



**A University of Sussex DPhil thesis**

Available online via Sussex Research Online:

<http://eprints.sussex.ac.uk/>

This thesis is protected by copyright which belongs to the author.

This thesis cannot be reproduced or quoted extensively from without first obtaining permission in writing from the Author

The content must not be changed in any way or sold commercially in any format or medium without the formal permission of the Author

When referring to this work, full bibliographic details including the author, title, awarding institution and date of the thesis must be given

Please visit Sussex Research Online for more information and further details

# Regulation and function of the Synaptonemal Complex during meiosis in *Saccharomyces cerevisiae*

Louise Joanna Newnham

Thesis for the qualification of DPhil

University of Sussex

April 2010

# Acknowledgements

First and foremost, I would like to thank Dr Eva Hoffmann for her superb guidance and unwavering support throughout my PhD. I have learnt so much from Eva and I am eternally grateful for her investment of time and patience with me.

I am also very grateful to all members of the Hoffmann and Neale laboratories for their insightful suggestions and valuable advice surrounding my research project.

Thanks is also owed to my co-supervisor Prof. Alan Lehmann for all of his helpful advice and for providing guidance when the going got a little tough.

I would also like to acknowledge the Medical Research Council for funding my 3-year studentship. Without this financial support, I simply would not have been able to carry out this research project.

Also deserving of special thanks are those that started off as colleagues at the GDSC and have since become my closest friends. I really would not have remained sane without their banter and reassurance that a failed experiment (or series of failed experiments) was not the end of the world. Thank you guys for making the journey so much fun!

This thesis would not exist without the unconditional love and support of my family. Thank you Mum and Dad for providing me with the solid foundations that have equipped me with the strength needed to combat my demons and make it this far. Thank you for never pushing me in one direction or the other and making me feel like whatever path I chose, you would be behind me. Thank you Matt, not only for being an inspirational big brother, but also for being a great friend.

Finally, a very special thanks is owed to my partner-in-crime, Andy who has kept me laughing throughout and has done an amazing job of putting up with me during my numerous freak-outs. Thank you for having remarkable faith in me at times when I didn't and for your reassurance that if it all goes wrong, we'd go and open a beach bar somewhere hot! Most of all though, thank you for your love. I hope this thesis goes some way to explain my need to 'homologously pair' your socks.

## **Declaration**

I hereby declare that this thesis was composed by me, and the research presented is my own, except where otherwise stated.

Louise Joanna Newnham

April 2010

# University of Sussex

## DPhil. Biochemistry

### **Regulation and function of the Synaptonemal Complex during meiosis in *Saccharomyces cerevisiae*.**

The Synaptonemal Complex (SC) is a proteinaceous structure that connects homologous chromosomes lengthwise during meiotic prophase. In budding yeast, the SC consists of two parallel axes that become connected by the central element protein, Zip1 that extends along the chromosome axes (Sym, Engbrecht et al. 1993). Extension of the SC is coordinated to crossover formation by a group of proteins known as the 'ZMM's (Zip1, Zip2, Zip3, Zip4, Msh4, Msh5 and Mer3) (Borner, Kleckner et al. 2004). Work outlined here demonstrates a role for the mismatch repair paralogue, Msh4 in preventing SC extension from being de-coupled from crossover formation. Furthermore, increased temperature serves as a positive effector for this de-coupling. These findings suggest that SC extension is highly regulated to ensure that it is coupled with crossing over.

As well as its role in crossover formation (Storlazzi, Xu et al. 1996), the work outlined here demonstrates an independent role for Zip1 in promoting the segregation of non-exchange chromosome pairs (NECs). Zip1 pairs the centromeres of NECs in pachytene through to metaphase I, where it aids their segregation at the first meiotic division. The localisation and function of Zip1 at the centromeres of non-exchange chromosomes depends on Zip3 and Zip2, respectively. Zip1 is observed at the centromeres of all chromosomes following SC disassembly through to the first meiotic division, where it promotes the segregation of exchange pairs also. A model is suggested whereby Zip1 promotes the segregation of both non-exchange and exchange chromosome pairs by tethering homologous centromeres throughout meiotic prophase. Finally, a parallel pathway for NEC segregation is also described that depends upon the spindle checkpoint component, Mad3. When both *ZIP1* and *MAD3* are deleted, NECs segregate at random.

# Table of Contents

## Chapter 1. Introduction

<b>1.1. Meiosis.....</b>	<b>page 1</b>
1.1.1. Meiosis – An Overview.....	page 1
1.1.2. Pre-meiotic Establishment of Sister Chromatid Cohesion.....	page 4
1.1.3. Meiotic Prophase.....	page 12
1.1.3.1. <i>Meiotic Prophase – An Overview.....</i>	<i>page 12</i>
1.1.3.2. <i>Early Prophase Chromosome Dynamics.....</i>	<i>page 14</i>
1.1.3.3. <i>Meiotic Recombination.....</i>	<i>page 18</i>
1.1.4. Meiotic Divisions.....	page 31
1.1.4.1. <i>Mono-orientation of Sister Chromatids at Meiosis I.....</i>	<i>page 31</i>
1.1.4.2. <i>The Spindle Checkpoint and the Onset of Anaphase.....</i>	<i>page 37</i>
1.1.4.3. <i>Protection of Centromeric Cohesin during Meiosis I.....</i>	<i>page 48</i>
<b>1.2. The Synaptonemal Complex.....</b>	<b>page 55</b>
1.2.1. The Architecture of the Synaptonemal Complex.....	page 55
1.2.1.1. <i>The Structure of the Synaptonemal Complex in Yeast.....</i>	<i>page 55</i>
1.2.1.2. <i>The Structure of the Synaptonemal Complex in Worms.....</i>	<i>page 61</i>
1.2.1.3. <i>The Structure of the Synaptonemal Complex in Flies.....</i>	<i>page 63</i>
1.2.1.4. <i>The Structure of the Synaptonemal Complex in Mammals.....</i>	<i>page 65</i>
1.2.2. Regulation of Synaptonemal Complex Assembly.....	page 69
1.2.3. The Role(s) of Synaptonemal Complex Proteins.....	page 77
1.2.4. Synaptonemal Complex Disassembly.....	page 81
<b>1.3. Non-Exchange Chromosome Segregation (NECS).....</b>	<b>page 85</b>
1.3.1. NECS in yeast.....	page 86
1.3.2. NECS in Flies & Worms.....	page 92
1.3.3. NECS in Plants.....	page 99
1.3.4. NECS in Mammals.....	page 100

## Chapter 2. Materials and Methods

### 2.1. Materials

2.1.1 Growth Media.....	page 104
-------------------------	----------

2.1.1.1. <i>Bacterial Media</i> .....	page 104
2.1.1.2. <i>Yeast Media</i> .....	page 104
2.1.2. <i>Buffers</i> .....	page 106
2.1.3. <i>Enzymes</i> .....	page 107
2.1.4. <i>Drugs &amp; Antibiotics</i> .....	page 107
2.1.5. <i>Antibodies</i> .....	page 108
2.1.6. <i>Oligonucleotides</i> .....	page 110
2.1.7. <i>Yeast Strains</i> .....	page 120
2.1.8. <i>Plasmids</i> .....	page 125
<b>2.2. Methods</b>	
2.2.1. <i>Bacterial Methods</i> .....	page 127
2.2.1.1. <i>Growth conditions</i> .....	page 127
2.2.1.2. <i>Plasmid extractions</i> .....	page 127
2.2.1.3. <i>Preparation of chemically competent DH5α cells</i> .....	page 127
2.2.1.4. <i>Transformation of chemically competent DH5α cells</i> .....	page 128
2.2.1.5. <i>Transformation of STBL2 cells</i> .....	page 128
2.2.1.6. <i>Storage of bacterial strains</i> .....	page 128
2.2.2. <i>Yeast Growth Conditions</i> .....	page 129
2.2.2.1. <i>Vegetative growth conditions</i> .....	page 129
2.2.2.2. <i>Sporulation conditions</i> .....	page 129
2.2.3. <i>Yeast Strain Construction</i> .....	page 130
2.2.3.1. <i>Transformation of yeast cells</i> .....	page 130
2.2.3.2. <i>PCR-based gene deletion</i> .....	page 131
2.2.3.3. <i>PCR-based promoter replacement</i> .....	page 132
2.2.3.4. <i>PCR-based C-terminal gene tagging</i> .....	page 133
2.2.3.5. <i>Genetic crosses</i> .....	page 134
2.2.3.6. <i>Diploid isolation</i> .....	page 135
2.2.3.7. <i>Storage of yeast strains</i> .....	page 136
2.2.4. <i>Cytological Methods</i> .....	page 136
2.2.4.1. <i>Assessment of nuclear divisions using DAPI</i> .....	page 136
2.2.4.2. <i>Sporulation counts</i> .....	page 136
2.2.4.3. <i>Visualisation of GFP in tetrads and live cells</i> .....	page 137
2.2.4.4. <i>In situ immunofluorescence of fixed cells</i> .....	page 137
2.2.4.5. <i>Preparation and immuno-staining of chromosome spreads</i> .....	page 138

2.2.4.6. Image capture.....	page 140
2.2.5. DNA Methods.....	page 141
2.2.5.1. General PCR.....	page 141
2.2.5.2. Genomic DNA extraction (yeast).....	page 142
2.2.5.3. Phenol-Chloroform DNA extraction.....	page 143
2.2.5.4. Restriction Digests of DNA.....	page 143
2.2.5.5. DNA Ligation.....	page 143
2.2.5.6. Agarose Gel Electrophoresis.....	page 144
2.2.5.7. Gel extraction of DNA.....	page 144
2.2.6. Protein Methods.....	page 145
2.2.6.1. Protein Extraction.....	page 145
2.2.6.1.1. Protein Extraction using NaOH.....	page 145
2.2.6.1.2. Tri-Chloroacetic Acid (TCA) extraction of proteins.....	page 145
2.2.6.1.3. Preparation of non-denaturing nuclear/chromatin extracts.....	page 146
2.2.6.2. SDS-PAGE separation of proteins.....	page 148
2.2.6.3. Western Blotting.....	page 149
2.2.6.5. Immunoprecipitation.....	page 150
2.2.6. Computational Tools.....	page 152
2.2.6.1. Websites used.....	page 152
2.2.6.2. Software used.....	page 152
2.2.6.3. Overview of ColoS.....	page 153

## **Chapter 3. Synaptonemal Complex (SC) formation is both promoted and prohibited by Msh4.**

3.1. Introduction.....	page 156
3.2. Results.....	page 159
3.2.1. <i>msh4Δ</i> mutants display improved chromosome synapsis at 33 °C	
.....	page 159
3.2.2. <i>Zip2</i> is required for synapsis at 33 °C.....	page 166
3.2.3. <i>Zip2</i> -independent synapsis can occur in the absence of <i>MSH4</i>	
.....	page 166
3.2.4. <i>Zip2</i> extends polymers of <i>Zip1</i> in <i>msh4Δ</i> mutants at 33 °C...	page 169

<b>3.2.5. Zip1 polymerisation is unaffected by temperature and MSH4 status in zip3Δ mutants.....</b>	<b>page 170</b>
<b>3.2.6. The improved synapsis observed in msh4Δ mutants at 33 °C is predominately centromere-associated.....</b>	<b>page 172</b>
<b>3.2.7. Zip1 localisation at centromeres is similar in zip2Δ and msh4Δ zip2Δ mutants at both temperatures.....</b>	<b>page 174</b>
<b>3.2.8. Msh4 foci are juxtaposed to centromeres at both temperatures .....</b>	<b>page 176</b>
<b>3.2.9. Msh4-GFP foci behaviour at zygotene and pachytene is unaffected by temperature.....</b>	<b>page 178</b>
<b>3.2.10. Zip1 extension occurs both uni- and bi-directionally from Msh4-GFP foci.....</b>	<b>page 180</b>
<b>3.3. Discussion.....</b>	<b>page 186</b>

## **Chapter 4. Zip1 promotes the segregation of non-exchange chromosomes.**

<b>4.1. Introduction.....</b>	<b>page 195</b>
<b>4.2. Results.....</b>	<b>page 199</b>
<b>4.2.1. Deletion of ZIP1 increases non-disjunction of an obligate non-exchange pair and correlates with a defect in centromere pairing.....</b>	<b>page 199</b>
<b>4.2.2. Differential requirements for the 'ZMM' proteins in non-exchange chromosome segregation.....</b>	<b>page 204</b>
<b>4.2.3. Zip1-dependent centromere pairing is observed throughout meiotic prophase.....</b>	<b>page 206</b>
<b>4.2.4. Zip1 is observed at neCEN5s throughout meiotic prophase...page</b>	<b>212</b>
<b>4.2.5. Localisation of Zip1 to neCEN5s depends upon Zip3.....page</b>	<b>213</b>
<b>4.2.6. Synapsis initiation proteins, Zip2 and Zip4 are required for Zip1-mediated centromere pairing.....page</b>	<b>219</b>
<b>4.2.7. Zip1 does not facilitate centromere pairing when C-terminally tagged with LacI.....page</b>	<b>223</b>
<b>4.2.8. Zip1 also co-localises with the centromeres of exchange chromosomes following SC disassembly.....page</b>	<b>225</b>
<b>4.2.9. Zip1 promotes the segregation of exchange chromosomes...page</b>	<b>226</b>

4.3. Discussion.....	page 230
----------------------	----------

## Chapter 5. Distinct roles for Zip2 and Zip3 in synaptonemal complex formation.

5.1. Introduction.....	page 237
5.2. Results.....	page 240
5.2.1. <i>Zip1 shows strong association with centromeres in zip2Δ mutants, but is depleted from centromeres in zip3Δ mutants.</i> .....	page 240
5.2.2. <i>Development of a program to quantify Zip1-Ctf19 co-localisation</i> .....	page 243
5.2.3. <i>Smt3<sup>SUMO</sup> does not accumulate at centromeres in zip2Δ mutants and is moderately depleted from centromeres in zip3Δ mutants.</i> .....	page 251
5.2.4. <i>Zip3 acts upstream of Zip2 in both synapsis and in the localisation of Zip1 to centromeres.</i> .....	page 255
5.2.5. <i>Zip2- and Zip3-independent centromere ‘coupling’ persists to mid-prophase in spo11Δ cells.</i> .....	page 259
5.3. Discussion.....	page 265

## Chapter 6. The role of spindle checkpoint proteins in non-exchange chromosome segregation.

6.1. Introduction.....	page 272
6.2. Results.....	page 276
6.2.1. <i>Mad3 promotes centromere pairing, but also acts in a parallel pathway to Zip1 in promoting NECS.</i> .....	page 276
6.2.2. <i>Mad2 is also involved in NECS.</i> .....	page 279
6.2.3. <i>Ipl1/Aurora B kinase activity is required for NECS.</i> .....	page 282
6.2.4. <i>ipl1-mn mutants exhibit an SC disassembly defect.</i> .....	page 284
6.2.5. <i>Exploiting the ipl-mn SC disassembly phenotype to identify the Smt3 species that co-localise with Zip1 on synapsed chromosomes.</i> .....	page 286
6.2.6. <i>Preliminary work on TAP-tagged Zip1.</i> .....	page 290
6.3 Discussion.....	page 294

<b>Chapter 7. Discussion.....</b>	<b>page 303</b>
<b>7.1. Discussion.....</b>	<b>page 303</b>
<b>7.2. Conclusions and Future work.....</b>	<b>page 307</b>
<b>Bibliography.....</b>	<b>page 309</b>
<b>Appendix.....</b>	<b>page 329</b>
<b>Appendix: Figures.....</b>	<b>page 329</b>
<b>Appendix: Published Work.....</b>	<b>follows page 338</b>

# List of Figures

**Figure 1.1.** Diagram outlining the differences between mitotic and meiotic cell divisions.

**Figure 1.2.** Proposed structure of the cohesin complex and models for how cohesin may mediate sister chromatid cohesion.

**Figure 1.3.** Stages of meiotic prophase

**Figure 1.4.** Original DNA double-strand break repair model.

**Figure 1.5.** Pathways of meiotic DSB repair in *Saccharomyces cerevisiae*.

**Figure 1.6.** Sister kinetochore orientation in the first and second meiotic divisions.

**Figure 1.7.** Homolog bi-orientation generates spindle tension.

**Figure 1.8.** Diagram outlining how the chromosomal passenger proteins regulate the spindle checkpoint in response to spindle tension.

**Figure 1.9.** The structure of the Synaptonemal Complex.

**Figure 1.10.** Structural models of the synaptonemal complex in different organisms.

**Figure 1.11.** Model for the initiation of SC formation by the 'ZMM's.

**Figure 1.13.** Non-exchange chromosome segregation.

**Figure 2.1.** PCR-based gene-deletion.

**Figure 2.2.** PCR-based promoter replacement.

**Figure 2.3.** PCR-based C-terminal gene tagging.

**Figure 2.4.** A program for automated object-detection.

**Figure 3.1.** Improved synapsis in *msh4Δ* nuclei at 33 °C in the BR strain background.

**Figure 3.2.** Improved synapsis in *msh4Δ* nuclei at 33 °C precedes meiotic nuclear divisions in Y55 strains.

**Figure 3.3.** *msh4Δ* mutants do not form extensive SCs at 25 °C even when arrested in pachytene.

**Figure 3.4.** Deletion of *MSH4* improves Zip1 polymerization in *zip2Δ* mutants of the BR background, at 33 °C.

**Figure 3.5.** Improved synapsis precedes meiotic nuclear divisions in *msh4Δ zip2Δ* double mutants of the Y55 background, at 33 °C.

**Figure 3.6.** Synapsis is unaffected by both temperature and deletion of *MSH4* in *zip3Δ* mutants.

**Figure 3.7.** Zip1 stretches observed in *msh4Δ* and *msh4Δ zip2Δ* mutants at 33 °C are predominantly associated with centromeres (Ctf19-13Myc).

**Figure 3.8.** Centromeres frequently co-localise with Zip1 foci in early zygotene nuclei of *msh4Δ* and *msh4Δzip2Δ* mutants.

**Figure 3.9.** Zip1 association with centromeres (Ctf19-13Myc) is similar in *zip2Δ* and *msh4Δ zip2Δ* strains and is irrespective of temperature.

**Figure 3.10.** Msh4-GFP foci are frequently juxtaposed to centromeres at both zygotene and pachytene.

**Figure 3.11.** The number of Msh4-GFP foci *per* nucleus is unaffected by temperature.

**Figure 3.12.** Zip1 stretches are found to one side or both sides of Msh4-GFP foci.

**Figure 3.13.** Model outlining the regulation of Synaptonemal Complex (SC) formation by the 'ZMM' ensemble and temperature.

**Figure 4.1.** Decreased centromere pairing frequencies correlate with increased meiosis I non-disjunction of a non-exchange chromosome pair.

**Figure 4.2.** Histograms showing the distribution of distances between *neCEN5* foci in spread pachytene nuclei.

**Figure 4.3.** Differing *ZMM* mutant phenotypes for centromere pairing and meiosis I segregation of the non-exchange chromosome pair.

**Figure 4.4.** Time course analysis of *neCEN5* pairing frequencies for wild type and *zip1Δ* cells.

**Figure 4.5.** *neCEN5* pairing frequencies in pachytene, diplotene and metaphase I nuclei.

**Figure 4.6.** Analysis of *neCEN5* position relative to the metaphase I spindle for wild type, *zip1Δ* and *zip2Δ* cells.

**Figure 4.7.** Zip1 co-localises with *neCEN5*s at diplotene and metaphase I.

**Figure 4.8.** Zip1 co-localises with *neCEN5s* in pachytene nuclei in a Zip3-dependent manner.

**Figure 4.9.** Flow diagram detailing the *neCEN5*-Zip1 co-localisation analysis using 'ColoR'.

**Figure 4.10.** A representative image of a wild type pachytene nucleus used for the 'ColoR' analysis.

**Figure 4.11.** Analysis of Zip1-*neCEN5* co-localisation using ColoR.

**Figure 4.12.** Zip2 and Zip4 are dispensable for localisation of Zip1 to *neCEN5s* in pachytene nuclei.

**Figure 4.13.** Zip1-LacI fusion protein fails to 'tether' centromeres of the non-exchange chromosomes despite proficient localisation to *LacO* repeats.

**Figure 4.14.** Zip1 remains associated with the centromeres of exchange chromosomes following SC disassembly.

**Figure 4.15.** Zip1 is detected following SC disassembly in three different strain backgrounds.

**Figure 4.16.** Model for how Zip1 promotes the segregation of both non-exchange and exchange chromosomes at meiosis I.

**Figure 5.1.** Zip1 localisation to centromeres during pachytene is different in *zip2Δ* and *zip3Δ* mutants.

**Figure 5.2.** Schematic flow diagram of how 'ColoS' performs automated object detection and quantifies protein co-localisation.

**Figure 5.3.** Typical example of the output file generated for each image by 'ColoS'.

**Figure 5.4.** A comparison of the raw, unprocessed images with corresponding graphical outputs following automated object-detection.

**Figure 5.5.** The results of Zip1-Ctf19 co-localisation analysis done using 'ColoS'.

**Figure 5.6.** Localisation of Smt3<sup>SUMO</sup> during pachytene in wild type, *zip2Δ* and *zip3Δ* nuclei.

**Figure 5.7.** Box plots comparing the co-localisation of Zip1 and Smt3<sup>SUMO</sup> with centromeres, during pachytene.

**Figure 5.8.** Synapsis is indistinguishable in *zip3Δ* and *zip2Δzip3Δ* mutants.

**Figure 5.9.** The association of Zip1 with centromeres in *zip2Δzip3Δ* pachytene nuclei.

**Figure 5.10.** Pair-wise associations of centromeres in *spo11Δ* mutants during pachytene.

**Figure 5.11.** Co-localisation of Zip1 with Ctf19 foci during pachytene in *spo11Δ*, *spo11Δzip2Δ* and *spo11Δzip3Δ* mutants.

**Figure 5.12.** Diagram summarising the *zip2Δ* and *zip3Δ* synapsis phenotypes.

**Figure 6.1.** Mad3 promotes centromere pairing and the segregation of non-exchange chromosomes not 'paired' by Zip1.

**Figure 6.2.** Mad2 promotes centromere pairing and the segregation of non-exchange chromosomes not 'paired' by Zip1.

**Figure 6.3.** Ipl1/Aurora B kinase activity is required for non-exchange chromosome segregation.

**Figure 6.4.** The synaptonemal complex fails to disassemble in *ipl1-mn* cells.

**Figure 6.5.** Smt3<sup>SUMO</sup> fails to become diffuse or dotty following exit from pachytene in *ipl1-mn* cells.

**Figure 6.6.** Experimental outline for identifying the sumoylated protein species present along the chromosomal axes.

**Figure 6.7.** Smt3 immunoprecipitation on crude chromatin extracts from wild type and *ipl1-mn* cells one hour after pachytene exit.

**Figure 6.8.** Preliminary work on Zip1-TAP strains.

**Figure 6.9.** Model for non-exchange chromosome segregation in budding yeast.

**Appendix Figure 1.** Chromosome pairing occurs normally in *msh4* strains.

**Appendix Figure 2.** GFP signal is not detected in un-tagged Msh4 strains.

**Appendix Figure 3.** Zip1 co-localises with neCEN5s during metaphase I.

**Appendix Figure 4.** Staining controls for Zip1 localisation to metaphase I spindles.

**Appendix Figure 5.** Histograms representing the same data shown in Figure 5.5.

**Appendix Figure 6.** Representative images of Smt3 and Zip1 co-staining in pachytene nuclei of *zip2Δ* and *zip3Δ* mutants.

**Appendix Figure 7.** Analysis of the 'proportion' of each neCEN5 covered by Zip1 during pachytene in *zip2Δ* mutants.

**Appendix Figure 8.** Scatterplot of the mean Zip1 and mean Ctf19 pixel intensities for 80 randomly selected Ctf19 foci from *zip2Δ* mutants.

**Appendix Figure 9.** Protein extracts for Smt3 IP experiment.

**Appendix Figure 10.** A typical histogram from a single bootstrapping analysis of our dataset.

# List of Abbreviations

APC	Anaphase promoting complex
ATP	Adenosine Triphosphate
bp	Base pair
ChIP	Chromatin Immuno-precipitation
Cy5	Cyanine 5
DAPI	4',6-diamidino-2-phenylindole
dHJ	Double Holliday Junction
DSB	Double strand break
DTT	Dithiothreitol
EDTA	Ethylenediaminetetraacetic acid
FISH	Fluorescent <i>in situ</i> hybridisation
FITC	Fluorescein isothiocyanate
g	Gram
ml	Millilitre
mM	Millimolar
mmol	Millimole
NDJ	Non-disjunction
NECS	Non-exchange chromosome segregation
<i>neCEN5</i>	Centromere of non-exchange chromosome 5
NEM	<i>N</i> -Ethylmaleimide
ORF	Open reading frame
PBS	Phosphate Buffered Saline
PCR	Polymerase chain reaction
µg	microgram
µl	microlitre
µm	micrometre
Q-PCR	Quantitative polymerase chain reaction
SC	Synaptonemal complex
SEI	Single end invasion
SNP	Single nucleotide polymorphism
SUMO	Small Ubiquitin-like Modifier
w/v	Weight per unit volume
v/v	Volume per unit volume
YEPD	Yeast Extract, Peptone, Dextrose

# Chapter 1. Introduction

## 1.1. Meiosis

### 1.1.1. Meiosis – an overview

Central to sexual reproduction is the production of gametes (eggs and sperm in humans) with half the chromosome complement compared to the original parent cell. This enables restoration of the original chromosome complement when two gametes fuse. Meiosis is the cell division responsible for gamete production and is characterised by a single round of DNA replication followed by two successive rounds of chromosome segregation. The net result is four daughter cells with half the number of chromosomes of the original parent cell (Figure 1.1). During the first meiotic division homologous chromosomes that differ in parental origin are segregated from each other and this is sometimes referred to as the 'reductional division'. The second meiotic division partitions replicated sister chromatids from one another, much like a mitotic cell division (Figure 1.1). This is often referred to as the 'equational division'. The segregation of homologous chromosomes during the first meiotic division requires several modifications to chromosome behaviour that will be outlined in detail in the following sections. Briefly, this involves the formation of chiasmata between homologous chromosomes that are the result of reciprocal crossover recombination events. This imparts homologous chromosomes with a physical linkage that allows the cell to identify them as segregating partners. As well as assisting in the fidelity of chromosome segregation at meiosis I, crossing over generates novel combinations of alleles that

Figure 1.1.

break up gene linkage groups and contribute to genetic diversity in the resulting offspring. Meiosis also promotes genetic diversity through Mendel's second law of 'independent assortment' of chromosomes. That is, chromosomes of different parental origin are inter-mixed in meiosis I. By providing new combinations of alleles, meiosis has provided much broader genetic diversity than could be afforded by mutation alone.

Meiosis is not faultless however, and errors in meiotic chromosome segregation in humans can result in reduced fertility and miscarriage. Although the majority of aneuploid fetuses undergo spontaneous abortion, some chromosomal aneuploidies can be tolerated to birth but are associated with severe mental retardation and developmental abnormalities (Hassold and Hunt, 2001). These include Down's syndrome (trisomy 21), Edward's syndrome (trisomy 18), Patau syndrome (trisomy 13), Klinefelter's syndrome (XXY) and Triple X syndrome (XXX). Monosomies are less well tolerated with the majority of monosomic offspring undergoing spontaneous abortion during fetal development. The only whole chromosome monosomy that can be tolerated during fetal development is Turner's syndrome in which only one copy of the X chromosome is present. This syndrome is characterised by severe developmental abnormalities and sterility of the affected individual. The incidence of meiotically-derived aneuploidy increases sharply with increasing maternal age (Hassold and Hunt, 2001), suggesting that the fidelity of meiotic chromosome segregation decreases in ageing mothers. Therefore, understanding the processes that underpin meiotic chromosome segregation is paramount to understanding why the incidence of aneuploidy increases with increasing maternal age. Age-related infertility has large

implications in modern society where women are increasingly waiting later in life to start families (office for national statistics [www.statistics.gov.uk](http://www.statistics.gov.uk)).

### **1.1.2. Pre-meiotic Establishment of Sister Chromatid Cohesion**

The first cellular landmark in the meiotic program is pre-meiotic DNA replication. Although the mechanisms underlying DNA replication are thought to be very similar in mitotic and meiotic cells, some subtle differences do exist. For example, DNA replication takes longer to complete in meiotic cells as compared to mitotic cells (Cha et al., 2000). In *S. cerevisiae*, pre-meiotic S-phase takes three times as long as mitotic S-phase (mitotic S-phase: 17 min, meiotic S phase: 61 min)(Cha et al., 2000). This is thought to be due to changes in chromatin structure that occur during pre-meiotic S-phase that are necessary for later meiotic events. Consistent with DNA replication being coupled to later meiotic events is the observation that meiotic S-phase is shortened and lengthened by deletion of *SPO11* and *REC8*, respectively (Cha et al., 2000). Spo11 is a topoisomerase II-like protein that is responsible for initiation of meiotic recombination (Keeney et al., 1997) and Rec8 is the meiosis-specific kleisin subunit of cohesin (Klein et al., 1999). The fact that these proteins influence the length of S-phase suggests that S-phase progression is linked to meiotic recombination and changes to chromatin structure that accompany establishment of sister chromatid cohesion. Consistent with this is the observation that preventing DNA replication by treatment with hydroxyurea or deletion of the genes encoding S-phase cyclins Clb5/Clb6, abolishes DSB formation (Borde et al., 2000). Furthermore, delaying DNA replication on one chromosome arm results in a corresponding delay (~ 1 hour) in

DSB formation on the same chromosome arm. The interval between DNA replication and DSB formation is therefore fixed regardless of whether regions were replicated early or late (Borde et al., 2000). This has led to a model whereby DNA replication is linked to DSB formation in a regional, rather than genome-wide basis. Taken together, these findings imply that the DSB machinery may assemble onto newly replicated regions and this assembly may regulate S-phase progression.

Another unique feature of meiotic S-phase is the requirement for the meiosis-specific Mum2 protein for successful DNA replication. Mutants deleted for *mum2Δ* fail to replicate their DNA and arrest without entering into the meiotic divisions (sporulation efficiency <0.1 %) (Engelbrecht et al., 1998). It is unknown precisely why Mum2 is so important for pre-meiotic, but not vegetative S-phase.

Why does meiosis even require a round of DNA replication? Surely halving of the chromosome number could be achieved by bypassing DNA replication all together and instead undertaking a single reductional division? Indeed, many meiotic events such as homolog pairing, recombination and SC formation can occur proficiently in the absence of sister chromatids. This is evidenced by meiotic chromosome behaviour in *cdc6-mn* mutants that do not replicate their DNA (Brar et al., 2008; Hochwagen et al., 2005). Despite this, sister chromatids are required (in many organisms) to ensure the disjunction of homologous chromosomes at meiosis I. This is because sister chromatids and the cohesion between them, together with inter-homolog crossover recombination, impart homologous chromosomes with a physical connection that is crucial for their correct segregation at meiosis I (Figure 1.6 A). Therefore, pre-meiotic S-phase is crucial for meiotic

chromosome segregation in that it generates of sister chromatids and establishes of sister chromatid cohesion (Klein et al., 1999; Uhlmann and Nasmyth, 1998).

Cohesin was first discovered in budding yeast with the identification of Smc1, Smc3, Scc1 and later Scc3 that form a protein complex capable of holding sister chromatids together (Michaelis et al., 1997; Toth et al., 1999). SMC (structural maintenance of chromosomes) proteins are characterised by two globular C- and N-terminal domains and a flexible 'hinge' region in the middle of the protein that is flanked by two coiled-coil domains (Michaelis et al., 1997). Electron micrographs have revealed that Smc1 and Smc3 fold back on themselves to form intra-molecular, anti-parallel coiled coils that, in turn form V-shaped Smc1-Smc3 heterodimers through their flexible hinge domains (Haering et al., 2002)(Figure 1.2). Intra-molecular folding of SMC proteins unites the globular domains of N and C termini that contain Walker A and B motifs, respectively, forming a putative ABC (ATP binding cassette) ATPase domain (Lowe et al., 2001). The globular heads of Smc1 and Smc3 proteins are connected by the kleisin subunit, Scc1. In particular, the N-terminus of Scc1 contacts the globular head of Smc3 and the C-terminus contacts that of Smc1. The fourth cohesin protein, Scc3 also interacts with the C-terminus of Scc1 (Haering et al., 2002) (Figure 1.2). However, in meiotic cells Scc1 is substituted for the meiosis-specific kleisin subunit Rec8 (Klein et al., 1999). Rec8 and Scc1 share 38 % amino acid similarity (16 % identity) with the most highly conserved regions being the C- and N- terminal domains (Klein et al., 1999; Michaelis et al., 1997).

Figure 1.2.

In *rec8Δ* mutants, homolog pairing is reduced, no SC formation occurs and DSBs are not repaired (Klein et al., 1999). However, as previously mentioned sister chromatids are not required for homolog pairing, DSB repair and SC formation as these processes occur normally in *cdc6-mn* mutants that fail to replicate their DNA (Brar et al., 2008; Hochwagen et al., 2005). This suggests that Rec8 plays a direct role in these processes that is independent from its role in sister chromatid cohesion.

The ring-like structure, 40 nm in diameter formed by the cohesin complex has led to the suggestion that cohesin 'entrap' two newly replicated sister chromatids which is retained until the cleavage of the kleisin subunit at anaphase (Haering et al., 2002) (Figure 1.2, Model 1). Support for a model whereby cohesin rings 'entrap' sister chromatids comes from work using circular mini-chromosomes. Linearization of the chromosomes with a restriction enzyme resulted in decreased association of the cohesin complex with the DNA whereas histone proteins remained bound to the DNA (Ivanov and Nasmyth, 2005). This was interpreted to be because the cohesin rings could slide off the ends of the linearized DNA. However, other models have since been suggested for how the cohesin complex mediates sister chromatid cohesion that could also explain the above findings (reviewed in Guacci 2007). An alternative model was suggested whereby cohesin complexes encircle individual chromatids and interact with each other thus 'tethering' sister chromatids together (Figure 1.2, Model 2). This model is based on work into the association of cohesin with silent chromatin domains, such as the *HMR* mating locus. Recombinase sites flanking the *HMR* locus allowed excision by a site-specific recombinase and *LacO/LacI*-GFP allowed the excised HMR circles

to be followed cytologically (Chang et al., 2005). In silencing mutants (*sir2Δ*), *HMR* circles were not cohesed as evidenced by the presence of two GFP dots in M-phase arrested cells. This correlated with decreased co-immunoprecipitation of cohesin subunits with the *HMR* locus. Crucially however, inactivation of Sir2 in M phase-arrested cells resulted in severely decreased cohesion of the *HMR* circles (two GFP dots), despite high levels of associated cohesin. (Chang et al., 2005). This finding is hard to reconcile with the previous model whereby cohesin entraps both helices of sister chromatids and so a modified version of the model has been proposed (for the *HMR* locus at least) in which cohesin complexes encircle individual chromatids and through interaction with cohesin complexes on the sister chromatid, provide sister chromatid cohesion. Finally, a third model suggests that cohesin complexes do not encircle DNA at all and instead tether sister chromatids through directly binding DNA and other cohesin complexes bound to the sister chromatid (Huang et al., 2005; Milutinovich and Koshland, 2003) (Figure 1.2, Model 3). Further experimental evidence is required before any of these models can be fully accepted or ruled out.

How is sister chromatid cohesion established? Cohesin complexes are thought to be loaded onto the DNA prior to DNA replication in vegetative cells by the proteins Scc2 and Scc4 (Ciosk et al., 2000; Toth et al., 1999). Mutants lacking Scc2 or Scc4 have markedly less Smc1 and Scc1 present in chromatin extracts than wild type cells, which correlates with precocious sister chromatid separation (Ciosk et al., 2000). Use of temperature sensitive *scc2* and *scc4* alleles showed that the defect is not in the maintenance of cohesin, but is in the establishment of

cohesin (Ciosk et al., 2000). However, precisely how cohesin loading is achieved remains elusive owing to the ambiguity surrounding how cohesin associates with the DNA (see above).

If cohesin is established during G1, cohesin must be modified during DNA replication to facilitate cohesion between nascent sister chromatids, possibly by transient opening of the cohesin ring to permit passage of the replication fork or unloading/re-loading onto nascent sister chromatids. In either case this process requires Eco1/Ctf7, a conserved protein that is thought to act at the replication fork to couple DNA replication to the establishment of cohesion (Toth et al., 1999). Mutants lacking Eco1 (*eco1-1*) load cohesin onto DNA as determined from chromosome spreads, but sister chromatids are not cohesed according to the presence of two *CENV*-GFP dots in many of the cells assayed (Toth et al., 1999). This phenotype is not observed when cells (containing a temperature sensitive *eco1* allele) are shifted to the restrictive temperature after S-phase, suggesting Eco1 functions during S-phase (Toth et al., 1999). More recent work has revealed that Eco1 binds directly to PCNA, the sliding clamp that travels with the replicative DNA polymerase at the replication fork (Moldovan et al., 2006). Point mutations in Eco1 that abolish its binding to PCNA has the same effect on sister chromatid cohesion as an *ECO1* deletion mutant, suggesting that this interaction is paramount to its function (Moldovan et al., 2006). These observations indeed suggest that establishment of cohesion between sister chromatids is coupled to DNA replication.

The timing at which sister chromatid cohesion is established in the meiotic cell cycle has important implications for human fertility. Sister chromatid cohesion, together with crossovers, holds homologous chromosomes together until their eventual segregation at meiosis I (Figure 1.6 A). During oogenesis, DNA replication occurs in the primordial germ cells within the developing fetus whereas the first meiotic division does not proceed until ovulation that may occur up to several decades later. If establishment of sister chromatid cohesion is confined to DNA replication, cohesin must be sustained in the developing oocyte for decades. However, experiments in yeast show that cohesin is re-loaded onto chromatin in G2 cells following DNA damage (Heidinger-Pauli et al., 2008; Strom et al., 2007; Strom et al., 2004). This suggests that replenishing of cohesin after DNA replication may indeed occur in oocytes *in vivo* where they are likely to endure substantial levels of DNA damage over several decades of meiotic arrest.

Clearly cohesin is important for mammalian fertility. In mammals, there exist meiosis specific isoforms of cohesin proteins including SMC1- $\beta$ , the meiosis specific SMC1 variant. Both male and female SMC1- $\beta$  -/- knock out mice are infertile, which correlates with multiple meiotic defects (synapsis, recombination and cohesion affected) (Revenkova et al., 2004). This serves to highlight the importance of cohesin for the generation of healthy gametes in mammals.

### **1.1.3. Meiotic prophase**

#### ***1.1.3.1. Meiotic prophase – An overview***

Having completed duplication of the genome, meiotic cells engage in an extended prophase in which the chromosomes prepare for the ensuing meiotic divisions. Meiotic prophase comprises of several stages that are characterised by distinct landmark events (Figure 1.3). During the first stage named 'Leptotene' (from the greek meaning "thin threads") chromosomes undergo dynamic rearrangements such as telomere clustering and centromere 'coupling' (Tsubouchi and Roeder, 2005; Zickler and Kleckner, 1998). Another hallmark of leptotene is the initiation of meiotic recombination with the formation of programmed double-strand breaks (DSBs) in the DNA. During 'Zygotene' ("paired threads") homologous chromosomes become paired allowing inter-homolog repair of the DSBs (Borner et al., 2004). Another feature of zygotene is the formation of the synaptonemal complex (SC), a tripartite proteinaceous structure that synapses homologous chromosomes along their lengths. The next stage is 'Pachytene' ("thick threads") characterised by full-length SC (Figure 1.3), highly condensed DNA and the resolution of a subset of recombination intermediates into non-crossovers. Pachytene is also characterised by the presence of unresolved double Holiday junctions (dHJ), the precursors to crossover recombination events (Allers and Lichten, 2001). Cells exit pachytene and enter 'Diplotene' ("two threads"), characterised by separated spindle pole bodies, diffuse DNA, disassembly of the SC and resolution of dHJ into crossovers (Allers and Lichten, 2001). In some organisms, diplotene is followed by 'Diakinesis' in which chromosomes once again become highly condensed and chiasmata are cytologically detectable (Petronczki

Figure 1.3

et al. 2003). Assembly of the meiosis I metaphase spindle signals the end of meiotic prophase the start of the meiotic divisions. The following sections describe these events in greater detail, apart from the synaptonemal complex, which is discussed, in depth, in Section 1.2.

#### **1.1.3.2. Early prophase chromosome dynamics**

Following completion of DNA replication and establishment of sister chromatid cohesion, the next task facing the meiotic cell is to unite homologous chromosomes (homolog pairing). The process by which this occurs varies depending on the organism, but generally involves dynamic chromosome interactions that facilitate the assessment of homology. In many organisms “bouquet formation” in which the telomeres cluster near the spindle pole body, is a hallmark of early meiotic prophase (Zickler and Kleckner, 1998). Bouquet formation is proposed to assist homolog pairing by tethering the telomeres at a single fixed point of the nuclear envelope uniting the chromosomes in close proximity, allowing homology to be assessed. In *S. cerevisiae*, this process requires a protein named Ndj1 (Chua and Roeder, 1997; Conrad et al., 1997). Defects in bouquet formation that result from deletion of *NDJ1* causes delayed homolog alignment and synaptonemal complex formation as well as increased homolog non-disjunction (Chua and Roeder, 1997; Conrad et al., 1997). Ndj1 directly binds the telomeres and interacts with a SUN-domain containing protein called Mps3 that spans the inner nuclear membrane and interacts with another unknown protein (possibly Mps2) that spans the outer nuclear envelope and contacts the cytoskeleton. SUN-domain proteins have recently been identified as playing conserved meiotic

functions in the nematode, *C. elegans* (Penkner et al., 2009; Sato et al., 2009).

These interactions are stabilised by a fourth protein, named Csm4 (Conrad et al., 2008).

Following bouquet formation, the telomeres are dispersed around the nuclear envelope and undergo rapid telomere-led movements that persist throughout meiotic prophase (Conrad et al., 2008; Koszul et al., 2008; Wanat et al., 2008). This process is dependent upon the same proteins and mechanism that mediate bouquet formation (Ndj1, Csm4 and Mps3). Three-dimensional live-cell imaging revealed that telomeres travel independently of one another along common 'tracks' within the nucleus at speeds of up to 1  $\mu\text{m}$  per second (Conrad et al., 2008). Given that the yeast nucleus is  $\sim 4 \mu\text{m}$  in diameter, these represent very rapid chromosome movements.

An analogous, but more dramatic process occurs during meiotic prophase in fission yeast in which the entire nucleus oscillates between opposite ends of the cell. This so-called 'horsetail movement' is driven by cytoplasmic microtubules that are tethered to the telomeres through the nuclear membrane and persists throughout meiotic prophase (Chikashige et al., 1994). It is thought that such movements (which are distinct from earlier bouquet formation) may disrupt inappropriate recombination events as well as helping to untangle chromosomes so that they do not become interlocked during recombination (reviewed in Koszul and Kleckner 2009).

In addition to bouquet formation, another process believed to assist in homolog pairing in *S. cerevisiae* is 'centromere coupling'. This process, which also occurs during leptotene, is characterised by pair-wise centromeric associations

between non-homologous chromosomes. The central element protein, Zip1 is responsible for 'coupling' centromeres together independently of homology and this process is distinct from telomere clustering as it is unaffected by deletion of *NDJ1* (Tsubouchi and Roeder, 2005). It is thought that this process assists in the homology search by allowing chromosomes to switch partners until they become 'coupled' to their homologous partner chromosome.

Although *NDJ1*-dependent telomere clustering and *ZIP1*-dependent centromere coupling are thought to assist in homolog pairing, neither are essential as homolog alignment eventually occurs in *ndj1Δ* (Chua and Roeder, 1997; Conrad et al., 1997) and *zip1Δ* mutants (Sym et al., 1993). However, it is tempting to speculate that the timely alignment of homologs provided by these two independent pathways that is important for successful completion of later meiotic events.

In many organisms, the precise mechanism by which homologous chromosomes become paired remains an elusive area of study. Recombination and synapsis cannot occur until homologs have paired, but pairing cannot be established/stabilised without recombination and synapsis. This apparent interdependence, coupled with the fact that the two events occur simultaneously, has made the study of homolog pairing difficult in these organisms. However, the situation is clearer in *C. elegans*, which have chromosome-specific 'pairing centres' that allow homologous chromosomes to pair prior to undergoing synapsis and recombination (MacQueen et al., 2005). These pairing centres are found near the ends of chromosomes and are bound by zinc finger proteins that tether the pairing

centres to the nuclear envelope where they initiate homolog pairing (Phillips and Dernburg, 2006). However, this study revealed just four genes encoding such zinc finger proteins (or *zim* genes) and there are six pairs of chromosomes in *C. elegans*, ruling out the possibility that each chromosome pair has their own 'ZIM' protein. Indeed further experimentation showed that two of these proteins function for two different chromosome pairs, but despite this, the chromosomes 'sharing' the same ZIM protein still underwent accurate homolog pairing, suggesting that there are other as yet unidentified proteins that must contribute to homolog recognition (Phillips and Dernburg, 2006). Nevertheless, this is a clear example of active homolog pairing that is clearly separable from both synapsis and recombination (MacQueen et al., 2005).

An analogous system exists in *Drosophila* males in which chromosomes do not crossover, but still manage to pair with high efficacy (Hawley, 2002). RNAi knock down of Rad51 has no effect on homolog pairing or fertility in *Drosophila* males, suggesting that they have alternative mechanisms that are independent of DSB repair for pairing homologs (Yoo and McKee, 2005).

In *S. cerevisiae*, Spo11 is required for homolog pairing as *spo11Δ* mutants do not pair their homologous chromosomes. However, a mutant of *spo11* that does not form breaks (*spo11-Y135F*) successfully pairs homologous chromosomes (Cha et al., 2000). This suggests that in budding yeast, DSB formation is not required for homolog alignment, but Spo11 protein is. However, the mechanism by which this occurs remains elusive.

### **1.1.3.3. *Meiotic recombination***

Meiotic recombination is essential in most organisms in generating crossovers that impart homologous chromosomes with a physical connection to assist their disjunction at the first meiotic division. Meiotic recombination is initiated by the formation of double-strand breaks (DSBs) in the DNA by the topoisomerase II-like protein Spo11 (Keeney et al., 1997). Spo11 attacks the phosphodiester backbone of DNA by a transesterase reaction between a tyrosine residue (Y135) and a 5' phosphate group on the DNA. This occurs simultaneously on both strands of the DNA duplex, the net result being two Spo11 monomers covalently bound to the two 5' ends of the DSB and two free 3' ends (Keeney et al., 1997). Although this role of Spo11 was first unravelled in budding yeast, orthologs have since been identified in fission yeast (Keeney et al., 1997; Lin and Smith, 1994), worms (Dernburg et al., 1998), flies (McKim and Hayashi-Hagihara, 1998), plants (Grelon et al., 2001) and mammals (Baudat et al., 2000; Romanienko and Camerini-Otero, 2000), suggesting that this mechanism of programmed DSB induction is highly conserved.

Also required for the formation of DSBs are a group of accessory proteins that regulate Spo11 activity. These include Rec102, Rec104, Rec114, Mei4, Mer2, Ski8, Mre11, Rad50 and Xrs2, which in turn, form four distinct sub-complexes that assist in Spo11-mediated DSB formation. The sub-complexes consist of Rec102-Rec104 (Jiao et al., 2003; Kee and Keeney, 2002; Kee et al., 2004), Rec114-Mei4-Mer2 (Li et al., 2006; Maleki et al., 2007), Ski8-Spo11 (Arora et al., 2004) and Mre11-Rad50-Xrs2 (Johzuka and Ogawa, 1995; Ohta et al., 1998). Although the precise mechanism for how these proteins assist Spo11 in DSB formation is unknown, there are clues as to how each sub-complex may act. For example, Ski8

is important for the association of Spo11 with chromatin suggesting that it may recruit or stabilise Spo11 on the chromatin (Arora et al., 2004). Furthermore, changes in chromatin structure are observed in mutants of the MRX complex suggesting that this complex may be important for changes in chromatin structure that accompany DSB formation (Ohta et al., 1998). The lack of co-localisation between Rec102 and Mer2 suggests that their respective sub-complexes may act at distinct regions on the chromatin (e.g. chromatin loops or axes), which may provide insight into their distinct functions (Li et al., 2006).

DSB formation is controlled by the same cell-cycle kinases that are responsible for initiation of DNA replication, namely CDK-S (Cdc28-Clb5) and DDK (Cdc7-Dbf4) (Hardy et al., 1997). CDK-S phosphorylates Mer2 on serine 30 and mutation of this serine to a non-phosphorylatable alanine residue abolishes DSB formation (Henderson et al., 2006). Mer2 is also phosphorylated by DDK on serine 29 and again, mutation of this residue to an alanine abolishes DSB formation (Wan et al., 2008). *In vitro* kinase assays revealed that DDK phosphorylation of S29 only occurs when S30 is phosphorylated (Wan et al., 2008). This suggests that CDK-S phosphorylation of S30 'primes' DDK-dependent phosphorylation of S29. Consistent with this, Mer2 phospho-shifts are completely abolished in the *mer2-S30A* mutant, but some residual Mer2 phosphorylation is observed in the *mer2-S29A* mutant (Wan et al., 2008). Mutation of S29 and S30 to aspartate, which mimics the negative charge conferred by a phosphate group, supports wild type-levels of DSBs (Wan et al., 2008). However, this only occurs in the presence of CDK-S and DDK, suggesting that these kinases have other roles in promoting DSB formation that are independent of S30 and S29 phosphorylation, respectively.

Nonetheless, the finding that the same kinases responsible for initiation of pre-meiotic DNA replication are important for DSB formation helps explain how these two processes are temporally closely linked (Borde et al., 2000).

The positioning of DSBs is non-random with particular regions of the genome experiencing higher frequencies of DSBs than others. Such regions are known as 'DSB hotspots' and have been well documented from yeast (Wu and Lichten, 1994) and mammals (Lichten and Goldman, 1995). In yeast, DSB hotspots tend to cluster in regions of high GC content and open chromatin such as inter-genic and gene promoter regions (Gerton et al., 2000). Consistent with this, certain histone modifications are enriched in regions of DSB hotspots, suggesting a mechanistic link between chromatin structure and DSB induction. A recent genome-wide mapping study of Histone H3 lysine 4 trimethylation (H3K4me3) revealed a positive correlation between H3K4me3 and increased DSB frequencies (Borde et al., 2008). This study demonstrated that this correlation was independent of transcription levels and therefore was not due to 'incidental' placement of DSBs in gene promoter regions. Thus, histone modifications that result in open chromatin configurations predispose such regions of the genome to experiencing high levels of meiotic DSBs.

This concept has developed further with the recent identification of DNA sequence motifs that control DNA hotspot distribution in mice, primates and humans (Baudat et al. 2010, ; Myers et al. 2010, ; Parvanov et al. 2010). These DNA sequences are recognised by the ring finger-containing protein encoded by the *PRDM9* gene. Crucially, this protein also has histone H3K4 trimethylation activity (Hayashi et al., 2005), suggesting that a DNA sequence motif directly

controls H3K4 trimethylation that 'opens' the chromatin and therefore makes that region more likely to experience a DSB. These studies are particularly interesting from the evolutionary perspective, as they can explain why humans and chimpanzees do not share the same DSB hotspots despite 99% DNA sequence conservation. This conundrum is solved by the revelation that the *PRDM9* gene is subject to rapid evolution, particularly in those amino acids comprising the RING finger that bind DNA. Consequently, the human and chimp *PRDM9* genes have undergone substantial divergence. This is matched by rapid co-evolution of the DNA sequence that the encoded protein recognises. Therefore, the sequences that correlate with DSB hotspots in humans are not the same as the sequences found in chimps (Hochwagen and Marais). These findings provide an explanation for how DSB hotspot distributions are controlled and why these distributions differ in closely related species.

Following DSB formation, Spo11 is removed from the DNA by an endonucleolytic release reaction that generates short oligonucleotides bound to Spo11 protein (Neale et al., 2005). Intriguingly, in budding yeast Spo11 is bound to oligonucleotides of two distinct sizes in seemingly equal abundance, suggesting that Spo11 may be cleaved asymmetrically at the DSB site (Neale et al., 2005). However, only a single Spo11-oligo species is present in mouse testis extracts (Neale et al., 2005), suggesting that asymmetric release is not a universal feature of Spo11 removal. Both the MRX complex and Sae2 protein are required for this endonucleolytic release step (Neale et al., 2005; Prinz et al., 1997; Tsubouchi and Ogawa, 1998; Usui et al., 1998). Separation-of-function alleles of Mre11 have revealed that the different domains of the protein are required for DSB formation

and processing, with mutations in the nuclease domain specifically influencing post-DSB processing, without affecting DSB formation (Tsubouchi and Ogawa, 1998; Usui et al., 1998). Sae2, which also has endonuclease activity (Lengsfeld et al., 2007), is also important for this step, suggesting that Sae2 may cooperate with the MRN complex to release Spo11-oligo complexes.

The next step in the repair pathway is the resection of 5' DNA ends to yield recombinogenic 3' overhangs. In budding yeast, the resection step is thought to be catalysed by the nuclease activity of Dna2 (in conjunction with Sgs1 helicase) and the 5' to 3' exonuclease activity of Exo1, whose roles have been studied extensively in DNA repair in mitotic cells (Mimitou and Symington, 2008). In meiotic cells, deletion of *EXO1* results in a decrease in the appearance of resected DNA ends, at least at the *HIS4:LEU2* hotspot (Tsubouchi and Ogawa, 2000). In a different study, a direct assay was used to detect the extent of resection at the *YCR048W* hotspot. This was done using restriction sites at regular intervals from a DSB site. Single-stranded resection of the DSB abolishes restriction sites and so larger restriction fragments are indicative of further resection (Manfrini et al.). This assay showed that resection occurred at similar levels to the wild type in *sgs1-mn* mutants, but resection was significantly reduced in *exo1Δ* (and *dna2Δ*) mutants. Curiously, a further decrease in resection was seen in the *exo1Δ sgs1-mn* double mutant, suggesting that Sgs1 is responsible for the residual resection observed in *exo1Δ* mutants (Manfrini et al.). This is very similar to the resection phenotypes reported for mitotic cells (Mimitou and Symington, 2008) and suggests that Sgs1-Dna2 act independently of Exo1 in meiotic DSB resection.

Single-stranded 3' overhangs generated by resection of the 5' ends become bound by Rad51 and Dmc1, orthologs of the bacterial RecA protein that form helical nucleofilaments with ssDNA (Bishop et al., 1992; Shinohara et al., 1997). Deletion of *RAD52* abolishes Rad51 foci formation and reduces the number of Dmc1 foci by two-fold (Lao et al., 2008). Whereas deletion of *MEI5* and *SAE3* virtually abolishes Dmc1 foci formation without affecting the numbers of Rad51 foci that form (Hayase et al., 2004). These findings suggest that loading of Rad51 and Dmc1 have distinct genetic requirements. Rad51/Dmc1 nucleofilaments catalyse homology searches with an intact DNA duplex (Shinohara et al., 1997). Whilst Rad51 functions in both mitotic and meiotic DNA repair (Shinohara et al., 1997; Shinohara and Ogawa, 1998), Dmc1 is expressed specifically in meiotic cells (Bishop et al., 1992). There is evidence to suggest that the two proteins play overlapping, but non-identical roles in meiotic recombination with both proteins required for wild type levels of meiotic recombination (Shinohara et al., 1997). Rad51 activity is attenuated by the meiosis-specific Hed1 protein that prevents excessive inter-sister recombination (Busygina et al., 2008). Dmc1 therefore predominates meiotic strand exchange ensuring high levels of inter-homolog rather than inter-sister recombination (Niu et al., 2009; Schwacha and Kleckner, 1997).

The 3' end then invades a homologous DNA duplex and carries out a search for homology (Figure 1.4). The Rad51-mediated strand invasion is catalysed by the recombinase Rad52 protein as shown by *in vitro* strand invasion assays (Shinohara and Ogawa, 1998). Rad52 has been suggested to do so by promoting strand annealing of complementary DNA sequences (Lao et al., 2008).

Figure 1.4.

The invading 3' end is then extended using the intact DNA duplex as a template resulting in the extrusion of a D-loop (Figure 1.4). Continued extension of the 3' end displaces more of the D-loop, which then anneals with the other 3' end of the break in a step referred to as 'second end capture' (Figure 1.4) that also requires the strand annealing function of Rad52 (Lao et al., 2008). The second 3' end can then be polymerised using the D-loop as a template and the two extended 3' ends are ligated to the resected 5' ends to form a double 'Holliday Junction' (Szostak et al., 1983). This model of DSB repair, first proposed by Szostak *et al.* (1983) originally proposed that non-crossover and crossover recombinants were derived by cleavage of the same strands or different strands of the double Holliday Junction (dHJ), respectively (Figure 1.4). However, subsequent research has revealed both temporal and genetic differences in crossover and non-crossover formation, suggesting that they may arise from separate pathways (Allers and Lichten, 2001). Molecular analyses showed that non-crossovers form without a stable single-end invasion (SEI) step, whilst stable SEIs and dHJs are specific precursors to the crossover-only pathway (Hunter and Kleckner, 2001). Moreover, mutations in a particular group of genes called the '*ZMM*'s (see below) reduce SEIs, dHJs and crossovers to a similar extent, whilst levels of non-crossovers are not compromised (Borner et al., 2004). Similarly, molecular analyses of recombination intermediates in *ndt80Δ* mutants that are arrested in pachytene revealed that non-crossover products form normally, whereas virtually no crossover products are detected (Allers and Lichten, 2001). Instead, dHJs accumulate in *ndt80Δ* mutants, making it likely that they are the precursors to crossovers that form following exit from pachytene (Allers and Lichten, 2001;

Sourirajan and Lichten, 2008). Indeed, expression of polo-like kinase (Cdc5) in *ndt80Δ* cells causes the disappearance of dHJs and the formation of crossovers, providing clear evidence that dHJs are the precursors to crossovers and that Cdc5 is sufficient for this transition (Sourirajan and Lichten, 2008).

These findings have led to an updated model of meiotic DSB repair (Figure 1.5) in which DSBs are designated to become crossovers or non-crossovers very early on, potentially prior to strand invasion, and the two pathways are temporally and genetically distinct. It is thought that non-crossovers are exclusively derived from the synthesis dependent strand-annealing (SDSA) pathway with only a transient SEI intermediate (Paques and Haber, 1999), whilst crossovers are derived from cleavage of opposing DNA strands of a dHJ (Allers and Lichten, 2001) (Figure 1.5).

The situation is made more complex in budding yeast by the existence of a third repair pathway that controls the formation of a distinct subset of crossovers (Figure 1.5). This pathway is dependent upon the Mus81-Mms4 endonuclease and does not involve a dHJ intermediate (de los Santos et al., 2003; de los Santos et al., 2001; Hollingsworth and Brill, 2004). As well as the mechanistic differences, this subset of crossovers are distinct to those arising from the aforementioned DSB repair pathway in that they are not subject to the phenomenon known as crossover interference. Crossover interference describes how a crossover at one position decreases the likelihood of a crossover occurring nearby on the same chromosome. This process ensures that crossovers are placed non-randomly and so are evenly spaced along the chromosome. The crossovers formed by the

Figure 1.5

Mus81-Mms4 pathway, however, do not display interference (de los Santos et al., 2003; Hollingsworth and Brill, 2004).

It is the ZMM-dependent crossovers that show an interference distribution in budding yeast (Borner et al., 2004). These crossovers are promoted by a group of proteins known collectively as the 'ZMM's. These include synaptonemal complex proteins Zip1, Zip2, Zip3, Zip4 and Spo16, the DNA helicase Mer3 and mismatch repair paralogs Msh4 and Msh5 (Borner et al., 2004; Shinohara et al., 2008). Mutation of any of the genes encoding these proteins results in a severe reduction of SEIs, dHJs and crossovers, whilst non-crossovers are largely unaffected. Two-dimensional gel electrophoresis revealed the defect to be at the SEI to dHJ transition in these mutants, leading to the suggestion that 'ZMM's stabilise these intermediates (Borner et al., 2004). Whilst synaptonemal complex proteins are thought to serve a structural role in this process, Msh4 and Msh5 directly stabilise recombination intermediates in the crossover pathway, supported by *in vitro* evidence that human Msh4-Msh5 heterodimers bind dHJs (Snowden et al., 2004). All 'ZMM' proteins cooperate to protect crossover intermediates from the anti-recombination activity of Sgs1 helicase (Jessop et al., 2006; Oh et al., 2007). Mismatch repair proteins, Mlh1 and Mlh3 form a heterodimer that functions downstream of Msh4-Msh5 in promoting crossovers arising from this pathway (Hunter and Borts, 1997; Wang et al., 1999). The final step in this pathway is cleavage of the double Holliday junction to yield crossover products. This may be catalysed by the recently discovered Holliday junction resolvase Yen1 (Gen1 in humans) (Ip et al., 2008). Although, there is no *in vivo* evidence to determine whether Yen1 resolves dHJs in budding yeast. These ZMM-dependent crossovers

(which comprise between 80-95% of crossovers in budding yeast, Borner *et al.* 2004) are subject to crossover interference that means the majority of crossovers are evenly spaced along chromosomes in *S. cerevisiae*. This may be conserved in mammals as *MUS81*<sup>-/-</sup> mice have a reduced testis size, less mature sperm are formed and a subset of DSBs that are not repaired (Holloway *et al.*, 2008). Despite this, *MUS81*<sup>-/-</sup> mice are fertile, suggesting that the MUS81 pathway plays a minor role in meiotic recombination as compared to the MSH4 pathway (*MSH4*<sup>-/-</sup> mice are infertile, Kneitz *et al.* 2000). Finally, there may exist a third pathway for crossover formation as, in budding yeast, some residual crossovers form in *mms4Δ msh5Δ* double mutants (de los Santos *et al.*, 2003).

Various models have been suggested for the mechanism(s) underlying crossover interference. These include the spread of an inhibitory signal outward from a newly formed crossover site by the synaptonemal complex (Egel, 1978) and more recently, the stress-release model, which posits that commitment to crossing over is imposed by torsional stress on the chromatin axes (Borner *et al.* 2004). Once a critical level of stress builds up, crossover-designation occurs that results in local relaxation of the axes in the immediate vicinity, meaning that another crossover will not occur nearby. This model currently lacks experimental evidence and so must only be considered theoretical at this stage.

Mus81-dependent crossovers have been proposed to be background noise from the 'mitotic' recombination pathway, which does not experience interference. *S. cerevisiae* is not the only organism that experiences non-interfering Mus81-dependent crossovers. In *S. pombe*, all crossovers derive from a Mus81-dependent pathway and no crossover interference exists in this organism,

suggesting that interference may be specific to the ZMM-dependent crossover pathway (Cromie et al., 2006). Consistent with this are findings in *Arabidopsis thaliana* in which the majority of crossovers are derived from an AtMSH4-dependent pathway, but the residual crossovers that form in *Atmsh4* mutants do not display interference (Franklin et al., 2006). These findings strongly suggest that crossover interference is confined to the ZMM-dependent class of crossovers.

Another feature of crossover formation is that of crossover assurance. This is the phenomenon of ensuring that each chromosome pair receives at least one crossover. The recent discovery of a new 'ZMM' member has revealed that crossover assurance and crossover interference can be genetically separated. Although the 'ZMM's were originally thought to act as a single functional unit with respect to promoting crossovers, a recent study has suggested that distinct sub-complexes operate within the 'ZMM' to control crossover interference and crossover assurance (Shinohara et al., 2008). This study characterises the new ZMM mutant, *spo16Δ* in which crossover interference is proficient. This correlates with proficient localisation of Msh4-Msh5 foci on meiotic chromosomes, implicating that focal formation of these proteins implements crossover interference (Shinohara et al., 2008). However, as with all *zmm* mutants, crossover assurance is abolished in *spo16Δ* mutants suggesting that assurance and interference may arise through distinct mechanisms.

Another phenomenon controlling crossover formation is the process of crossover homeostasis. This was first described in budding yeast with the identification of hypomorphic *spo11* alleles that experience decreased DSB formation (Martini et al., 2006). Despite decreasing numbers of DSBs, the number

of crossovers did not show a corresponding decrease and instead remained relatively stable at the expense of non-crossovers. Thus this may help explain why the number of DSBs (~200 per nucleus) greatly exceeds that of crossovers (~90 per nucleus). With a 'reserve pool' of non-crossovers, the cell can adjust the flux of DSBs entering the crossover pathway to ensure that a baseline level of crossovers are formed even if DSBs are compromised. This occurs down to a critical point, past which further reduction of DSBs results in a corresponding reduction of crossovers (Martini et al., 2006). It has been suggested that homeostasis is mechanistically linked to interference, as certain mutations tend to abolish both processes (Chen et al., 2008). It will be interesting to see how future research will shed light on the interplay between crossover assurance, interference and homeostasis and the underlying mechanisms that are responsible for each.

#### **1.1.4. Meiotic divisions**

##### ***1.1.4.1. Mono-orientation of sister chromatids at meiosis I***

The first meiotic division or 'reductional division' requires that homologous chromosomes, rather than sister chromatids attach to microtubules emanating from opposite spindle poles. This requires sister kinetochores to co-orient towards the same spindle pole, a configuration that is prohibited during meiosis II and mitosis in which sister kinetochores must be bi-oriented (Figure 1.6).

How is co-orientation of sister kinetochores achieved during the first meiotic division? It has been proposed that one of the sister kinetochores may be 'masked' and so only one of the pair is functional during meiosis I. Alternatively, sister

Figure 1.6

kinetochores may 'fuse' at meiosis I and so function as a single unit (Li and Dawe, 2009).

The first insight into the mechanism by which this process occurs came from the discovery of Mam1 in budding yeast (Toth et al., 2000). Mam1 was identified in a candidate-based screen for genes that, when mutated, result in meiotic chromosome missegregation. Mam1 co-localises with kinetochores throughout meiotic prophase until the onset of anaphase I. Mutants lacking *MAM1* fail to undergo the first meiotic division and instead undertake a single round of chromosome segregation on the meiosis II spindle in which sister kinetochores are segregated (Toth et al., 2000). The explanation for this phenotype is that in the absence of Mam1, sister kinetochores form a bipolar spindle attachment during meiosis I but cannot segregate owing to the protection of centromeric cohesin (Section 1.1.4.3). Instead, the diploid nucleus reattempts chromosome segregation at meiosis II and owing to the de-protection of centromeric cohesin, sister chromatids segregate away from each other. The net result is two diploid daughter cells (Toth et al., 2000). Therefore, Mam1 is clearly important for preventing sister kinetochore bi-orientation at meiosis I.

In addition to Mam1, other proteins have since been identified in assisting in co-orientation of sister kinetochores. Amongst these are Csm1 and Lrs4, which reside in the nucleolus throughout the cell cycle where they are involved in rDNA silencing (Rabitsch et al., 2003). However, they are released from the nucleolus in late meiotic prophase until metaphase I where they associate with centromeres. Csm1 and Lrs4 are mutually dependent on one another for their release from the nucleolus (Rabitsch et al., 2003). The phenotypes of either *csm1* $\Delta$  or *lrs4* $\Delta$  mutants

are indistinguishable from *mam1 $\Delta$*  mutants, which is consistent with all three proteins forming a complex that together assists in co-orientation of sister kinetochores at the first meiotic division (Rabitsch et al., 2003). Assembly of this monopolin complex is controlled by the cell cycle kinase DDK, which is also important for pre-meiotic DNA replication and DSB formation. In the absence of post-replicative Cdc7 activity Mam1 foci fail to form, which may be due to reduced phosphorylation of Lrs4 (Matos et al., 2008). In this way, DDK coordinates many important meiotic events, such as pre-meiotic DNA replication, DSB formation and control of the reductional meiotic division.

Another protein important for co-orientation of sister kinetochores at meiosis I is Spo13. Spo13 is required for the centromeric localisation of Mam1 during late meiotic prophase (Katis et al., 2004). Spo13 is also involved in the protection of centromeric cohesin at meiosis I (Klein et al., 1999; Shonn et al., 2002). Similarly, polo-like kinase (Cdc5) is also required for localisation of Lrs4 and Mam1 to centromeres (Clyne et al., 2003). Furthermore, Lrs4 phosphorylation is reduced to similar extents in *cdc5-mn* and *spo13 $\Delta$*  mutants (Katis et al., 2004). Therefore, it is possible that Spo13 and Cdc5 cooperate in Lrs4 phosphorylation that regulates the assembly of monopolin complexes at the centromeres. DDK is also thought to collaborate with Cdc5 to ensure hyper-phosphorylation of Lrs4 (Matos et al., 2008). The overlapping functions of multiple kinases are a recurring theme in meiosis (see sections 1.1.2. and 1.1.3.3), probably helping to ensure the coordination of major landmark events in the meiotic program.

Finally, casein kinase 1 (Hrr25 in *S. cerevisiae*) was the most recent member of the monopolin complex to be identified (Petronczki et al., 2006). It binds with high affinity to Mam1, thus forming a quaternary complex comprising Csm1, Lrs4, Mam1 and Hrr25. Two residues on the surface of Hrr25 are necessary for interaction with Mam1, which is crucial for the latter's localisation to centromeres (Petronczki et al., 2006). In addition, the kinase activity of Hrr25 is also important for mono-orientation of sister kinetochores as evidenced by the mono-orientation phenotype that results from inhibiting the kinase activity of Hrr25 (using a *hrr25-as* allele). Targets of Hrr25 may include Rec8 and Mam1, but whether these are the targets that are responsible for mono-orientation is unclear (Petronczki et al., 2006). Finally, casein kinases are highly conserved proteins and so it is possible that their roles in mono-orientation of sister kinetochores at meiosis I are conserved in higher organisms.

Curiously, orthologs of most of the monopolin proteins identified in *S. cerevisiae* have not been identified in other organisms. Although a putative ortholog of Csm1 exists in *S. pombe* (Pcs1), its function is confined to mitosis where it 'clamps' together microtubule sites within the same kinetochore, thus preventing merotelic spindle attachments (Rabitsch et al., 2003). This suggests that different mechanisms are responsible for mono-orientation of sister kinetochores at meiosis I in these organisms. Indeed, in fission yeast, Rec8-mediated cohesin at the core centromeres together with Moa1 have been shown to underpin mono-orientation of sister kinetochores at meiosis I, whereas cohesion at the peri-centromeric regions is important for sister kinetochore bi-orientation at meiosis II and mitosis (Sakuno et al., 2009; Sakuno and Watanabe, 2009). In

contrast, cohesin does not appear to play an active role in mono-orientation of sister kinetochores in budding yeast as replacement of *REC8* for the *SCC1* gene results in a reductional division with two sister chromatids (marked by URA3-GFP) frequently segregating to the same daughter cell (Toth et al., 2000).

Although the underlying mechanisms are clearly distinct in budding and fission yeasts, Aurora B kinase is involved either directly or indirectly in both yeast species (Hauf et al., 2007; Monje-Casas et al., 2007). In Maize meiosis, the kinetochore protein Mis12 together with the Ndc80 complex fuses sister kinetochores so they attach to microtubules emanating from the same spindle pole. Knock-down of Mis12 results in increased equational sister chromatid segregation at meiosis I and lagging chromosomes during anaphase due to merotelic spindle attachments (Li and Dawe, 2009). In mammals, the lateral element proteins SYCP2 and SYCP3, together with the mitotic cohesin protein RAD21, have been suggested to constrain sister kinetochores to adopt a mono-polar orientation on meiosis I spindles (Parra et al., 2004).

Taken together, these observations suggest that the mechanisms in place to ensure mono-orientation of sister kinetochores at meiosis I differ vastly between organisms. It is possible that these diverse mechanisms arose as a result of the differences in centromere size and kinetochore structure between species that meant a single, conserved mechanism was not suitable. For example, budding yeast have a simple, 'point centromere' comprising a 120 bp core centromere and no flanking heterochromatin. In contrast, fission yeast centromeres are, on average, 70 kb comprising a central core flanked by inner- and outer-most repeats that form heterochromatin. In humans, centromeres are on average 3 Mb in size

consisting of heterochromatin containing tandem alpha-satellite repeats (Brar and Amon, 2008). Furthermore, budding yeast kinetochores attach to a single microtubule (Winey et al., 1995), whereas in fission yeast and higher eukaryotes, several microtubule-binding sites exist within a single kinetochore (Ding et al., 1993). It is therefore likely that as centromeres and kinetochores became increasingly complex during the course of evolution, they were accompanied by changes in the mechanism for ensuring mono-orientation of sister kinetochores during meiosis I. Therefore, a common ancestral mechanism may have been phased out by the species-specific mechanisms we observe today.

#### ***1.1.4.2. The Spindle Checkpoint and the Onset of Anaphase.***

The spindle checkpoint is a highly conserved group of proteins that together, delay the onset of anaphase until all chromosomes are correctly aligned on the metaphase spindle. The spindle checkpoint was first discovered in budding yeast with the identification of Mad1, Mad2, Mad3, Bub1 and Bub3 (Hoyt et al., 1991; Li and Murray, 1991). Many homologs of these proteins have since been identified in flies (Buffin et al., 2007), worms (Kitagawa and Rose, 1999) and humans (Li and Benezra, 1996), suggesting that the spindle checkpoint is a highly conserved mechanism that underpins the fidelity of chromosome segregation in many organisms. Although originally discovered in mitotic cells (Li and Murray, 1991), the spindle checkpoint also operates during meiotic divisions. In fact, the first meiotic division relies more heavily upon the spindle checkpoint than mitotic or the second meiotic divisions do. This is based on the observations that spindle checkpoint mutants do not have much of a phenotype in an unperturbed mitotic cell cycle (i.e.

in the absence of microtubule de-polymerising drugs), but they experience elevated chromosome missegregation at the first meiotic division during an otherwise wild-type meiosis (Shonn et al., 2000). This is likely to be due to the fact that homologous chromosomes, rather than sister chromatids are the segregating partners during meiosis I. Owing to the fact that homologous chromosomes are held together by the cohesin distal to chiasmata (Figure 1.6 A), it is likely that the kinetochores belonging to each chromosome are allowed rotational freedom with respect to each other and so are not constrained to adopt a bipolar spindle attachment in the same way that sister kinetochores are.

The precursor to faithful chromosome segregation is the correct orientation of kinetochores upon the metaphase spindle. In the case of meiosis I, homologous chromosomes must be positioned so that both sister kinetochores face in one direction whilst the sister kinetochores of the other homologous chromosome face in the other direction (this requires co-orientation of sister kinetochores, see Section 1.1.4.1). This configuration is referred to as 'homolog bi-orientation' and once achieved results in spindle tension. This is owing to the opposing pulling forces of the spindle, antagonised by the sister chromatid cohesin distal to the crossover site that connects homologous chromosomes together (Maguire, 1995) (Figure 1.7). This tension inactivates the spindle checkpoint, which consequently triggers the onset of anaphase.

Chromosomes often require several attempts to attain a bipolar orientation. This is achieved through severing of kinetochore – microtubule attachments in the absence of spindle tension and implementation of a delay while the chromosomes reattempt a bipolar spindle attachment. Spindle tension is monitored by a group of

Figure 1.7

proteins known as the chromosomal passenger proteins. These proteins consist of INCENP, Survivin, Borealin, and Aurora B kinase (Ruchaud et al., 2007). The ability of these proteins to activate the spindle checkpoint depends upon Aurora B kinase activity (Tanaka et al., 2002). In the absence of spindle tension, such as when kinetochores of each segregating partner are attached to microtubules emanating from the same spindle pole, Aurora B kinase phosphorylates the kinetochore protein, Dam1 (Cheeseman et al., 2002) as well as the spindle checkpoint protein, Mad3 (King et al., 2007). Phosphorylation of Dam1 causes release of kinetochore – microtubule attachments. These unattached kinetochores activate the spindle checkpoint (Pinsky et al., 2006), which orchestrate a corresponding delay of anaphase onset. Aurora B kinase also directly activates the spindle checkpoint by phosphorylation of Mad3 (King et al., 2007) (Figure 1.8). How might the chromosomal passenger complex sense and respond to spindle tension? Current models suggest that spindle tension results in a conformational change to the complex that attenuates Aurora B kinase activity, either by inactivation or by spatial separation of Aurora B kinase from its substrates (Kelly and Funabiki, 2009).

In addition to the chromosomal passenger complex, a second kinase has been identified in meiotic cells that fulfills a similar function to Aurora B kinase (Straight et al., 2000). The activity of this kinase, called Mps1, is also modulated by spindle tension (Maure et al., 2007), which activates or silences the spindle checkpoint accordingly. Mps1 phosphorylates the kinetochore protein Dam1 on six serine residues *in vitro*, but these are not the same sites phosphorylated by

Figure 1.8

Ipl1/Aurora B kinase (Cheeseman et al., 2002; Shimogawa et al., 2006).

Furthermore, the functional importance of these phosphorylation events is less clear than for Ipl1-mediated phosphorylation of Dam1. Mutation of two of these six serine residues (S218 and S221) abolishes the ability of kinetochores to bind to the plus-ends of microtubules. Despite this, cells are viable and chromosome bi-orientation is achieved with normal kinetics (Shimogawa et al., 2006). Of more functional importance is the phosphorylation of the kinetochore protein Ndc80 by Mps1. Mutation of 14 serine residues to alanine in Ndc80 (*ndc80-14A*) abolishes spindle checkpoint activation, and the phospho-mimetic Ndc80 mutant results in constitutive activation of the spindle checkpoint (Kemmler et al., 2009). Moreover, this activation is not due to unattached kinetochores as *ndc80-14D* mutants arrest with kinetochores attached to the microtubules in a bipolar configuration. These findings suggest that Mps1-mediated phosphorylation of Ndc80 directly activates the spindle checkpoint. Despite their highly similar cellular functions, Mps1 and Ipl1 do not appear to regulate each other as their localisation and respective *in vitro* kinase activities were normal when the opposing kinase was mutated (Maure et al., 2007). This reveals that at least two kinases control spindle checkpoint activation in budding yeast.

In addition to their roles in correcting aberrant spindle attachments, Ipl1/Aurora B kinase and Mps1 have additional meiotic functions. For example, Aurora B kinase is required for maintenance of centromeric cohesin (Resnick et al., 2006; Yu and Koshland, 2007), microtubule dynamics and for synaptonemal complex disassembly (Jordan et al., 2009). In contrast, Mps1 is involved in spindle pole body duplication and spore formation (Straight et al., 2000).

In order to explain how the spindle checkpoint mediates a metaphase delay, it is necessary to first outline the mechanism that underpins the onset of anaphase. Regardless of whether homologous chromosomes (meiosis I) or sister chromatids (mitosis and meiosis II) are the segregating partners during anaphase, the principle underlying their segregation is the same. In order for their partitioning to opposite spindle poles, the physical connections holding them together must be removed. Sister chromatids are held together along their lengths by cohesin and homologous chromosomes are held together by sister chromatid cohesin distal to the crossover site (Klein et al., 1999). Therefore, instrumental to their segregation at the onset of anaphase is removal of cohesin. This is achieved by an enzyme known as separase (Esp1 in *S. cerevisiae*) that cleaves the kleisin subunit of cohesin, Scc1 in mitotic cells (Ciosk et al., 1998; Uhlmann et al., 2000) and Rec8 in meiotic cells (Buonomo et al., 2000). This breaks the cohesin 'ring' and thus liberates sister chromatids from one another. Separase is kept inactive until commitment to anaphase by binding of securin (Pds1 in yeast) which blocks separase activity (Ciosk et al., 1998; Tinker-Kulberg and Morgan, 1999). Anaphase is triggered by activation of the anaphase-promoting complex (APC), an E3 ubiquitin ligase that targets securin (Pds1) for degradation by the 26S proteasome (Cohen-Fix et al., 1996; Zachariae and Nasmyth, 1999). The resulting separase activity allows the dissolution of sister chromatid cohesin and thus relieves the antagonism to the pole-ward forces of the spindle. This allows segregation of chromosomes or chromatids to opposite spindle poles.

The spindle checkpoint delays the onset of anaphase by tight regulation of APC activation. Mad2 forms a complex at the kinetochores with the APC activator,

Cdc20. As long as Cdc20 is bound to Mad2, it cannot activate the APC (Nasmyth, 2005). Mad1 binds Mad2 at kinetochores (Chen et al., 1999), which is thought to recruit another Mad2 molecule through the ability of Mad2 to dimerise (Mapelli et al., 2006). It has been suggested that this second Mad2 molecule adopts an “open” configuration that after Cdc20 binding becomes “closed” (Mapelli et al., 2006; Nezi et al., 2006). It is less clear how the other spindle checkpoint proteins (Mad3, Bub1 and Bub3) cooperate in this process, but it is thought that they help stabilise the Mad1-Mad2-Cdc20 protein complex as they have been shown to interact biochemically with these proteins as well as each other (Hardwick et al., 2000; Hwang et al., 1998).

In the absence of kinetochore-microtubule tension, as sensed by the chromosomal passenger proteins and Mps1, the spindle checkpoint is active and sequesters Cdc20 at kinetochores, away from the APC. Once bi-orientation is achieved and spindle tension is formed, the spindle checkpoint is silenced, leading to the liberation of Cdc20, which together with the APC triggers anaphase (Figure 1.8). A curious feature of this mode of regulation is how a single mal-oriented chromosome is sufficient to delay segregation of all the other correctly oriented chromosomes (reviewed by Nasmyth 2005). The most likely explanation for this is that Cdc20 is not liberated from any of the kinetochores until all are correctly oriented, rather than on a chromosome-by-chromosome basis.

Although much of the insight into the spindle checkpoint has been uncovered in lower eukaryotes and in mitotic cells, there is now a growing body of evidence that suggests the same mechanism is responsible for meiotic chromosome segregation in mammals. In fact, mammalian cells may be even more

dependent on spindle checkp In *rec8Δ* mutants, homolog pairing is reduced, no SC formation occurs and DSBs are not repaired (Klein et al., 1999). However, as previously mentioned sister chromatids are not required for homolog pairing, DSB repair and SC formation as these processes occur normally in *cdc6-mn* mutants that fail to replicate their DNA (Brar et al., 2008; Hochwagen et al., 2005). This suggests that Rec8 plays a direct role in these processes that is independent from its role in sister chromatid cohesion.

The ring-like structure, 40 nm in diameter formed by the cohesin complex has led to the suggestion that cohesin 'entraps' two newly replicated sister chromatids which is retained until the cleavage of the kleisin subunit at anaphase (Haering et al., 2002) (Figure 1.2, Model 1). Support for a model whereby cohesin rings 'entrap' sister chromatids comes from work using circular mini-chromosomes. Linearization of the chromosomes with a restriction enzyme resulted in decreased association of the cohesin complex with the DNA whereas histone proteins remained bound to the DNA (Ivanov and Nasmyth, 2005). This was interpreted to be because the cohesin rings could slide off the ends of the linearized DNA. However, other models have since been suggested for how the cohesin complex mediates sister chromatid cohesion that could also explain the above findings (reviewed in Guacci 2007). An alternative model was suggested whereby cohesin complexes encircle individual chromatids and interact with each other thus 'tethering' sister chromatids together (Figure 1.2, Model 2). This model is based on work into the association of cohesin with silent chromatin domains, such as the *HMR* mating locus. Recombinase sites flanking the *HMR* locus allowed excision by a site-specific recombinase and *LacO/LacI*-GFP allowed the excised HMR circles

ooint activity owing to the fact that their kinetochores contain multiple microtubule binding sites (as opposed to a single site in budding yeast, Winey et al 1995), which may predispose them to making aberrant spindle attachments. Evidence that the spindle checkpoint operates in the same way in mammalian meiosis includes the work showing that separase-mediated cleavage of Rec8 operates in mouse oocytes (Kudo et al., 2009; Kudo et al., 2006). Furthermore, homologs of spindle checkpoint proteins have also been shown to play conserved roles in mammals. For example, depletion of Bub1 in mouse oocytes results in premature APC activation with incorrectly oriented chromosomes (McGuinness et al., 2009). Similar defects are observed when Mad2 was depleted in mouse oocytes (Homer et al., 2005). Conversely, anaphase onset is inhibited in oocytes over-expressing Mad2, which means that an excess of Mad2 must be capable of binding sufficient Cdc20 to prevent anaphase onset (Homer et al., 2005; Wassmann et al., 2003).

There now exists an abundance of evidence that suggests the spindle checkpoint is active in mammalian meiosis, however there was one study that called this view into question. This was the lack of any detectable delay to anaphase in mouse oocytes containing a univalent X chromosome. This was despite the absence of a partner chromosome and a failure of the univalent to align properly during metaphase I (LeMaire-Adkins et al., 1997). This may be reconciled by the finding that univalent chromosomes in *sycp3*<sup>-/-</sup> mice can evade the spindle checkpoint by segregating equationally at meiosis I (Kouznetsova et al., 2007).

The existence of the spindle checkpoint operating in mammalian meiosis has led to the suggestion that a less efficient spindle checkpoint may account for the age-related increase in aneuploidy observed in human females (Hassold and

Hunt, 2001; Mailhes, 2008). This model posits that age-related aneuploidy may be explained by “two hits”. The “first hit” is a chromosome pair with an error-prone crossover configuration such as having a crossover far from the centromere (or no crossover at all). This is age-independent and the model suggests that in young oocytes these error-prone chromosomes are segregated by an efficient spindle checkpoint. However, the “second hit” comes from dilapidation over time of the spindle checkpoint operating in oocytes. Therefore, the segregation of the error-prone chromosome pair cannot be corrected by the spindle checkpoint in these ageing oocytes and they subsequently missegregate at the first meiotic division (Hassold and Hunt, 2001). There are several lines of evidence that support such a model. For example, transcripts of the *MAD2* and *BUB1* genes are found to decrease in oocytes with increasing maternal age (Steuerwald et al., 2001). However, it is possible that this does not reflect a change in protein levels. Crossover mapping of non-disjoining chromosome 21 pairs in humans has revealed that they frequently contained distally-located crossovers (or no crossover at all) that pose the “first hit” to age-related non-disjunction (Lamb et al., 1996). Finally, there appears to exist some level of sexual dimorphism in spindle checkpoint surveillance in humans, with males appearing to exert a more stringent checkpoint than females (Hunt and Hassold, 2002). This may explain the higher incidence of maternally derived trisomies (Hassold and Hunt, 2001).

Finally, discussion of the spindle checkpoint during meiosis would not be complete without brief outline of the additional meiotic roles of spindle checkpoint proteins. For example, in addition to Mad2’s role in sequestering Cdc20 until chromosomes are correctly oriented on the meiotic spindle, Mad2 may also play a

role in promoting homolog bi-orientation that is independent from its canonical spindle checkpoint role (Shonn et al., 2003). Mad3 also has roles that are distinct from its role in the spindle checkpoint that operates at metaphase I. For example, in *S. cerevisiae* Mad3 has been shown to have a distinct role in mediating a prophase I delay during every meiosis that specifically assists in the segregation of non-exchange chromosomes (Cheslock et al., 2005). Moreover, this seems to be conserved in mammals in which the mammalian Mad3 homolog BubR1 is required for maintaining a prophase I arrest in developing mouse oocytes (Homer et al., 2009). This study also highlighted roles for BubR1 in completion of anaphase by limiting the abundance of securin and in establishing kinetochore-microtubule attachments. Thus it seems that spindle checkpoint proteins are central to many meiotic processes that are directly applicable to human fertility.

#### **1.1.4.3. Protection of centromeric cohesin during meiosis**

Homologous chromosomes are held together by sister chromatid cohesin distal to the crossover site (Figure 1.7 B). In order for disjunction of homologous chromosomes at the first meiotic division this cohesin must be removed. However, removal of sister chromatid cohesin along the entire length of the chromosomes at anaphase I would result in precocious sister chromatid separation. With no physical connection between sister chromatids, they would be doomed to segregate at random during meiosis II. Luckily, this conundrum is solved by a elegant mechanism that results in the step-wise loss of cohesin during meiosis. Cohesin is removed specifically from the chromosome arms during meiosis I, but is retained at the centromeres until meiosis II. This allows the removal of physical

connections between homologous chromosomes at meiosis I, whilst retaining cohesion between sister chromatids until their segregation at anaphase II.

The factor responsible for protection of centromeric cohesin at meiosis I has been identified and named 'Shugoshin'. Shugoshin (or Sgo1) was originally identified in genome-wide screens carried out in budding and fission yeasts for mutants that cannot maintain centromeric cohesion at the first meiotic division (Kitajima et al., 2004; Marston et al., 2004). In budding yeast, additional proteins identified in this screen included the kinetochore proteins Chl4 and Iml3, which were shown to act in the same pathway for protecting centromeric cohesin (Marston et al., 2004). Sgo1 localises with the centromere marker Ndc10 throughout meiosis until anaphase II, which is also the point that centromeric Rec8 signal disappears (Klein et al., 1999). This is consistent with Sgo1 playing a role in maintaining cohesin until this stage. The spindle checkpoint protein Bub1 is required for Sgo1's localisation to kinetochores (Kiburz et al., 2005; Kitajima et al., 2004) and a paralogue of shugoshin (Sgo2) exists in fission yeast that is important for mitotic chromosome segregation (Kitajima et al., 2004).

What is the mechanism by which Sgo1 protects centromeric cohesin during the first meiotic division? Fundamental to the separation of homologous chromosomes during anaphase I is the resolution of chiasmata at anaphase I. This is achieved by separase-mediated cleavage of Rec8, at two sites that removes cohesins from chromosome arms (Buonomo et al., 2000). It was previously thought that phosphorylation of Rec8 by the polo-like kinase, Cdc5 facilitated Rec8 cleavage by separase at anaphase I (Brar et al., 2006; Lee and Amon, 2003). This probably stemmed from the observation that Cdc5 is required for removal of a

subset of cohesin complexes that occurs prior to anaphase I in the so-called 'prophase pathway' of cohesin removal (Yu and Koshland, 2005). However, when all putative Cdc5 phosphorylation sites were mutated in Rec8 (*rec8-17A*), cleavage of Rec8 still occurred but with a delay owing to a delay in cells entering anaphase I (Brar et al., 2006). However, there exists evidence for Cdc5-independent Rec8 phosphorylation at chromosome arm regions that correlates with loss of cohesin at anaphase I (Brar et al., 2008). Furthermore, substantial Rec8 phosphorylation is observed in *cdc5-meiotic null* mutants (Lee and Amon, 2003). These findings may now be explained by the finding that Rec8 is also phosphorylated by casein kinase (Hrr25) and DDK (Cdc7-Dbf4) (Katis et al.). This study showed that phosphorylation of Rec8 by these two kinases, but not Cdc5, is essential for Rec8 cleavage *in vitro* and *in vivo*. Mutation of the 24 phosphorylated Rec8 residues identified in this study to non-phosphorylatable alanine residues completely abolished *in vivo* Rec8 cleavage (Katis et al.). Furthermore, in the phosphomimetic mutant (*rec8-14D*) no Rec8 was detectable in metaphase II cells consistent with the interpretation that all Rec8 is cleaved during anaphase I in this mutant (Katis et al.). These findings show that Rec8 phosphorylation by casein kinase and DDK is essential for its cleavage at anaphase I.

Shugoshin protects centromeric Rec8 by recruiting the phosphatase, PP2A through direct interaction with its regulatory subunit Rts1 (Kitajima et al., 2006; Riedel et al., 2006). De-phosphorylation of Rec8 by PP2A renders it refractive to separase-mediated cleavage in both yeast and humans (Kitajima et al., 2006; Riedel et al., 2006). In budding yeast, this region of cohesin protection spans 50kb of the centromere (Kiburz et al., 2005). Although Bub1 is required for the initial

recruitment of Sgo1, which subsequently recruits PP2A, Ipl1/Aurora B is required for the maintenance of PP2A at centromeres beyond anaphase I (Yu and Koshland, 2007). This is likely to be conserved as Aurora B kinase and INCENP are required for centromeric localisation of Shugoshin (MEI-S332) in *Drosophila* (Resnick et al., 2006).

In addition to recruiting PP2A, recent work has uncovered an additional role for Sgo1 in preventing Rec8 cleavage in the vicinity of centromeres. This stemmed from the observation in budding yeast that depletion of *SGO1* restored timely cleavage of Rec8-17A, which could not be phosphorylated by Cdc5 (Brar et al., 2006). This finding suggested that Sgo1 is capable of preventing Rec8 cleavage independently of modulating the phosphorylation status of Rec8. Moreover, in budding yeast, deletion of *PDS1* (securin) still leads to the timely segregation of chromatids in mitotic cells, suggesting that other mechanisms exist to confine separase activity to the correct window of the cell cycle. Indeed, subsequent work has elucidated a second role for Sgo1 in inhibition of separase activity (Clift et al., 2009). This work showed that over-expression of Sgo1 in vegetative cells arrested cells in metaphase with no cleavage of the mitotic counterpart, Scc1. This was dependent on the mitotic PP2A regulatory subunit, Cdc55. This work went on to show that un-phosphorylated Rec8 (in cells depleted for *CDC5*) could be cleaved when *SGO1* or *CDC55* were depleted (Clift et al., 2009). Therefore, in the absence of the inhibitory activities of Sgo1-Cdc55, separase is able to cleave Rec8 even in the absence of the 'priming' phosphorylation events. This suggests that Sgo1-Cdc55 directly inhibits separase activity in a manner that is independent of Rec8 phosphorylation.

In addition to the dual roles of Shugoshin in protecting centromeric cohesin during meiosis I, inter-homolog recombination has also been shown to play an important role in the step-wise loss of cohesin during meiosis (Brar et al., 2006). This is based on the intriguing observation that deletion of *SPO11* restores the timely cleavage of non-phosphorylatable Rec8 (*rec8-17A*) as well as increasing sister chromatid disjunction during meiosis II in cells depleted for *SGO1* (Brar et al., 2006; Clift et al., 2009). The explanation for these observations is that in the absence of crossovers between homologous chromosomes but mono-orientation of sister kinetochores, spindle tension cannot be achieved. Therefore, the spindle checkpoint is active, which keeps separase in an inactive state. However, owing to the absence of any inter-homolog connections to antagonise the pulling forces of the meiotic spindle, the achiasmate chromosomes segregate (at random) in the presence of an active spindle checkpoint. As separase is kept inactive, cohesin is retained along the lengths of chromosomes where it stays until anaphase II, promoting the disjunction of sister chromatids. Inactivation of the spindle checkpoint (by deletion of *Mad2*) randomises sister chromatid segregation at meiosis II, presumably due to complete cohesin removal at anaphase I (Brar et al., 2006). This suggests that the spindle checkpoint is responsible for retention of cohesin in *spo11Δ SGO1*-depleted cells.

There exists mounting evidence that this mechanism of ensuring the stepwise loss of cohesins during meiosis is conserved in mammals. For example, Rec8 from mice is hyper-phosphorylated and this phosphorylation precedes its cleavage by separase *in vitro*. Expression of a non-cleavable variant of Rec8

(Rec8-N) causes sterility in male mice due to a failure to complete either nuclear division during spermatogenesis (Kudo et al., 2009). These observations, together with the evidence that shugoshin together with PP2A play conserved molecular functions in HeLa cells (Kitajima et al., 2006) and mouse oocytes (Lee et al., 2008), suggests that the mechanism is widely conserved from yeast to mammals.

Although a lot of the original work into the role of Shugoshin in protection of centromeric cohesin has been carried out in yeast, a recent study using a combination of HeLa cells and mouse oocytes has provided new insight into the mechanism by which this process occurs (Lee et al., 2008). The elegant cytology performed in this work revealed that during metaphase II and mitotic metaphase, shugoshin proteins relocate from the inner centromeres towards the kinetochores. This renders the cohesin present at the inner centromeres de-protected and thus cleavable by separase. This relocation of shugoshin proteins to the outer kinetochore is dependent upon tension between the sister chromatids. Therefore, during the first meiotic division when no tension exists between sister chromatids, shugoshin remains at its inner centromere location where it protects Rec8 from separase cleavage. Then during the second meiotic division when sister chromatids come under tension, shugoshin is displaced from the inner centromere and Rec8 is subsequently free to be cleaved by separase. This study not only confirms the highly conserved requirement for shugoshin in the stepwise loss of cohesin during meiosis, but also provides novel insight into how this process works. However, one problem with applying this mechanism to yeast is the observation that in *mam1* $\Delta$  mutants, sister chromatids bi-orient at the first meiotic

division. Despite this inter-sister tension, however, centromeric cohesin cannot be cleaved and the nuclear division is therefore aborted (Toth et al., 2000). This suggests that tension between sister chromatids is not sufficient to de-protect centromeric cohesin in yeast cells. It is therefore possible that different mechanisms exist in yeast and mammals.

## 1.2. The Synaptonemal Complex

### 1.2.1. The Architecture of the Synaptonemal Complex

The Synaptonemal Complex (SC) is a proteinaceous structure that connects homologous chromosomes lengthwise during meiotic prophase. The SC consists of two parallel axial elements that become connected by the deposition of transverse proteins that form the central element between adjacent axes (Figure 1.9). The SC is a structurally conserved protein complex found in organisms as diverse as yeast, worms, flies and mammals where it assists in homolog alignment, inter-homolog recombination and in some organisms, chromosome segregation. In this section, the proteins comprising the synaptonemal complex in different organisms are described with particular emphasis on the structural conservation of these proteins between organisms. Although the transverse filament proteins that make up the central element of the SC show weak conservation of amino acid sequences, they are all characterised by an  $\alpha$ -helical coiled-coil domain that is central to their structure (Page and Hawley, 2004). The central element proteins should therefore be thought of as 'functional orthologs' rather than *bona fide* orthologs.

#### 1.2.1.1. The Structure of the Synaptonemal Complex in Yeast

In *Saccharomyces cerevisiae*, a single protein comprises the central element named Zip1 (Sym et al., 1993). Zip1 consists of 875 amino acids and contains a central coiled-coil domain flanked by C- and N-terminal globular domains (Tung and Roeder, 1998). Electron micrographs and protein

Figure 1.9

fractionation has revealed that Zip1 dimerises through its coiled-coil domain uniting two C-termini at one end and N-termini at the other. These dimers are arranged in a head-to-head configuration with the C-termini contacting the lateral elements and the N-termini facing inwards forming the electron-dense central element between aligned axes (Dong and Roeder, 2000) (Figure 1.10). Electron micrographs reveal the space between aligned lateral elements to be ~110 nm, consistent with two Zip1 dimers, each ~60 nm in length, lying in a head-to-head configuration (Dong and Roeder, 2000). In-frame deletions within the coiled-coil domain of Zip1 result in corresponding decreases in the width of the SC (Tung and Roeder, 1998). Similarly, a mutation that extends the length of the coiled-coil region of Zip1 (*zip1-3XH2*) extends the width of the SC by 1.7-fold (Dong and Roeder, 2000). These results are consistent with Zip1 spanning the gap between adjacent lateral elements. Zip1 connects homologous chromosomes along their lengths in an end-to-end fashion during mid-pachytene, culminating in the appearance of clear 'lines' of Zip1 in surface-spread pachytene nuclei (Sym et al., 1993).

The lateral elements consist of an assortment of different proteins in budding yeast. These include Red1 and Hop1, which together with the meiosis-specific Rad53 homolog Mek1 are well known for their roles in biasing DSB repair toward homologous chromosomes rather than sister chromatids (Carballo et al., 2008; Lin et al., 2009; Niu et al., 2007; Schwacha and Kleckner, 1997). Mutants deleted for *RED1* or *HOP1* experience severely defective chromosome synapsis with only very few short stretches of densely staining synaptonemal complexes present in electron micrographs of pachytene nuclei (Woltering et al., 2000).

Figure 1.10

Red1 and Hop1 co-localise with Zip1 in zygotene nuclei, although the staining pattern does not reveal the continuous lines characteristic of Zip1 staining. Rather, Red1 and Hop1 are characterised by punctuate staining patterns that co-localise with the 'lines' of Zip1 present on meiotic chromosomes (Smith and Roeder 1997). The staining pattern of Hop1, however, becomes less continuous than Red1 during pachytene (Smith and Roeder, 1997). Hop1 and Red1 physically interact in meiotic cell extracts (Woltering et al., 2000). This interaction is abolished when the lysine present at position 348 in Red1 is mutated to glutamate. The *red1-K348E* mutant experiences severely reduced synapsis, suggesting that the Red1-Hop1 interaction is important for formation of the synaptonemal complex (Woltering et al., 2000). Yeast two-hybrid experiments show that Red1 and Zip1 physically interact, suggesting that Red1 is the binding partner for Zip1 (Cheng et al., 2006).

There is also evidence that Zip1 binds Smt3<sup>SUMO</sup> both in yeast two-hybrid assays and *in vitro* binding assays (Cheng et al., 2006). Zip1 contains a putative SUMO binding motif in its C-terminus that when deleted, abolishes SC formation (Cheng et al., 2006). This suggests that the ability of Zip1 to bind Smt3<sup>SUMO</sup> may be of functional importance for the formation of the SC. On the other hand, it may be that mutation of these hydrophobic residues disrupts the folding of the entire C-terminus, which would obviously have severe consequences for SC formation. Smt3<sup>SUMO</sup> and Zip1 show near-perfect co-localisation during both zygotene and pachytene and are inter-dependent for their localisation to meiotic chromosomes as shown by defective SUMO staining in a *zip1Δ* mutant and delayed and incomplete Zip1 staining in a *ubc9-t* mutant (Hooker and Roeder, 2006). This suggests that sumoylation is central to the polymerisation of Zip1 along meiotic

chromosomes. However, attempts to detect sumoylation of Zip1 have been unsuccessful suggesting that Zip1 binds Smt3<sup>SUMO</sup>, rather than being sumoylated itself. The observations that Zip1 interacts with both Red1 and Smt3<sup>SUMO</sup>, but does not appear to be sumoylated raises the possibility that sumoylated Red1 is the binding partner for Zip1. Although sumoylation of Red1 is detectable in meiotic cell extracts, this is only observed when the gene encoding the SUMO-deconjugating enzyme *ULP2* is deleted and only comprises a small proportion of total Red1 protein (Cheng et al., 2006). More recently, a model has been suggested whereby Zip1 and Red1 interact through 'sandwiching' polymeric Smt3<sup>SUMO</sup> chains (Lin et al., 2009). However, whether the Smt3<sup>SUMO</sup> species that co-localises with Zip1 in pachytene nuclei correspond to Smt3<sup>SUMO</sup> chains is controversial as the *smt3-allR* mutants that cannot form polymeric chains (in which all nine lysine residues have been mutated to arginine) can still form SC (Cheng et al., 2006). Therefore, the precise nature of the Smt3<sup>SUMO</sup> species that are central to SC formation and co-localise with Zip1 on pachytene chromosomes remains unclear.

Another crucial component of the lateral elements in *Saccharomyces cerevisiae* is the cohesin complex. The cohesin proteins, Rec8 (the kleisin subunit of cohesin) and Smc3 form linear stretches during pachytene, very similar to the Zip1 staining pattern (Klein et al., 1999). Mutants lacking Rec8 fail to form linear stretches of Zip1 and instead large aggregates of Zip1 protein known as poly-complexes are frequently observed (Klein et al., 1999). Poly-complexes (PCs) consist of an ordered network of Zip1 protein that are not associated with the chromatin and are generally associated with defective SC formation (although PCs are observed in wild-type SK1 strains). Chromatin-immunoprecipitation of cohesin

proteins and Red1 revealed very similar localisation profiles, suggesting that cohesin is present with Red1 (Hop1 and Smt3<sup>SUMO</sup>) at the lateral elements (Blat et al., 2002). Finally, point mutations in Rec8 in which six of the serine residues have been mutated to alanines (*rec8-6A*) render SC formation severely defective, whilst sister chromatid cohesion and recombination occurs normally (Brar et al., 2008). This finding implies that Rec8 plays an active role in SC formation that is independent of its roles in recombination and sister chromatid cohesion. However, at present there is no evidence for a direct physical interaction between Rec8 and Zip1, suggesting that Rec8 assists in SC formation without directly binding Zip1.

To summarise, in *Saccharomyces cerevisiae* the synaptonemal complex consists of the lateral element proteins Red1, Hop1, Smt3<sup>SUMO</sup> and cohesin whereas the central element comprises solely of Zip1 (Figure 1.10).

#### **1.2.1.2. The Structure of the Synaptonemal Complex in Worms**

Another model organism known to form synaptonemal complexes during meiotic prophase is the nematode *Caenorhabditis elegans*. Unlike in yeast, two proteins are known to form the transverse filaments of the central element. These are SYP-1 and SYP-2, which are 484 and 213 amino acids in size, respectively (Colaiacovo et al., 2003; MacQueen et al., 2002). Both contain coiled-coil domains and localise to the synapsed regions of chromosomes, but not the unsynapsed regions, consistent with the notion that these proteins form the central element. However, Colaiacovo *et al.* point out that the width of the SC remains similar (~100 nm) across many organisms (including *C. elegans*) but SYP-1 and SYP-2 are both relatively small proteins compared to the functional orthologs in other species. The

authors explain this by proposing that SYP-1 and SYP-2 cooperate to form a single structural module that together equates to the length of other central element proteins (Figure 1.10 B). Or put another way, SYP-1 and SYP-2 represent two halves of an equivalent transverse filament protein (such as Zip1).

The lateral elements in *C. elegans* consists of four proteins HIM-3 and the related proteins HTP-1, HTP-2 and HTP-3 (Severson et al., 2009; Zetka et al., 1999). Hypomorphic mutants or RNAi knock down of any of these components lead to synapsis defects with the central element protein SYP-1 failing to form any linear structures in pachytene nuclei and instead forming poly-complexes (Goodyer et al., 2008; Severson et al., 2009). These proteins form linear 'ribbon'-like staining patterns in pachytene nuclei that co-localise with the central element proteins (Severson et al., 2009; Zetka et al., 1999). These proteins are all members of the HIM-3 family that share a common HORMA domain (Also found in **Hop1**, **Rev7** and **Mad2** in *S. cerevisiae*), which is characterised by conserved hydrophobic residues that are predicted to form a globular structure, potentially as a complex  $\beta$ -sheet with associated  $\alpha$ -helices (Aravind and Koonin, 1998). The lateral element protein, Hop1 in budding yeast also contains a HORMA domain, suggesting a plausible evolutionary link between these proteins.

The cohesin complex is also an important structural component of the SC in *C. elegans*. RNAi knock down of the cohesin component SCC3 or simultaneous knock down of the three known kleisin subunits (REC-8, COH-3 and COH-4) results in complete failure to form SCs with the central element (SYP-1) and lateral element proteins (HTP-3 and HIM-3) aggregating as poly-complexes (Severson et al., 2009).

In summary, the synaptonemal complex in *C. elegans* is composed of two smaller central element proteins, SYP-1 and SYP-2 and four HORMA-domain containing lateral element proteins HIM-3, HTP-1, HTP-2 and HTP-3. In addition to these proteins, the cohesin complex is also an integral component of the SC (Figure 1.10 B).

#### **1.2.1.3. The Structure of the Synaptonemal Complex in Flies**

The Synaptonemal Complex is only found in females of *Drosophila melanogaster* and again consists of lateral element proteins connected by a transverse filament protein that form the central element. In *Drosophila*, a single central element protein spans the gap between adjacent lateral elements. This protein, named C(3)G, contains a predicted coiled-coil domain flanked by globular C- and N-terminal domains, analogous to central element proteins in other species (Page and Hawley, 2001). C(3)G localises to the synapsed regions of homologously paired chromosomes in female oocytes and in-frame deletions of the coiled-coil region of C(3)G result in a high incidence of unsynapsed chromosomes (Page and Hawley, 2001). The predicted length of the coiled-coil domain of C(3)G is 68 nm, very similar to that predicted for Zip1 (Page and Hawley, 2001). Electron micrographs reveal that the C-terminus of C(3)G binds the lateral elements whilst the N-terminus is found at the middle of the central element (Anderson et al., 2005). This arrangement is identical to those reported for the central element proteins Zip1 (Tung and Roeder, 1998) and mammalian SYCP1 (Liu et al., 1996) (Figure 1.10).

In addition to C(3)G, another protein has recently been discovered that stabilises the assembly of the transverse filaments of the central element. This protein, named *corona* (CONA) co-localises extensively with C(3)G both as linear SC structures and in poly-complexes. The two proteins are mutually dependent for their localisation, but axial elements form normally in the absence of CONA (Page et al., 2008). The authors suggest that CONA may act in an analogous manner to Tex12 and Syce2 in mammalian SC (Section 1.2.1.4) either in stabilising head-to-head interactions between the N-terminus of C(3)G, or in promoting the 'stacking' of transverse filaments (Page et al., 2008).

The lateral elements are thought to be composed of the ORD protein in *Drosophila*, with ORD staining co-localising with the central element protein C(3)G in oocyte nuclei (Webber et al., 2004). In the absence of ORD, both C(3)G and the putative cohesin kleisin subunit C(2)M initially associate with meiotic chromosomes, but dissociate prematurely before the pachytene stage. In these mutants, lateral elements are not observed but some transient central element-like structures are observed by electron microscopy (Webber et al., 2004). Page and Hawley (2004) have suggested that the inability to maintain the central element in *ord* mutants is due to the loss of cohesin as the departure of SMC1 and SMC3 from the chromosomes is closely followed by departure of C(3)G. Furthermore, over-expression of the Rec8 homolog C(2)M results in an accumulation of C(3)G staining (Manheim and McKim, 2003). It is clear that both ORD and cohesin are important members of the lateral elements that ensure the stable assembly of the central element protein C(3)G.

#### **1.2.1.4. The Structure of the Synaptonemal Complex in Mammals**

The overall architecture of the SC in mammals conforms to the tripartite configuration described for lower eukaryotes. However, the existence of additional central element proteins and their subsequent mutation has provided novel insight into the three-dimensional organisation of the SC that may have otherwise evaded detection (Bolcun-Filas et al., 2009). The lateral elements in mammals consist of two proteins named SYCP2 and SYCP3 (Cor1 in rats) (Dobson et al., 1994; Offenberg et al., 1998; Schalk et al., 1998). These proteins localise to the lateral elements of both synapsed and unsynapsed regions as shown by electron microscopy (Offenberg et al., 1998; Schalk et al., 1998). Consistent with this, SYCP3 is present as linear structures during zygotene, prior to the onset of synapsis as well as during diplotene after the disassembly of the central element (de la Fuente et al., 2007; Wojtasz et al., 2009). SYCP2 shares amino acid sequence similarity to the yeast protein Red1 that also forms lateral elements, suggesting a possible evolutionary link between these two proteins (Offenberg et al., 1998). Two additional proteins have recently been identified in mice, each containing the HORMA domains that are present in the yeast Hop1 and *C. elegans* HIM-3 family of lateral element proteins (Severson et al., 2009; Wojtasz et al., 2009). Curiously, these proteins named HORMAD1 and HORMAD2 co-localise with the axial elements (SYCP3) during leptotene, but during zygotene, HORMAD1/2 are only present on unsynapsed regions in both spermatocytes and oocytes. In pachytene spermatocytes, HORMAD1 and 2 are completely absent (as detected cytologically) from the synapsed chromosome axes and only remain at the unsynapsed sex chromosomes (Wojtasz et al., 2009). By diplotene when the

SC has disassembled, HORMAD1 is once again observed as linear structures. These observations suggest that the HORMAD proteins are specifically depleted from synapsed regions of chromosomes and so are unlikely to participate directly in the tripartite SC structure. This is analogous, although not identical to the staining pattern reported for Hop1 in *S. cerevisiae*, the HORMA domain-containing protein present in axial elements. Hop1 staining appears less continuous during pachytene as compared to zygotene, however some faint staining remains co-localised with Zip1 at these stages (Borner et al., 2008; Smith and Roeder, 1997). Moreover, the depletion of HORMAD1 and 2 from synapsed regions depends upon TRIP13 (Wojtasz et al., 2009), the mammalian ortholog of the yeast Pch2 protein. Pch2 is a highly conserved AAA ATPase required for the partial depletion of Hop1 from Zip1-containing regions of meiotic chromosomes (Borner et al., 2008). Taken together, these observations suggest that depletion of HORMA-domain proteins from synapsed chromosomal regions are controlled by the conserved AAA ATPases TRIP13 in mammals and Pch2 in yeast.

Cohesin also plays an important role in organisation of the lateral elements within the mammalian SC. The cohesin proteins SMC3 and STAG3 form linear staining patterns in pachytene nuclei that correspond to the synapsed chromosome axes (Prieto et al., 2001; Xu et al., 2005). When the meiosis-specific SMC1 isoform, SMC1- $\beta$  is knocked out in mice, the axial elements are grossly shortened and the chromatin loops are expanded (Revenkova et al., 2004). This suggests that cohesin is important for fixation of the chromatin loops onto the chromosome axes. Furthermore, when the kleisin subunit REC8 is knocked out, some limited and incomplete synapsis occurs between sister chromatids (Xu et al., 2005). This

suggests that Rec8 is required for uniting sister chromatids onto a single axial element so that synapsis is prevented from forming between them. This is analogous to the *pds5Δ* mutant phenotype in *S. cerevisiae* where chromosome axes are shortened and SC forms between sister chromatids (Jin et al., 2009). Pds5 is a cohesin-maintenance protein, suggesting the cohesin may play conserved roles in the correct organisation of the axial elements that ensures SC forms between homologous chromosomes rather than sister chromatids.

The central element of the SC in mammals consists of several proteins known as SYCP1, SYCE1, SYCE2, SYCE3 and TEX12 (Figure 1.10). SYCP1 was the first of these to be discovered and forms the transverse filaments characteristic of the central element. SYCP1 is a 946 amino acid protein containing a central coiled-coil domain flanked by globular domains and is the functional ortholog of Zip1 (Meuwissen et al., 1992). Electron micrographs show that SYCP1 dimers are organised in the same configuration as Zip1 within the central element with the C-terminus contacting the lateral elements and the N-terminus facing inwards contacting the N-terminus of another SYCP1 dimer (Liu et al., 1996). The C-terminus of SYCP1 binds to the C-terminus of the lateral element protein SYCP2, which in turn interacts with SYCP3, thus linking the central element to the lateral elements (Winkel et al., 2008). SYCP1 recruits two additional central element proteins named SYCE1 and SYCE2 (Costa et al., 2005). SYCE1 and SYCE2 show extensive co-localisation with SYCP1 in wild type and *sycp3*<sup>-/-</sup> mice. Furthermore, electron microscopy using immuno-gold labeled antibodies against SYCE1 and SYCE2 illustrated that these proteins localise to the central region of the central element where the N-terminus of SYCP1 is found. Consistent with this, both

SYCE1 and SYCE2 interact with the N-terminus of SYCP1 as shown by co-immunoprecipitation experiments from testis extracts (Costa et al., 2005). In addition to these proteins, another central element protein has been identified called TEX12 (Hamer et al., 2006). TEX12 co-localises and co-immunoprecipitates specifically with SYCE2 (but not SYCP1 or SYCE1) and localises to the central element of the SC in electron micrographs of mouse and rat spermatocytes (Hamer et al., 2006). These observations led the authors to suggest that SYCE2 and TEX12 form a complex that interacts with SYCP1 (through SYCE2). In further support of this, *syce2*<sup>-/-</sup> and *tex12*<sup>-/-</sup> knock out mice have very similar synapsis phenotypes whereby synapsis is initiated, but fails to extend outwards from synapsis initiation sites (Bolcun-Filas et al., 2007; Hamer et al., 2008). This culminates in the appearance of very short regions of central element-containing SCs in electron micrographs and limited SYCP1 staining in immuno-stained pachytene nuclei. *Syce2*<sup>-/-</sup> and *tex12*<sup>-/-</sup> mice form axial elements normally, but fail to undergo synapsis. Instead axes are joined at specific sites that correspond to sites of limited SYCP1 staining (Hamer et al., 2008). These may be analogous to the axial associations observed in *zip2Δ* and *zip4Δ* mutants in *S. cerevisiae* that contain Zip1 staining (Chua and Roeder, 1998; Tsubouchi et al., 2006). In contrast, *syce1*<sup>-/-</sup> mice exhibit a distinct synapsis phenotype, indicative of distinct roles for these proteins in SC assembly. Rather than SYCP1 staining being largely confined to 'axial associations' in *syce1*<sup>-/-</sup> mice, SYCP1 forms faint discontinuous lines along the axial elements but with no detectable central element observed by electron microscopy (Bolcun-Filas et al., 2009). This suggests that in the absence

of SYCE1, synapsis does not even initiate. The lack of any detectable SC at the EM level despite the presence of the three remaining central element proteins led the authors to propose that SYCE1 is important for three-dimensional 'stacking' of the transverse filaments. Thus a model whereby SYCE2 and TEX12 promote the lengthwise polymerisation of SYCP1 along the axes and SYCE1 ensures the stacking of SYCP1 that gives the mammalian SC depth is suggested (Bolcun-Filas et al., 2009) (Figure 1.10 D).

### **1.2.2. Regulation of Synaptonemal Complex Assembly**

Formation of the synaptonemal complex is a highly regulated process in meiotic prophase with multiple safeguards in place to prevent inappropriate synapsis and to coordinate synapsis with other cell cycle events. In both yeast and mammals, synapsis is dependent upon initiation of recombination (Baudat et al., 2000; Henderson and Keeney, 2004). However, the same cannot be said for flies (*Drosophila*) and worms (*C. elegans*), whereby mutations eliminating their respective *SPO11* orthologs result in seemingly normal levels of chromosome synapsis (Dernburg et al., 1998; McKim and Hayashi-Hagihara, 1998). In these organisms, additional mechanisms are in place to ensure that synapsis is contingent upon successful pairing of homologous chromosomes. Although this section is focussed on the regulation of SC initiation in budding yeast, comparisons are made to other organisms where relevant.

The first step in formation of the synaptonemal complex in *S. cerevisiae* is the deposition of the central element protein, Zip1 at synapsis initiation sites that are believed to include both centromeres (Tsubouchi et al., 2008) and sites of

crossover-designated recombination events (Henderson and Keeney, 2004). This is dependent on the synapsis-initiation protein, Zip3 (Agarwal and Roeder, 2000; Shinohara et al., 2008) (Figure 1.11). In the absence of Zip3, synapsis is delayed and incomplete and Zip1 frequently aggregates into large poly-complexes that are not associated with the chromatin (Agarwal and Roeder, 2000). Zip3 is a putative SUMO E3 ligase containing a RING finger motif shared by other SUMO E3 ligases, Siz1 and Siz2 (Cheng et al., 2006). Smt3<sup>SUMO</sup> co-localises extensively with Zip1 during meiotic prophase and shows inter-dependence with Zip1 for its localisation to meiotic chromosomes (Hooker and Roeder, 2006) (Section 1.2.1.1.). Other studies have claimed that Zip3 is actually a ubiquitin E3 ligase (Perry et al., 2005), however several observations suggest otherwise. These include the observations that Zip3 has SUMO E3 ligase activity *in vitro* and protein sequence alignments showing that Zip3 has a conserved histidine residue (at position 80) within the ring finger motif that is unique to SUMO E3 ligases, with the equivalent residue being a cysteine in ubiquitin E3 ligases (Cheng et al., 2006). Mutation of this residue to an alanine results in aberrant SC formation as well as <5% sporulation efficiency, leading the authors to suggest that the function of Zip3 in meiosis is highly dependent on its sumoylation activity (Cheng et al., 2006). However, there is no *zip3Δ* data to compare the point mutant phenotype to, so it is impossible to say whether mutation of this residue completely abolishes Zip3 function. Nonetheless, this histidine residue is clearly important. Finally, any changes to global ubiquitin conjugation patterns were not observed by western blot in cells lacking Zip3 (Cheng et al., 2006). These findings strongly suggest that Zip3 is indeed a SUMO E3 ligase.

Figure 1.11

Following initial deposition, Zip1 must be polymerised outwards from synapsis initiation sites (Figure 1.11). Deletion of *ZIP2*, *ZIP4* or *SPO16* results in dotted Zip1 staining that corresponds to sites of axial associations (Chua and Roeder, 1998; Shinohara et al., 2008; Tsubouchi et al., 2006). Furthermore, these proteins form foci on meiotic chromosomes that have been proposed to 'move' at the leading edge of synapsis (Shinohara et al., 2008; Tsubouchi et al., 2008). These observations have led to a model whereby Zip2, Zip4 and Spo16 polymerise Zip1, culminating in the appearance of cytologically detectable Zip1 'lines' (Figure 1.11). Zip3 is required to recruit these proteins (at least at levels detectable cytologically) to synapsis initiation sites (Agarwal and Roeder, 2000; Shinohara et al., 2008). Mutants lacking any of these proteins fail to extend polymers of Zip1, which instead accumulate into foci corresponding to sites of axial associations, as well as forming poly-complexes (Chua and Roeder, 1998; Tsubouchi et al., 2006). Very little is known regarding the biochemical activities of these proteins and much of the putative activities of these proteins have been inferred from bioinformatic approaches. Zip2 contains 14 WD40 repeats that may form a linked pair of 7-blade propellers. Such motifs are frequently found in proteins associated with ubiquitination complexes, such as Cdc20 and Cdh1, which are co-activators of the anaphase-promoting complex (Kraft et al., 2005; Perry et al., 2005). Furthermore, Zip2 has been shown to interact by yeast two-hybrid with the cullin protein Cdc53, a member of the SCF ubiquitin ligase complex (Seol et al., 2001; Uetz et al., 2000). These findings implicate that Zip2 is involved in the ubiquitin pathway, although there is no experimental evidence to date supporting this claim. Zip4 contains a 22-unit tetratricopeptide repeat shared by Cdc16, Cdc23, and Cdc27, which are all

members of the anaphase-promoting complex (Perry et al., 2005). This implicates Zip4 as having a role in the ubiquitin pathway, although as with Zip2, this claim currently lacks experimental evidence. It will be interesting to see whether future studies can pinpoint the mechanism by which these proteins promote the polymerisation of Zip1 along chromosomal axes.

Where does synapsis initiate? There exists a large body of evidence that suggests synapsis initiates from sites of recombination in *S. cerevisiae*. This includes the observation that the extent of synapsis correlates with the number of DSBs formed in *spo11* hypomorphs (Henderson and Keeney, 2004). Moreover, the synapsis initiation protein Zip3 physically interacts with the recombination proteins Rad51, Mre11 and Msh4-Msh5 in meiotic cell extracts and both Zip3 and Zip2 foci show high levels of co-localisation with Mre11 foci (Agarwal and Roeder, 2000; Chua and Roeder, 1998). Mutants that fail to extend SC accumulate Zip1 at axial associations thought to be synapsis initiation sites. Axial associations are dependent on the strand invasion proteins, Rad51 and Dmc1 suggesting that axial associations, and therefore synapsis initiation, occurs at sites of recombination (Rockmill et al., 1995). Electron-dense 'recombination nodules' are observed in late zygotene nuclei from electron micrographs and mutations that cause reduced crossing over display corresponding reductions of both recombination nodules and synapsis initiation events in *Sordaria* (Zickler et al., 1992). This adds support to the model of SC initiating at crossover-designated recombination sites. In budding yeast, the number of synapsis initiation sites (Zip2 and Zip3 foci) per nucleus is similar to the number of crossovers and Zip2 foci, like crossovers, show interference in their position along each chromosome (Fung et al., 2004). This

strongly suggests a link between crossover designation and initiation of synapsis. However Tsubouchi et al (2008) argues that not all SICs mark crossover sites, with a subset co-localising with centromeres where crossing over is suppressed (Lambie and Roeder, 1988). Finally, mutations in any of the genes encoding *ZMM* proteins (Section 1.2.3 and 1.1.3.3) results in reduced crossing over corresponding and synapsis defects, suggesting a mechanistic link between the two processes (Borner et al., 2004). Furthermore, restoration of crossovers in *zmm* mutants by deletion of *SGS1* is accompanied by a restoration of end-to-end synapsis in many nuclei (Jessop et al., 2006). A link between recombination and synapsis has also been implicated in mice where synapsis is dependent on recombination and the central element protein SYCE2 physically interacts with RAD51 (Baudat et al., 2000; Bolcun-Filas et al., 2009).

A recent study in budding yeast argues that synapsis initiates from centromeres, where crossing over is strongly suppressed (Tsubouchi et al., 2008). This is based on the observations that short stretches of Zip1 are frequently associated with centromeres in zygotene nuclei and axial associations are frequently observed at centromeres in *zip4Δ* mutants, but not *zip1Δ* mutants (Tsubouchi et al., 2008). Moreover, Zip3 co-localises with centromeres and Zip1 during early meiotic prophase. It is therefore possible that in budding yeast, synapsis initiates at both centromeres and crossover-designated sites. Alternatively, the apparent synapsis from centromeres may actually be emanating from crossover-designated sites proximal to the centromere.

The initiation of synapsis from centromeres, where crossing over is strongly suppressed (Lambie and Roeder, 1988), is analogous to the initiation of synapsis in *C. elegans*. In this organism, synapsis initiates at a single site on each pair of chromosomes known as the pairing centre (MacQueen et al., 2005). Pairing centres are both necessary and sufficient to trigger synapsis along the entire length of chromosomes, even in the absence of recombination and chromosomal homology (Dernburg et al., 1998; MacQueen et al., 2005). This example serves to highlight the fact that initiation of synapsis can occur at sites other than those of ongoing recombination.

The finding that non-homologous chromosomes can efficiently undergo synapsis in *C. elegans* raises the interesting question of how synapsis is regulated to ensure that it only occurs between homologous chromosomes? In *S. cerevisiae* several proteins have been identified as important in preventing inappropriate synapsis. These include Hop2, Fpr3, Zip3 and Pds5. Hop2 forms a complex with Mnd1 that is vital for repair of meiotic DSBs (Tsubouchi and Roeder, 2002). Mutation of either *MND1* or *HOP2* results in extensive synapsis between non-homologous chromosomes, suggesting that these proteins are important for achieving homolog pairing and/or preventing inappropriate synapsis (Leu et al., 1998; Tsubouchi and Roeder, 2002). The proline isomerase Fpr3 and synapsis initiation protein Zip3 are also important for preventing inappropriate synapsis. These two proteins act in parallel pathways to block synapsis in the absence of recombination (*spo11Δ*) where homologous chromosomes fail to pair (MacQueen and Roeder, 2009). This finding may explain why Zip3 co-localises with

centromeres prior to the onset of recombination in wild type meiosis (Tsubouchi et al., 2008).

In addition to preventing synapsis between non-homologous chromosomes, SC formation must also be prevented from forming between sister chromatids. This is normally prevented by the fixation of sister chromatids onto a single, common axes. However, in the absence of the cohesin maintenance protein, Pds5, synapsis occurs between sister chromatids (Jin et al., 2009). This is Rec8-dependent as deletion of Rec8 abolished axial element formation in both *PDS5* and *pds5-mn* (meiotic null) cells. Replacement of Rec8 with its mitotic counterpart, Scc1 in *pds5-mn* cells abolished inter-sister synapsis, suggesting that Rec8, rather than cohesin in general, is required for inter-sister synapsis (Jin et al., 2009). A similar phenotype has been described for *REC8*<sup>-/-</sup> knock-out mice where synapsis occurs between sister chromatids (Xu et al., 2005), although this contrasts to the situation in yeast where Rec8 is clearly required for inter-sister synapsis (Jin et al., 2009). Regardless, the findings that synapsis can occur between sister chromatids in the absence of the cohesin maintenance factor (yeast) or the kleisin cohesin (mammals) suggests that cohesin is important for preventing sister chromatid synapsis. It is likely that cohesin unites sister chromatids by fixing them onto a common axes and in doing so, prevents them from undergoing synapsis.

In budding yeast and mammals, synapsis is dependent on the initiation of recombination, however this is not the case in *C. elegans* where synapsis can occur proficiently in the absence of Spo11p (Dernburg et al., 1998). How is synapsis confined to homologous chromosomes in this organism? Surprisingly, the lateral element protein HTP-1 seems to be important for preventing synapsis until

homolog alignment has been attained. In *htp-1* mutants, homologous chromosomes do not pair but extensive synapsis is observed between non-homologous chromosomes (Couteau and Zetka, 2005). Thus, it seems that HTP-1 serves to coordinate synapsis with successful homolog pairing.

These examples highlight the tightly regulated process of synaptonemal complex assembly. It is clear that synapsis is capable of forming independently of chromosomal homology through the inherent ability of the SC to polymerise along the chromosomes. Because of this, regulatory mechanisms are in place to ensure that synapsis is only triggered when homologous partner chromosomes have paired. The absence of such mechanisms would result in extensive non-homologous synapsis, which would clearly have disastrous consequences for DSB repair and subsequent attempts at chromosome segregation. It is therefore clear to see why such mechanisms have evolved.

### **1.2.3. The Role(s) of Synaptonemal Complex Proteins**

In addition to assisting the stable juxtapositioning of homologs, the synaptonemal complex proteins have other roles, distinct from their canonical roles in chromosome synapsis. The most widely documented being the role of SC proteins in crossing over. Crossing over is abolished in mutants lacking central element proteins in *Drosophila* females and *C. elegans* (Colaiacovo et al., 2003; Page and Hawley, 2001), which is interesting given that synapsis occurs independently of recombination in both organisms (Dernburg et al., 1998; McKim and Hayashi-Hagihara, 1998). This suggests that whilst synapsis does not require recombination, completion of recombination is heavily dependent on the SC in

these organisms. Similarly, in mammals the SC is required for completion of crossover recombination with very few Mlh1 foci (which mark crossovers) present in mutants lacking central element proteins. Such mutants are consequently infertile (Bolcun-Filas et al., 2007; de Vries et al., 2005; Hamer et al., 2006).

In budding yeast, crossing over is closely coupled to SC formation by a group of proteins known collectively as the 'ZMM's. The 'ZMM's consist of synaptonemal complex proteins Zip1, Zip2, Zip3, Zip4 and the recently discovered Spo16 as well as the mismatch repair paralogs Msh4 and Msh5 and the DNA helicase, Mer3 (Borner et al., 2004; Shinohara et al., 2008). Deletion of any of the genes encoding these proteins results in reduced crossing over, the extent of which is modulated by temperature (~ 15% and 5 % of wild type levels at 25 °C and 33 °C, respectively) and concomitant synapsis defects (Borner, Kleckner et al. 2004). Non-crossovers however form proficiently in these mutants. Moreover, the *ZMM* mutants fall into the same epistasis group for crossing over, suggesting they act in the same pathway in crossover-promotion (Borner et al., 2004; Novak et al., 2001). Why is crossing over reduced in SC mutants? The finding that crossovers are reduced in *zip2*Δ, *zip4*Δ and *spo16*Δ mutants, despite proficient deposition of Zip1 at synapsis initiation sites, suggests that local nucleation of the SC is not sufficient for crossover maturation. Rather, this would suggest that extension of the SC is required for crossing over. However, this is not the case. In *red1*Δ mutants, no detectable SC is formed and crossing over is reduced. If the role of the SC proteins in crossing over is dependent on their ability to form SC, no further decrease in crossing over should be observed when *ZIP1* is deleted in *red1*Δ

mutants. However, in actual fact *red1Δ zip1Δ* mutants exhibit an additive crossover defect compared to the two single mutants (Storlazzi et al., 1996). This finding suggests that Zip1 promotes crossing over independently of forming extensive SC.

The synaptonemal complex has previously been implicated as mediating crossover interference (Egel, 1978). This theory was supported by the evidence that in budding yeast, interference is dependent on *ZIP1* and the extent of synapsis in a series of *ZIP1* deletion mutants correlated with the extent of interference (Tung and Roeder, 1998). Further correlations between SC and interference came from the observation that in *Schizosaccharomyces pombe*, no SC forms and no crossover interference occurs in this organism. However, there is now an increasing body of evidence that suggests that crossover interference is not dependent on the SC. This includes the observation that Zip2 foci (that are thought to mark crossover sites) show an interference distribution even though they assemble prior to and independently of synapsis (Fung et al., 2004). Moreover, the recent discovery of a new *ZMM* mutant, *spo16Δ* in which SC is not extended, but crossovers still display interference again suggests that SC extension is not the means by which the interference signal is spread (Shinohara et al., 2008). Finally, there is evidence to suggest that DSBs are designated to become crossovers very early, prior to strand invasion and more importantly, SC formation (Borner et al., 2004). This suggests that the interference distribution is implemented prior to SC extension. Collectively, these findings are incompatible with the model that SC extension mediates crossover interference. Therefore, there is now compelling evidence that separates crossover interference from SC formation. An alternative

model has been suggested in which crossover designation is triggered by compaction of the chromosome axes. Eventually this build up of 'stress' on the axes results in crossover designation, which relieves the stress in the vicinity of the crossover and so another crossover cannot be designated nearby. In this model, local stress release serves as an inhibitory signal for crossing over (Borner et al., 2004).

Another role for the synaptonemal complex protein, Zip1 is in preventing crossing over at the centromeres. In the absence of *ZIP1*, suppression of centromeric crossing over is eliminated (Chen et al., 2008). Crossovers are normally prevented at the centromeres (Lambie and Roeder, 1988), presumably because they are associated with precocious sister chromatid separation in both yeast and humans (Lamb et al., 1996; Rockmill et al., 2006). Therefore, Zip1 serves to safeguard the chromosomes from experiencing centromere-proximal crossovers that may result in precocious separation of sister chromatids.

In mammals, SC proteins have also been implicated in mono-orientation of sister kinetochores at meiosis I. These include the lateral element proteins SYCP2 and SYCP3, which together with RAD21 are thought to constrain sister kinetochores to adopt a mono-polar orientation. This is based largely on the localisation pattern of these proteins at the outer kinetochore during metaphase I. These proteins are proposed to form a 'double-cornet' structure holding sister kinetochores in the same orientation (Parra et al., 2004). Support for this suggestion comes from the observations that univalent chromosomes frequently bi-orient in oocytes of *sycp3*<sup>-/-</sup> mice (Kouznetsova et al., 2007).

Another role for SC proteins that is independent of their canonical role in chromosome synapsis is in 'centromere coupling'. In budding yeast, centromeres are observed to engage in pair wise interactions during early meiotic prophase, prior to and independently of recombination (Tsubouchi and Roeder, 2005). This so-called centromere coupling occurs between non-homologous chromosomes and is dependent on the central element protein, Zip1, but not synapsis initiation proteins Zip2 or Zip3. It has been suggested that centromere coupling unites chromosomes to allow homology to be assessed. In doing so, chromosomes may switch partners until they are united with their homologous partner. It will be interesting to see whether future research will uncover a similar role for SC proteins in other organisms.

Finally, SC proteins are also involved in non-exchange chromosome segregation in many organisms, which is described in detail in the next section (Section 1.3).

It is clear that the synaptonemal complex proteins have many distinct cellular roles in meiosis that are independent from their canonical roles in chromosome synapsis. They should therefore be thought of as flexible proteins that have evolved to carry out a multitude of different functions that are central to many key events in meiosis.

#### **1.2.4. Synaptonemal Complex Disassembly**

Exit from the pachytene stage of meiosis is characterised by disassembly of the synaptonemal complex, leaving homologous chromosomes connected only at sites of chiasmata. Less is known about the disassembly of the SC compared to the

assembly, but recent studies are beginning to shed light on how this process is controlled.

In *C. elegans*, the SC is disassembled asymmetrically with central element proteins being lost from one “arm” of each chromosome pair. Chromosomes in *C. elegans* are holocentric and so crossovers rather than centromeres define the chromosome “arms”. Asymmetric SC disassembly is controlled by the Zip3 ortholog, ZHP-3, which together with SUMO (SMO-1) coordinates crossover formation with asymmetric SC disassembly (Bhalla et al., 2008). This mode of SC disassembly is thought to assist in stable bivalent formation that promotes accurate chromosome segregation. This contrasts to the situation in budding yeast where Zip3 couples crossing over to SC assembly, rather than disassembly and is likely to reflect differing requirements for recombination in the initiation of synapsis in these two organisms.

In budding yeast, Zip1 is removed from the chromosome arms during diplotene, but remains at the centromeres (Newnham et al.). SC disassembly is coordinated with spindle pole body separation and resolution of dHJ into crossovers following exit from pachytene. In the absence of the transcription factor, Ndt80, cells arrest in pachytene with full SC, unresolved Holliday junctions and unseparated spindle pole bodies (Allers and Lichten, 2001; Xu et al., 1995). Expression of polo-like kinase (Cdc5) is sufficient to drive dHJ resolution and SC disassembly in *ndt80* $\Delta$  cells (Sourirajan and Lichten, 2008). *CDC5* expression is induced by Ndt80, suggesting that expression of *NDT80* at late pachytene triggers SC disassembly by turning on expression of *CDC5*. However, the finding that *cdc5*-

*mn* mutants only exhibit a mild SC disassembly phenotype (Clyne et al., 2003), suggests that even though Cdc5 is sufficient for SC disassembly in *ndt80Δ* cells, it may not be required in an otherwise wild-type meiosis. Indeed, subsequent research has revealed that Aurora B kinase (Ipl1) is required for SC disassembly (Jordan et al., 2009). In *ipl1-mn* mutants, SC fails to disassemble following exit from pachytene despite proficient continuation of other cell cycle events such as spindle pole body separation, crossover formation and entry into the meiotic divisions. This suggests that Ipl1 is required to coordinate SC disassembly with other cell cycle events in late meiotic prophase. Ipl1 is required for Cdc5-mediated SC disassembly that occurs when *CDC5* is induced in *ndt80Δ* backgrounds (Jordan et al., 2009). The precise mechanism by which the SC is disassembled is unclear. Although several Aurora B consensus phosphorylation sites exist in Zip1, mutation of these does not recapitulate the SC disassembly phenotype of *ipl1-mn* mutants, ruling out the possibility that phosphorylation of Zip1 by Ipl1 is the mechanism by which SC disassembles. It is therefore likely that Ipl1 phosphorylates other protein targets that are responsible for SC disassembly.

A similar phenotype has been reported for *in vitro* cultured mouse spermatocytes treated with the Aurora kinase inhibitor, ZM447439 at the G2-M transition (Sun and Handel, 2008). Although, the central element protein SYCP1 disassembles normally in these spermatocytes, SYCP3 staining remains linear, suggesting that Aurora kinase activity is required for removal of lateral element proteins, but not central element proteins, in mammals (Sun and Handel, 2008).

This suggests that lateral element proteins may in fact be the targets of Aurora kinases.

SC disassembly in *Drosophila* oocytes is dependent on the histone kinase NHK-1 as *nhk-1*<sup>-/-</sup> mutant females fail to disassemble their SC. This is shown by the persistent 'ribbon-like' staining of the central element protein, C(3)G in later stages of oogenesis in *nhk-1*<sup>-/-</sup> mutants whereas C(3)G staining is absent at the corresponding stage in wild-type oocytes (Ivanovska et al., 2005). This example suggests that histone modifications control higher order chromosome dynamics during meiosis that may be applicable to other organisms (Ivanovska and Orr-Weaver, 2006).

Although many questions remain regarding the underlying mechanisms of SC disassembly, the discovery of crucial regulators of this process may help narrow down the search for other proteins that may be involved. For example, identification of protein targets of Aurora B kinase in yeast and mammals or NHK-1 in *Drosophila* may provide novel insight into the mechanism of SC disassembly in these organisms.

### **1. 3. Non-Exchange Chromosome Segregation (NECS)**

Many organisms primarily rely on crossovers between homologous chromosome pairs to ensure their disjunction at the first meiotic division. However, there are examples of organisms that lack crossovers all together or contain a particular chromosome pair that fails to recombine. In these organisms, alternative mechanisms are in place to ensure high fidelity segregation of the non-exchange or 'achiasmate' chromosome pairs. There are also examples of organisms that primarily rely on crossover-mediated chromosome segregation, but are capable of segregating non-exchange chromosomes should they arise. Such 'back-up' mechanisms have been discovered in many organisms, including some in which non-exchange chromosomes are normally extremely rare.

Non-exchange chromosome segregation is highly relevant to human trisomies, with an estimated 40% of maternally derived cases of trisomy 21 involving an achiasmate chromosome pair (Lamb et al., 1996). Moreover, similar frequencies are observed for other trisomies, such as chromosome 15, 18 and the sex chromosomes (Hassold et al., 2000). Furthermore, cytological work on developing human oocytes estimates that as many as 25 % of chromosome pairs are non-exchange (do not contain an Mlh1 foci) (Cheng et al., 2009). As well as failing to crossover, another factor predisposing chromosomes to missegregate in human oocytes is the sub-optimal positioning of chromosomes either too close, or too distal to the centromere (Cheng et al., 2009). In this section, the mechanisms underlying non-exchange chromosome segregation (NECS) in various organisms are described.

### 1.3.1. NECS in Yeast

In both budding yeast (*S. cerevisiae*) and fission yeast (*S. pombe*) chromosome segregation during the first meiotic division primarily relies on crossovers between chromosome pairs. However, in both organisms there exist mechanisms to segregate non-exchange chromosome pairs (Davis and Smith, 2005; Dawson et al., 1986).

The existence of a mechanism for NECS in budding yeast was first discovered over two decades ago using artificial chromosomes that do not recombine (Dawson et al., 1986). This study showed that despite frequently failing to cross over (>97% of meioses), these artificial chromosome pairs underwent high levels of disjunction at meiosis I, segregating to opposite daughter cells in 90% of tetrads examined. Moreover, this appeared to be independent of DNA sequence homology. This was demonstrated by a strain containing two artificial yeast chromosomes that share four genes (*LEU2*, *TRP1*, *URA3*, *HIS3*) in a co-linear configuration, as well as an ARS element and a yeast centromere all embedded within a bacteriophage lambda DNA backbone. This diploid strain also contained a single copy of a mini chromosome *III* that was non-homologous to the artificial chromosome pair. The segregation pattern of these three non-exchange chromosomes was consistent with those predicted if all three were equally capable of acting as segregating partners (i.e. the three possible segregation outcomes were observed in ~ equal frequencies) (Dawson et al., 1986). This suggests that DNA sequence homology does not bias which non-exchange chromosomes will act as segregating partners. This finding was confirmed using artificial chromosomes containing higher levels of DNA sequence homology (30 kb), but still

with little or no crossing over between the non-exchange chromosomes (Ross et al., 1996). However, a later study suggested that extensive DNA sequence homology (~400 kb) between non-exchange chromosomes does, in fact, bias their likelihood of being segregating partners in the presence of a third mini-chromosome (Maxfield Boumil et al., 2003). The authors suggest that extensive DNA sequence homology allows some level of strand invasion that although does not give rise to crossovers, can bias their tendency to act as segregating partners.

The use of artificial chromosomes to demonstrate NECS in yeast begs the question of whether genuine non-exchange yeast chromosomes behave in the same way. This question led Guacci and Kaback (1991) to construct a yeast strain that was doubly monosomic for chromosomes 1 and 3. If normal yeast chromosomes behave as artificial chromosomes then these univalent chromosomes should act as segregating partners. Indeed, these chromosomes disjoined at meiosis I with similar frequencies (89 %) to those reported for the artificial chromosome pairs and spore viability of having a single monosome indicates that the segregation of exchange chromosomes was not affected (Guacci and Kaback, 1991). This suggests that the same mechanism is responsible for the segregation of both artificial and genuine non-exchange chromosomes in yeast meiosis.

More recently, yeast strains have been constructed that contain 'homeologous' chromosome pairs. These are made by replacement of one copy of a chromosome in a diploid yeast strain with a single copy of the equivalent chromosome from a closely related species. For example, replacing one copy of *Saccharomyces cerevisiae* chromosome 5 with the closely related *Saccharomyces*

*carlsbergensis* chromosome 5 (Shubochkina et al., 2001). These chromosomes share 70% DNA sequence homology and a co-linear gene arrangement, which owing to the anti-recombination activity of mismatch repair proteins (Chambers et al., 1996) prevents crossover recombination between them (Maxfield Boumil et al., 2003). These homeologs disjoin at similar frequencies to all of the other non-exchange chromosomes studied (92%), again suggesting that all non-exchange chromosomes are segregated by the same mechanism(s) in yeast.

What is the basis for non-exchange chromosome segregation in yeast? It was hypothesised that non-exchange chromosomes may physically interact prior to their disjunction at meiosis I. Indeed, Loidl *et al.* showed by electron microscopy and fluorescence *in situ* hybridization (FISH) that the monosomic chromosome 1 and 3 physically interact during pachytene when all of the other chromosome pairs are fully synapsed (Loidl et al., 1994). Furthermore, they showed that the frequency with which they were observed as 'paired' correlated with the observed non-disjunction frequencies. It was later shown using homeologous chromosomes that non-exchange chromosomes were 'paired' specifically at their centromeres during pachytene (Kemp et al., 2004). This was shown using *LacO* repeats placed either on the chromosome arms (180 kb from the centromere), or near to the centromere (12 kb) to which constitutively expressed LacI-GFP binds. By visualisation of the GFP foci, pairing of the arm regions or centromeres of the non-exchange pair could be assayed. A single focus was visible when the chromosomes were paired, whereas two were visible when they were unpaired. This analysis revealed that the non-exchange chromosomes were frequently paired (54 %) specifically at their centromeres and not arm regions during

pachytene (Kemp et al., 2004). However, their centromeres were not paired as frequently as the centromeres of homologous chromosomes (77%), suggesting that non-exchange chromosomes were not paired in all nuclei. Crucially, centromere pairing of the non-exchange chromosomes was disrupted when a centromere-containing plasmid or artificial chromosome was introduced and this resulted in a corresponding increase in meiosis I non-disjunction of the non-exchange chromosome pair. The pairing of homologous, exchange chromosomes was unaffected consistent with the artificial chromosome/plasmid only interfering with the non-exchange chromosome pair (Kemp et al., 2004). This strongly suggests that centromere pairing of non-exchange chromosomes during pachytene is the basis for their disjunction at meiosis I.

What mediates centromere pairing between non-exchange chromosomes? Kemp *et al.* originally ruled out a role for the central element protein Zip1 in this process, based on tetrad analysis that relies on the recovery of live spores. However, this study failed to account for the reduced spore viability in *zip1Δ* mutants that results from increased non-disjunction of the remaining 15 chromosome pairs. This meant that the elevated non-disjunction, specifically of the non-exchange chromosome pair, went undetected in *zip1Δ* mutants. However, subsequent studies have established that Zip1 is in fact required for centromere pairing and NECS (Gladstone et al., 2009; Newnham et al.). To circumvent the issue of reduced spore viability in *zip1Δ* mutants, chromosome segregation was inferred by direct visualisation of non-exchange (homeologous) chromosomes using the LacO/LacI-GFP system in tetrads and bi-nucleate cells. Meiosis I non-

disjunction of the non-exchange chromosomes increased ~3-fold in cells deleted for *ZIP1* and this correlated with reduced centromere pairing throughout meiotic prophase. Furthermore, these studies showed that the synapsis-initiation proteins, Zip2, Zip3 and Zip4 are also required for Zip1-dependent NECS and that Zip1 co-localises with the centromeres of non-exchange chromosomes throughout meiotic prophase. Both studies also propose that Zip1 may also promote the segregation of exchange chromosome pairs through the same mechanism (Gladstone et al., 2009; Newnham et al.) (see Chapter 4).

In addition to Zip1-mediated centromere pairing, spindle checkpoint proteins Mad1, Mad2 and Mad3 also function in NECS (Cheslock et al., 2005; Lacefield and Murray, 2007; Newnham et al.). It is thought that they function in a parallel pathway to Zip1-mediated NECS. This is based on the observation that elimination of both *ZIP1* and *MAD3* has an additive effect on NECS with the non-exchange pair segregating at random (50 % non-disjunction) (Newnham et al.). A similar effect is seen for homologous chromosome pairs when both *ZIP1* and *MAD2* are deleted, although no crossover control was analysed to account for the crossover defect associated with deletion of *ZIP1* (Gladstone et al., 2009). Mad2 has also been shown to aid the segregation of chromosome pairs that lack a crossover near the centromere (Lacefield and Murray, 2007). Precisely how the spindle checkpoint proteins mediate NECS is unclear. Whilst deletion of *MAD1* or *MAD2* influences the segregation of both exchange and non-exchange chromosomes, deletion of *MAD3* only influences the segregation of non-exchange chromosomes, suggesting that these proteins may exert their actions through distinct mechanisms. Consistent with this, Mad3 mediates a 2-3 hour prophase delay in every meioses, whereas

Mad1 and Mad2 mediate a metaphase I delay only in response to mal-oriented chromosome pairs (Cheslock et al., 2005). However, there is also evidence to suggest that Mad2 may have earlier roles in meiotic prophase that influences centromere pairing of non-exchange chromosomes (see Chapter 6).

Although the bulk of the work into NECS in yeast has been carried out in *S. cerevisiae*, another study has demonstrated the existence of a NECS mechanism in *S. pombe* (Davis and Smith, 2005). This mechanism is dependent on the dynein heavy and light chains. In mutants in which the Spo11 ortholog *REC12* is deleted, the pairing of homologous chromosomes is reduced but not eliminated and this residual pairing between centromeric regions depends upon the dynein heavy chain, Dhc1 (Ding et al., 2004). Furthermore, deletion of the genes encoding the dynein heavy (*DHC1*) or light (*DLC1*) chains increased meiosis I non-disjunction of a non-exchange chromosome pair as assayed using the LacO/LacI-GFP system (Davis and Smith, 2005). Whereas deletion of *DHC1* increased non-disjunction of both exchange and non-exchange chromosomes, deletion of *DLC1* specifically influenced the segregation of non-exchange chromosomes, suggesting that the dynein light chain plays a specific role in NECS in *S. pombe* (Davis and Smith, 2005).

Although the proteins responsible for NECS in the two yeasts are in no way similar, they may mediate NECS through analogous mechanisms. The observation that the centromeres of chromosomes are associated in the absence of recombination in *S. pombe* in a Dhc1-dependent manner is analogous to the centromere pairing of non-exchange chromosomes reported in *S. cerevisiae* (Ding

et al., 2004; Kemp et al., 2004). The different proteins responsible may simply be a reflection of there being no synaptonemal complex in *S. pombe* (Figure 1.12).

### 1.3.2. NECS in Flies & Worms

*Drosophila melanogaster* has provided an excellent model organism for the study of non-exchange chromosome segregation. In males, recombination is completely absent and so the chromosomes are segregated through alternative mechanisms (Hawley, 2002). In females, the 4<sup>th</sup> chromosome pair does not recombine, but manages to segregate correctly in 99.9 % of oocytes (Carpenter, 1973). Similar levels of segregation fidelity are observed for the X chromosomes that fail to recombine in 5-10 % of meioses (Sturtevant and Beadle, 1936). How is NECS mediated in *Drosophila*? Interestingly, the mechanisms underlying NECS are quite different for male and females and are likely to represent the fact that crossovers are completely absent in males, whereas they are only absent from a single chromosome pair in females (Orr-Weaver, 1995). In *Drosophila* males, the first insight into the behaviour of meiotic chromosomes came from a pioneering study using LacO/LacI-GFP to follow the chromosomes in living spermatocytes (Vazquez et al., 2002).

This study showed that homologous chromosomes are tightly paired at regions of euchromatin very early in spermatogenesis, possibly representing a persistence of somatic pairing. In addition to these euchromatic associations, the centromeres appear to undergo dynamic clustering throughout this period between non-homologous chromosomes. These chromosomal interactions persist from early G1, through S phase until mid-G2 where each pair of chromosomes are

Figure 1.12

sequestered to distinct territories of the nucleus, near the nuclear envelope. Coupled with this chromosomal sequestration is the abrupt loss of euchromatic associations between both sister chromatids and homologous chromosomes. Chromosomes remain associated, however, until the first meiotic division. The mechanism responsible for the continued chromosome pairing in late G2 may be chromosome entanglements that become resolved by a topoisomerase-II catalysed reaction at anaphase I. Alternatively, heterochromatic associations that are independent of homology may be responsible for holding chromosome pairs together in their distinct territories until they congress on the metaphase spindle (Vazquez et al., 2002). Support for the latter comes from a model suggested from much earlier work that the X-Y initially pair through rDNA sequences, but then homology-independent heterochromatic associations take over in holding the chromosomes together in late G2 (Cooper, 1964)(reviewed in Hawley 2002). Moreover, heterochromatic associations are the reported mechanism by which the achiasmate 4<sup>th</sup> chromosome pairs are segregated in *Drosophila* females (Dernburg et al., 1996). It is therefore conceivable that a similar mechanism exists to segregate achiasmate chromosomes in males.

There are several proteins responsible for associations between achiasmate chromosome pairs in *Drosophila* males. When mutated, chromosome pairing/conjunction is impaired and chromosome pairs therefore missegregate at the first meiotic division. One of the factors important for this process has been mapped to the teflon gene. In *tef* mutants, pairing of all four autosomes is impaired whereas the sex chromosomes are unaffected. This perturbation of chromosome pairing correlates with increased missegregation of the autosomes at meiosis I

(Tomkiel et al., 2001). In addition to *teflon*, two additional proteins have been identified that are important for the segregation of all chromosome pairs (including sex chromosomes) in *Drosophila* males (Thomas et al., 2005). Mutations in either gene encoding these two proteins named SNM (**S**tromalin in **M**eiosis) and MNM (**M**odifier of MDG4 in **M**eiosis), cause elevated meiosis I non-disjunction of autosomes and sex chromosomes. This correlates with abolished homolog pairing during pro-metaphase I, and failure to congress into single chromosome mass during metaphase I. Although initial pairing appears to be established normally in these mutants, sequestration of homologs to nuclear territories is defective. This suggests that SNM and MNM are important for the maintenance, rather than the establishment of pairing. It is likely that these proteins act alongside *teflon* as their localisation to autosomes is dependent upon *teflon* (Thomas et al., 2005) (Figure 1.12).

Precisely how these proteins collaborate to ensure associations between achiasmate chromosome pairs is unclear. SNM is a homolog of the cohesin protein, SCC3, but analysis of protein co-localisation suggests that it does not form part of the cohesin complex and so is unlikely to mediate pairing through a cohesin-dependent mechanism. Further research is required to identify the mechanisms responsible for holding achiasmate chromosome pairs together until their segregation at meiosis I in *Drosophila* spermatogenesis.

How is NECS mediated in *Drosophila* females? As mentioned earlier, the 4<sup>th</sup> chromosome pair never recombines and yet segregates correctly in 99.9 % of oocytes (Carpenter, 1973). What is responsible for the high fidelity of NECS in *Drosophila* females? Experiments using a combination of FISH and high-resolution

microscopy of intact oocytes revealed the existence of two distinct NECS mechanisms operating in *Drosophila* females (Dernburg et al., 1996). One mechanism ensures the segregation of homologous non-exchange chromosomes and involves pairing at regions of heterochromatin from pachytene until the first meiotic division. The other mechanism ensures the segregation of heterologous non-exchange chromosomes and does not involve pairing. Instead, it was proposed to involve a “crowded spindle” in which limited kinetochore binding sites are available and so heterologous pairs are forced to adopt positions on opposite half-spindles (Dernburg et al., 1996). However, the recent finding that achiasmate X chromosomes engage in dynamic chromosome oscillations between opposite half-spindles suggests that that spindle is not “crowded” and non-exchange chromosomes are in no way spatially confined on the metaphase I spindle (Hughes et al., 2009).

In addition to these two mechanisms, the protein encoded by the *NOD* (No distributive disjunction) gene is also important for NECS in *Drosophila* females (Carpenter, 1973). *NOD* is known to encode a kinesin-like motor protein that may propel the achiasmate chromosomes away from their respective spindle poles and towards the main chromosome mass at metaphase I and in doing so, substitute for a chiasma (Hawley and Theurkauf, 1993; Orr-Weaver, 1995).

It was previously thought that metaphase I was characterised by a single chromosome mass at the spindle mid-zone and achiasmate chromosomes on opposite half spindles, mid-way between the main chromosome mass and the spindle poles (Hawley and Theurkauf, 1993). However, it has since been shown that this stage actually corresponds to mid pro-metaphase I and that the

achiasmate chromosome pairs eventually congress to join the main chromosome mass at metaphase I (Gilliland et al., 2009). Further insight into the behaviour of non-exchange chromosomes at this stage was gained from elegant live-cell imaging of *Drosophila* oocytes (Hughes et al., 2009). These studies revealed that achiasmate chromosomes frequently oscillate between the two half spindles during pro-metaphase. Thus, at any one time, both chromosomes may be on the same or opposite half spindles. This oscillation was increased when the plus-end directed kinesin protein NOD that is responsible for the polar ejection force, was mutated, suggesting that such forces normally restrict oscillating movements (Hughes et al., 2009). Furthermore, this study demonstrated that centric heterochromatic threads connect the oscillating non-exchange chromosomes (Hughes et al., 2009). These threads can span large distances allowing the chromosomes the freedom to oscillate between opposite spindle poles (Figure 1.12). This is analogous to reports from mitotic cells in which sister chromatids are connected by threads of centromeric heterochromatin containing PICH (Plk1 interacting checkpoint helicase) protein (Baumann et al., 2007). PICH is thought to act in conjunction with the spindle checkpoint to sense tension during mitosis. These chromatin threads vanish during anaphase in a manner that has been proposed as being mediated by topoisomerase activity. Collectively, these studies help explain the functional importance of the vast regions of heterochromatin present at the centromeres of many diverse organisms (Brar and Amon, 2008).

The finding that non-exchange chromosomes oscillate to opposite halves of the spindle during pro-metaphase highlights the strength of using live-cell imaging over fixed samples to decipher dynamic chromosome behaviours. This finding may

in fact, be applicable to the behaviour of non-exchange chromosomes during metaphase I in budding yeast. Kemp *et al.* reported that non-exchange chromosomes separate precociously in metaphase I, as shown by their centromeres being positioned at, or near to, opposite spindle poles in *pds1*-arrested cells (Kemp *et al.*, 2004). However, the finding that non-exchange chromosomes oscillate between opposite spindle poles before finally congressing towards the exchange chromosomes in *Drosophila* females, suggests that the same may be true of budding yeast. This could easily be addressed by using live-cell imaging to follow the movements of non-exchange chromosomes in yeast cells.

In addition to *Drosophila melanogaster*, another invertebrate that is characterised by its ability to segregate homologous chromosomes in the absence of crossovers is the female silk worm (*Bombyx mori*). *Bombyx mori* females do not experience crossing over and instead use a modified form of the synaptonemal complex to segregate their chromosomes at the first meiotic division (Rasmussen, 1977). Observations of the chromosomes in *Bombyx mori* oocytes showed that the SC appears to undergo morphological changes following exit from pachytene, in which the central element becomes extruded and the dense lateral elements are connected. The dense lateral elements appear to become shorter and thicker and eventually form a single end-to-end structure at metaphase with the chromatin of each chromosome to either side (Rasmussen, 1977) (Figure 1.12).

These examples highlight the diverse mechanisms employed by invertebrates to segregate non-exchange chromosomes. Even between the two sexes in *Drosophila*, the mechanisms are quite distinct. However, these are likely

to represent the fact that crossovers are completely absent in males, whereas they are only absent for the 4<sup>th</sup> chromosome pair in females. The use of the synaptonemal complex in NECS of *Bombyx mori* females is analogous to what is now known in organisms as diverse as budding yeast, plants and mammals (Sections 1.3.1, 1.3.3 and 1.3.4, respectively).

### 1.3.3. NECS in plants

The investigation of non-exchange chromosome segregation (NECS) in plants has focussed on the study of univalents in *Arabidopsis thaliana* (Pradillo et al., 2007). This study examined four mutants, *spo11-1-3*, *dsy1*, *mpa1*, and *asy1*, each of which is characterised by a high level of univalent (non-exchange) chromosomes in meiosis. The *SPO11* and *ASY1* genes encode the *SPO11* and *HOP1* orthologs, respectively, whereas *DSY1* and *MPA1* are poorly characterised, but are known to have important meiotic functions in crossing over (Sanchez Moran et al., 2001). Whilst the *dsy1* and *mpa1* mutants displayed extensive synapsis in pachytene nuclei, synapsis was severely defective in the *spo11* and *asy1* mutants. Crucially, meiosis I non-disjunction frequencies (as assayed using FISH) were similar to those expected if the non-exchange chromosomes were segregating at random in the *spo11* and *asy1* mutants. In contrast, non-disjunction frequencies were significantly lower than those expected from random segregation of the non-exchange pairs in the *dsy1* and *asy1* mutants (Pradillo et al., 2007). These findings correlate the extent of synapsis with the disjunction of non-exchange chromosomes at meiosis I. This suggests that perhaps the SC mediates NECS in *Arabidopsis*. However, more experimental evidence is required to substantiate this

claim. For example, it may be that homolog pairing is defective in the *spo11* and *asy1* mutants and this is the reason for the increased non-disjunction of univalents at meiosis I. Defective synapsis may therefore merely be a read-out of earlier problems in homolog pairing. This highlights the two steps that are important for any NECS mechanism; firstly segregating partners must be identified (e.g. by homology pairing) and secondly a disjunction mechanism must exist to substitute for chiasmata at meiosis I (e.g. the SC). It is unclear which of these steps are defective in these mutants.

#### **1.3.4. NECS in Mammals**

The study of non-exchange chromosome segregation in mammals is confined to those organisms whose sex chromosomes are achiasmate. These include the marsupial *Thylamys elegans* and the eutherian mammal, *Meriones unguiculatus* (de la Fuente et al., 2007; Page et al., 2006). The more commonly studied meiotic model organism, *Mus musculus* (mouse) cannot be used for the study of NECS as each chromosome pair receives an obligate crossover, including the XY pair (Burgoyne, 1982).

Study of the achiasmate (non-exchange) XY pair in marsupial meiosis demonstrated the existence of an SC-derived structure that holds the X and Y chromosomes together until their segregation at meiosis I (Page et al., 2006). The authors first verified that the XY pair was indeed achiasmate by examining the staining of STAG3, a meiotic cohesin subunit, within each bivalent of metaphase I nuclei. Unlike the exchange chromosomes that contained cruciform STAG3 staining that was interrupted at the site of the chiasmata, the X- and Y-

chromosomes each contained uninterrupted STAG3 staining that was not connected in any way. This indicated that unlike the autosomes, the XY chromosomes were not connected by chiasmata. Despite this, the X- and Y-chromosomes were associated with each other at this stage. As the sex chromosomes were connected distally, it was possible that heterochromatin between the telomeres was holding the chromosomes together. However, FISH probes to telomeric DNA sequences did not expose any associations between telomeric sequences of the chromosome pair. Instead, a region containing the lateral element protein, SCP3 seemed to connect the chromosomes. Following the disassembly of the synaptonemal complex at diplotene, the SCP3 staining appeared diffuse and discontinuous for the autosomes but remained as a dense-staining region corresponding to the sex chromosomes. This SCP3-derived 'dense plate' is known to assist pairing of the XY chromosomes (Page et al., 2003). Rather than forming lengthways between the XY pair, the dense plate connects the ends of the X and Y chromosomes. Curiously, the central element protein SCP1 was also observed within this 'dense plate' at both diplotene and metaphase I. This is especially surprising given that the XY chromosomes do not contain SCP1 staining at pachytene (Page et al., 2003). The authors suggest that the 'dense plate' is a linear structure of SCP3 that connects the telomeres of the XY pair and unites them into close proximity by folding back on itself. The central element SCP1 has been proposed to secure the 'folded sheet' structure of SCP3, holding the ends of the XY pair together (Page et al., 2006) (Figure 1.12).

The finding that SC proteins promote NECS was not confined to marsupial meiosis with an analogous finding reported in *Meriones unguiculatus* (de la Fuente

et al., 2007). In this study, the XY pair were inferred as being non-exchange by the absence of an Mlh1 focus (indicative of crossovers) during late pachytene. Whether this method alone is sufficient to conclude that the X-Y pair are non-exchange is controversial. Nonetheless, during diplotene and diakinesis, SYCP3 was observed to undergo morphological changes specifically on the sex chromosomes forming a dense staining structure on the Y chromosome. Unlike marsupial males, this SYCP3-rich structure did not contain SYCP1 staining, indicating that no central element was present. The XY pair remained paired from pachytene until late metaphase I where they appeared associated at their chromosome ends. Even after the XY pair started to separate at anaphase I, “threads” of SYCP3 were clearly visible between them. These threads are devoid of DAPI staining leading the authors to suggest that they represent proteinaceous links between the chromosomes (de la Fuente et al., 2007). However, it is unclear whether DAPI staining would be sensitive enough to detect fine chromatin threads in these preparations. Nonetheless, this study provides strong evidence that SYCP3 is responsible for holding together the ends of non-exchange sex chromosomes until their disjunction at meiosis I.

These examples present a previously unknown role for the lateral element protein SYCP3/SCP3 in the segregation of non-exchange chromosomes in mammals. Although these studies have only looked at sex chromosomes, it is possible that the same, or an analogous mechanism may be capable of segregating autosomes that fail to crossover. This would be consistent with the observation that SYCP3 is found at the centromeres of all autosomes at metaphase I in male mice (Parra et al., 2004; Wojtasz et al., 2009). Furthermore, in

marsupial males the central element protein SCP1 co-localises with the centromeres until diakinesis (Page et al., 2006). However, the rarity of naturally occurring non-exchange chromosomes in mammals makes this a difficult area of study.

The examples described here highlight the diverse mechanisms employed by different organisms to segregate non-exchange chromosomes at meiosis I (Wolf, 1994). Although each organism has its own distinct way of dealing with non-exchange chromosomes in meiosis, there are common themes amongst these mechanisms that may hint towards a common ancestral mechanism. For example, the role of SC proteins in NECS is a reoccurring theme shared by many organisms, suggesting that the role of the SC in meiotic chromosome segregation may be deep-rooted in evolution (for full discussion see Chapter 7).

## Chapter 2. Materials and Methods

### 2.1. Materials

#### 2.1.1 Growth Media

##### 2.1.1.1. Bacterial Media

Most bacterial strains used in this work were grown in Luria Broth (1% w/v bacto-tryptone, 0.5% w/v yeast extract, 0.5% w/v NaCl, pH 7.0) at 37 °C. For solid media, 2% w/v agar was added before autoclaving. Selection of a particular plasmid was achieved through addition of relevant antibiotics at the concentrations listed in section 2.1.4.

STBL2 cells (Invitrogen) were used when using plasmids containing *LacO* repeats. These cells were grown in SOC medium (2% w/v bacto-tryptone, 0.5% w/v yeast extract, 10 mM NaCl, 2.5 mM KCl, 10 mM MgCl<sub>2</sub>, 10 mM MgSO<sub>4</sub>, 20 mM glucose, pH 7.0).

##### 2.1.1.2. Yeast Media

Yeast cells were generally grown in 'rich' YPD medium (1% w/v yeast extract, 2% w/v bacto-peptone, 2% w/v glucose, 500 µM adenine, pH 6.5). For solid media, 2% w/v agar was added before autoclaving. For selection of drug-resistance markers, the relevant antibiotic was added at the concentrations listed in Section 2.1.4. For enrichment of yeast cells with functional mitochondria, cells were grown in YEPEG media (1% w/v succinate, 1% w/v yeast extract, 2% w/v bacto-Peptone, 2% v/v

glycerol, 500  $\mu$ M adenine, pH 5.5. 2% v/v ethanol added after autoclaving). Minimal media contained 0.17% w/v yeast nitrogen base, 2% w/v D-glucose, 0.5% ammonium sulphate, pH 7.25. 'Complete media' was the same as minimal media but with 0.087% w/v of a nutrient mix containing all amino acids. 'Drop-out' media was the same as complete media but with the appropriate amino acid omitted from the nutrient mix. 'Complete' amino acid mix was made by combining the appropriate quantities of each amino acid given in Table 2.1. 'Drop out' powders were made in the same way as 'complete' powders but the relevant amino acid was omitted from the mix.

Amino Acid	Amount (mg)	Final conc. in media (% w/v)
Adenine (hemisulfate salt)	800	0.003
L-arginine (HCl)	800	0.003
L-aspartic acid	4000	0.016
L-histidine	800	0.003
L-leucine	800	0.003
L-lysine (mono-HCl)	1200	0.005
L-methionine	800	0.003
L-phenylalanine	2000	0.007
L-threonine	8000	0.032
L-tryptophan	800	0.003
L-tyrosine	1200	0.005
Uracil	800	0.003

**Table 2.1.** Amino acids used to make complete and drop out powders. For drop out powders, the appropriate amino acid is omitted from the blend. All amino acids were supplied by Sigma.

### 2.1.2. Buffers

Buffer	Composition
TAE:	40mM Tris·acetate 2 mM Na <sub>2</sub> EDTA·2H <sub>2</sub> O pH 8.5
TE:	10 mM Tris·Cl 1 mM EDTA pH 8.0
PBS:	137 mM NaCl 2.7 mM KCl 4.3 mM Na <sub>2</sub> PO <sub>4</sub> ·7H <sub>2</sub> O 1.4 mM KH <sub>2</sub> PO <sub>4</sub>
11.1 $\chi$ buffer:	45 mM Tris•HCl (pH 8.8) 11 mM ammonium sulphate 4.5 mM magnesium chloride 6.7 mM 2- $\beta$ -mercaptoethanol 4.4 $\mu$ M EDTA (pH 8.0) 1 mM adenine dNTP 1mM cytosine dNTP 1mM guanine dNTP 1mM thymine dNTP 113 $\mu$ g/ml BSA
10 $\chi$ SDS running buffer:	250 mM Tris base 1.92 M Glycine 35 mM SDS

### 2.1.2. Buffers *continued*.

Buffer	Composition
Semi-Dry transfer buffer:	50 mM Tris base 39 mM Glycine 1.3 mM SDS

### 2.1.3. Enzymes

Enzyme	Supplier
Taq DNA polymerase:	Thermo Scientific
KOD Hotstart DNA polymerase:	Novagen
T4 DNA ligase:	New England Biolabs
Antartic phosphatase:	New England Biolabs
Restriction enzymes:	New England Biolabs
Zymolyase (100T):	Seikagaku Corporations
Zymolyase (20T):	Seikagaku Corporations
RNase:	Sigma
DNase:	Sigma

### 2.1.4. Drugs & Antibiotics

Drug	Concentration used	Supplier
Ampicillin	100 µg/ml	Sigma
Chloramphenicol	100 µg/ml	Sigma
G418	400 µg/ml	Invitrogen
Hygromycin B	300 µg/ml	Invitrogen
Nourseothricin	100 µg/ml	Werner Biotech
Tetracyclin	100 µg/ml	Sigma

### 2.1.5. Antibodies

Primary antibodies	Working dilution	Supplier	Catalogue number
Mouse anti-Myc (9E10)	1:100	Cambridge Bioscience	MMS-150P-200
Mouse anti-HA (HA11)	1:100	Cambridge Bioscience	MMS-101P-200
Guinea pig anti-GFP	1:100	Roeder Lab (Tsubouchi <i>et al.</i> 2008)	n/a
Rabbit anti-Zip1	1:100	Roeder Lab (Sym <i>et al.</i> , 1993)	n/a
Mouse anti-Zip1	1:100	Roeder Lab (Chua & Roeder, 1998)	n/a
Rat anti-tubulin	1:400	Strattech	T9154-04
Goat anti-GFP	1:1000	AbCam	ab5450-25
Rabbit anti-Zip1	1:100	Hoffmann Lab (Jordan <i>et al.</i> 2009)	n/a
Mouse anti-3-phosphoglycerate kinase	1:2000 (WB*)	Invitrogen	459250
Rabbit anti-Smt3	1:100 1:1000 (WB)	Santa Cruz	sc-28649
Goat anti-Zip1 (N-terminus)	1:1000 (WB)	Santa Cruz	sc-48716

**\*WB depicts dilutions used for western blot**

<b>Secondary antibodies</b>	<b>Working dilution</b>	<b>Supplier</b>	<b>Catalogue number</b>
Donkey anti-rabbit, FITC	1:100	Jackson ImmunoResearch	711-095-152
Donkey anti-rabbit, Texas Red	1:100	Jackson ImmunoResearch	711-075-152
Donkey anti-rabbit, Cy5	1:100	Jackson ImmunoResearch	711-175-152
Donkey anti-rat, FITC	1:100	Jackson ImmunoResearch	712-095-153
Donkey anti-rat, Texas Red	1:100	Jackson ImmunoResearch	712-075-153
Donkey anti-rat, Cy5	1:100	Jackson ImmunoResearch	712-175-153
Donkey anti-mouse, FITC	1:100	Jackson ImmunoResearch	715-095-151
Donkey anti-mouse, Texas Red	1:100	Jackson ImmunoResearch	715-075-151
Donkey anti-mouse, Cy5	1:100	Jackson ImmunoResearch	715-175-151
Donkey anti-mouse, AMCA	1:100	Jackson ImmunoResearch	715-155-151
Donkey anti-mouse, Alexafluor	1:100	Invitrogen	A-21202
Donkey anti-guinea pig, FITC	1:100	Jackson ImmunoResearch	706-095-148
Donkey anti- guinea pig, Texas Red	1:100	Jackson ImmunoResearch	706-075-148
Donkey anti - guinea pig, Cy5	1:100	Jackson ImmunoResearch	706-175-148
Donkey anti -goat, FITC	1:100	Jackson ImmunoResearch	705-096-147
Donkey anti - goat, Texas Red	1:100	Jackson ImmunoResearch	705-075-147
Donkey anti - goat, Cy5	1:100	Jackson ImmunoResearch	705-175-147
Rabbit anti - rat IG, HRP	1:2000 (WB)	Dako	
Swine anti - rabbit IG, HRP	1:2000 (WB)	Dako	
Rabbit anti - mouse IG, HRP	1:2000 (WB)	Dako	
Rabbit anti - goat IG, HRP	1:2000 (WB)	Dako	

### 2.1.6. Oligonucleotides.

**Table 2.2.** Oligonucleotides used in this work.

EH oligo no.	Name	Sequence (5' to 3')	Application
O61	ZIP1-MX4.R	ATGAAATGTATTTCGCACAAAACGATTTCAAATTTT CCATTATCCTATCGATGAATTCGAGCTCG	Reverse primer for amplification of cassettes to replace <i>ZIP1</i> ORF
O62	ZIP1-A1	GAAGAGCTGCTTCTTCACTTG	Forward primer upstream of <i>ZIP1</i> ORF to check integration of cassette
O63	ZIP1-A4	GCAATCTAGATGACCTCTT	Reverse primer downstream of <i>ZIP1</i> ORF to check integration of cassette
O64	ZIP3-MX4.F	CAGGTCGACACGTCTGTGAAGTTGACGCTTTGTG CCGCGGCCAACAAGGGCGTACGCTG	Forward primer for amplification of cassettes to replace <i>ZIP3</i> ORF
O65	ZIP3-MX4.R	TCTGAAGGCTGTTTTCGTCACGGGGAATCCTTAC ACCTATATCGATGAATTCGAGCTCG	Reverse primer for amplification of cassettes to replace <i>ZIP3</i> ORF
O66	ZIP3-A1	TGTTCTAGAGGCCAATGGCC	Forward primer upstream of <i>ZIP3</i> ORF to check integration of cassette
O67	ZIP3-A4	CTCTCCTTGTGCCTTCGTATTG	Reverse primer downstream of <i>ZIP3</i> ORF to check integration of cassette
O68	MER3-MX4.F	TTGATACCTCAAGGTGGATTTGACAACTTAAGAG GCGTCGTAAGGCGTACGCTGCAGGTC	Forward primer for amplification of cassettes to replace <i>MER3</i> ORF
O69	MER3-MX4.R	GGGGTAATGAATATCAGTAATGTCTATTGTTCCC GGCCATGCCGCATCGATGAATTCGAG	Reverse primer for amplification of cassettes to replace <i>MER3</i> ORF

EH oligo no.	Name	Sequence (5' to 3')	Application
O70	MER3-A1	ACGAATGGATGCAGGCTCG	Forward primer upstream of <i>MER3</i> ORF to check integration of cassette
O71	MER3-A4	GTAAACTCTCACACATGCT	Reverse primer downstream of <i>MER3</i> ORF to check integration of cassette
O73	K2	TTCAGAAACAACTCTGGCGCA	Reverse primer ~600bp into <i>KANMX6</i> cassette for checking integration of <i>KANMX6</i> cassettes
O74	K3	CATCCTATGGAAGTGCCTCGG	Forward primer ~400bp from the end of <i>KANMX6</i> cassette for checking integration of <i>KANMX6</i> cassettes
O75	MSH4-MX4.R	AGAAATAATGGATTATAGTTTTAAGCTAAGCGGAA AAGCCAAA-ATCGATGAATTCTGAGCT	Reverse primer for amplification of cassettes to replace <i>MSH4</i> ORF
O76	MSH4-A1	TAGCAAAAGAGCAGTTGG	Forward primer upstream of <i>MSH4</i> ORF to check integration of cassette
O77	MSH4-A4	CTATCTACTGAGACCATGTG	Reverse primer downstream of <i>MSH4</i> ORF to check integration of cassette
O80	MSH4-MX4.F	ATAGCATTGAAATCTGTAGCTGATCAACGCAAAC TATATGCA-CGTACGCTGCAGGTCGAC	Forward primer for amplification of cassettes to replace <i>MSH4</i> ORF

**Table 2.2 continued.** Oligonucleotides used in this work.

EH oligo no.	Name	Sequence (5' to 3')	Application
O98	ZIP2_A1	ACTGATCGTGGGAAATCCTG	Forward primer upstream of <i>ZIP2</i> ORF to check integration of cassette
O99	ZIP2_A4	CTCATTTTCCGTGCGGTATT	Reverse primer downstream of <i>ZIP2</i> ORF to check integration of cassette
O105	ZIP1_MX4.F	TGAGATTCGGAAGTAAAATACCCTCGGCGGCTAA ATTTTATAGAGACGTACGCTGCAGGTCGAC	Forward primer for amplification of cassettes to replace <i>ZIP1</i> ORF
O110	MSH4_A0	ACCCTCACTGGGGTCGTTTTT	Forward primer to check integration of cassette made using <i>MSH4_A1</i> and <i>MSH4_A4</i> primers
O111	MSH4_A5	GTTAATGGGGCCAAGCAGTGAT	Reverse primer to check integration of cassette made using <i>MSH4_A1</i> and <i>MSH4_A4</i> primers
O141	MAD3_MX4.F	AATCATGCGAAAATACAATAAAAGACGTAACTTG ATAGACGTACGCTGCAGGTCGAC	Forward primer for amplification of cassettes to replace <i>MAD3</i> ORF
O142	MAD3_MX4.R	TTGGCCAGTATACTTACTCATTCATGGGATTAGTT TTATTATCGATGAATTCGAGCTCG	Reverse primer for amplification of cassettes to replace <i>MAD3</i> ORF
O149	H2	CGGCGGGAGATGCAATAGG	Reverse primer ~700bp into <i>HPHMX4</i> cassette for checking correct integration of <i>HPHMX4</i> cassette

**Table 2.2 continued.** Oligonucleotides used in this work.

EH oligo no.	Name	Sequence (5' to 3')	Application
O150	H3	TCGCCCCGCAGAAGCGCGGCC	Forward primer ~400bp to end of <i>HPHMX4</i> cassette for checking correct integration of <i>HPHMX4</i> cassette
O151	N2	GATTCGTCGTCCGATTCGTC	Reverse primer ~600bp into <i>NATMX4</i> cassette for checking correct integration of <i>NATMX4</i> cassette
O152	N3	AGGTCACCAACGTCAACGCA	Forward primer ~400bp to end of <i>NATMX4</i> cassette for checking correct integration of <i>NATMX4</i> cassette
O179	ZIP2mx_F	GTAATTGAATCAATTTAGAGAAATAGATCATATTA CAAAAATACTCGTACGCTGCAGGTC	Forward primer for amplification of cassettes to replace <i>ZIP2</i> ORF
O180	ZIP2mx_R	CAGGCGTAGTATAAATAGTTTACCGGGTAACGAT CCTTGCTGGATATCGATGAATTCGAG	Reverse primer for amplification of cassettes to replace <i>ZIP2</i> ORF
O304	ZIP4_mxF	TAATATTAGTAAAAGGCTATGTTCTAAAGTGATCA ACAAGTTTCACGTACGCTGCAGGTCGAC	Forward primer for amplification of cassettes to replace <i>ZIP4</i> ORF
O305	ZIP4_mxR	TAAGGGTCAGCCAGTATAAACGACAGTAAATGGA ATAAAAAAGGTATCGATGAATTCGAGCTCG	Reverse primer for amplification of cassettes to replace <i>ZIP4</i> ORF
O309	Ctf19.F	GCTGTGCAAGTTACTCAT	Forward primer 200bp upstream of <i>CTF19</i> ORF

**Table 2.2 continued.** Oligonucleotides used in this work.

EH oligo no.	Name	Sequence (5' to 3')	Application
O310	Ctf19.R	CGGGAAGAGAATACTACA	Reverse primer 200bp downstream of <i>CTF19</i> ORF
O445	ZIP3_A	TTAAATGACAGTAACGTCCAAATCA	Forward primer ~ 400bp upstream of <i>ZIP3</i> ORF
O446	ZIP3_B	TAAACAAAGGGCTGTTCAAAAATAG	Reverse primer ~150bp into <i>ZIP3</i> ORF
O447	ZIP3_C	AATTGCATCATTCAAATACACCTTT	Forward primer ~ 300bp from the end of <i>ZIP3</i> ORF
O448	ZIP3_D	CTTTTAAAACACCCCCATAAGTTT	Reverse primer ~350bp downstream of <i>ZIP3</i> ORF
O449	ZIP2_A	GCCTTCTTTTTCGTTTGTATAGTCA	Forward primer ~ 400bp upstream of <i>ZIP2</i> ORF
O450	ZIP2_B	CAGTGGTTTAAGTTGCAAATTTCTT	Reverse primer ~150bp into <i>ZIP2</i> ORF
O451	ZIP2_C	GCGATTTTCATTATAAACCATTCAAC	Forward primer ~ 500bp from the end of <i>ZIP2</i> ORF
O452	ZIP2_D	GGTAATTTTTAGTTTCAAGTCACGC	Reverse primer ~300bp downstream of <i>ZIP2</i> ORF
O464	MAD2_F4	AACGAACATTTGAAGTGCACATACCATTGCTGAC CTACTGCTTTAGAATTCGAGCTCGTTTAAAC	Forward primer for promoter replacement of <i>MAD2</i>
O465	MAD2_R3	TGTAAGTGTCTTGTGTAACCTTTAGTGATATTG ATTGTGACATGCACTGAGCAGCGTAATCTG	Reverse primer for promoter replacement of <i>MAD2</i>
O466	MAD2_A	TTTCGTCTTGAAGTCTCTTTTGTCT	Forward primer to check integration of <i>MAD2</i> promoter replacement cassette

**Table 2.2 continued.** Oligonucleotides used in this work.

EH oligo no.	Name	Sequence (5' to 3')	Application
O467	MAD2_B	TGGAATTAATGCTGTACTCGAAAA	Reverse primer to check integration of <i>MAD2</i> promoter replacement cassette
O481	ZIP1_A	TTTGTTCTAAACGGTCAAACCTTTTC	Forward primer ~250bp upstream of <i>ZIP1</i> ORF
O482	ZIP1_B	TTTTGCTACTCCTTCACTCACTTCT	Reverse primer ~400bp into <i>ZIP1</i> ORF
O483	ZIP1_C	GAAATCGGAGAAGCAAGATATAACA	Forward primer ~ 500bp from the end of <i>ZIP3</i> ORF
O484	ZIP1_D	AGTCAACATAACTGACCGAAGAAAC	Reverse primer ~350bp downstream of <i>ZIP3</i> ORF
O497	Msh4.F2	AAATTAAGAAAGAAATAAACTCCGACTTCATCGAAAA TTTTGAAGAACGGATCCCCGGGTAAATTAA	Forward primer for C-terminal tagging of Msh4
O498	Msh4.R1	GAAATAATGGATTATAGTTTTAAGCTAAGCGGAAA AGCCAAATTAGAATTCGAGCTCGTTTAAAC	Reverse primer for C-terminal tagging of Msh4
O503	Cdc14.F2	AGCGCCGCCGGTGGTATAAGAAAAATAAGTGGC TCCATCAAGAAACGGATCCCCGGGTAAATTAA	Forward primer for C-terminal tagging of Cdc14
O504	Cdc14_R1	GTAAGTTTTTTTATTATATGATATATATATATAA AAATGAAATAAAGAATTCGAGCTCGTTTAAAC	Reverse primer for C-terminal tagging of Cdc14
O505	Pds1.F2	AGCGAAGAAGGCCTCGATCCTGAAGAACTAGAG GACTTAGTTACTCGGATCCCCGGGTAAATTAA	Forward primer for C-terminal tagging of Pds1
O506	Pds1.R1	TATATACGTGTATATATGTTGTGTGTATGTGAATG AGCAGTGGATGAATTCGAGCTCGTTTAAAC	Reverse primer for C-terminal tagging of Pds1

**Table 2.2 continued.** Oligonucleotides used in this work.

EH oligo no.	Name	Sequence (5' to 3')	Application
O517	CDC14_A	CTAGAACAACAATCACACACACACA	Forward primer ~ 350bp upstream of <i>CDC14</i> ORF
O518	CDC14_B	AAATCCAAATGGAACTGTTGTAAA	Reverse primer ~150bp into <i>CDC14</i> ORF
O519	CDC14_C	CAACAATAATCGTAATCCAACCTTC	Forward primer ~ 300bp from the end of <i>CDC14</i> ORF
O520	CDC14_D	GATTTTAAGATTGGCATATCGAGAA	Reverse primer ~300bp downstream of <i>CDC14</i> ORF
O523	PDS1_A	GTGTATTTGTTAGCGTAGGTTGCTT	Forward primer ~ 250bp upstream of <i>PDS1</i> ORF
O524	PDS1_B	ATAGTCCTAGGCCACCATTTAATTC	Reverse primer ~700bp into <i>PDS1</i> ORF
O525	PDS1_C	GAATTAAATGGTGGCCTAGGACTAT	Forward primer ~ 500bp from the end of <i>PDS1</i> ORF
O526	PDS1_D	TTATGACGAAGTACTTTGAGAACCC	Reverse primer ~250bp downstream of <i>PDS1</i> ORF
O605	NDT80_A	GTGACTTTACATTGTTACTTCCGC	Forward primer ~ 300bp upstream of <i>NDT80</i> ORF
O606	NDT80_B	TCTCTCACTAATTCAAATGGAGGTC	Reverse primer ~200bp into <i>NDT80</i> ORF
O607	NDT80_C	AATATGAAGCAAATCGAACTGAAAC	Forward primer ~ 500bp from the end of <i>NDT80</i> ORF
O608	NDT80_D	TCAAATTATTCACCCAATCTTCATT	Reverse primer ~200bp downstream of <i>NDT80</i> ORF

**Table 2.2 continued.** Oligonucleotides used in this work.

EH oligo no.	Name	Sequence (5' to 3')	Application
O615	CTF19_C	ATTACAATGCCCGGTGAGAG	Forward primer ~ 200bp from the end of <i>CTF19</i> ORF
O616	CTF19_D	CGCATCCCATATCAAAAAGG	Reverse primer ~200bp downstream of <i>CTF19</i> ORF
O630	NDT80_MX.F	TAAAAAGCGCTTAAAATGGATGTCCACGAGGTCT CTATTGCATGTCAAGGCAGCCCCGTACGCTGCA GGTCGAC	Forward primer for amplification of cassettes to replace <i>NDT80</i> ORF
O631	NDT80_MX.R	AAATCATTAGTTTATTTACGGTGTCTCGGTCTCGTAG GCTCAGCATCAAGCACATTAATCGATGAATTCGA GCTCG	Reverse primer for amplification of cassettes to replace <i>NDT80</i> ORF
O634	FPR3_MX4.F	TGAAAGTTCATACATAATTGAAAGCAAGCATCCAA CCAGCCCAATCGTACGCTGCAGGTCGAC	Forward primer for amplification of cassettes to replace <i>FPR3</i> ORF
O635	FPR3_MX4.R	AAAAAGAATAATATATATAAACATCTATCCGTACG AGCGCGTGTAATCGATGAATTCGAGCTCG	Reverse primer for amplification of cassettes to replace <i>FPR3</i> ORF
O636	FPR3_A1	GCTTGCTTCCTCTACCTTTC	Forward primer upstream of <i>FPR3</i> ORF to check correct integration of gene-replacement cassette
O637	FPR3_A4	CTTCACCTTTCTTGACGACC	Reverse primer downstream of <i>FPR3</i> ORF to check correct integration of gene-replacement cassette
O734	LacI_SV40_tac.F	ATGgtgAAAtatGTAACGTTATACG	Forward primer for amplification of LacI sequence

**Table 2.2 continued.** Oligonucleotides used in this work.

EH oligo no.	Name	Sequence (5' to 3')	Application
O735	LacI_SV40_fusion. R	GTCGACCTGCAGCGTACGTTAGGCAACCTTTCTC TTCTTC	Reverse primer for amplification of LacI sequence and for overlapping PCR with <i>HPHMX4</i> fragment
O741	LacI_408_427.F	GGAAGCTGCCTGCACTAATG	Forward primer ~ 400bp into LacI sequence
O742	LacI_758_788,R	ACTCGGTAATGGCGCGCATTG	Reverse primer ~ 800bp into LacI sequence
O743	LacI_1056_1080.R	CTGCCCGCTTTCCAGTCGGGAAACC	Reverse primer ~ 1100bp into LacI sequence
O744	Zip1_LacI_minusS BM	AAATCAAGAAGGGTTCAAATTGCATGAAACCTCC AATTTCTTCAAATGGTGAAATATGTAAACGTTATAC G	Reverse primer for truncation of Zip1 to remove SUMO-binding motif and C-terminal tagging of Zip1 with LacI- <i>HPHMX4</i> fusion PCR product
O745	Zip1_LacI_R	AAATGTATTTCGCACAAAACGATTTCAAATTTTCCA TTATCCTCTAATCGATGAATTCGAGCTCG	Reverse primer for C-terminal tagging of Zip1 with LacI- <i>HPHMX4</i> fusion PCR product
O746	Zip1_LacI_withSB M	GACGAAGACCAGTCATTAAAAATAAGCAAGAAAA GGAGAAGGAAAATGGTGAAATATGTAAACGTTATA CG	Reverse primer for C-terminal tagging of Zip1 with LacI- <i>HPHMX4</i> fusion PCR product
O891	Zip1_C_up	GAATTGGAGCTTGAAGAGCAG	Forward primer to check integration of cassettes made using Zip1_C and Zip1_D

**Table 2.2 continued.** Oligonucleotides used in this work.

EH oligo no.	Name	Sequence (5' to 3')	Application
O892	Zip1_D_down	TGTGGGTTATGCGATCAAGC	Reverse primer to check integration of cassettes made using Zip1_C and Zip1_D
O893	Zip2_C_up	GCATAGCCGTAAATGAAAAC	Forward primer to check integration of cassettes made using Zip2_C and Zip2_D
O894	Zip2_D_down	TATTCGGTGGGTCCTCCATT	Reverse primer to check integration of cassettes made using Zip2_C and Zip2_D
O895	Zip3_C_up	AGCTTCTCTCCAACCCTCTT	Forward primer to check integration of cassettes made using Zip3_C and Zip3_D
O896	Zip3_D_down	GAAGAAAGACACCTTACGCC	Reverse primer to check integration of cassettes made using Zip3_C and Zip3_D

**Table 2.2 *continued*.** Oligonucleotides used in this work.

### 2.1.7. Yeast Strains

**Table 2.3.** Base yeast strains used in this work

EH Strain no.	Strain Background	Ploidy	Genotype
Y636	BR	2N	<i>MATa/MAT<math>\alpha</math> LacO::CEN3/LacO::CEN3 LacI-GFP::URA3/LacI-GFP::URA3 ura3/ura3 CTF19-13MYC:KANMX4/CTF19-13MYC:KANMX4</i>
Y1291	BR	1N	<i>CTF19-13MYC::KANMX4, his4-260, leu2-3, ade2-1, trp1-289, thr1-4, ura3-1, MATa</i>
Y1292	BR	1N	<i>CTF19-13MYC::KANMX4, his4-260, leu2-3, ade2-1, trp1-289, arg4-1, ura3-1, MAT<math>\alpha</math></i>
Y1293	BR	2N	Diploid of Y1291 and Y1292
Y713	S288C	1N	<i>MATa his3 leu2, 112 lys2BgIII CEN5-lacO-LEU2 P<sub>CYC1</sub>LacI-GFP-HIS3 ilv1 (S. carlsbergensis chromosome V)</i>
Y714	S288C	1N	<i>MAT<math>\alpha</math> his3 leu2, 112 lys2BgIII CEN5-lacO-LEU2 P<sub>CYC1</sub>LacI-GFP-HIS3 ilv1 (S. cerevisiae chromosome V)</i>
Y712	S288C	2N	Diploid of Y713 and Y714
Y957	SK1	1N	<i>his3::hisG, leu2::hisG, ADE1, trp1::hisG, MET13, lys2, ura3, ho::L YS2, MAT<math>\alpha</math></i>
Y958	SK1	1N	<i>his3::hisG, leu2::hisG, ADE1, trp1::hisG, MET13, lys2, ura3, ho::L YS2, MATa</i>
Y1381	SK1	2N	Diploid of Y957 and Y958
Y965	SK1	1N	<i>his3::hisG, leu2::hisG, ADE1, trp1::hisG, MET13, lys2, ura3, ho::L YS2, Estrogen Receptor-GAL4::URA3, pGAL1-NDT80::TRP1, MATa</i>

EH Strain no.	Strain Background	Ploidy	Genotype
Y966	SK1	1N	<i>his3::hisG, leu2::hisG, trp1::hisG, lys2, ura3, ho::LYS2, Estrogen Receptor-GAL4::URA3, pGAL1-NDT80::TRP1, MAT<math>\alpha</math></i>
Y1602	SK1	2N	Diploid of Y965 and Y966
Y128	Y55	1N	<i>his4::HhaI, leu2-r, met13-2, lys2-d, ura3-1,, BIK1-Pvull, MAT<math>\underline{a}</math></i>
Y256	Y55	1N	<i>his4::HhaI, leu2-r, met13-2, lys2-d, ura3-1,, BIK1-Pvull, MAT<math>\alpha</math></i>
Y650	Y55	2N	Diploid of Y128 and Y256

**Table 2.3 continued.** Base yeast strains used in this work.

**Table 2.4.**Yeast strains used in this work.

EH Strain no.	Strain Background	Ploidy	Genotype
Y644	BR	2N	As Y636, but <i>msh4::ADE2</i> / <i>msh4::ADE2</i>
Y859	BR	2N	As Y636, but <i>zip1::NATMX4</i> / <i>zip1::NATMX4</i> and <i>msh4::ADE2</i> / <i>msh4::ADE2</i>
Y860	BR	2N	As Y636, but <i>zip1::NATMX4</i> / <i>zip1::NATMX4</i>
Y861	BR	2N	As Y636, but <i>zip2::HPHMX4</i> / <i>zip2::HPHMX4</i> and <i>msh4::ADE2</i> / <i>msh4::ADE2</i>
Y862	BR	2N	As Y636, but <i>zip2::HPHMX4</i> / <i>zip2::HPHMX4</i>
Y1136	BR	2N	As Y1293, but <i>spo11::ADE2</i> / <i>spo11::ADE2</i>
Y1185	BR	2N	As Y1136, but <i>zip1::NATMX4</i> / <i>zip1::NATMX4</i>
Y1188	BR	2N	As Y1136, but <i>zip2::HPHMX4</i> / <i>zip2::HPHMX4</i>
Y1266	BR	2N	As Y1136, but <i>zip3::HPHMX4</i> / <i>zip3::HPHMX4</i>
Y1269	BR	2N	As Y1293, but <i>zip2::HPHMX4</i> / <i>zip2::HPHMX4</i>
Y1274	BR	2N	As Y1293, but <i>zip3::HPHMX4</i> / <i>zip3::HPHMX4</i>
Y1350	BR	2N	As Y1293, but <i>msh4::ADE2</i> / <i>msh4::ADE2</i> and <i>zip3::HPHMX4</i> / <i>zip3::HPHMX4</i>
Y2248	BR	2N	As Y1293, but <i>msh4::NATMX4</i> / <i>msh4::NATMX4</i> and <i>zip2::HPHMX4</i> / <i>zip2::HPHMX4</i>
Y2251	BR	2N	As Y1293, but <i>msh4::HPHMX4</i> / <i>msh4::HPHMX4</i>

EH Strain no.	Strain Background	Ploidy	Genotype
Y2064	BR	2N	As Y1293, but <i>MSH4-GFP::KANMX6 / MSH4-GFP::KANMX6</i>
Y787	S288C	2N	As Y712, but <i>ZIP1::KANMX6 / ZIP1::KANMX6</i>
Y784	S288C	2N	As Y712, but <i>MAD3::NATMX4 / MAD3::NATMX4</i>
Y790	S288C	2N	As Y712, but <i>MSH4::KANMX6 / MSH4::KANMX6</i>
Y813	S288C	2N	As Y712, but <i>ZIP2::HPHMX4 / ZIP2::HPHMX4</i>
Y983	S288C	2N	As Y712, but <i>ZIP1::KANMX6 / ZIP1::KANMX6</i> and <i>ZIP2::HPHMX4 / ZIP2::HPHMX4</i>
Y1010	S288C	2N	As Y712, but <i>ZIP3::KANMX6 / ZIP3::KANMX6</i>
Y1133	S288C	2N	As Y712, but <i>ZIP4::KANMX6 / ZIP4::KANMX6</i>
Y1155	S288C	2N	As Y712, but <i>MAD3::NATMX4 / MAD3::NATMX4</i> and <i>ZIP1::KANMX6 / ZIP1::KANMX6</i>
Y1476	S288C	2N	As Y712, but <i>pCLB2-3HA-MAD2::KANMX6 / pCLB2-3HA-MAD2::KANMX6</i>
Y2116	S288C	2N	As Y712, but <i>ZIP1-SBMΔ-LACI::HPHMX4 / ZIP1::KANMX6</i>
Y2117	S288C	2N	As Y712, but <i>ZIP1--LACI::HPHMX4 / ZIP1::KANMX6</i>
Y2172	S288C	2N	As Y712, but <i>MER3::HPHMX4 / MER3::HPHMX4</i>
Y2502	S288C	2N	As Y712, but <i>PPH3::HPHMX4 / PPH3::HPHMX4</i>

**Table 2.4 continued.** Yeast strains used in this work

EH Strain no.	Strain Background	Ploidy	Genotype
Y1538	SK1	2N	As Y1602, but <i>pCLB2-3HA-IPL1::KANMX6 / pCLB2-3HA-IPL1::KANMX6</i>
Y2121	SK1	2N	As Y1381, but <i>ZIP1-TAP::klURA3 / ZIP1-TAP::klURA3</i>
Y750	Y55	2N	As Y650, but <i>ZIP2::KANMX6 / ZIP2::KANMX6</i> and <i>MSH4::KANMX6 / MSH4::KANMX6</i>
Y1465	Y55	2N	As Y650, but <i>MSH4::KANMX6 / MSH4::KANMX6</i>
Y1571	Y55	2N	As Y650, but <i>ZIP2::KANMX6 / ZIP2::KANMX6</i>
Y1789	Y55	2N	As Y650, but <i>ZIP3::KANMX6 / ZIP3::KANMX6</i>
Y1792	Y55	2N	As Y650, but <i>MSH4::KANMX6 / MSH4::KANMX6</i> and <i>ZIP3::KANMX6 / ZIP3::KANMX6</i>
Y1815	Y55	2N	As Y650, but <i>NDT80::HPHMX4 / NDT80::HPHMX4</i>
Y1816	Y55	2N	As Y650, but <i>NDT80::HPHMX4 / NDT80::HPHMX4</i> and <i>MSH4::KANMX6 / MSH4::KANMX6</i>
Y1841	Y55	2N	As Y650, but <i>MSH4::HPHMX4 / MSH4::HPHMX4</i> and <i>FPR3::KANMX6 / FPR3::KANMX6</i>

**Table 2.4 continued.** Yeast strains used in this work

### 2.1.8. Plasmids

**Table 2.5.** Plasmids used in this work.

pEH plasmid no.	Other Name	Description	Source
pEH89	pAG25	For amplification of <i>NATMX4</i> cassette	Yeast 15: 1541-1553
pEH90	pAG32	For amplification of <i>HPHMX4</i> cassette	Yeast 15: 1541-1553
pEH95	pAFS6a	Contains <i>GFP(S65T)::KANMX6</i> for amplification of C-terminal tagging cassettes.	Longtine <i>et al.</i> (1998) Yeast <b>14</b> . 953-961
pEH96	pAFS6a	Contains <i>GFP(S65T)::TRP1</i> for amplification of C-terminal tagging cassettes.	Longtine <i>et al.</i> (1998) Yeast <b>14</b> . 953-961
pEH97	pAFS6a	Contains <i>GFP(S65T)::HIS3MX6</i> for amplification of C-terminal tagging cassettes.	Longtine <i>et al.</i> (1998) Yeast <b>14</b> . 953-961
pEH98	pAFS6a	Contains <i>3HA::KANMX6</i> for amplification of C-terminal tagging cassettes.	Longtine <i>et al.</i> (1998) Yeast <b>14</b> . 953-961
pEH101	pAFS6a	Contains <i>13Myc::KANMX6</i> for amplification of C-terminal tagging cassettes.	Longtine <i>et al.</i> (1998) Yeast <b>14</b> . 953-961
pEH110	pAFS6a	Contains <i>pGAL1-3HA::KANMX6</i> for amplification of N-terminal tagging and promoter replacement cassettes.	Longtine <i>et al.</i> (1998) Yeast <b>14</b> . 953-961
pEH137	pMR1591	<i>KAR1Δ13</i> loop in-loop out plasmid.	Vallen <i>et al.</i> (1992) Journal of Cell Biology <b>117</b> . 1277-1287
pEH170	pAFS6a	As pEH110, but <i>pSCC1</i> instead of <i>pGAL1</i>	Angelika Amon
pEH172	pAFS6a	For amplification of <i>KANMX4</i> cassette	Yeast 15: 1541-1553

pEH plasmid no.	Other Name	Description	Source
pEH188	pAFS6a	As pEH110, but <i>pCLB2</i> instead of <i>pGAL1</i>	Angelika Amon
pEH283	pAFS52	<i>LacO</i> (256 repeats), integrates at <i>TRP1</i>	Lacefield & Murray (2008) Nature Genetics <b>39</b> (10) 1273 - 1277
pEH284	pAFS152	<i>pCYC1-LacI<sub>2</sub></i> , integrates at <i>URA3</i>	Lacefield & Murray (2008) Nature Genetics <b>39</b> (10) 1273 - 1277
pEH285	pSLB8	<i>PCYC1-LacI<sub>4</sub></i> , integrates at <i>URA3</i>	Lacefield & Murray (2008) Nature Genetics <b>39</b> (10) 1273 - 1277

**Table 2.5 continued.** Plasmids used in this work.

## **2.2. Methods**

### **2.2.1. Bacterial Methods**

#### **2.2.1.1. Growth conditions**

Cells were grown at 37 °C in Luria Broth (Section 2.1.1.1.). For liquid cultures cells were grown overnight at 37 °C shaking at 180 rpm. STBL2 cells (Invitrogen) bearing *LacO* repeat-containing plasmids were grown to stationary phase in SOC media at 30 °C.

#### **2.2.1.2. Plasmid extractions**

Plasmids were extracted from DH5 $\alpha$  cells using a QIAprep Spin Miniprep kit as described in manufacturer's instructions.

#### **2.2.1.3. Preparation of chemically competent DH5 $\alpha$ cells**

A single colony of *E. coli* DH5 $\alpha$  cells was inoculated into 50 ml of LB and grown overnight in a shaking incubator at 37 °C and 180 rpm. Cells were then diluted 100-fold into 400 ml LB and grown to an OD<sub>590</sub> of 0.375 at which point 50 ml aliquots were taken and chilled on ice for 15 minutes. Following this, cells were centrifuged at 3500 rpm at 4 °C for 10 minutes and pellets were resuspended in 10 ml of pre-chilled CaCl<sub>2</sub> solution (60 mM CaCl<sub>2</sub>, 15% glycerol, 10 mM PIPES, pH 7.0). Cells were centrifuged once more at 2500 rpm at 4 °C for 5 minutes and cell pellets were resuspended in 10 ml of pre-chilled CaCl<sub>2</sub> solution. Cell suspensions were dispensed into 400  $\mu$ l aliquots and snap-frozen in liquid nitrogen.

#### **2.2.1.4. Transformation of chemically competent DH5 $\alpha$ cells**

Aliquots of chemically competent DH5 $\alpha$  cells were thawed on ice in the cold room. Once thawed, 100  $\mu$ l of cell suspension was transferred to a pre-chilled polypropylene tube for each transformation reaction. Using a pre-chilled pipette tip, 10 ng (in around 10-30  $\mu$ l volume) of plasmid DNA was added to the cell suspension, gently mixed with a pipette tip and left on ice for 20 minutes in the cold room. The cells were then placed in a 42 °C water bath for 45 seconds and then placed on ice for a further 2 minutes. 500  $\mu$ l of LB medium (minus drug) was added to the cell suspension and incubated at 37 °C for 1 hour. Cells were plated on LB agar plates containing the appropriate drug for selection of cells harbouring the plasmid. Plates were incubated overnight at 37 °C.

#### **2.2.1.5. Transformation of STBL2 cells**

Transformation of STBL2 cells was carried out as instructed by the accompanying information supplied with the cells by Invitrogen (Cat. No. 10268-019).

#### **2.2.1.6. Storage of bacterial strains**

For long-term storage of bacterial strains, cells were grown overnight in 5 ml LB. The following day, cells were spun down, re-suspended in 1 ml 30% glycerol and transferred to a 1.5 ml screw-top tube. Tubes were then frozen and stored at -80 °C. For short-term storage, cells were kept on LB plates at 4 °C.

## **2.2.2 Yeast Growth Conditions**

### **2.2.2.1. Vegetative growth conditions**

For growth of yeast cells in liquid media, a single colony was inoculated into ~50 ml YPD (see section 2.1.1.2) for growth in a shaking 30 °C incubator until cells had reached the appropriate OD<sub>600</sub>. For growth on solid media, cells were streaked onto the appropriate agar media and incubated at 30 °C overnight. For growth of single colonies/spore germination, plates were left in the incubator for 2 days.

### **2.2.2.2. Sporulation conditions**

Prior to sporulation, diploid cells were streaked onto YEPEG medium (section 2.1.1.2). A single colony was inoculated into 50 ml YEPD medium and incubated overnight in a 30 °C shaking incubator set to 180 rpm. The following day when cells had grown to saturation they were inoculated into pre-sporulation media at a starting OD<sup>600</sup> of ~ 0.2. For S288C strains, the pre-sporulation media used was YPA (1% yeast extract, 2% bacto-peptone, 2% potassium acetate pH 7.0), for SK1 and Y55 strains, SPS media (0.5% yeast extract, 1% peptone, 0.17% yeast nitrogen base, 1% potassium acetate, 0.5% ammonium sulfate, 0.05M potassium hydrogen phthalate, pH 5.5) was used. When cultures reached a density of 4-5 × 10<sup>7</sup> cells/ml, cells were spun down at 3500 rpm and washed in pre-warmed sporulation media (S288C: 2% KAc + 0.02% raffinose + 0.01% Antifoam 204 (Sigma), pH 7.0 and 1% KAc + 0.02% raffinose + 0.01% Antifoam 204 (Sigma), pH 7.0 for SK1 and Y55 strains). Finally, cells were inoculated into the same volume of pre-warmed sporulation media as they were grown in pre-sporulation media and

incubated in a shaking (250 rpm) incubator at the appropriate temperature. BR strains were inoculated directly from overnight cultures of YEPD to 2% KAc + 0.01% Antifoam 204 (Sigma), pH 7.0. Cells were then harvested at the appropriate time point(s) for analysis. Sporulation was carried out at 30 °C unless otherwise stated. For sporulation on solid media, cells were replica plated directly from a YEPD plate to a KAc-COM plate and incubated at 30 °C. Tetrads were formed by 3 days of incubation.

### **2.2.3. Yeast Strain Construction**

#### **2.2.3.1. Transformation of yeast cells**

Yeast cells were transformed using the lithium acetate procedure (Gietz and Schiestl, 2007; Gietz et al., 1995). Cells to be transformed were grown overnight in 50 ml YEPD medium and then diluted 25-fold into fresh YEPD the following morning. Cultures were grown for 3-4 hours and then harvested by centrifugation at 2000 rpm for 3 minutes. Cell pellets were then washed twice in 10ml of 100 mM LiAc and the final cell pellet was resuspended in 1ml 100 mM LiAc and transferred to a sterile 1.5ml Eppendorf tube. Cells were centrifuged for 30 seconds in a bench-top centrifuge (Eppendorf 5415D) set to 13,000rpm and cell pellets were resuspended in 250 µl LiAc. 50 µl of this cell suspension was aliquoted into separate sterile 1.5 ml Eppendorf tubes for each transformation reaction. These tubes were centrifuged for 30 seconds in a bench-top centrifuge (Eppendorf 5415D) set to 13,000rpm and the supernatant was removed. The following reagents were layered onto the cell pellets in the order 240 µl 50% (w/v) PEG-

3500, 36  $\mu$ l 1M LiAc, 50  $\mu$ l boiled salmon sperm DNA and  $\sim$ 1  $\mu$ g DNA in a volume of  $\sim$  50  $\mu$ l (or 50  $\mu$ l sterile dH<sub>2</sub>O for the negative control). Cells were then gently mixed with the layered reagents using a pipette tip and left at 30 °C for 30 minutes. Following this, the tubes containing the cells/transformation mix were transferred to a 42 °C water bath for 20 minutes (SK1), 30 minutes (S288C, BR) or 40 minutes (Y55) after which 1 ml of sterile distilled H<sub>2</sub>O was added to the tubes and cells were centrifuged at 4000 rpm in a bench-top centrifuge (Eppendorf 5415D). When selecting for prototrophy, cell pellets were resuspended in 500  $\mu$ l dH<sub>2</sub>O and 250  $\mu$ l was plated onto each plate containing the appropriate drop out media. When selecting for drug-resistance, cell pellets were resuspended in YEPD (minus drugs) and left in a shaking 30 °C incubator for 3 hours. Cells were then centrifuged at 4000 rpm for 1 minute and resuspended in 500  $\mu$ l dH<sub>2</sub>O and 250  $\mu$ l was plated onto YEPD plates containing the appropriate drug selection. Plates were incubated at 30 °C for 3 days for growth of transformants.

#### **2.2.3.2. PCR-based gene deletion**

Gene deletion cassettes were made by PCR-based amplification of drug-resistance genes from a plasmid vector (*NATMX4*, *HYGMX4* and *KANMX6* genes, see Table 2.5) with flanking regions of  $\sim$ 45 bp homology to the intended site of integration (Longtine et al., 1998). This is achieved through designing primers to include the 45 bp flanking regions of homology. Correct integration of the gene-deletion cassette was checked by performing PCR using primers that flank the junction between upstream/downstream sequences and the gene-deletion cassette (Figure 2.1 and (Longtine et al., 1998).

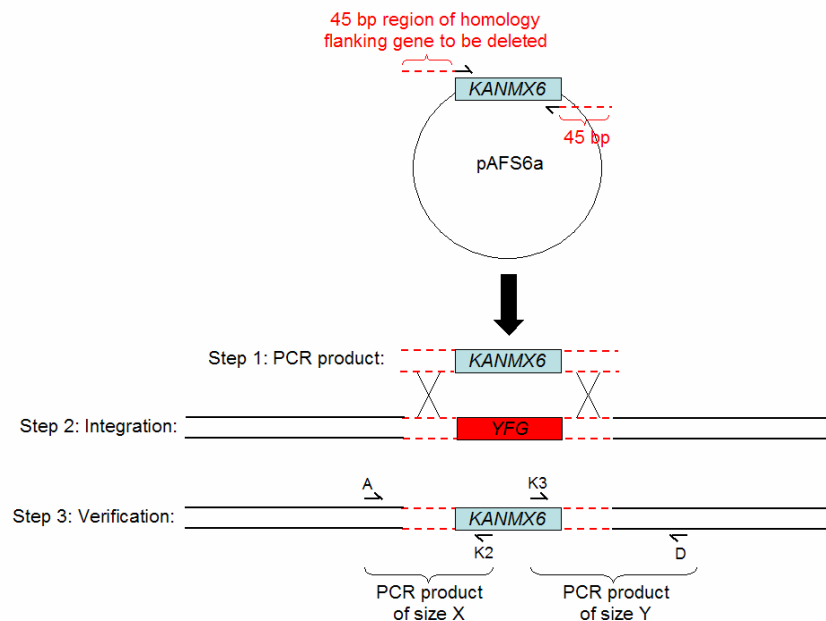


**Figure 2.1. PCR-based gene-deletion.** A gene deletion cassette is amplified by PCR using primers that anneal upstream and downstream of the selectable marker (light blue box). These primers have 45 bp ‘tails’ homologous to the desired site of cassette integration (red dotted lines). Integration of the cassette was achieved through homologous recombination. Correct integration of the deletion cassette was assessed by PCR using primers flanking the integration sites and recovery of a DNA fragment of the correct size. Red box denotes gene to be deleted (“YFG” represents your favourite gene).

#### 2.2.3.3. PCR-based promoter replacement

Promoter-replacement cassettes were made by PCR-based amplification of the desired promoter together with a drug-resistance gene and an N-terminal protein tag from a plasmid vector (see table 2.5 for different vectors) with flanking regions of ~45 bp homology to the intended site of integration (Longtine et al., 1998).

Primers were designed so that the gene’s native promoter was replaced by the promoter on the cassette. Correct integration of the promoter-replacement cassette was checked by performing PCR using primers that flank the junction between

upstream/downstream sequences and the cassette (Figure 2.2 and (Longtine et al., 1998) and by Western blotting of the tagged protein.

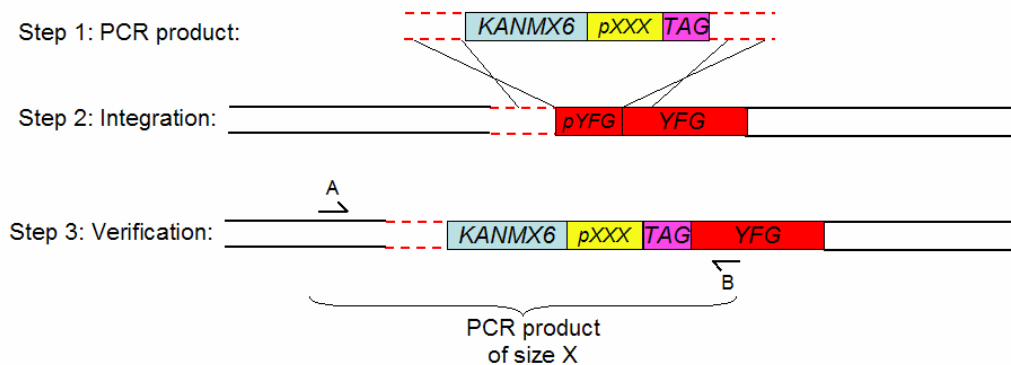


**Figure 2.2. Diagram outlining PCR-based promoter replacement.** A promoter-replacement cassette comprises a selectable marker (light blue box), a promoter (yellow box) and an N-terminal protein tag (purple box). A cassette was amplified by PCR using primers that anneal upstream of the selectable marker and downstream of the tag. These primers have 45 bp ‘tails’ that are homologous to the desired site of cassette integration (red dotted lines). Integration of the cassette was achieved through homologous recombination. Correct integration of the promoter cassette was assessed by PCR using primers flanking the integration sites and recovery of a DNA fragment of the correct size (Longtine et al., 1998). Red box denotes gene whose promoter is replaced. “YFG” represents Your Favourite Gene. pXXX represents the promoter that replaces the native gene promoter. “TAG” represents the sequence encoding the protein tag.

#### 2.2.3.4. PCR-based C-terminal gene tagging

C-terminal tagging cassettes were made by PCR-based amplification of the desired C-terminal tag together with a drug-resistance gene from a plasmid vector (see table 2.5 for different vectors) with flanking regions of ~45 bp homology to the intended site of integration. Primers were designed so that the site of cassette integration was immediately upstream of the stop codon of the gene. Correct integration of the C-terminal gene tagging cassette was checked by performing

PCR using primers that flank the junction between the cassette and downstream sequences (Figure 2.3 and (Longtine et al., 1998) and by western blotting of the tagged protein.

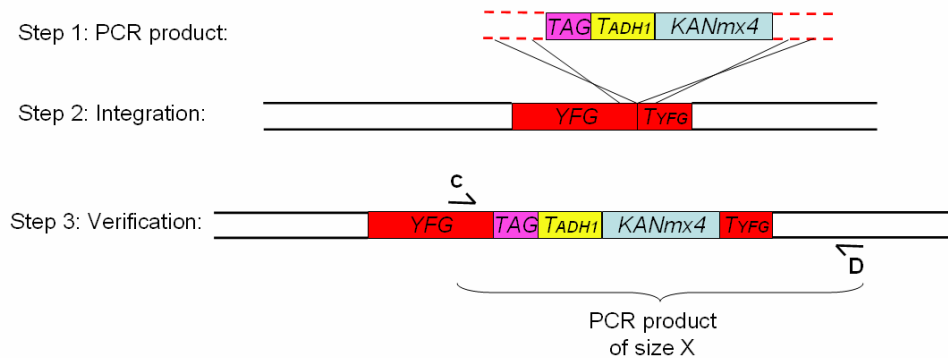


**Figure 2.3. Diagram outlining PCR-based C-terminal gene tagging.** A C-terminal gene tagging cassette comprises a C-terminal protein tag (purple box), an *ADH1* terminator sequence (yellow box) and a selectable marker (light blue box). A cassette is amplified by PCR using primers that anneal upstream of the tag sequence and downstream of the selectable marker. These primers have 45 bp ‘tails’ homologous to the desired site of cassette integration (red dotted lines). Integration of the cassette is achieved through homologous recombination. Correct integration of the tagging cassette is assessed by PCR using primers flanking the integration sites and recovery of a DNA fragment of the correct size. Red box denotes gene to be tagged. “YFG” represents **Y**our **F**avourite **G**ene. “T<sub>ADH1</sub>” represents the terminator sequence of *ADH1*. “TAG” represents the sequence encoding the protein tag.

### 2.2.3.5. Genetic crosses

Genetic crosses were performed by thoroughly mixing two haploid strains on a YEPD plate using a wooden dowel/toothpick. Cells were left to mate for 5 hours in a 30 °C incubator after which, cells were replica-plated onto KAc-COM (2% KAc and 0.0875% w/v COM powder, pH 7.0, Section 2.1.1.2) and incubated at 30 °C. After 3 days, sporulation was assessed by taking a small amount of cells from the sporulation plate and looking for tetrad formation under the light microscope. When sporulation was complete cells were taken from the plate using a wooden dowel

and placed in a 1.5 ml Eppendorf tube containing 100 µl dissecting buffer (10 mM EDTA, 1M Sorbitol and 10mM NaH<sub>2</sub>PO<sub>4</sub>) with 5 µl of 10 mg/ml Zymolyase (20T). Cells were incubated at 37 °C for 30 minutes and then 400 µl of dissecting buffer was added. Samples were then either used straight away or stored at 4 °C for no longer than a month. Tetrad dissection was achieved by streaking zymolyase-treated tetrads onto a dissection plate (YEPD plate poured on a flat surface) and using a Nikon Eclipse 50i microscope and micromanipulator to separate each ascospore from within a tetrad. Spores were incubated at 30 °C to germinate for 3 days and then replica-plated onto the appropriate media for selection of markers.

#### **2.2.3.6. Diploid isolation**

Diploids were obtained by thorough mixing of two haploid strains on a YEPD plate and incubation for a minimum of 5 hours at 30 °C. For SK1 strains, mated strains were streaked onto a fresh YEPD plate for single colonies and incubated at 30 °C for two days. Owing to the morphological differences of diploid and haploid SK1 cells, diploid candidates (characterised by growth of a 'smooth' colony) were picked for screening. For S288C, BR and Y55 strains, zygotes were picked using a micromanipulator microscope (as outlined in section 2.2.3.5). Diploid candidates were screened by replica plating to sporulation plates or mating tester strains (failure of the candidate to mate with either tester strain indicates that the candidate is diploid).

#### **2.2.3.7. Storage of yeast strains**

For long-term storage of yeast strains, cells were grown overnight in 5 ml YEPD. The following day, cells were spun down, resuspended in 1 ml 30% glycerol and transferred to a 1.5 ml screw-top tube. Tubes were then frozen and stored at -80 °C. For short-term storage, cells were kept on agar plates at 4 °C.

#### **2.2.4. Cytological Methods**

##### **2.2.4.1. Assessment of nuclear divisions using DAPI**

500 µl samples were harvested from sporulation cultures at the appropriate time points and placed in sterile 1.5 ml Eppendorf tubes. Samples were centrifuged in a bench-top centrifuge (Eppendorf 5415D) at 4000 rpm and cell pellets were resuspended in 100% ethanol. Samples were stored at 4 °C until ready to be processed. Samples were processed by centrifugation in a bench-top centrifuge at 4000 rpm, removal of the supernatant and addition of 20 µl DAPI-mount solution (1 mg/ml p-phenylenediamin in 10% v/v PBS and 90% v/v glycerol and DAPI 1 µg/ml). 5 µl of DAPI-stained cells were applied to a glass slide and a 22 x 22 mm<sup>2</sup> cover slip was added. Nuclei were visualised using the DAPI filter on the Nikon Eclipse 50i microscope.

##### **2.2.4.2. Sporulation counts**

Sporulation counts were carried out by taking 10 µl sporulation media after an appropriate time for sporulation to have occurred, applied to a glass slide and covered with a 22 x 22<sup>2</sup> mm cover slip. Cells were visualised using a light

microscope and the proportion of total cells that had formed tetrads were counted. >100 cells were counted to obtain a sporulation frequency.

#### **2.2.4.3. Visualisation of GFP in tetrads and live cells**

For visualisation of GFP in live cells or tetrads 500 µl of sporulation culture was harvested and placed in a sterile 1.5 ml Eppendorf tube. Samples were centrifuged at 4000 x g in a bench-top centrifuge (Eppendorf 5415D) for 1 minute and the supernatant was discarded. Cell pellets were resuspended in 20 µl PBS and 5 µl of cell suspension was applied to a glass slide and covered by a 22 x 22<sup>2</sup> mm cover slip. Cells were visualised using the transmitted light on a Nikon Eclipse 50i microscope and GFP was visualised using the fluorescent FITC filters.

#### **2.2.4.4. *In situ* immunofluorescence of fixed cells**

8 ml of sporulation culture was harvested at the appropriate time point and placed into a 14 ml round-bottomed polypropylene tube (Falcon). Formaldehyde was added to a final concentration of 4% and cells were left for up to 1 hour at room temperature. 2 ml of SKP solution (1.2 M sorbitol, 50 mM KPO<sub>4</sub> pH 7.0) was added and cells were centrifuged at 3500 rpm for 3 minutes. This was repeated twice to ensure removal of all of the formaldehyde. Following the third spin, the cell pellets were resuspended in 100 µl SKP and transferred to a 1.5 ml Eppendorf tube. To this, 2 µl of 1M DTT and 10 µl of 10 mg/ml zymolyase (100T) were added and tubes were incubated at 37 °C until spheroplasting was complete. Spheroplasting was assessed by mixing 2 µl of cell suspension with 2 µl distilled H<sub>2</sub>O on a glass slide and observing the cells under a light microscope.

Spheroplasting is complete when cells lose their dark 'halo' and some cells burst. 100 µl of PBS was added to the spheroplast solution and tubes were centrifuged for 1 minute at 4000 rpm in a bench-top centrifuge (Eppendorf 5415D). Cell pellets were then gently resuspended in 67 µl PBS + 0.1% NP40 and left at room temperature for 30 minutes. 33 µl fetal bovine serum (FBS) was added followed by the appropriate dilutions of primary antibodies (section 2.1.5). Cells were incubated with the primary antibodies overnight at 4 °C. The following day, cells were washed gently three times in 100 µl PBS and after the last wash, cell pellets were gently resuspended in 100 µl PBS + 4% BSA with the appropriate dilutions of secondary antibodies (section 2.1.5). Cells were incubated in the dark at room temperature for 2 hours and then washed three times in PBS. 50 µl of DAPI mount solution (1 mg/ml p-phenylenediamin in 10% v/v PBS and 90% v/v glycerol) containing DAPI (1 µg/ml mount), was used to resuspend the cells and ~20 µl was dispensed onto a 22 x 50 cover slip (Menzel-Glaser) balanced on an Eppendorf rack. A Superfrost<sup>®</sup> microscope slide (Thermo Scientific) pre-cleaned in ethanol was added face-down to the cover slip and immediately rotated 180°. The cover slip was sealed to the slide with clear nail varnish.

#### **2.2.4.5. Preparation and immuno-staining of chromosome spreads**

4 - 8 ml of sporulation culture was harvested at the appropriate time point and placed into a 14 ml round-bottomed polypropylene tube. Cells were centrifuged at 4000 rpm for 5 minutes and cell pellets were resuspended in 500 µl KAc-Sorbitol (2% KAc, 1 M Sorbitol, pH 7.0) to which 5 µl 1M DTT were added as well as 12 µl zymolyase (100T, 10 mg/ml). Cells were incubated in a roller-drum incubator at 30

°C for 30 min (BR, S288C & Y55 strains) or 10-15 minutes (SK1 strains). Tubes were then placed on ice while spheroplasting was assessed (see Section 2.2.4.4). Once spheroplasting was complete, 2 ml of cold (4 °C) MES-Sorbitol (0.1 M MES, 1 mM EDTA, 0.5 mM MgCl<sub>2</sub>, 1 M sorbitol) was added and the spheroplasts were centrifuged at 1100 rpm (271 x g). The supernatant was carefully decanted and the tube was drained by briefly upturning it on a piece of tissue. 50 µl chilled MES solution (0.1M MES, 1 mM EDTA, 0.5 mM MgCl<sub>2</sub>, pH 6.4) was added to the side of the tube and then flicked gently to mix with the spheroplasts in the pellet. The tube was flicked for no longer than 10 seconds after which 100 µl of chilled 4% para-formaldehyde (pH 8.5) was added and gently pipetted up and down 8 times. 50 µl of cell suspension was dispensed onto a 22 x 50 cover slip (Menzel-Glaser) balanced on an Eppendorf rack. An upturned Superfrost® Slide (Thermo Scientific) that had been pre-cleaned in ethanol was added to the cover slip and immediately rotated 180°. Slides were left for 1 hour at room temperature and then cover slips were washed off using 0.4% Photo-Flo 200 (KODAK) solution (made up in PBS). Slides were left to air-dry for at least an hour. Primary antibodies were applied to a fresh 22 x 50 cover slip diluted in 50 µl of 1 part FBS: 2 parts PBS-4% BSA to which the air-dried slides were placed face-down and again rotated 180°. Slides were kept in a 'humidity chamber' overnight at 4 °C and the following day, the cover slips were removed and the slides were washed for 5 minutes in PBS. This was repeated 3 times in total. Secondary antibodies were applied to a fresh 22 x 50 cover slip diluted in 50 µl of PBS-4% BSA to which the slides were placed face-down and rotated 180°. Slides were placed in a humidity chamber and incubated for 2 hours in the dark, at room temperature. Cover slips were then removed and

the slides were washed for 5 minutes in PBS as before. The slides were then mounted with DAPI-Mount solution (1 mg/ml p-phenylenediamin in 10% v/v PBS and 90% v/v glycerol) and DAPI (1 µg/ml mount), a fresh cover slip was added and the edges sealed with nail varnish.

#### **2.2.4.6. Image capture**

Images were captured using a Deltavision IX70 system (Applied Precision) using the accompanying *softWoRx* software, and an Olympus Plan Apo 100× 1.4 numerical aperture objective lens. Emission and excitation filters for DAPI (DAPI-5060B, FF01-387/11-25 and FF409-Em02-25), FITC (FITC-3540B, FF506-Ex04-25 and FF506-Em02-25), Texas Red (TXRED-4040B, FF593-Ex03-25 and FF593-Em02-25), and Cy5 (Cy5-4040A, FF660-Ex03-25 and FF660-Em02-25) were obtained from Semrock. The ranges of excitation wavelengths for each filter set are, DAPI (350 nm to 410 nm), FITC (465 nm to 500 nm), Texas red (542 nm to 582nm) and Cy5 (608 nm to 648nm). Images were captured by a 12-bit CoolSnap HQ CCD camera (Roper Scientific) and deconvolved using the proprietary constrained iterative deconvolution algorithm until the standard residual,  $r$ , was  $<0.02$ . The exposure times of the camera were optimised for each channel to allow detection of ~3000 – 3600 counts on the 12-bit CoolSnap HQ CCD camera (Roper Scientific). The *softworx* software was used to take Z-stack images (set at 0.2 µm increments) and to do 2D-projections of such images.

## 2.2.5. DNA Methods

### 2.2.5.1 General PCR

PCR-based DNA amplification was used for the amplification of cassettes for gene tagging/gene deletion and for verification of cassette integration (see Figures 2.1, 2.2 and 2.3). For PCR reactions not requiring a stringent proof-reading activity, 1 unit of *Taq* polymerase (Abgene) was used per 20  $\mu$ l PCR reaction. The accompanying buffer contained 45 mM Tris-HCL pH 8.8, 11mM ammonium sulphate, 4.5 mM  $MgCl_2$ , 6.7 mM  $\beta$ -mercaptoethanol, 4.4  $\mu$ M EDTA, 113  $\mu$ g/ml BSA and 1 mM of each dNTP. This buffer was used in an 11.1  $\times$  dilution. Primers were diluted 100-fold to a final concentration of 1  $\mu$ M. 50 – 250ng of template DNA was used in a volume of 1  $\mu$ l per 20  $\mu$ l reaction. Volumes were made up to 20  $\mu$ l with  $dH_2O$ . All PCR reactions were performed using an Eppendorf Mastercycler RP-Gradient with the following standard program:

Step 1: 95 °C for 3 minutes

Step 2: 35 cycles of;

95 °C for 30 seconds

50 – 60 °C (subject to the  $T_m$  of each primer pair)

72 °C for 1minute/kb

Step 3: 72 °C for 10 minutes

Step 4: Hold at 14 °C

Alternatively, for PCR reactions that required a polymerase with a stringent high level of proof-reading activity, KOD Hotstart DNA Polymerase (Novagen) was used. PCR was performed as per manufacturer's instructions.

#### **2.2.5.2. Genomic DNA extraction (yeast)**

Cells were grown overnight in 14 ml polypropylene tubes containing 5 ml YEPD and were centrifuged at 3500 rpm for 3 minutes. Cell pellets were resuspended in 1 ml sterile dH<sub>2</sub>O and were transferred to 1.5 ml Eppendorf tubes. Tubes were centrifuged for 1 minute at 13,000 rpm in a bench-top centrifuge (Eppendorf 5415D), supernatant was discarded and cell pellets were resuspended in 500 µl 1M sorbitol. 15 µl of 1 M DTT and 8 µl of zymolyase (100T, 10mg/ml) was added to the cell suspension and placed in a shaking incubator set to 37 °C for 1 hour. After this, 200 µl TE and 70 µl 10% SDS were added to each tube and incubated in a 65°C water bath for 10 minutes. 320 µl 5M KAc was added to each tube, inverted six times and left on ice for 30 minutes. Tubes were then spun at 13,000 rpm in a bench-top centrifuge for 6 minutes and 650 µl of the resulting supernatant was added to a fresh 2ml Eppendorf tube containing 1 ml isopropanol and 200 µl 5M ammonium acetate and inverted 6 times. Each 2 ml tube was then spun down in a bench-top centrifuge at 4000 rpm for 1 minute, the supernatant was discarded and the pellets were dried in a vacuum. 300 µl TE was added to the pellets with 10 µl of 10mg/ml RNase and tubes were placed in a 37 °C water bath for 30 minutes. DNA was then quantified and used in the appropriate dilution for PCR reactions.

#### **2.2.5.3. Phenol-Chloroform DNA extraction**

An equal volume of phenol/chloroform was added to the DNA sample, thoroughly vortexed and centrifuged at 13,000 rpm in a bench-top centrifuge. The aqueous phase was taken and mixed with 0.1  $\times$  volume of 3 M NaOAc and 2.5  $\times$  volume of 100% ice-cold ethanol. Tubes were left on ice for 5 minutes and then centrifuged in a bench-top centrifuge for 10 minutes at full-speed. The pellet was washed in 500  $\mu$ l 70% ethanol and spun at full-speed again for 5 minutes. The supernatant was aspirated away and the pellet was air-dried before final resuspension in 10  $\mu$ l TE.

#### **2.2.5.4. Restriction Digests of DNA**

Restriction digests of plasmid DNA was carried out in 50  $\mu$ l reaction volumes using ~10 Units (or 1  $\mu$ l) of the relevant restriction enzyme (New England Biolabs) and 1  $\mu$ g of DNA. The appropriate NE Buffer is used in a 10-fold dilution and BSA is added to a final concentration of 100  $\mu$ g/ml. Tubes containing all reagents were placed in a 37 °C water bath for 2 hours and 2  $\mu$ l of this was run on an agarose gel alongside un-digested plasmid DNA.

#### **2.2.5.5. DNA Ligation**

Ligation of DNA fragments into a cut plasmid was performed using T4 DNA Ligase (New England Biolabs). Insert DNA and linearised plasmid DNA were mixed in a molar ratio of 3:1, respectively as per the following equation:

$$\frac{Z \times Y \times 3}{X}$$

Where:

Z = the length in base pairs of insert DNA

X = the length in base pairs of vector DNA

Y = the amount (in ng) of vector used

10 Units of T4 DNA Ligase was added to the DNA along with 1  $\times$  T4 DNA Ligase buffer and was incubated overnight at 16 °C. Ligation reactions were checked by running 2  $\mu$ l on an agarose gel.

#### **2.2.5.6. Agarose Gel Electrophoresis**

Agarose gel electrophoresis was used to separate DNA fragments by size (and/or conformation). Generally, 150 mm x 150 mm, 1% agarose (made using 1  $\times$  TAE buffer, section 2.1.5) gels were used, but higher or lower percentage gels were made for separation of especially small or large DNA species. DNA was loaded into the gel lanes with 1  $\times$  loading buffer (1 part loading dye, 5 parts 30% glycerol) usually in a volume of ~15  $\mu$ l. 250 ng of 1kb or 100 bp ladder (New England Biolabs) were also loaded. Gels were run in Fisherbrand electrophoresis tanks filled with 1  $\times$  TAE buffer. Gels were run by applying a charge difference of 4 volts/cm of agarose gel at room temperature. Gels were stained for 30 minutes in 500 ml 1  $\times$  TAE containing 5  $\mu$ M ethidium bromide and images using SYNGENE INGenius BIO Imager.

#### **2.2.5.7. Gel extraction of DNA**

DNA fragments were visualised using a blue light imager and cut out of the gel using a clean scalpel. DNA was extracted from the agarose gel matrix using a QIAgen QIAquick Gel Extraction Kit and following manufacturer's instructions.

## **2.2.6. Protein Methods**

### **2.2.6.1. Protein Extraction**

#### **2.2.6.1.1. Protein Extraction using NaOH**

4 ml of cell culture was harvested, placed in 14 ml polypropylene tubes and centrifuged at 3500 rpm for 3 minutes. Cell pellets were resuspended in 100  $\mu$ l sterile dH<sub>2</sub>O and transferred to a 1.5 ml Eppendorf tube. To this, 100  $\mu$ l of 0.2 M NaOH was added, left at room temperature for 5 minutes and then tubes were spun at 13,000 rpm at 4 °C in an Eppendorf bench-top cooling centrifuge. The supernatant was discarded and the pellets were thoroughly resuspended in 100  $\mu$ l 1  $\times$  Laemmli sample buffer (2% SDS, 10% glycerol, 0.002% bromophenol blue, 0.06 M Tris HCl, with 40  $\mu$ l  $\beta$ -mercaptoethanol per ml sample buffer added before use) and boiled at 100 °C for 5 minutes. Tubes were centrifuged at max-speed in a cooling bench-top centrifuge and the supernatant was collected and kept.

#### **2.2.6.1.2. Tri-Chloroacetic Acid (TCA) extraction of proteins**

4 ml of cell culture ( $\sim 4.5 \times 10^7$  cells/ml) was harvested, placed in 14 ml polypropylene tubes and 1 ml of cold 100% TCA was added (final conc. 20%). Cells were spun at 4000 rpm at 4 °C for 10 minutes, cell pellets were resuspended in 1 ml cold 10% TCA and transferred to a 2 ml Ribolyser tubes. Cells were centrifuged at 4 °C for 10 minutes at 10,000 rpm in a cooling bench-top centrifuge and pellets were snap-frozen in liquid nitrogen for processing at a later date, or resuspended in 200  $\mu$ l cold 10% TCA for immediate processing. To this, a small scoop of 425 – 600  $\mu$ m acid-washed glass beads (Sigma) were added and tubes

were ribolysed five times in an MP Biomedicals FastPrep®-24 Ribolyser set to 6.5 m/s with an intervening 5 minute resting of the tubes on ice. Cells were checked for complete and uniform lysis under the light microscope and once fully lysed the supernatant was collected from the beads (taking care not to withdraw any beads into the pipette tip) and placed into a fresh 2 ml Eppendorf tube. The beads were washed once using 200 µl of cold 10% TCA and a further two times with 400 µl cold 10% TCA, vortexing thoroughly during each wash and pooling the supernatants from each wash into the corresponding 2 ml tube. The beads were discarded and the 10% TCA wash solution was centrifuged at 5000 rpm for 10 minutes in a bench-top cooling centrifuge set at 4 °C. The cell pellet was thoroughly resuspended in 100-200 µl 4 × sample buffer (0.25 M Tris-HCl pH 6.8, 8% SDS, 10% β-mercaptoethanol, 30% glycerol, 0.02% bromophenol blue) and 35 µl of 1.5 M Tris-HCl pH 8.8 to neutralise the acidity. Samples were boiled at 100 °C for 3 minutes and immediately centrifuged at max-speed in a bench-top cooling centrifuge for 2 minutes. The supernatant was collected and kept.

#### **2.2.6.1.3. Preparation of non-denaturing nuclear/chromatin extracts**

Protocol adapted from Kee and Keeney 2002 and Kee *et al.* 2004. 200 ml of sporulating cultures ( $\sim 4.5 \times 10^7$  cells/ml so  $\sim 9 \times 10^9$  cells in total) were taken and centrifuged in a large Sorvall SLA-1500 rotor at 4000 rpm for 10 minutes. The cell pellet was weighed and used to find the pelleted cell volume (PCV, 1g = 1 ml). Cell pellets were washed 3 times in 3 × PCV of ice-cold, sterile dH<sub>2</sub>O and transferred to a round-bottomed sterile polypropylene tube. Following the final wash, cells were

resuspended in 4 ml zymolyase buffer (10 mM  $\text{MgCl}_2$ , 50 mM Tris-HCl pH 7.5, 30 mM DTT) containing the following protease inhibitors; 100  $\mu\text{l}$  per 2g (wet weight) cells of Sigma Protease inhibitor cocktail, 50  $\mu\text{l}$  of 10 mM Chymostatin, 10  $\mu\text{l}$  of 10 mg/ml Aprotinin, 100  $\mu\text{l}$  of 0.2 M Benzamidine, 400  $\mu\text{l}$  of 25  $\chi$  Roche Protease inhibitor cocktail, 10 mM NEM and 40  $\mu\text{l}$  of 0.5 M EDTA. To this, 500  $\mu\text{l}$  of 10 mg/ml zymolyase (100T) was added and the cells were digested for 15 minutes in a 37 °C shaking incubator. When spheroplasting was complete, the cell suspension was gently layered onto a 4 ml 30% sucrose 'step' (with protease inhibitors) held in a fresh round-bottomed 14 ml polypropylene tube. The tubes were then centrifuged at 10,000 rpm in a swing-bucket HB-4 rotor for 10 minutes. The supernatant and sucrose were carefully removed and the pellet was resuspended in 10 ml Hypotonic Lysis Buffer (100 mM MES-NaOH pH 6.4, 1 mM EDTA, 0.5 mM  $\text{MgCl}_2$ , plus protease inhibitors) and transferred to a 50 ml polypropylene tube, where a further 25 ml HLB (plus protease inhibitors) was added. Cells were given 2 strokes in a pre-chilled dounce homogeniser (pestle A, 1 – 3  $\mu\text{m}$  clearance) and left to swell on ice for 10 minutes. Cells were given a further 8 strokes in a dounce homogeniser and cells were carefully layered onto a 10 ml 30% sucrose 'step' in a 50 ml polycarbonate round-bottomed tube (Nalgene). The tubes were then centrifuged at 11,000 rpm in a swing-bucket HB-4 rotor for 15 minutes, following which the supernatant and sucrose was carefully removed and the pellet was resuspended in 1 ml EBX buffer (50 mM HEPES-NaOH pH 7.5, 100 mM KCl, 2.5 mM  $\text{MgCl}_2$ , 0.05% Triton-X, plus protease inhibitors) and transferred to a 2 ml Eppendorf tube. For liberation of chromatin-bound proteins, 6  $\mu\text{l}$  of 15 U/ $\mu\text{l}$  DNase and  $\text{MgCl}_2$  (4.5 mM) was added and left on ice for 2 hours. The

efficacy of the DNase treatment was checked by assessment of the viscosity of the sample (samples should be less viscous following successful DNase treatment).

When DNase treatment is complete, the sample was then centrifuged at 9000 rpm for 10 minutes in a cooling bench-top centrifuge set to 4 °C. The supernatant was then kept for analysis.

#### **2.2.6.2. SDS-PAGE separation of proteins**

One-dimensional separation of proteins on basis of protein size was achieved by SDS-PAGE. Generally this was done with 100 mm x 70 mm mini-gels, but for better resolution of bands (e.g. Smt3 IP), larger-format 180 mm x 160 mm gels were run. A typical 5 ml 10% resolving gel consisted of 2 ml H<sub>2</sub>O, 2 ml of 30% Bis-acrylamide, 1.3 ml 1.5 M Tris pH 8.8, 50 µl 10% SDS, 50 µl 10% APS, 2 µl TEMED. Amounts were adjusted appropriately for gels of different percentages. H<sub>2</sub>O-saturated butanol was applied to the top of the resolving gel to ensure even polymerisation at the top of the gel. After the resolving gel had set, the butanol was removed and 2 ml of stacking gel was applied to the top of the gel with the desired gel comb. 1 ml of stacking gel consisted of 680 µl of H<sub>2</sub>O, 170 µl of 30% Bis-acrylamide, 130 µl of 1 M Tris pH 6.8, 10 µl of 10% SDS, 10 µl of 10% APS and 1 µl TEMED. Small and large format gels were run in a Mini-PROTEAN® Tetra Cell (BIORAD) and an SE 600 Ruby dual cooled gel electrophoresis unit (Amersham Biosciences), respectively, with 1 × SDS running buffer (Section 2.1.2). Small gels were run at 200 volts for ~30 minutes or until the dye front ran off the gel and large-format gels were run at 25 mA for ~5 hours at 4 °C. Full range RAINBOW™ protein markers (GE Healthcare) were used to determine protein size (15 µl per lane).

### **2.2.6.3. Western Blotting**

After SDS-PAGE, proteins were transferred to nitrocellulose membrane for immuno-blotting. Nitrocellulose membranes (WHATMAN Protran™ 0.45 µm pore size) were cut slightly larger than the gel and two pieces of filter paper (BIORAD extra-thick filter paper) was cut to the same size as the gel. Filter paper and nitrocellulose membrane was soaked in semi-dry transfer buffer (section 2.1.2) for 5 minutes. The nitrocellulose membrane was placed on top of the filter paper and the gel was placed on top of the membrane. The other piece of filter paper was placed on top of the gel and the 'sandwich' was rolled with a glass tube to remove air bubbles. The membrane/gel sandwich was placed onto a pre-wetted semi-dry transfer chamber and transferred at 15 volts for 1 hour (or more for larger gels). When transfer was complete the membrane was carefully removed rinsed with Ponceau (1 g Ponceau, 15 g TCA, 500 ml dH<sub>2</sub>O) followed by dH<sub>2</sub>O to visualise protein bands. Membranes were then incubated in 5% milk (Marvel milk powder made up in PBS) at room temperature for 30 minutes and washed 3 times in PBS-Tween (1 ml TWEEN in 1000 ml PBS). Primary antibodies were then added to the membrane at the appropriate dilution in 5% milk and were incubated overnight at 4 °C. The following day, the membrane was washed 3 times in PBS-Tween and the secondary antibodies diluted in 5% milk were added to the membrane. The membrane was incubated with the secondary antibodies (conjugated to horseradish peroxidase) for one hour at room temperature and then washed 3 times with PBS-Tween. Pierce® ECL Western Blotting Substrate was used for chemiluminescent detection of secondary antibodies and blots were exposed to

chemiluminescent film (18 x 24 cm Hyperfilm ECL, GE Healthcare) in the dark room, following which films were developed.

#### **2.2.6.5. Immunoprecipitation**

Immunoprecipitation reactions were carried out using Dynabeads® (Invitrogen) covalently bound to Protein G (Invitrogen). Dynabeads were completely resuspended by pipetting or vortexing and 50 µl was added to a sterile 1.5 ml Eppendorf tube. The tube was placed against a magnet (DynaMag™, Invitrogen) to separate the beads from the solution and the solution was removed and discarded. 1 ml of sample was added to the beads, thoroughly mixed and incubated on a rotating wheel for 10 minutes at room temperature. The tube was placed against a magnet and the solution containing unbound material was pipetted off and transferred to a fresh tube for the subsequent IP step (pre-clearing the sample). The beads were washed 3 times in 200 µl PBS and after the final wash beads were resuspended in 100 µl PBS and transferred to a fresh tube. These beads were kept on ice for elution of non-specific proteins. In a fresh 1.5 ml Eppendorf tube, 50 µl Dynabeads were added and placed against a magnet to remove storage solution. To this, 1 – 10 µg antibody diluted in 200 µl PBS-TWEEN (1 ml TWEEN in 1000 ml PBS) was added and incubated on a rotating wheel for 10 minutes at room temperature. The tube was then placed against a magnet and the supernatant was removed and discarded. The beads were washed once with 200 µl PBS-TWEEN and then the 1 ml of pre-cleared sample was added to the beads and mixed thoroughly. The tube was incubated on a rotating wheel for 10 minutes at room temperature and then placed against a magnet for removal of unbound

material. The beads were washed 3 times in 200  $\mu$ l PBS and following the final wash beads were resuspended in 100  $\mu$ l PBS and transferred to a fresh tube. The tube was placed against a magnet and the PBS was removed and discarded. To elute material bound to the beads, 50  $\mu$ l of 4  $\times$  sample buffer (0.25 M Tris-HCl pH 6.8, 8% SDS, 10% 2-mercaptoethanol, 30% glycerol, 0.02% bromophenol blue) was added to the tube and then placed in a 70 °C water bath for 10 minutes. The tube was placed against a magnet one last time and the sample was loaded onto a gel for analysis.

## **2.2.6. Computational Tools**

### **2.2.6.1. Websites used**

Saccharomyces Genome Database:

<http://www.yeastgenome.org/>

SwissProt:

<http://www.expasy.ch/sprot/>

Reverse Complement:

[http://www.bioinformatics.org/sms/rev\\_comp.html](http://www.bioinformatics.org/sms/rev_comp.html)

BLAST:

<http://www.ncbi.nlm.nih.gov/>

BioGRID:

[www.thebiogrid.org/](http://www.thebiogrid.org/)

R-project:

[www.r-project.org/](http://www.r-project.org/)

Power/Sample size calculator:

<http://www.stat.ubc.ca/~rollin/stats/ssize/b1.html>

### **2.2.6.2. Software used**

ColoR written in R ([www.r-project.com](http://www.r-project.com))

ColoS written in C# by Matthew Newnham

Adobe Photoshop, version 9

*Softworx* Deltavision software

### **2.2.6.3. Overview of ColoS**

A computer program was developed that performed automated object-detection. This was achieved by first extracting the pixel intensities from each image for the relevant channel(s). Then using an algorithm based on the range and frequency of pixel intensities for each image, the program set a threshold for background subtraction (Figure 2.4 A and B). Any objects above this threshold were subjected to a further round of processing whereby an edge-detection algorithm was used to define individual foci (Figure 2.4 C). This was able to resolve two closely apposed foci, even if the intervening 'dip' in pixel intensities (or 'local minimum') between them was above the threshold set in the previous step (Figure 2.4 D). Finally, the program generates graphical outputs that allow the user to see which foci were identified and counted (Figure 2.4 E). This allowed the user to verify that image processing had occurred correctly.

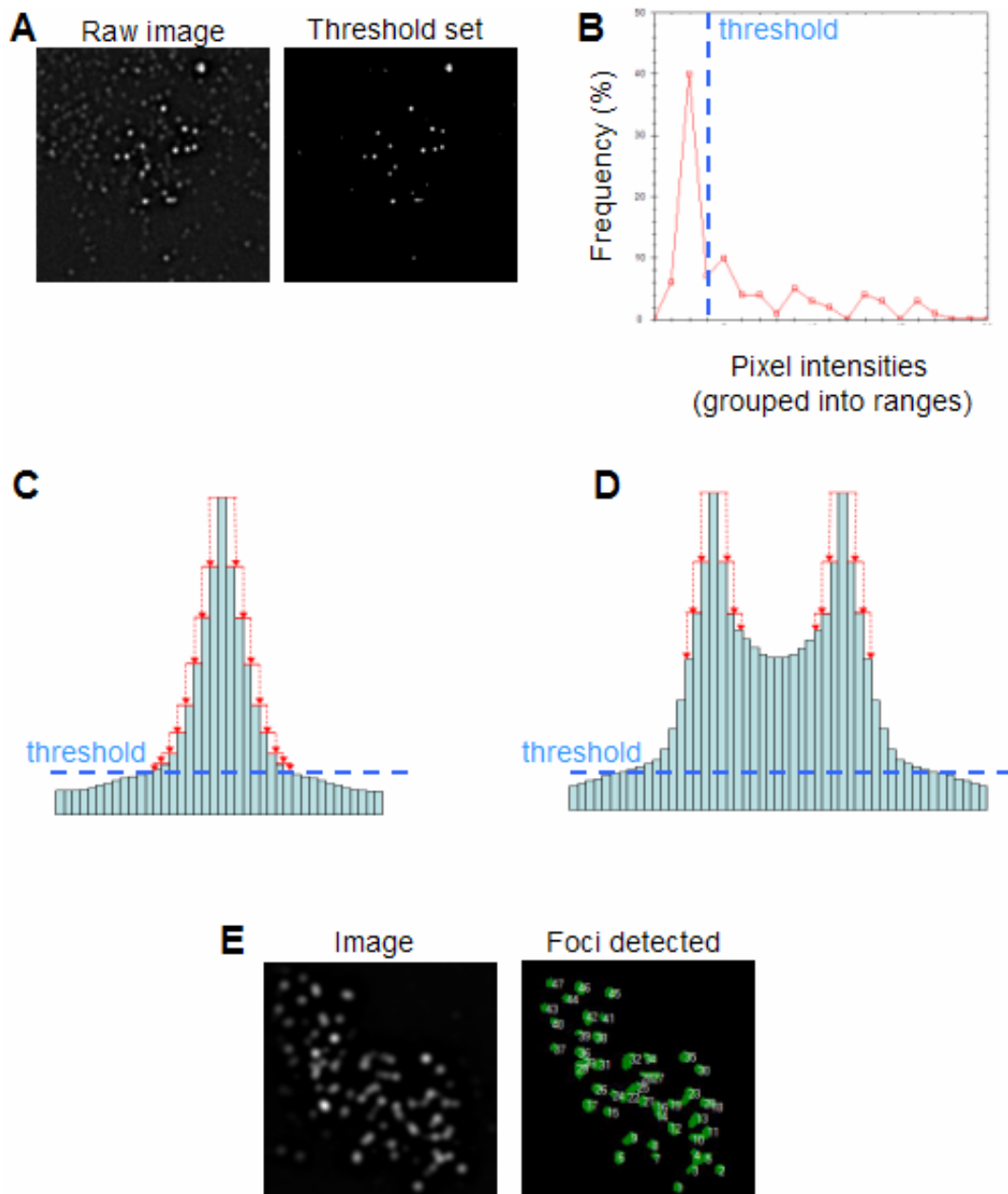


**Figure 2.4.** A program for automated object-detection. (A) Example of the signal present in an unprocessed image (left) and after the program has set a threshold for background subtraction (right). The program initially identifies all ‘peaks’ in an image and plots them based on maximum pixel intensities (B). Note the high frequency of low intensity peaks that correspond to background signal. The program sets the threshold just above this point (blue dotted line). After this, a second round of processing identifies all peaks above the threshold using edge-detection (using symmetric nearest neighbor algorithms). (C) Schematic detailing how edge-detection works by starting at the top of each peak and working outward to surrounding pixels. So long as the outermost pixels are lower in intensity, they

are grouped into the object. This continues until it reaches the threshold set in the previous step or the local minimum between two closely opposed 'peaks' (D). Identified objects are then assigned an ID depicted in the graphical output (E, left).

# **Chapter 3. Synaptonemal Complex (SC)**

## **formation is both promoted and prohibited by Msh4.**

### **3.1. Introduction**

Assembly of the synaptonemal complex (SC) and formation of crossovers are intimately coupled events in meiotic prophase with aberrations in one, affecting proficiency of the other. The proteins responsible for coordinating these two events are known as the 'ZMM's (Zip1, Zip2, Zip3, Zip4, Msh4, Msh5 and Mer3). Mutants lacking any one of these components fall into the same epistasis group for crossing over, characterised by a severe defect at the DSB-SEI transition culminating in a reduction of crossover products (5-20 % of wild type levels). Another hallmark of the *ZMM* mutants are synapsis defects with Zip1 frequently failing to extend along the chromosomes and instead tending to form large aggregates known as poly-complexes (PCs). Furthermore, these mutant phenotypes are modulated by temperature, with a greater reduction in crossing over (and corresponding intermediates) observed at 33 °C, compared to 25 °C (Borner et al., 2004).

Consistent with the notion that SC formation is coupled to crossover formation, mutants lacking the cellular machinery required for SC extension (Zip2-Zip4-Spo16), or the SC itself (Zip1), not only display synapsis defects, but also a severe reduction in crossing over (Agarwal and Roeder, 2000; Chua and Roeder, 1998; Shinohara et al., 2008; Tsubouchi et al., 2006; Tung and Roeder,

1998). Similarly, mutants lacking any of the components important for crossover-designated DNA transactions, such as Msh4-Msh5 or Mer3 helicase, display corresponding synapsis defects, although the reported severity of *msh4* $\Delta$  and *msh5* $\Delta$  phenotypes vary (Borner et al., 2004; Novak et al., 2001; Ross-Macdonald and Roeder, 1994). Both the SC extension (Zip2-Zip4-Spo16) and the DNA transaction sub-complexes (Msh4-Msh5 and Mer3) depend upon Zip3 for their chromosomal localisation, which has led to the suggestion that Zip3 is the primary regulator of the 'ZMM' ensemble (Agarwal and Roeder, 2000; Shinohara et al., 2008). Mutants lacking Zip3 experience reduced crossing over as well as delayed and incomplete synapsis (Agarwal and Roeder, 2000).

In addition to genetic interactions, proteins belonging to the 'ZMM' ensemble also show physical interactions during meiotic prophase. A combination of immuno-precipitation and yeast two-hybrid assays revealed that Zip3 interacts with the synaptonemal complex proteins Zip1 and Zip2, as well as the Msh4-Msh5 heterodimer (Agarwal and Roeder, 2000). Furthermore, Zip3 also interacts with non-ZMM members that are involved in recombination such as Mre11, Rad51 and Rad57 (Agarwal and Roeder, 2000), suggesting a link between recombination and the primary regulator of the 'ZMM' (Zip3). Consistently, Zip2 and Zip3 foci that mark synapsis initiation sites co-localise with Mre11 and Msh4 foci (Agarwal and Roeder, 2000; Chua and Roeder, 1998). This is also in agreement with the proposition that SC initiation occurs at sites of recombination (Henderson and Keeney, 2004, 2005). A model whereby synaptonemal complex formation initiates at sites of future crossovers fits with the way in which these two processes are closely coupled events.

How does the cell ensure that extension of the SC is coupled to crossover formation? A previous study investigating the roles of the 'ZMM's in these processes was carried out in a strain background that experiences arrest at 33 °C with a concomitant crossover defect at the leptotene to zygotene transition. This arrest may therefore have hampered the investigation of SC extension in these mutants, which occurs during zygotene (Borner et al., 2004). However, *ZMM* mutants of the BR and Y55 strain backgrounds do not display this arrest phenotype, despite similar crossover defects (Chan et al., 2009). The ability to progress beyond the leptotene-zygotene transition (at which point SC extension normally occurs), provided a tool to gain further insight into how the 'ZMM's regulate SC extension.

If the 'ZMM' proteins are responsible for regulating SC extension so that it is closely coupled to crossing over, mutant situations in which the former may be de-coupled from the latter must exist. In order to test this, the SC extension phenotypes of various *ZMM* mutants were examined in BR and Y55 strain backgrounds that do not arrest at 33 °C.

## 3.2. Results

### 3.2.1. *msh4*Δ mutants display improved chromosome synapsis at 33 °C

Previous work has shown that *MSH4* and *MSH5* mutants display improved meiotic chromosome segregation at 33 °C as compared to 23 °C. This improvement depends upon Zip1, alluding to the possibility that Zip1 may be modulated by temperature in these mutants (Chan et al., 2009). In order to investigate this, BR strains were used that display proficient meiotic progression at 33 °C (Chan et al., 2009), unlike SK1 strains (Borner et al., 2004; Chan et al., 2009). Cells from sporulating cultures were harvested at ~16 hours and immuno-stained, surface spread nuclei were prepared. DAPI staining of the DNA showed that many (~30-40% of Zip1 positive nuclei) wild type nuclei at this time point had highly condensed, worm-like chromosomes indicative of the cells being in pachytene. Immuno-staining for Zip1 revealed three categories of nuclei with distinct Zip1 staining patterns. The first category consists of nuclei containing dotty Zip1 staining and leptotene-like diffuse DNA ('Dotty' Figure 3.1.A). Nuclei with a mixture of Zip1 dots and short lines fell into the second category ('Dot-linear' Figure 3.1.C). These nuclei are interpreted as representing SC extending from synapsis initiation sites. The final category consists of nuclei with extensive linear stretches of Zip1, typical of situations whereby all 16 chromosome pairs are fully synapsed along their lengths ('Linear' Figure 3.1.E). The relative proportions of these different categories of nuclei were similar at both 25 °C and 33 °C and poly-complexes (PCs) were absent, suggesting that in wild type cells SC extension occurs proficiently at both temperatures (Figure 3.1.G and H).

Figure 3.1

However, deletion of *MSH4* resulted in an increase of nuclei with 'dotty' Zip1 and a concomitant decrease in nuclei with 'dot-linear' or 'linear' Zip1 staining at 25 °C (Figure 3.1.B, D, F and G). A large proportion of nuclei that contained PCs were also observed, indicative of defective SC assembly (Figure 3.1.H). In contrast, at 33 °C the *msh4Δ* mutant displayed more extensive SC formation, which is herein referred to as 'improved synapsis' (although whether this is identical in nature to the 'synapsis' occurring in wild type cells is unclear). Of the Zip1-positive nuclei, ~50% contained 'linear' Zip1 staining and highly condensed DNA, whilst the leptotene-like nuclei with 'dotty' Zip1 staining only comprised a relatively small minority (<10%, Figure 3.1.G). The synapsis that occurs at either temperature is likely to involve homologous chromosomes as fluorescence *in situ* hybridisation (FISH) revealed a single focus for two different chromosome pairs in ~90% of nuclei examined (as opposed to two foci when homologous chromosomes are unpaired, Appendix Figure 1-data courtesy of E.H.). Furthermore, the proportion of nuclei that contained PCs was reduced from 44% at 25 °C, to just 6% at 33 °C. Thus, synapsis is significantly improved at 33 °C in *msh4Δ* mutants. These observations may therefore account for the conflicting SC formation phenotypes described previously for *msh4Δ* mutants (Borner et al., 2004; Novak et al., 2001; Ross-Macdonald and Roeder, 1994).

It is possible that the different synapsis phenotypes observed in *msh4Δ* mutants was due to different meiotic progression profiles at the two temperatures. In order to investigate this possibility, the same experiment was carried out using the Y55 strain background that undergoes synchronous meiosis under liquid culture conditions, but like BR strains does not arrest at 33 °C (Chan et al., 2009). This allowed the kinetics of Zip1 behaviour and

Figure 3.2

chromosome morphology to be followed during meiotic prophase and correlated with nuclear divisions. Wild type cells showed proficient meiotic progression at both temperatures with ~80% of cells completing meiosis I by 24 hours (Figure 3.2.O and P). Similar to BR, the majority of wild type nuclei exhibited 'dot-linear' or 'linear' Zip1 staining at both temperatures and a low frequency of PCs. The incidence of nuclei with 'dotty' Zip1 staining steadily increased throughout the time course as the majority of cells entered and completed the meiotic divisions (Figure 3.2. G, H, O and P). These are likely to represent the small subset of cells that had not yet entered the meiotic divisions.

*msh4*Δ mutants behaved similarly to BR strains at 25 °C with nuclei containing 'dotty' Zip1 predominating throughout the meiotic time course, whilst at 33 °C (8 hr) a greater proportion of nuclei with 'dot-linear' and 'linear' Zip1 staining were observed (Figure 3.2. B, D, F, I and J). Again, these nuclei were largely replaced by nuclei with 'dotty' Zip1 staining as cells progressed through the meiotic divisions. This suggests that the cells exhibiting improved synapsis in *msh4*Δ mutants (at 33 °C) at early time points (8 hr), enter and complete the meiotic divisions at later time points (12-24 hr), whilst a small minority with 'dotty' Zip1 staining remain at later time points. These are likely to represent cells that had not yet entered the meiotic divisions. Curiously, despite formation of extensive SCs in *msh4*Δ mutants (at 33 °C), every nucleus examined at 8 hours contained a PC (Figure 3.2 N). This implies that the SC may not be structurally the same as wild type where only ~10% of nuclei contain PCs.

It is possible that *msh4*Δ cells experience a shortened prophase at 25 °C, whereby the stage corresponding to 'linear' Zip1 staining (pachytene) is so transient that detection of such nuclei is extremely rare. In order to address this,

cells were arrested in pachytene by deletion of *NDT80*. Ndt80 is a transcription factor that induces expression of ~200 genes required for exit from pachytene (Chu and Herskowitz, 1998; Hepworth et al., 1998; Xu et al., 1995). *ndt80Δ* mutants arrest in pachytene with unresolved Holliday junctions (Allers and Lichten, 2001) and fully synapsed chromosomes. The *ndt80Δ msh4Δ* double mutant failed to form any Zip1 stretches at 25 °C despite the imposed block in cells exiting pachytene (Figure 3.3. B, D and H). However, synapsis was improved at 33 °C in the double mutant (Figure 3.3 B, D and I). This suggests that the lack of extensive synapsis in *msh4Δ* mutants at 25 °C is not due to transient passage through the pachytene stage. Strangely, the synapsis observed in the *ndt80Δ msh4Δ* double mutant was not as extensive as that observed in the *msh4Δ* mutant (compare figure 3.3 I with 3.2 J). Similarly, the synapsis observed in *ndt80Δ* single mutants was not identical to that of wild type cells. Despite, *ndt80Δ* mutants initially displaying similar proportions of all three nuclear categories as wild type, a large proportion of nuclei contained a PC at 33 °C suggesting that Zip1 may be misregulated in cells lacking *NDT80* (12 hours, Figure 3.3 G and K). In addition, a reduction in the proportion of nuclei with 'linear' Zip1 were observed after prolonged arrest (24 hours, Figure 3.3. F and G). These findings suggest that deletion of *NDT80* may influence SC assembly and/or stability. Nonetheless, these findings support that notion that Msh4 is important for SC extension that occurs at lower temperature (25 °C), but is partly dispensable at 33 °C.

Figure 3.3

### 3.2.2. Zip2 is required for synapsis at 33 °C

Within the ZMM ensemble, Zip2, together with Zip4 and Spo16 are thought to extend Zip1 polymers outward from synapsis initiation sites, culminating in the appearance of end-to-end SCs (Zip1 stretches). Cells lacking any one of these proteins exhibit severely defective SC extension. Zip1 appears as foci at axial associations and these fail to extend into cytologically detectable stretches (Chua and Roeder, 1998; Shinohara et al., 2008; Tsubouchi et al., 2006). In order to determine whether improved synapsis (at 33 °C) depends upon Zip2-Zip4-Spo16, the *zip2*Δ mutant was assessed. Both BR and Y55 strains deleted for *ZIP2* displayed a high proportion of cells (> 80%) with 'dotty' Zip1 staining and a PC, irrespective of temperature (Figures 3.4 and 3.5). Therefore, *zip2*Δ mutants suffer a severe failure to extend Zip1 polymers at either temperature.

### 3.2.3. Zip2-independent synapsis can occur in the absence of *MSH4*

What causes the improved synapsis observed in *msh4*Δ mutants? Msh4 may simply be dispensable for synapsis that occurs at higher temperatures; alternatively Msh4 may actively prevent this mode of SC extension. To help distinguish between these two possibilities, *MSH4* was deleted in *zip2*Δ mutants. Having ascertained that Zip2 is required for synapsis at both temperatures, one might expect the *msh4*Δ *zip2*Δ double mutant phenotype to mimic that of *zip2*Δ. However, this was not the case. Despite *msh4*Δ *zip2*Δ double mutants (for both BR and Y55) appearing much like either single mutant at 25 °C, improved synapsis was again observed at 33 °C (Figures 3.4 and 3.5).

Figure 3.4

Figure 3.5

An increased proportion of *msh4Δ zip2Δ* nuclei with 'dot-linear' Zip1 were observed as compared to 25 °C (for both BR and Y55\_12 hr this category increased from ~ 10% at 25 °C, to ~60% at 33 °C) and even some nuclei containing 'linear' Zip1 staining were observed (BR: 25% and Y55\_12 hr: 4%). In both strain backgrounds, ~40% of *msh4Δ zip2Δ* nuclei contained a PC (Figure 3.4.F and Figure 3.5.M). In summary, deletion of *MSH4* partially bypasses the requirement for Zip2 in extending the SC, suggesting that Msh4 inhibits Zip2-independent synapsis that can occur at higher temperatures (33 °C).

#### **3.2.4. Zip2 extends polymers of Zip1 in *msh4Δ* mutants at 33 °C**

In order to determine whether Zip2 was in any way responsible for the improved synapsis observed in *msh4Δ* mutants, the synapsis phenotype of the *msh4Δ zip2Δ* double mutant was compared to that of the *msh4Δ* single mutant at 33 °C. The proportion of nuclei containing linear Zip1 staining was significantly decreased from 38 % (8hr, Figure 3.2.J) in the *msh4Δ* mutant to just 4 % in the *msh4Δ zip2Δ* double mutant (12 hr, figure 3.5 I). The same was true of the BR strain background (compare figure 3.1 G with 3.4 F). Thus, synapsis is less extensive in *msh4Δzip2Δ* double mutants than in *msh4Δ* mutants at 33 °C. Furthermore, there were a higher proportion of nuclei that contained PCs in the *msh4Δzip2Δ* double mutant at 33 °C than the *msh4Δ* mutant (Figure 3.4 G and Figure 3.1 H). These findings suggest that Zip2 contributes towards the extensive synapsis observed in *msh4Δ* mutants at 33 °C.

### 3.2.5. Zip1 polymerisation is unaffected by temperature and *MSH4* status in *zip3Δ* mutants.

Previous models have placed Zip3 upstream of both Msh4 and Zip2 as the primary regulator of the 'ZMM' ensemble (Agarwal and Roeder, 2000; Shinohara et al., 2008). *zip3Δ* mutants are characterised by delayed and incomplete synapsis relative to wild type (Agarwal and Roeder, 2000). If Zip3 is truly acting upstream of the other 'ZMM' proteins and temperature exerts its influence via these proteins, the limited synapsis observed in *zip3Δ* mutants should be unaffected by temperature. Indeed, both the number and length of Zip1 stretches (defined as 'lines' of Zip1) were indistinguishable at either temperature for the *zip3Δ* mutant (Figure 3.6 A, C and E) suggesting that Zip3-independent synapsis is unaffected by temperature.

Models that place Zip3 upstream of the other 'ZMM's predict that deletion of *MSH4* should have no influence on Zip3-independent synapsis. Consistent with this prediction, the number of Zip1 stretches observed in the *zip3Δ msh4Δ* double mutant was similar to those observed for the *zip3Δ* single mutant (Figure 3.6). However, the distribution of Zip1 stretch length appeared to marginally differ for the two mutants (Figure 3.6 E). The difference being that the few longer Zip1 stretches (>3 μm) observed in *zip3Δ* mutants were not observed in the *zip3Δ msh4Δ* double mutant. However, owing to the very small number of these 'long' Zip1 stretches in the *zip3Δ* mutant, more nuclei would have to be examined before concluding a *bona fide* difference between the two mutants. Nonetheless, the fact that Zip3-independent synapsis is not improved by deletion of *MSH4* suggests that Msh4 only blocks SC extension within the context of the 'ZMM' ensemble. In sum, neither temperature nor *MSH4* deletion

Figure 3.6

improves Zip3-independent synapsis, suggesting that the regulation of SC extension by temperature and Msh4 only occurs within the context of the 'ZMM'.

### **3.2.6. The improved synapsis observed in *msh4Δ* mutants at 33 °C is predominantly centromere-associated**

There is evidence that synapsis initiates from both centromeres (Tsubouchi et al., 2008) and crossover sites (Henderson and Keeney, 2004). In an attempt to determine where synapsis had initiated in *msh4Δ* and *msh4Δ zip2Δ* mutants at 33 °C, the association of short Zip1 stretches with centromeres was examined. To try and confine the analysis to single synapsis initiation events, only short Zip1 stretches (< 1 μm, or slightly longer if DAPI staining revealed the stretch belonged to a long, well-separated chromosome) were studied in zygotene nuclei with 'dot-linear' Zip1 staining. Nuclei with 'linear' Zip1 staining were excluded from this analysis as, of course, all Zip1 stretches would be associated with a centromere regardless of where synapsis had initiated. By using 13Myc-tagged Ctf19 (a kinetochore protein) to identify centromeres, >90% (84 stretches) and >80% (114 stretches) of short Zip1 stretches were associated with a centromere in *msh4Δ* and *msh4Δ zip2Δ* mutants, respectively (Figure 3.7. B, C and D). This was significantly higher than that observed in wild type zygotene nuclei (49%, Figure 3.7. A and D), suggesting that centromere-associated Zip1 stretches are enriched in cells lacking Msh4. The reciprocal analysis was carried out whereby the proportion of centromeres associated with a Zip1 stretch was assessed. This proportion was 38% and 27% for *msh4Δ* and *msh4Δ zip2Δ* mutants, respectively. This implies

Figure 3.7

some degree of inter-chromosomal heterogeneity either in the timing or the proficiency of synapsis initiation at centromeres.

The finding that short Zip1 stretches are predominantly centromere-associated in cells lacking *msh4* $\Delta$  could be interpreted as Msh4 specifically preventing SC extension from centromeres. However, it remains controversial whether centromere-associated Zip1 stretches are a good read-out of synapsis that has initiated from centromeres, as all of the short Zip1 stretches observed in wild type zygotene nuclei also include crossover sites (see discussion). If synapsis is initiated from centromeres in *msh4* $\Delta$  and *msh4* $\Delta$ *zip2* $\Delta$  mutants at 33 °C, Zip1 foci should co-localise with centromeres in early zygotene nuclei that have not yet started forming stretches of Zip1. To this end, the association of Zip1 foci with centromeres was assessed in early zygotene nuclei of *msh4* $\Delta$  and *msh4* $\Delta$ *zip2* $\Delta$  mutants. During early zygotene, centromeres frequently co-localised with Zip1 foci, but there were often more Zip1 foci than there were centromeres, suggesting that Zip1 loading sites are not confined to centromeres in these mutants (Figure 3.8 A and B).

### **3.2.7. Zip1 localisation at centromeres is similar in *zip2* $\Delta$ and *msh4* $\Delta$ *zip2* $\Delta$ mutants at both temperatures**

Failure to form extensive SC in *zip2* $\Delta$  mutants (and *msh4* $\Delta$  *zip2* $\Delta$  mutants at 25 °C) could either be caused by faulty deposition of Zip1 at synapsis initiation sites and/or failure to extend Zip1 outward from these sites. To determine whether Msh4 actively blocks SC extension from centromeres, or influences Zip1 deposition at synapsis initiation sites, the association of Zip1

Figure 3.8

with centromeres was examined. At 25 °C and 33 °C, both *zip2Δ* and *msh4Δ* *zip2Δ* mutants had a similar proportion of centromeres either directly co-localised (70-80%) or juxtaposed to Zip1 foci/stretches (10-20%, Figure 3.9). Only a small minority of centromeres lacked any association with Zip1. Furthermore, frequently the foci of Zip1 found in *zip2Δ* mutants were brighter at the centromere than those found elsewhere, suggestive of Zip1 accumulating at centromeres in the absence of SC extension (see Chapter 5). The fainter Zip1 foci observed at non-centromeric locations are likely to represent synapsis initiation at crossover-designated sites. Thus, Zip1 loading at synapsis initiation sites appears proficient in *zip2Δ* mutants irrespective of temperature.

### **3.2.8. *Msh4* foci are juxtaposed to centromeres at both temperatures**

The synapsis that occurs in the absence of Msh4 (at 33 °C) is predominantly centromere-associated. If Msh4 blocks SC extension from centromeres or sites nearby, Msh4 should localise to centromeres at times when SC is being formed. To address this, Msh4 was tagged at the C-terminus with GFP, which allowed the identification of Msh4 in spread meiotic nuclei using anti-GFP antibodies. Staining was also performed on an un-tagged control strain to ensure that the signal was specific to the GFP epitope (Appendix Figure 2). However, this allele showed partial loss of function as synapsis was slightly improved in *zip2Δ* mutants carrying this allele. Msh4 foci were not generally observed in leptotene nuclei. Although some nuclei contained occasional foci, these were often very faint and barely above background (Figure 3.10 A). In contrast, Msh4 foci were easily detectable in all zygotene and pachytene nuclei examined (Figure 3.10 B and C). As well as

Figure 3.9

appearing as foci along chromosome arm regions, Msh4 foci were frequently flanking or to one side of a centromere, rather than directly overlapping. This pattern was similar in zygotene to pachytene nuclei and was not affected by temperature (Figure 3.10 D and E). These findings suggest that Msh4 localisation (at least with respect to centromeres) is unaffected by temperature. Rather than being directly co-localised, Msh4 foci are frequently juxtaposed to centromeres. It is possible that Msh4 may block SC extension from these centromere-proximal sites that may also mark crossovers (see discussion).

### **3.2.9. Msh4-GFP foci behaviour at zygotene and pachytene is unaffected by temperature.**

To determine whether temperature influences the number of Msh4 foci at other (i.e. non-centromeric) chromosomal sites, all foci were counted in both zygotene and pachytene nuclei at both temperatures. In an attempt to count these foci in a robust, standardised way across all nuclei, a computer program was developed that performed automated object-detection (see materials and methods section 2.2.6.3 for description of how the program defines objects). This analysis revealed a similar number of Msh4 foci at both temperatures in zygotene nuclei (average of  $38 \pm 11.5$  (S.D.) and  $35 \pm 11.3$  (S.D.) for 25 °C and 33 °C respectively, Figure 3.11 A and C). This number increased in pachytene nuclei (25 °C:  $48 \pm 9.7$ , 33 °C:  $44 \pm 10.0$ ) but values remained similar at either temperature (Figure 3.11 B and C). To verify that these foci-counts were similar whether using 'automated' or 'manual' methods of assessment, the two methods were compared. Figure 3.11.D shows that the counts done 'manually' were slightly more conservative than those done computationally, however the

Figure 3.10

methods were compared. Figure 3.11.D shows that the counts done 'manually' were slightly more conservative than those done computationally, however the range was similar. As the 'automated' method was believed to be more consistent between nuclei, this was the preferred method.

These findings suggest that the majority of Msh4 foci are static from zygotene to pachytene and localisation is unaffected by temperature. A subset of foci, however, appear later in pachytene nuclei. The fact that the location of Msh4-GFP foci with respect to centromeres did not change much between zygotene and pachytene (section 3.2.8) suggests that these foci may form first whilst more foci form elsewhere later on during pachytene.

#### **3.2.10. Zip1 extension occurs both uni- and bi-directionally from Msh4-GFP foci.**

Sites of crossover recombination (believed to be marked by Msh4 foci) have been proposed to be the sites from which synapsis initiates (Henderson and Keeney, 2004, 2005). However, a recent study has suggested that synapsis actually initiates at centromeres, where crossing over is strongly suppressed (Tsubouchi et al., 2008).

When and where do Zip1 stretches form relative to Msh4-GFP foci? Each individual Msh4-GFP focus within wild type zygotene nuclei were examined and their position relative to Zip1 was scored. 64% were associated with a Zip1 stretch (and all Zip1 stretches examined contained at least one Msh4-GFP focus), but roughly half of these (46%) also contained a centromere within the same Zip1 stretch. In these instances, synapsis could have initiated

Figure 3.11

from either the Msh4-GFP focus or the centromere (or both) making it impossible to infer unequivocally where synapsis had initiated.

In order to further examine the non-centromeric synapsis initiation events, short Zip1 stretches ( $\sim 1 \mu\text{m}$ ) that did not contain a centromere were analysed. This was done in wild type zygotene nuclei in which all 16 Ctf19 foci were identifiable, to control for any centromeres that may have evaded detection. A total of 58 non-centromeric Zip1 stretches from 26 nuclei were analysed. Firstly, this analysis revealed that all Zip1 stretches contained at least one Msh4 focus. Secondly, short Zip1 stretches were often observed with a single Msh4 focus in the middle (46%, Figure 3.12 A, category 1). These could represent bidirectional synapsis emanating from the Msh4 focus. Thirdly, 28% of these short Zip1 stretches had a single Msh4 focus at one end, suggestive of unidirectional synapsis (Figure 3.12 A, category 2). Finally, the remaining 26% of Zip1 stretches contained more than one Msh4 focus making the interpretation of individual synapsis initiation events more ambiguous (Figure 3.12 A, categories 3, 4 and 5). However, it is likely that short Zip1 stretches with Msh4 at opposing ends (category 3) arose from unidirectional synapsis from one or both Msh4 foci. If so, then unidirectional synapsis accounts for 42% of these non-centromeric Zip1 stretches (category 2 and 3 combined). Thus in wild type cells, short Zip1 stretches are observed to one or both sides of an Msh4-GFP focus. These may represent uni- and bi-directional synapsis occurring from crossover sites.

Figure 3.12

If crossover sites, marked by Msh4-GFP foci, do serve as synapsis initiation sites then Msh4 foci should co-localise with Zip1 foci that are the precursors to the short Zip1 stretches (described above). Indeed, those Msh4-GFP foci that were not associated with a Zip1 stretch were frequently overlapping with (38%), or juxtaposed to (26%) a Zip1 focus (Figure 3.12 B, categories 1 and 3). This is consistent with the notion that synapsis can initiate from crossover sites, thought to be marked by Msh4-GFP foci. However, the fact that not all Msh4-GFP foci were associated with a Zip1 focus might be explained by variability in the timing, or proficiency of each Msh4-GFP focus to initiate synapsis. In summary, SC extension appears to occur both uni- and bi-directionally from Msh4-GFP foci that also mark sites of future crossovers in wild type cells.

### **Table 3.1**

### 3.3. Discussion

The results presented here allude to a previously unknown role for the mismatch repair paralogue, Msh4 in regulating SC extension. Synapsis is much more extensive in *msh4* $\Delta$  mutants at 33 °C compared to 25 °C in Y55 and BR strains. However, crossing over (as estimated from genetic map distances) is similar at either temperature (Chan et al., 2009). This implies that the SC extension observed at 33 °C in *msh4* $\Delta$  mutants must have been de-coupled from crossing over. Thus, Msh4 appears to regulate SC extension ensuring that it is coupled to crossing over. *zip2* $\Delta$  mutants do not experience extensive synapsis at either temperature, suggesting that Zip2 is required for SC extension that owing to the presence of Msh4, is coupled to crossing over. Therefore, Msh4 serves to enforce Zip2-dependent SC extension that is coupled to crossing over.

However, removal of Msh4 allows SC extension to become de-coupled from crossing over at elevated temperatures (33 °C). This mode of SC extension is only partially dependent upon Zip2. These data suggest a model whereby temperature serves as a positive regulator of SC extension that has been de-coupled from crossover formation and that Msh4 normally prevents this (Figure 3.13).

This model can accommodate previous findings that concluded that Zip2 is absolutely required for the extension of Zip1 outward from synapsis initiation sites. A failure to do so in *zip2* $\Delta$  mutants, results in accumulation of Zip1 at sites of axial associations (Chua and Roeder, 1998). However, work described in this chapter alludes to Zip2-independent synapsis that is normally prevented by Msh4.

Figure 3.13

Therefore the *zip2* $\Delta$  SC extension phenotype can be explained by the presence of Msh4 blocking Zip2-independent synapsis and thereby enforcing Zip2-dependent synapsis (Table 3.1).

The SC extension phenotype of *msh4* $\Delta$  mutants, at 25 °C, is similar to that observed for the *zip2* $\Delta$  mutant (section 3.2.1 and 3.2.2). But if ‘DNA transaction’ and ‘SC extension’ sub-complexes occupy different branches within the ‘ZMM’ ensemble, how can removal of a component involved in the former (Msh4) have such severe consequences for the latter? One possible explanation is that at 25 °C, crossing over and SC extension are intimately coupled events, so that aberrations in one affect proficiency of the other (see section 3.1). This in turn could explain why *zip2* $\Delta$  mutants display crossover defects despite the presence of Msh4, Msh5 and Mer3 (Borner et al., 2004; Chua and Roeder, 1998). The synapsis phenotype of *msh4* $\Delta$  mutants at 25 °C is similar to that reported for *MSH4* knockout mice (Kneitz et al., 2000), suggesting these mechanisms of regulation may be conserved in mammals. However, the severity of the synapsis phenotype was slightly unexpected as a previous study using SK1 strains reports the *msh4* $\Delta$  phenotype to be less marked with up to 20% of nuclei capable of forming full SCs, albeit with a delay (Novak et al., 2001; Ross-Macdonald and Roeder, 1994). Similarly, *msh4* $\Delta$  mutants of the S288C background frequently form extensive SCs (Chapter 4). How can these apparent discrepancies be accounted for? As the SK1 and S288C *msh4* $\Delta$  mutants both underwent meiosis at 30 °C, it is possible that at this intermediate temperature (between 25 °C and 33 °C) an intermediate synapsis phenotype is observed. Alternatively, it may be that allelic differences between the strain backgrounds give rise to the differing penetrance of the

*MSH4* mutation. Nonetheless, in both strain backgrounds studied in this work (Y55 and BR), Msh4 is important for SC extension at 25 °C.

In contrast, an 8 °C shift in temperature (up to 33 °C) results in vastly improved SC extension in the *msh4Δ* mutant. The proportions of nuclei with 'dot-linear' and 'linear' SCs at this temperature closely mimicked that of wild type. These findings strongly suggest that different modes of SC extension operate at 25 °C and 33 °C, the former heavily dependent on Msh4 and the latter occurs in the absence of Msh4.

The fact that the synapsis defect of *zip2Δ* mutants can be partially overcome by deletion of *MSH4*, specifically at 33 °C, suggests that Msh4 normally blocks Zip2-independent SC extension that can occur at higher temperature (section 3.2.3). However, the same is not observed at 25 °C suggesting that Zip2-independent synapsis can only occur at higher temperature (33 °C) or some other factor is blocking it at 25 °C. It would be interesting to see if synapsis could be rescued in *msh4Δ* mutants at 25 °C by deletion of *SGS1*, which rescues the crossover defect (Jessop et al., 2006). Owing to the similar decrease in map distances at either temperature in cells deleted for *MSH4* (Chan et al., 2009), the SC extension that occurs at 33 °C must be de-coupled from crossing over (see above).

Interestingly, the synapsis observed in the *msh4Δ zip2Δ* double mutant at 33 °C was not as extensive as that observed for the *msh4Δ* mutant (compare Figure 3.2.J with 3.5.I). This could either be because both Zip2-dependent and Zip2-independent modes of SC extension are active in *msh4Δ* mutants at 33 °C that together give rise to the extensive stretches of Zip1 observed. An

alternative interpretation is that Zip2-dependent synapsis (active in the *msh4Δ* mutant at 33 °C) is better than the Zip2-independent mechanism (active in the *msh4Δ zip2Δ* mutant at 33 °C) at extending SC. Regardless, as both pathways proceed in the absence of Msh4 and are only observed at 33 °C, a model whereby temperature promotes SC extension (both Zip2-dependent and – independent) that has been de-coupled from crossing over is proposed (Figure 3.13). In this model, Msh4 blocks these alternative modes of SC extension thus keeping SC extension coupled to crossing over.

The apparent ‘cross-talk’ between ‘DNA transaction’ and ‘SC extension’ sub-complexes may be explained by checkpoint activity. In budding yeast, two separate pathways monitoring ongoing recombination intermediates and SC formation are believed to exist. Rad17 and Sae2 comprise the recombination checkpoint while Pch2 monitors synapsis (Wu and Burgess, 2006). It is possible that the SC defects of *msh4Δ* mutants and the crossover defects of *zip2Δ* mutants may be explained by these checkpoints. For example, the SC defects that are a direct result of deletion of *ZIP2* may be detected by Pch2, which imposes a checkpoint arrest that indirectly affects crossing over (at least those mediated by the ‘ZMM’s) and *vice versa*.

This hypothesis may also account for the improved meiotic progression of *msh4Δ zip2Δ* double mutant compared to the *zip2Δ* mutant, at 33 °C (compare figure 3.5 O and Q). In these cells the improved synapsis may satisfy the SC checkpoint and allow more cells to progress through the meiotic divisions. Furthermore, meiotic progression is better in the *msh4Δ* mutant than the *msh4Δ zip2Δ* double mutant at 33 °C, which is matched by improved synapsis (compare figure 3.2 R with 3.5 Q). Meiotic progression is better in all

mutants at 25 °C where synapsis is aberrant, which may be explained by slightly higher levels of crossing over at 25 °C in these mutants (Chan et al., 2009). One problem with this model, however is that improved synapsis may be able to satisfy the SC checkpoint, but presumably the recombination checkpoint would still be active in cells lacking Msh4. It is unclear precisely how meiotic progression is controlled by temperature in these strain backgrounds, but improved synapsis at 33 °C certainly correlates with improved meiotic progression suggesting that the two may be linked in some way.

Synapsis has been proposed to initiate from both centromeres (Macqueen and Roeder, 2009; Tsubouchi et al., 2008) and sites of developing crossovers (Henderson and Keeney, 2004). The short stretches of Zip1 that form in the absence of Msh4 are predominantly associated with centromeres (~80-90 %, Figure 3.7). This proportion is higher than observed for wild type (<50 %, Figure 3.7), which could be interpreted as evidence that synapsis initiation from the centromeres is enriched in cells deleted for *MSH4*. However, all of the short stretches of Zip1 observed in wild type zygotene nuclei also contained at least one Msh4-GFP focus thought to mark crossover-designated sites (see Figure 3.10 B). This raises the possibility that in wild type, synapsis initiates at crossover sites and polymerises outwards to include a centromere. Consistent with this, over half of the Msh4-GFP foci not associated with a Zip1 stretch were either overlapping with or juxtaposed to a Zip1 focus with only a small minority (<10%) involving centromeres (Figure 3.12 B). Furthermore, a number of short Zip1 stretches (56 %) were observed to be associated with an Msh4-GFP focus, but not a centromere (Figure 3.12 A, C and D). These findings suggest that at least a subset of synapsis initiation events occur at

crossover-designated sites (marked by Msh4-GFP foci) not near a centromere. This could mean that the centromere-associated short Zip1 stretches observed in wild type zygotene nuclei, which also contain Msh4 foci could have in fact arisen from the Msh4 focus and not the centromere. An alternative interpretation is that centromeres, rather than crossover sites act as synapsis initiation sites in the absence of Msh4. This would fit with the way in which crossing over is strongly suppressed at centromeres and so would be a suitable site to initiate synapsis that has been de-coupled from crossing over.

What is the evidence that Msh4 marks sites of future crossovers? Msh4 and Msh5 are mismatch repair paralogues that participate in meiotic crossing over, but not mismatch repair (Ross-Macdonald and Roeder, 1994). Msh4-Msh5 are proposed to form a heterodimer that bind single-end invasions (SEIs) and double Holliday junctions (dHJs) preventing their dissolution by Sgs1 (Jessop et al., 2006; Oh et al., 2007). Consistent with this, human Msh4-Msh5 binds Holliday junctions *in vitro* (Snowden et al., 2004). Electron-dense 'recombination nodules' are observed in late zygotene nuclei at sites of axial associations visible from electron micrographs (Zickler et al., 1992). Formation of axial associations depends upon Dmc1 and Rad51, further supporting the notion that these sites represent recombination intermediates (Rockmill et al., 1995). Moreover, in *Sordaria* mutations that reduce crossing over display similar reductions of both recombination nodules and synapsis initiation events (Zickler et al., 1992). This adds support to the model of SC initiating at crossover-designated sites. The synapsis initiation protein; Zip2 is observed at axial associations and Zip2 also co-localises with the DSB-processing factor, Mre11 in mutants that accumulate DSBs (Chua and Roeder, 1998). Furthermore, the

number of Zip2 foci per nucleus is similar to the number of crossovers and Zip2 foci, like crossovers, show interference in their position along each chromosome (Fung et al., 2004). Msh4 and Zip2 foci co-localise (Novak et al., 2001), implying that Msh4 also localises to these sites that the above evidence suggests are crossover-designated sites.

The finding that the majority of Msh4-GFP foci are formed in zygotene nuclei, but more appear by pachytene contrasts with that reported in mammals. In mouse spermatocytes, the number of Msh4 foci peaks during zygotene and then decreases ~four-fold by mid-pachytene (Kneitz et al., 2000). This could be interpreted as Msh4 marking all sites of recombination during zygotene in mice, but specifically marks sites of crossovers in pachytene. However, in yeast Msh4 only seems to mark sites of ongoing ZMM-mediated crossover recombination.

Why must crossing over and SC extension be coupled? If Msh4 has evolved to block synapsis that is de-coupled from crossing over, there must be some selective advantage to keeping SC extension and crossing over intimately coupled. It is possible that the unregulated spread of SCs along the chromosome may disrupt early recombination events. If so, Msh4 may serve to halt SC extension until more stable recombination intermediates have formed that can withstand the morphological changes that accompany 'zippering up' of homologous chromosomes. In support of this, genetic map distances are marginally reduced at 33 °C in *msh4Δ* mutants (Chan et al., 2009), which may in part due to the unregulated synapsis in these cells.

To conclude, this work has elucidated a model whereby Zip3 is the primary regulator committing SC formation to the 'ZMM' pathway. Zip3 deposits Zip1 at synapsis initiation sites believed to include both centromeres and

crossover sites. From these sites, Zip2 together with Zip4 and Spo16 polymerise Zip1 outwards along the chromosomal axes (Chua and Roeder, 1998; Shinohara et al., 2008; Tsubouchi et al., 2006). Concomitant with this is the stabilisation of crossover intermediates by Msh4, Msh5 and Mer3. Alternative pathways can extend the SC in the absence of crossing over, but these are subject to opposing positive and negative regulation by temperature and Msh4, respectively. Finally, in the absence of the primary regulator, Zip3, SC extension occurs in a manner that is independent of both temperature and Msh4 (Figure 3.13).

This adds to an increasingly complex picture of how formation of the synaptonemal complex is regulated. Recent work has shown how Zip3 and Fpr3 act to prevent synapsis initiating between non-homologous chromosomes during early meiotic prophase prior to the onset of recombination (Macqueen and Roeder, 2009). Hop2 is also important for preventing non-homologous synapsis by instead promoting synapsis that is contingent upon homolog pairing (Tsubouchi and Roeder, 2002). Synapsis is also regulated by the cohesin maintenance protein, Pds5, which prevents the assembly of the synaptonemal complex between sister chromatids rather than homologous chromosomes (Jin et al., 2009). The work outlined here adds another layer to this regulation in which synapsis between homologous chromosomes is also tightly regulated to ensure that it is coupled to crossing over.

# Chapter 4. Zip1 promotes the segregation of non-exchange chromosomes.

## 4.1. Introduction

Many organisms primarily rely on crossovers between homologous chromosomes to aid their segregation at the first meiotic division. However, there are many examples of organisms that are capable of correctly segregating chromosome pairs that lack crossovers and the mechanisms in place to do so are diverse (see section 1.3 and review by Wolf 1994).

In budding yeast, the existence of a mechanism for segregating non-exchange chromosome pairs was first reported by Dawson *et al.* 1986. This was demonstrated using artificial chromosome 'pairs' with very limited homology to model how chromosomes that fail to cross over segregate during meiosis. The authors found that despite the lack of crossovers, the artificial chromosomes segregated away from each other at the first meiotic division in 90% of meioses (Dawson *et al.*, 1986). This is far from the expected 50% if the chromosomes of non-exchange pairs were to segregate independently of each other. This therefore alluded to the existence of a mechanism to segregate non-exchange chromosomes. Similar levels of non-disjunction have been reported for several other artificial obligate non-exchange pairs, including mini-chromosomes (Ross *et al.*, 1996), two monosomic chromosomes (Loidl *et al.*, 1994) and more recently, homeologous chromosomes (Maxfield Boumil *et al.*, 2003). Homeologous chromosome pairs have related, but non-identical

sequences, which owing to the anti-recombination activity of mismatch repair proteins (reviewed by Borts *et al.* 2000) prevents recombination between them. Strains containing homeologous chromosomes are derived by replacing one copy of a particular chromosome with the equivalent chromosome from a closely related species. For example, replacing one copy of chromosome V in a diploid *Saccharomyces cerevisiae* strain with a single copy of chromosome V from *Saccharomyces carlsbergensis*. These homeologs share ~70% sequence identity and consequently recombine in less than 0.1% of tetrads (Maxfield Boumil et al., 2003). They therefore provide an excellent model for studying non-exchange chromosome segregation.

How is non-exchange chromosome segregation (NECS) mediated? Recent work has demonstrated that non-exchange chromosomes are paired specifically at their centromeres at pachytene (Kemp et al., 2004). This was shown by assaying the association ('pairing') between homeologous chromosomes in surface-spread pachytene nuclei using *LacO* repeats to which constitutively expressed LacI-GFP bound. When the *LacO* repeats were placed close to the centromeres, a single LacI-GFP signal was observed in just over half of the nuclei examined, consistent with the centromeres of the non-exchange chromosomes being 'paired'. However, when the *LacO* repeats were present on the chromosome arm regions, the incidence of a single LacI-GFP signal (indicative of the arms being 'paired') was reduced to the level expected to be observed by chance alone. Instead, a higher proportion of nuclei contained two GFP signals consistent with the arm regions being 'unpaired'. These observations were interpreted as meaning the homeologous (non-exchange) chromosome pairs were paired specifically at their centromeres

during pachytene. This is consistent with previous observations using a different non-exchange chromosome pair that showed the chromosomes were not paired along their lengths in an end-to-end fashion like the exchange chromosomes were, but rather they appeared 'paired' at a distinct site (Loidl et al., 1994). The functional significance of this 'centromere pairing' became apparent by the introduction of a centromere plasmid or a yeast artificial chromosome (YAC), which increased meiosis I non-disjunction of the homeologous (non-exchange) chromosome pair (Kemp et al., 2004). In both cases this was shown to be due to reduced centromere pairing of the homeologous pair because the centromere plasmid or YAC acted as a competitor for centromere pairing. These findings suggest that centromere pairing mediates NECS in *S.cerevisiae*.

What is facilitating centromere pairing of non-exchange chromosomes? Several observations implicate the synaptonemal complex protein, Zip1 as a good candidate. Firstly, Zip1 holds centromeres together in a pair-wise manner very early in meiotic prophase, prior to the onset of recombination. This so-called 'centromere coupling' is independent of homology, with chromosomes coupled together seemingly at random (Tsubouchi and Roeder, 2005). This shows that Zip1 is capable of holding together chromosome pairs at their centromeres. Secondly, a genome-wide screen for genes involved in centromeric cohesion detected elevated non-disjunction of the small chromosome *III* pair in *zip1* $\Delta$  mutants, but a similar increase was not observed for *msh4* $\Delta$  mutants (Marston et al., 2004). As *MSH4* and *ZIP1* are in the same epistasis group for crossing over, the increased non-disjunction observed in *zip1* $\Delta$  mutants cannot have been due to reduced levels of crossovers (Borner et al., 2004; Novak et al., 2001). This suggests that the increased non-disjunction

was not due to the crossover defect of *zip1* $\Delta$  but rather the absence of some other function of Zip1. Thirdly, chromosome segregation is improved in *msh4* $\Delta$  mutants at higher temperatures despite crossover levels remaining largely unchanged. This effect disappeared when *ZIP1* was deleted, suggesting that Zip1 is responsible for the improved chromosome segregation observed in these mutants (Chan et al., 2009). Finally, there are examples in other organisms whereby the synaptonemal complex (SC) assists in the segregation of non-exchange chromosomes. For example, in *Bombyx mori* females crossovers are absent and instead they utilise a modified form of the SC to segregate homologous chromosomes correctly at the first meiotic division (Rasmussen, 1977). Similarly, there is evidence from both plants (Pradillo et al., 2007) and mammals (de la Fuente et al., 2007) that the segregation of non-exchange chromosomes depends on synaptonemal complex proteins. Taken together, these observations imply that the synaptonemal complex protein, Zip1 is a good candidate for facilitating NECS in budding yeast.

## 4.2. Results

### 4.2.1. Deletion of *ZIP1* increases non-disjunction of an obligate non-exchange pair and correlates with a defect in centromere pairing.

In order to study the involvement of Zip1 in non-exchange chromosome segregation (NECS) a diploid strain bearing a homeologous chromosome V pair (*S.carlsbergensis* chromosome V replacing one copy of *S.cerevisiae* chromosome V) was used. The homeolog pair contained 256 *LacO* repeats ~12kb from CEN5 to which constitutively expressed LacI-GFP bound. This allowed the centromeres of the non-exchange pair to be followed cytologically throughout meiosis (referred to as *neCEN5* throughout). In order to examine whether deletion of *ZIP1* influenced segregation of the homeolog pair, the GFP foci corresponding to the non-exchange chromosomes were examined in tetrads. Normal meiosis yields a tetrad in which each of the four spores contains a single GFP focus (Figure 4.1 A, left), whereas a meiosis I non-disjunction event results in two spores that contain two GFP foci and two with none (Figure 4.1 A, right). As the GFP signal can be spontaneously lost, only tetrads in which all four GFP foci were discernable were included. Non-disjunction of the homeologs (herein referred to as 'non-exchange pair') occurred at a frequency of 11% in the wild type (Figure 4.1 C). This frequency is similar to that inferred from genetic data using the same non-exchange pair. This was done using different prototrophic markers on each chromosome of the non-exchange pair and inferring their segregation from prototrophic assessment of each spore in a tetrad (Cheslock et al., 2005; Maxfield Boumil et al., 2003). Deletion of *ZIP1* resulted in a ~3-fold increase in non-disjunction (27 %, Figure 4.1 C). In order to

Figure 4.1

rule out that tetrads with two GFP foci in two of the four spores were not the result of meiosis II non-disjunction, cells were examined at the binucleate stage. Hoechst-staining of the DNA allowed the identification of binucleates without having to fix the cells, which can attenuate the GFP signal. This method revealed meiosis I non-disjunction frequencies similar to those measured from tetrads (Figure 4.1 B and C).

Zip1 has recently been shown to be important for preventing crossing over at the centromere (Fung et al., 2004). Crossovers placed too close to centromeres increase the incidence of precocious sister chromatid separation (Rockmill et al., 2006). It was therefore formally possible that increased precocious sister chromatid separation of the non-exchange chromosomes may have been responsible for the increased proportion of tetrads that had experienced apparent meiosis I non-disjunction. However, precocious sister chromatid separation (two spores with one focus, one with two and one with none) occurred at a frequency <5% in the wild type and *zip1* $\Delta$  mutant. These findings verified the tetrad data that Zip1 is indeed important for the segregation of the non-exchange pair during the reductional division (meiosis I).

In order to examine whether the increased meiosis I non-disjunction observed in *zip1* $\Delta$  mutants was due to the reduced number of crossovers in *zip1* $\Delta$  mutants, *msh4* $\Delta$  mutants were analysed, which are in the same epistasis group as *zip1* $\Delta$  for crossing over (Borner et al., 2004; Novak et al., 2001). Unlike *zip1* $\Delta$  mutants, *msh4* $\Delta$  mutants displayed meiosis I non-disjunction frequencies similar to wild type (Figure 4.1. C), suggesting that the increased meiosis I non-disjunction of the non-exchange chromosome pair observed in *zip1* $\Delta$  mutants was not an indirect result of reduced crossing over.

Centromere pairing during pachytene is the proposed mechanism by which non-exchange chromosomes segregate at meiosis I (Kemp et al., 2004). In order to determine whether centromere pairing was also influenced by deletion of *ZIP1*, surface spread nuclei were prepared and immuno-stained with anti-GFP antibodies to follow the non-exchange pair (*neCEN5*). In wild type, pachytene is characterised by highly condensed DNA and fully synapsed chromosomes (linear Zip1 staining) that allowed unambiguous identification of pachytene nuclei. A single GFP focus was observed when the homeologous chromosomes were paired, whereas two were observed when they were unpaired (Figure 4.1 D). The frequency of paired *neCEN5*s in wild-type pachytene nuclei was 55%, similar to the 54% reported by Kemp et al. 2004 using FISH (Figure 4.1 E). Obviously, Zip1 could not be used as a marker for pachytene in *zip1Δ* cells, so condensed DNA and a single brush-like dot of tubulin was used to mark pachytene in these nuclei. When this method was done for the wild type, it revealed similar levels of *neCEN5* pairing as those assessed using Zip1 to select for pachytene nuclei (60 %, n = 40). This analysis revealed a ~4-fold decrease in *neCEN5* pairing in the *zip1Δ* mutant (14%, Figure 4.1 E). The distances between unpaired (>0.5 μm apart) *neCEN5* foci showed a similar distribution in wild type and *zip1Δ* mutants (Figure 4.2), suggesting the chromosomes were spread out to a similar extent in both cases. Despite this, wild type cells displayed frequencies of *neCEN5* pairing nearly 5-fold higher than that of the *zip1Δ* mutant (Figure 4.2). This suggests that Zip1 may be responsible for holding non-exchange chromosomes together at their centromeres.

Figure 4.2

In order to examine whether Zip1-dependent centromere pairing was also independent of Zip1's crossover-promoting role, pairing was assessed in the *msh4Δ* mutant (see above). As with non-disjunction frequencies, centromere pairing in the *msh4Δ* mutant was similar to wild type (Figure 4.1 E), further supporting the notion that general reductions in crossing over do not influence NECS. To summarise, Zip1 promotes centromere pairing at pachytene and this correlates with accurate disjunction of the non-exchange chromosome pair at meiosis I.

#### **4.2.2. Differential requirements for the 'ZMM' proteins in non-exchange chromosome segregation.**

The fact that the centromere pairing and meiosis I non-disjunction frequencies of the *msh4Δ* mutants were similar to wild type, despite *msh4Δ* and *zip1Δ* mutants belonging to the same epistasis group for crossing over raises the question of what other 'ZMM's participate in NECS. To this end, deletion mutants were made for most of the remaining *ZMM* genes (*zip2Δ*, *zip3Δ*, *zip4Δ* and *mer3Δ*) and each was assessed for centromere pairing and non-disjunction of the non-exchange pair. Like the *msh4Δ* mutant, *mer3Δ* mutants appeared indistinguishable from wild type for both centromere pairing and meiosis I non-disjunction (Figure 4.3). In contrast, *zip2Δ*, *zip3Δ* and *zip4Δ* mutants appeared more like *zip1Δ* mutants with respect to both *neCEN5* pairing and non-disjunction (Figure 4.3). These findings suggest there are differential requirements for the 'ZMM' proteins in NECS. The 'DNA transaction' proteins Msh4 and Mer3 (see Chapter 3) are dispensable, whereas the proteins required for the initial deposition (Zip3) and extension (Zip2 and Zip4) of Zip1 polymers

Figure 4.3

into synaptonemal complexes are involved in NECS. These results imply that the synaptonemal complex proteins promote centromere pairing that correlates with improved non-exchange chromosome segregation, whereas Msh4-Msh5 and Mer3 are dispensable for this process.

#### **4.2.3. Zip1-dependent centromere pairing is observed throughout meiotic prophase.**

In order for centromere pairing of non-exchange chromosomes to promote their segregation at the first meiotic division, the pairing must be retained beyond pachytene. To this end, *neCEN5* pairing was followed throughout a meiotic time course. Whole cells were taken at the indicated time point and individual cells were scored as having 'paired' or 'unpaired' *neCEN5*s depending on whether one or two GFP signals were discernable. For wild-type cells, *neCEN5* pairing remained fairly steady (~60%) until the onset of the meiotic nuclear divisions where the non-exchange chromosomes (and therefore GFP foci) were partitioned from one another (Figure 4.4 A). This is consistent with the centromeres remaining paired throughout prophase until the meiotic divisions. In contrast, the pairing frequencies remained relatively low throughout the time course in *zip1* $\Delta$  mutants, consistent with a failure to pair the centromeres throughout meiotic prophase in this mutant (Figure 4.4 B). However, owing to the asynchrony of meiotic cultures of this strain background (S288C), any transient loss of centromere pairing at a particular stage of meiotic prophase may have gone undetected. To account for this asynchrony, *neCEN5* pairing was also assessed in surface-spread nuclei at different stages. The diplotene stage follows pachytene and is characterised by de-condensed

Figure 4.4

chromatin and separated spindle pole bodies visualised as two ‘dots’ of tubulin (Figure 4.5 C). Metaphase I is defined by the presence of a short club-shaped spindle (~2  $\mu\text{m}$ , Figure 4.5 E). Pairing of the *neCEN5s* was reduced slightly at diplotene (40%) relative to pachytene (56%) for the wild type, but this difference was not significant ( $p = 0.12$ ). During metaphase I, *neCEN5s* were paired in 49% of nuclei examined. This was similar to the *msh4 $\Delta$*  crossover-control mutant (Figure 4.5 B, D and F). In contrast, *neCEN5* pairing remained low (~15-20%) for *zip1 $\Delta$*  and *zip3 $\Delta$*  mutants at both diplotene and metaphase I. Although pairing was marginally increased in the *zip3 $\Delta$*  mutant compared to *zip1 $\Delta$* , this difference was not significant ( $p = 0.25$ , Figure 4.5 D and F). In summary, the non-exchange chromosomes are paired at their centromeres in diplotene and metaphase I nuclei, which is consistent with the interpretation that centromeres remain paired throughout meiotic prophase until the first meiotic division. This pairing depends upon Zip1 and Zip3.

Surprisingly, despite *zip2 $\Delta$*  mutants exhibiting *zip1 $\Delta$* -like pairing frequencies at pachytene, in diplotene and metaphase I *neCEN5s* were paired just as frequently as in wild type nuclei (Figure 4.5 B, D and F). This ‘delayed’ pairing was at least partially Zip1-dependent as deletion of *ZIP1* returned the pairing frequency to <30%. Curiously, despite *zip2 $\Delta$*  mutants achieving wild type levels of *neCEN5* pairing by metaphase I, the non-exchange pair non-disjoined with similar frequencies to *zip1 $\Delta$*  mutants (Figure 4.3 B). This suggests that the delayed pairing observed in *zip2 $\Delta$*  mutants is not sufficient to support disjunction of the non-exchange pair at the reductional division.

Figure 4.5

In an attempt to understand better why wild type and *zip2Δ* mutants exhibit vastly different chromosome segregation phenotypes despite similar levels of *neCEN5* pairing at metaphase I, the positions of *neCEN5*s were plotted relative to the metaphase spindle as was done by Kemp *et al.* 2004 (Figure 4.6). Such plots are based on the position of *neCEN5*s in relation to the spindle as inferred from immuno-fluorescence of fixed nuclei. This study revealed that the centromeres of homeologous (non-exchange) chromosomes separated precociously to opposite spindle poles in metaphase I-arrested wild-type cells. This was unique to non-exchange chromosomes as homologous exchange chromosomes were generally paired and attached to the metaphase I spindle (Kemp *et al.*, 2004). In an attempt to identify differences in *neCEN5* behaviour between wild type and *zip2Δ* nuclei at metaphase I, plots similar to those presented by Kemp *et al.* were generated.

The spindle is represented by the green club-shaped symbol on the x-axis and the spindle length is shown on the y-axis (Figure 4.6). The black circles represent paired *neCEN5*s whereas the blue triangles and red squares represent unpaired chromosome pairs. Data points that fall between the two arrows on the x-axis represent *neCEN5*s that were on the spindle, whereas the data points either side of this range represent *neCEN5*s that were off the spindle. This analysis revealed that a proportion of *neCEN5*s do indeed appear at opposite spindle poles in wild type, as reported by Kemp *et al.* (Figure 4.6 A). It also revealed that a larger proportion of *neCEN5*s were not attached to the spindle in *zip1Δ* mutants (61 %) compared to wild type (35 %) and *zip2Δ* mutants (46 %). Crucially, this analysis revealed a higher proportion of unpaired *neCEN5*s that were at or near the same spindle pole in *zip1Δ* and *zip2Δ*

Figure 4.6

mutants (compare the distribution of blue triangles on the left-hand side of the plots for Figures 4.6 A-C). If these represent chromosomes that had segregated precociously, then this explains the increased non-disjunction in *zip1* $\Delta$  and *zip2* $\Delta$  mutants. However, there did not appear to be any striking differences in the distribution of paired *neCEN5*s between wild type and *zip2* $\Delta$  mutants (Figure 4.6 A and C). A similar proportion of paired *neCEN5*s were observed as being attached to the spindle for wild type (63%) and for *zip2* $\Delta$  mutants (61 %). It therefore remains unclear as to why the non-disjunction frequencies are so high in *zip2* $\Delta$  mutants despite *neCEN5* pairing frequencies during metaphase I being indistinguishable from those of wild type nuclei. It is likely that the defect in *zip2* $\Delta$  mutants may be more subtle than could be detected by this type of analysis (see discussion).

To conclude, these findings imply that the association of centromeres has to occur prior to diplotene in order to support correct disjunction of the non-exchange chromosome pair at meiosis I.

#### **4.2.4. Zip1 is observed at *neCEN5*s throughout meiotic prophase.**

If Zip1 is directly mediating centromere pairing of the non-exchange chromosomes, it should localise there. Non-exchange chromosomes do not undergo extensive synapsis like that observed for fully synapsed exchange chromosomes (Loidl et al., 1994). This is consistent with the observation that non-exchange chromosomes are only paired at their centromeres, not at arm regions (Kemp et al., 2004). Indeed, in well-spread pachytene nuclei, Zip1 was

frequently observed as a focus directly co-localised with *neCEN5s* (Figure 4.8 A, C and E). If Zip1 is responsible for the pairing of centromeres of non-exchange chromosomes throughout meiotic prophase until the first meiotic division, it should be detectable following SC disassembly at diplotene. To this end, wild type diplotene nuclei were stained for GFP (*neCEN5*), Zip1 and tubulin. The Zip1 staining observed at this stage was faint compared to pachytene nuclei, but several foci of Zip1 could be discerned. Foci of Zip1 frequently co-localised with both paired and unpaired *neCEN5* foci (Figure 4.7 A-C). Furthermore, Zip1 was detected even later in metaphase I nuclei frequently co-localising with the *neCEN5s* (4.7 D and E). This could not, however, be accurately quantified as Zip1 often showed confluent staining along the spindle where *neCEN5s* were also often found. Thus determining whether they directly co-localise at this stage was ambiguous. Direct co-localisation was easier to discern when the *neCEN5s* were not attached to the spindle (Appendix Figure 3). Thus, Zip1 frequently co-localised with *neCEN5s* during pachytene and beyond, supporting the notion that Zip1 holds the centromeres of non-exchange pairs together throughout meiotic prophase until the first meiotic division, where it promotes their disjunction.

#### **4.2.5. Localisation of Zip1 to *neCEN5s* depends upon Zip3.**

Zip3 has been proposed to be the upstream regulator of Zip1, responsible for the initial deposition of Zip1 at synapsis initiation sites (Agarwal and Roeder, 2000; Shinohara et al., 2008). In order to investigate whether Zip3 is also required for the deposition of Zip1 at the centromeres of non-exchange

Figure 4.7

Figure 4.8

chromosomes, the association of Zip1 with *neCEN5s* was assessed in *zip3Δ* mutants. In contrast to wild type, fewer of the *neCEN5s* co-localised with Zip1 during pachytene in *zip3Δ* mutants and those that lacked Zip1 were predominantly unpaired (Figure 4.8). These findings correlate the localisation of Zip1 to *neCEN5s* with their pairing capacity. Thus, the centromere pairing defect and increased non-disjunction observed in *zip3Δ* mutants may be explained by a failure to localise Zip1 to centromeres of the non-exchange pair.

During this analysis, it was noted that the intensity of any detectable Zip1 signal was often fainter for the unpaired *neCEN5s* and for the *zip3Δ* mutant. In an attempt to quantify this, analysis on the pixel intensities was performed using 'R' ([www.r-project.org](http://www.r-project.org)) (Figure 4.9). In brief, pixel intensities were extracted for each channel (Zip1 and *neCEN5*) and the background was subtracted (Figure 4.10 A-C). The channels were overlaid (Figure 4.10 E and F) and the regions surrounding each *neCEN5* focus were manually selected (Figure 4.10 H and I). For each *neCEN5* focus, the proportion of pixels that contained Zip1 signal was calculated whereby a value of '1' indicates that all *neCEN5* pixels also contained Zip1 signal and '0' when none of the *neCEN5* pixels were Zip1-positive ('Proportion', Figure 4.11). This analysis revealed a median value of 0.74 for paired *neCEN5s* compared to 0.25 for unpaired in wild type nuclei. This suggests that Zip1 covers a larger area of paired *neCEN5s*. Next, the total signal intensity of this overlapping Zip1 was averaged across either the whole *neCEN5* focus ('General Zip1 intensity'), or just those pixels overlapping with Zip1 ('Specific Zip1 intensity') and normalised to the mean Zip1 intensity of a synapsed pachytene chromosome. Thus, a value of '1' represents equal Zip1 intensity on the *neCEN5* and the synapsed pachytene chromosomes.

Figure 4.9

Figure 4.10

Interestingly, normalised Zip1 intensities were seldom >1 and were often much lower, suggesting that the Zip1 associated with *neCEN5s* is less abundant compared to the synapsed exchange chromosomes (Figure 4.11 B and C). Both 'General' and 'Specific' Zip1 intensities the values were generally higher for paired than for unpaired *neCEN5s*, suggesting that more Zip1 protein was present at paired centromeres. This supports the proposition that Zip1 is responsible for pairing centromeres of non-exchange chromosomes.

For the *zip3Δ* mutant both the 'proportion' of *neCEN5s* covered with Zip1 and the intensity of this Zip1 was decreased relative to wild type (Figure 4.11). Thus, *zip3Δ* mutants appear defective in steady-state localisation of Zip1 to *neCEN5s*.

To summarise, Zip1 co-localises with *neCEN5* signals. The extent of Zip1 localisation during pachytene correlates with pairing, suggesting that Zip1 may directly tether the centromeres of non-exchange chromosomes. This centromeric localisation of Zip1 depends on Zip3. This is analogous to the regulation of Zip1 at synapsis initiation sites where Zip3 is believed to be required for the initial deposition of Zip1.

#### **4.2.6. Synapsis initiation proteins, Zip2 and Zip4 are required for Zip1-mediated centromere pairing.**

Having ascertained the synapsis initiation protein Zip3 is required for the localisation of Zip1 to *neCEN5s*, the roles of two other synapsis initiation proteins (Zip2 and Zip4) were investigated. First, the co-localisation of Zip1 with

Figure 4.11

*neCEN5s* was assessed in *zip2* $\Delta$  and *zip4* $\Delta$  mutants. In contrast to *zip3* $\Delta$  mutants, *zip2* $\Delta$  mutants accumulated Zip1 at the centromeres of the non-exchange pair as shown by bright foci of Zip1 directly overlapping with *neCEN5* (Figure 4.12 A and C). This was irrespective of pairing, with the majority of *neCEN5s* unpaired but with Zip1 co-localised to both centromeres (78%, Figure 4.12 E). Thus, despite the accumulation of Zip1, the majority of *neCEN5s* were unpaired implying that Zip1 localisation to centromeres is not sufficient to pair them.

*zip4* $\Delta$  mutants appeared similar to *zip2* $\Delta$  mutants with a large proportion of *neCEN5s* unpaired but with Zip1 co-localised to both centromeres (60%, Figure 4.12 F). Therefore, as was the case for *zip2* $\Delta$  mutants, the majority of *neCEN5s* failed to pair despite proficient localisation of Zip1 to *neCEN5s* (Figure 4.12 D and E).

To conclude, Zip2 and Zip4 appear to be dispensable for the localisation of Zip1 to centromeres of non-exchange chromosomes. However, Zip1 localisation alone is not sufficient to 'tether' centromeres together. This function of Zip1 depends upon Zip2 and Zip4 activity, although precisely how these proteins regulate Zip1 remains to be determined.

Figure 4.12

#### **4.2.7. Zip1 does not facilitate centromere pairing when C-terminally tagged with LacI.**

A recent study showed that the introduction of an artificial 'tether' between non-exchange chromosomes partially rescued their segregation in *mad2Δ* mutants. However, this 'tether' only did so when positioned near the centromeres rather than at arm regions (Lacefield and Murray, 2007). In order to investigate whether Zip1's role in NECS was specific to its localisation at centromeres, Zip1 was tagged with LacI to force its localisation to *LacO* repeats that would be placed at various intervals along the non-exchange chromosomes (*i.e.* near and far from centromeres).

Zip1 is organised within the synaptonemal complex in a tetrameric, head-to-head configuration with the C-termini contacting the lateral elements and the N-termini positioned centrally within the gap between adjacent axes (Dong and Roeder, 2000). As the C-terminus of Zip1 is the part of the protein responsible for its binding to lateral elements, this was the end chosen for tagging with LacI. Moreover, recent work has demonstrated a role for the SUMO-binding motif (SBM) present in the C-terminus of Zip1 in facilitating axes binding (Cheng et al., 2006). This work showed that the staining of Zip1 on meiotic chromosomes was severely disrupted in mutants whereby the hydrophobic leucine, aspartate and glutamate residues present in the SBM were mutated to hydrophilic arginine residues (Cheng et al., 2006). Therefore, in order to control localisation of Zip1, Zip1-LacI fusion proteins were made that lacked the SBM (SBM-containing fusion proteins were also made for comparison, Figure 4.13 A).

Figure 4.13

First of all the Zip1-LacI fusion protein was expressed in strains in which the LacO repeats were ~12kb from the centromeres of the non-exchange pair. These strains also expressed LacI-GFP to allow visualisation of *neCEN5s*. However, when surface-spread pachytene nuclei were stained for Zip1 and GFP (*neCEN5*), the frequency of paired *neCEN5s* was indistinguishable to the *zip1Δ* mutant regardless of SBM status (Figure 4.13 B and C). This was despite Zip1 co-localising with 97% and 96% of *neCEN5s* for the *Zip1-LacI* and *Zip1-SBMΔ-LacI* strains, respectively (Figure 4.13 B). Therefore, despite proficient localisation of the Zip1-LacI fusion proteins to the *LacO* repeats, Zip1 failed to 'tether' the non-exchange chromosomes. Unsurprisingly, non-disjunction frequencies were similar to the *zip1Δ* mutant (Figure 4.13 D). The finding that the LacI-Zip1 fusion protein could not facilitate pairing of the non-exchange pair hampered continuation of the experiment and so the influence of having *LacO* repeats at arm regions was never examined.

#### **4.2.8. Zip1 also co-localises with the centromeres of exchange chromosomes following SC disassembly.**

Whilst analysing the Zip1 staining patterns in diplotene nuclei, it was noticed that the number of Zip1 foci roughly corresponds to the number of homologously paired centromeres (~16). It was therefore hypothesised that these Zip1 foci could co-localise with centromeres. If correct, it would suggest that Zip1 is retained and/or re-loaded at centromeres following SC disassembly. Indeed, when wild type nuclei containing Ctf19-13Myc (centromere marker) were stained for Myc, Zip1 and tubulin, it was revealed that Zip1 co-localised

with most Ctf19-12Myc foci at diplotene (Figure 4.14 A, 2<sup>nd</sup> column). Moreover, Zip1 also co-localised with Ctf19-13Myc at metaphase I when most of the 16 centromere pairs are attached to the spindle (Figure 4.14 A, 3<sup>rd</sup> column). Zip1 was even found juxtaposed to or overlapping with Ctf19-13Myc signals at anaphase I and telophase I after the first meiotic division (Figure 4.14 A, 4<sup>th</sup> and 5<sup>th</sup> columns). However, Zip1 staining was very faint at these stages and sometimes not detectable at all after the first nuclear division.

To verify these findings, the presence of Zip1 at later stages was identified in other strain backgrounds (Figure 4.15 A-C) and control experiments were carried out to confirm the specificity of the Zip1 antibody at these stages (Appendix Figure 4, carried out by Phil Jordan).

#### **4.2.9. Zip1 promotes the segregation of exchange chromosomes.**

As Zip1 is associated with the centromeres of exchange chromosomes, it raises the question as to whether Zip1 promotes the segregation of homologous exchange chromosomes also? To this end, chromosome *III* was labelled with LacO/LacI-GFP allowing the segregation of this chromosome pair to be inferred from tetrads. The chromosome pair non-disjoined at a frequency of 15% in *zip1* $\Delta$  mutants as compared to 7% in the *msh4* $\Delta$  crossover control strain (>100 tetrads examined for each strain), values very similar to that reported in a screen for centromere cohesion genes (Marston et al., 2004). This is despite similar crossover frequencies for chromosome *III* in the two mutants (Borner et al., 2004; Novak et al., 2001).

Figure 4.14

Figure 4.15

Taken together, these findings suggest that centromeric Zip1 is retained and/or re-loaded at all centromeres following SC disassembly until the first meiotic division where it can promote the segregation of both homologous and homeologous chromosome pairs.

### 4.3. Discussion

The results described here demonstrate a novel role for Zip1 in meiotic chromosome segregation. Specifically, Zip1 pairs the centromeres of non-exchange chromosomes and ‘tethers’ them throughout meiotic prophase until the first meiotic division (Figure 4.16). This is analogous to the pairing of the achiasmate chromosome *IV* pair in *Drosophila* females, which occurs throughout prophase until metaphase I (Dernburg et al., 1996). However, Zip1 is also important for the segregation of crossover-proficient chromosome pairs, suggesting that Zip1 may promote the segregation of all chromosome pairs (Figure 4.16). Whether Zip1 is simply a ‘back-up’ segregation mechanism should crossover levels be compromised, or acts in conjunction with crossovers even when the latter are plentiful, remains unclear. This is because of the pleiotropic phenotype of *zip1Δ* mutants that makes it difficult to separate out the individual roles of the protein (Borner et al., 2004; Fung et al., 2004; Sym et al., 1993).

Interestingly, centromere pairing is not completely abolished in *zip1Δ* mutants (14%, not 0%). This suggests that either there is some level of residual pairing, or that 14% is the lowest limit of detection by this assay. Should pairing be completely abolished would two GFP signals be discernable in 100% of nuclei? Previous work by Kemp *et al.* (2004) showed that the centromeres of two heterologous chromosomes, each with their own homologous partners, appear ‘paired’ (a single GFP dot visible) in 15-20% of wild type pachytene nuclei. This is unlikely to represent true ‘pairing’ as each chromosome would be fully synapsed with its partner chromosome at this stage. Instead it is probably

Figure 4.16

the result of two GFP foci being closely juxtaposed by chance or loss of one of the GFP signals due to *LacO*-repeat instability. Thus, it is likely that the 'residual pairing' observed in *zip1* $\Delta$  mutants does not represent true pairing. Regardless of whether pairing is 0% or 14%, there is a shortfall in the expected non-disjunction values assuming that all unpaired NECs segregate at random. For example, assuming centromeres are paired in 14% of *zip1* $\Delta$  nuclei and these chromosomes go on to segregate correctly, one may expect the remaining 86% to segregate at random and thus non-disjoin at a frequency of 43%. However, the observed non-disjunction falls short of this at 27%. A similar observation is true in wild type where the observed non-disjunction (11%) deviates from the 22% expected from pairing frequencies. These findings allude to the existence of a parallel pathway that aids the segregation of unpaired non-exchange chromosomes (see Chapter 6).

Why do non-exchange chromosomes missegregate so frequently in *zip2* $\Delta$  mutants despite proficient centromere pairing at metaphase I? This anomaly cannot be accounted for by aberrant positioning of the paired *neCEN5*s upon the metaphase spindle, nor can it be explained by defective spindle attachment (section 4.2.3). Therefore perhaps the defect could be due to a failure in achieving a bipolar spindle attachment ('bi-orientation'). The pairing observed in *zip2* $\Delta$  mutants may occur too late (diplotene) to support chromosome bi-orientation. For example, *neCEN5* pairing frequencies in *zip2* $\Delta$  mutants closely mimic those of *zip1* $\Delta$  mutants during pachytene, as does the segregation phenotype. These findings suggest that it is the timely formation of centromere pairs that promote improved segregation at meiosis I. It may be that Zip1 forms a scaffold at centromeres to which other proteins such as

kinetochore components assemble around, the net result being kinetochore bi-orientation of the non-exchange pair on the meiosis I spindle. In order to gain further insight into the temporal establishment of pairing and its significance for NECS, experiments could be done whereby *ZIP1* expression is confined to early or late stages in meiotic prophase. Such experiments may provide further insight into precisely how Zip1 promotes the segregation of chromosome pairs.

In contrast, *zip3Δ* mutants experience low centromere pairing frequencies throughout prophase, which correlate with depleted Zip1 signal at *neCEN5s*. Zip3 is a putative SUMO E3 ligase that has been proposed to catalyse the formation of SUMO conjugates at the leading edge of synapsis to which Zip1 binds (Cheng et al., 2006; Hooker and Roeder, 2006). Thus, it could be that Zip3 normally sumoylates a centromeric protein to which Zip1 can bind and pair centromeres.

These findings may appear at odds with a recent study that concluded Zip3 is dispensable for the localisation of Zip1 to the centromeres of non-exchange chromosomes (Gladstone et al., 2009). This conclusion was based on ChIP experiments where Zip1 was immuno-precipitated and PCR was used to amplify a 300bp region spanning *CEN5* of non-exchange chromosomes. The PCR products were similar in abundance for the wild type and *zip3Δ* mutants, which was concluded to mean that Zip3 is dispensable for the localisation of Zip1 to *neCEN5s*. How can this be reconciled with the data presented in this chapter? First, it is unclear what stage the cells represented in the ChIP experiments were in. Cultures were harvested at 13 hours, but no information was given as to what proportion of the cells were in each stage of meiosis at

this time point. Therefore the centromeric Zip1 signal in *zip3Δ* mutants could be a result of inclusion of nuclei in which Zip3-independent centromere 'coupling' is occurring. Secondly, the ChIP experiments only looked at 300bp of the core centromere while work described here looked at the association of Zip1 with the LacO arrays 12kb from *CENV*. It is formally possible that the association of Zip1 differs between these two regions. Finally, the ChIP experiments described by Gladstone *et al.* 2009 did not use real time PCR to quantify *CEN5* signal so a depleted (but not absent) Zip1 signal at the centromeres may have gone undetected by only looking examining the end-product of a PCR reaction. These factors may help account for the discrepancy in the results of the two studies.

The regulation of Zip1-mediated centromere pairing is analogous to the regulation of Zip1 at synapsis initiation sites. In the latter, Zip3 is required for the initial deposition of Zip1 following which Zip2 (together with Zip4 and Spo16) polymerise Zip1 outwards along the chromosomal axes enabling Zip1 to develop into mature SC (Shinohara *et al.*, 2008). A similar model could be proposed for the regulation of centromeric Zip1; Zip3 deposits Zip1 at centromeres, following which Zip2 and Zip4 enable Zip1 to 'tether' the centromeres together so they appear paired (Figure 4.16). The involvement of Zip2 and Zip3 in Zip1-mediated centromere 'pairing' was slightly unexpected given that Zip1-mediated centromere 'coupling' that occurs early, prior to recombination is independent of these proteins (Tsubouchi and Roeder, 2005).

The finding that Zip1 is retained at all centromeres following SC disassembly is reminiscent of the retention of SYCP3 at centromeres in

mammals. SYCP3 is a lateral element protein, which following SC disassembly in mouse and rat spermatocytes remain at the centromeres until metaphase I (Page et al., 2006). Here it is believed to aid both monopolar orientation of sister kinetochores (Kouznetsova et al., 2007; Parra et al., 2004) and potentially the segregation of achiasmate sex chromosomes (de la Fuente et al., 2007). Furthermore, in marsupial males it has been shown that a SYCP3-rich structure that also contains the central element protein SYCP1, which promote the segregation of the achiasmate XY chromosome pair (Page et al., 2006). Similarly, *Bombyx mori* females that lack crossing over all together use a modified form of the synaptonemal complex to segregate their chromosome pairs at meiosis I (Rasmussen, 1977). These findings suggest that the ability of the SC components to promote chromosome segregation is conserved from yeast through to mammals. Perhaps SC-mediated chromosome segregation represents an evolutionary relic from a time when cells had not yet evolved crossover-mediated chromosome segregation. Then owing to the improved fidelity of crossover-mediated segregation it was subject to strong evolutionary selection, rendering the SC-mediated mechanism largely dispensable. However, this SC-mediated mechanism would be called into play should crossover levels be compromised or a chromosome pair fail to cross over (such as the XY pair) and consequently this mechanism has been maintained by evolution.

Crossover position has important implications for meiotic chromosome segregation. Centromere-proximal crossovers are better at aiding bi-orientation and subsequent segregation of chromosome pairs at meiosis I than centromere-distal crossovers (Lacefield and Murray, 2007). However,

crossovers too close to centromeres are associated with precocious separation of sister chromatids in both yeast (Rockmill et al., 2006) and humans (Lamb et al., 1996). Thus a balance must be struck where crossovers are placed near enough to centromeres to support kinetochore bi-orientation, but not so close that they disrupt sister chromatid cohesion around the centromere. Zip1 provides a solution to this conundrum by both preventing centromeric crossing over (Chen et al., 2008) and promoting bi-orientation of chromosome pairs. In this fashion, Zip1 provides an excellent substitute for having crossovers directly at centromeres.

To conclude, the work outlined here reveals a novel role for the central element protein, Zip1 in the segregation of non-exchange chromosomes at the first meiotic division. Zip1 carries out this function by tethering the centromeres of non-exchange chromosomes during pachytene through to the first meiotic division. This process is dependent upon the synaptonemal complex proteins, Zip2, Zip3 and Zip4, but not 'DNA transaction' proteins, Mer3 and Msh4, highlighting a separation-of-function for the 'ZMM' proteins in NECS. Zip1 may also assist in the segregation of exchange chromosomes in situations when crossing over is compromised or crossover position is sub-optimal.

# Chapter 5. Distinct roles for Zip2 and Zip3 in synaptonemal complex formation.

## 5.1. Introduction

Assembly of the tripartite synaptonemal complex during meiotic prophase requires the activity of several synapsis-initiation proteins. These include Zip2, Zip3, Zip4 and Spo16. Together these proteins assist in the assembly of the central element protein, Zip1 at synapsis initiation sites and the extension of Zip1 protein along the axes of paired homologous chromosomes.

Mutants lacking these synapsis-initiation proteins are characterised by defective synapsis and large aggregates of Zip1 (poly-complexes) that are indicative of a failure to incorporate Zip1 into synaptonemal complexes. Although both Zip2 and Zip3 are involved in the initiation of synapsis, they are characterised by distinct synapsis phenotypes. Cells deleted for *ZIP2* accumulate Zip1 as foci at sites of axial associations and fail to polymerise Zip1 into cytologically detectable 'stretches' (Chua and Roeder, 1998). This is very similar to the phenotypes described for *zip4* $\Delta$  (Tsubouchi et al., 2006) and *spo16* $\Delta$  mutants (Shinohara et al., 2008). In contrast, *zip3* $\Delta$  mutants undergo some synapsis but this is delayed relative to wild type and incomplete, limited to only some of the 16 chromosome pairs (Agarwal and Roeder, 2000). A recent study has claimed that Zip3 is dispensable for a subset of synapsis initiation events as short stretches of Zip1 form in the absence of Zip3. These 'early' stretches of Zip1 that form are predominantly associated with centromeres

(Tsubouchi et al., 2008). However, whether the short Zip1 stretches that are observed in *zip3Δ* mutants represent the same short stretches that are seen in wild type is unclear. Especially given that Zip3 also has a role alongside Fpr3 in preventing premature synapsis (Macqueen and Roeder, 2009).

Both Zip2 and Zip3 are dispensable for Zip1-mediated 'centromere coupling' that occurs very early during meiotic prophase prior to the initiation of recombination (Tsubouchi and Roeder, 2005). Curiously, however Zip3 foci co-localise with centromeres during early meiotic prophase (Tsubouchi et al., 2008). Following the initiation of recombination, Zip2 and Zip3 are required for Zip1-mediated 'centromere pairing' that holds non-exchange chromosomes together at pachytene, although they appear to have distinct roles in this process (Chapter 4). Mutants deleted for *ZIP3* fail to localise Zip1 to the centromeres of non-exchange chromosomes, whereas mutants lacking *ZIP2* are proficient in Zip1 localisation, but the centromeres fail to pair. This suggests that Zip3 is required for re-loading of Zip1 at centromeres and Zip2 is required to enable Zip1 to 'tether' centromeres into pairs. It is unclear why 'centromere coupling' that appears mechanistically similar to this process does not require Zip2 or Zip3, but is likely to reflect temporal differences in the regulation of Zip1.

Zip3 is a putative SUMO E3 ligase containing a RING finger motif, shared by other SUMO E3 ligases (such as Siz1 and Siz2), which is thought to be important for E3 catalytic activity (Cheng et al., 2006). On the other hand, a bioinformatic study implicated Zip3 as a putative ubiquitin E3 ligase (Perry et al., 2005). However, this is generally disfavoured given several observations. First of all, Zip3 has been shown to have SUMO E3 activity *in vitro* (Cheng et al., 2006). Second, protein sequence alignments show that Zip3 has a conserved

histidine residue within the RING finger motif that is unique to SUMO E3 ligases. The equivalent residue is a cysteine in ubiquitin E3 ligases (Cheng et al., 2006). Finally, any changes to global ubiquitin conjugation patterns were not observed in cells lacking Zip3 (Cheng et al., 2006). These findings strongly suggest that Zip3 is indeed a SUMO E3 ligase. Mutations in the RING finger motif result in aberrant SC formation as well as <5% sporulation efficiency, suggesting that the function of Zip3 in meiosis is highly dependent on its SUMOylation activity.

Less is known about the biochemical activity of the Zip2 protein. It contains 14 WD40 repeats that may form a linked pair of 7-blade propellers. Such motifs are frequently found in proteins associated with ubiquitination complexes, such as Cdc20 and Cdh1, which are co-activators of the anaphase-promoting complex (Kraft et al., 2005; Perry et al., 2005). Furthermore, Zip2 has been shown to interact by yeast two-hybrid with the cullin protein Cdc53, a member of the SCF ubiquitin ligase complex (Seol et al., 2001; Uetz et al., 2000). These findings implicate that Zip2 is involved in the ubiquitin-labelling pathway.

Zip1 has unique functions at the centromeres in promoting chromosome segregation (Gladstone et al., 2009; Newnham et al.) as well as preventing centromere-proximal crossovers (Chen et al., 2008) that increase precocious separation of sister chromatids (Rockmill et al., 2006) and engaging chromosomes in 'centromere coupling' during early meiotic prophase. Given the importance of centromeric Zip1 and the clues that suggest it may be differentially regulated by Zip2 and Zip3 (Chapter 4), the behaviour of centromeric Zip1 was analysed in *zip2Δ* and *zip3Δ* mutants.

## 5.2. Results

### 5.2.1. Zip1 shows strong association with centromeres in *zip2* $\Delta$ mutants, but is depleted from centromeres in *zip3* $\Delta$ mutants.

The fact that Zip1 is retained at centromeres following SC disassembly suggests that centromeric Zip1 is subject to distinct regulation to the Zip1 present at arm regions. Furthermore, Zip1 is retained at the centromeres of both exchange and non-exchange chromosomes, suggesting that Zip1 present at centromeres is subject to the same regulation regardless of exchange status. Given that the centromeric association of Zip1 on non-exchange chromosomes differed strikingly for *zip2* $\Delta$  and *zip3* $\Delta$  mutants, it was investigated whether the same was true for exchange chromosomes. To this end, the kinetochore protein, Ctf19 was tagged with a 13 x Myc epitope to identify centromeres in surface-spread nuclei. Wild type pachytene nuclei stained for Zip1, Myc and DAPI revealed highly condensed DNA, fully synapsed chromosomes (end-to-end association of Zip1) and ~16 Ctf19 foci indicative of all 32 chromosomes being homologously paired (Figure 5.1.A). Unsurprisingly, in these nuclei with fully synapsed chromosomes a high proportion (80%) of the Ctf19-13Myc foci examined (n=213) directly overlapped with Zip1 (Figure 5.1.E). However, 14 % of Ctf19 foci were touching, but not overlapping with Zip1 signal ('juxtaposed'). This apparent juxtapositioning observed in wild type may be due to mature SC appearing discontinuous in places, which has been reported previously (Joshi et al., 2009). In contrast, *zip2* $\Delta$  mutants at the equivalent stage only contained dotted Zip1 staining, consistent with previous findings (Borner et al., 2004; Chua and Roeder, 1998). This made it difficult to stage the nuclei, so tubulin was used alongside condensed DNA to confirm that the nuclei were in pachytene.

Figure 5.1

High levels of co-localisation between Zip1 and Ctf19-13Myc foci were observed in these nuclei with 76% of Ctf19-13Myc foci examined (n=341) directly co-localised with Zip1 foci (Figure 5.1. B and E). However, Zip1 foci were not confined to centromeres with many more Zip1 foci than Ctf19 foci. These foci are likely to represent sites of axial associations that may mark future crossover sites (Chua and Roeder, 1998). Moreover, as was the case with *neCEN5s* (Chapter 4) the Zip1 signals present at centromeres frequently appeared brighter than the foci present elsewhere.

A contrasting pattern was observed for *zip3Δ* mutants. At stages where the DNA appeared highly condensed, Zip1 was frequently observed as extensive stretches along the chromosome arms but appeared depleted at the centromeres (Figure 5.1 C and D). Even when Ctf19 did co-localise with Zip1, the Zip1 signal often appeared very faint. The majority of Ctf19 foci were juxtaposed (41 %) to Zip1 rather than co-localised (31 %, Figure 5.1 E). This suggests that Zip3 is important for the stable localisation of Zip1 to centromeres of exchange chromosomes during pachytene.

These observations are similar to those observed for the non-exchange chromosomes, suggesting that centromeric Zip1 is regulated in the same way for exchange and non-exchange chromosomes. In the absence of Zip3, Zip1 is depleted from centromeres whereas in the absence of Zip2, Zip1 localises proficiently to centromeres and in some instances appears to accumulate at these sites.

### 5.2.2. Development of a program to quantify Zip1-Ctf19 co-localisation.

Classical co-localisation studies (as described above) are, by their nature, quite subjective. That is, what is deemed to be 'co-localised' is likely to vary depending on the criteria of the individual doing the assessment.

Moreover, by categorising foci as 'co-localised' or not makes the resulting data binary and fails to take into account the varying extent of co-localisation. For example, the fact that Zip1 signal often appeared brighter at centromeres than elsewhere in *zip2Δ* mutants is not represented in the classical co-localisation analysis shown in Figure 5.1.E. An ideal solution would be to undertake similar analysis as done for Zip1-*neCEN5* using 'R' (Chapter 4). Though effective, this analysis was very labour-intensive, owing to the need to manually define 'objects' for analysis, which was not trivial given the limited user interface.

Clearly, to do the same analysis when there are 16 centromeres per nucleus to analyse (rather than 1 or 2 for *neCEN5*) would be extremely arduous.

To this end, a computer program was developed to perform automated object-detection and subsequently quantify the extent of protein co-localisation. The program was named 'ColoS'. The main aim of the program was to standardise image analysis thereby minimising confounding variables such as when background is subtracted manually for each image. The program uses a combination of image filters and edge-detection algorithms to remove background 'noise' from each channel and define individual objects (Du et al., 2006) <http://www.codeproject.com>). Channels are then overlaid and the program computes the three same statistics defined in the *neCEN5*-Zip1 analysis (Chapter 4, detailed schematically in Figure 5.2). These include the proportion of each Ctf19 focus that contains Zip1 signal ('Proportion') and of

Figure 5.2

these Zip1-positive pixels, how the intensity compares to the Zip1 present at arm regions. This is done by taking the mean of Zip1-positive pixels in each Ctf19 focus and normalising it to the mean of all other Zip1 pixels in the image that do not overlap with a Ctf19 focus. In this way, the intensity of Zip1 at each centromere is compared to the intensity of non-centromeric Zip1. 'General' Zip1 intensity derives from taking the total Zip1 intensity of Zip1-positive pixels present within a Ctf19 focus and dividing it by the total number of pixels within that Ctf19 focus, whereas 'specific' Zip1 intensity is instead derived by dividing this number by just the number of Zip1-positive Ctf19 pixels within that Ctf19 focus. Or put simply, 'general' Zip1 intensity is averaged out across the whole centromere while 'specific' is averaged out across just the part that overlaps.

However, the presence of poly-complexes in *zip2Δ* and *zip3Δ* mutants would have skewed the normalised Zip1 intensity values. This is because poly-complexes (PCs) are so much brighter than chromatin-bound Zip1 signals that they often saturate the pixel 'counts' of the camera rendering the chromatin-bound Zip1 much less intense in comparison. Thus, if centromeric Zip1 were to be normalised to all non-centromeric Zip1 (which would include PCs) in these mutants, it would appear artificially low. To circumvent this problem, the program detects poly-complexes and removes them so that the mean non-centromeric Zip1 intensity only reflects chromatin-bound Zip1 present along the chromosome arms (Figure 5.2, box 3).

Finally, the program generates graphical outputs for each image analysed showing the raw image for each channel and the image following background subtraction. It also numbers each Ctf19 focus and displays the corresponding statistics, so the user can easily trace which data corresponds to

Figure 5.3

Figure 5.4

which centromere (Figure 5.3). Additional graphical outputs are also produced (Figure 5.4).

The results of such analysis revealed the following. The 'proportion' of each Ctf19 foci co-localised with Zip1 in wild type pachytene nuclei was on average  $0.85 \pm 0.13$  (S.D), where a value of 1 indicates that 100% of Ctf19 pixels contained Zip1 signal (Figure 5.5 A or Appendix Figure 5). The fairly narrow distribution either side of the median suggests that the majority of centromeres had ~80-90% of their area covered by Zip1. The normalised Zip1 intensity present at centromeres also showed a relatively narrow distribution around, or just above 1 (where a value of 1 represents centromeric Zip1 being of equal intensity to that of arm regions, Figure 5.5 B and C). These findings are consistent with cytological observations that Zip1 signal is evenly distributed along the chromosomal axes in pachytene nuclei and this pattern appears homogeneous between chromosomes (Figure 5.5 or Appendix Figure 5)

For the *zip2* $\Delta$  mutant, the proportion of each centromere containing Zip1 signal was similar although slightly decreased relative to wild type ( $0.69 \pm 0.34$ ) with the data showing a wider distribution to wild type. However, the fact that the median (0.83) is higher than the mean (0.69) is consistent with the data being skewed towards '1' (Figure 5.5 A). The majority of centromeres have most of their area covered by Zip1, but some did not contain any in *zip2* $\Delta$  mutants (33 out of 260 centromeres, 13 %). A similarly wide distribution was observed for both the 'specific' and 'general' Zip1 intensities. These values showed a broad distribution in *zip2* $\Delta$  mutants, ranging from 0 to 4 for 'specific' intensity (0 to 3.9 for 'general') with a mean of  $1.4 \pm 0.9$  ( $1.2 \pm 0.9$  for 'general').

Figure 5.5

This suggests that whilst many centromeres have similar levels of Zip1 to that found elsewhere along the chromosome arms, some centromeres lack any Zip1 and others accumulate up to four times as much Zip1 to that present at non-centromeric locations (Figure 5.5 B and C or Appendix Figure 5).

The same analysis was performed for *zip3Δ* mutants and this revealed an overall decrease in both the proportion of each centromere containing Zip1 and the relative intensity of centromeric Zip1 (Figure 5.5 or Appendix Figure 5). For example, the 'specific' Zip1 intensity was on average  $0.78 \pm 0.55$  (S.D) compared to  $1.34 \pm 0.37$  and  $1.4 \pm 0.92$  for wild type and *zip2Δ*, respectively ('general' Zip1 intensity for *zip3Δ*:  $0.59 \pm 0.54$ , *zip2Δ*:  $1.31 \pm 0.93$  and wild type  $1.16 \pm 0.4$ ). This suggests that, in general, there is less Zip1 present at centromeres, compared to arm regions in *zip3Δ* mutants.

This analysis has revealed heterogeneity in the association of Zip1 with centromeres in *zip2Δ* and *zip3Δ* mutants that had previously gone undetected. In *zip2Δ* mutants, some centromeres accumulate Zip1 up to four times as intense as Zip1 found elsewhere whilst a small minority do not contain any Zip1 signal, with the majority falling somewhere in between these extremes. However, in the *zip3Δ* mutant although some centromeres were covered extensively with Zip1, the intensity was generally decreased relative to wild type suggesting that the amount of Zip1 present at centromeres was decreased relative to arm regions in *zip3Δ* mutants (Figure 5.5 and Appendix Figure 5).

### **5.2.3. Smt3<sup>SUMO</sup> does not accumulate at centromeres in *zip2Δ* mutants and is moderately depleted from centromeres in *zip3Δ* mutants.**

There exists a growing body of evidence that suggests sumoylation plays a crucial role in synaptonemal complex formation (Brown et al., 2008; Cheng et al., 2006; Hooker and Roeder, 2006; Lin et al., 2009; Tarsounas et al., 1997). Specifically, SUMOylation has been proposed to occur at the leading edge of synapsis to which the SUMO-binding motif, present in the C-terminus of Zip1, binds (Hooker and Roeder, 2006). Smt3<sup>SUMO</sup> and Zip1 show near-perfect co-localisation in zygotene and pachytene nuclei; consistent with the model that Smt3<sup>SUMO</sup> provides a substrate to enable Zip1 binding. Given the observations that Zip1 has tendencies to be depleted and accumulated at centromeres in *zip3Δ* and *zip2Δ* mutants, respectively, it was investigated whether Smt3<sup>SUMO</sup> displayed a similar pattern in these mutants. To this end, surface spread nuclei were prepared and stained for DNA, Smt3<sup>SUMO</sup> and the centromere marker Ctf19-13Myc. Pachytene nuclei were identified as having highly condensed worm-like chromosomes (Figure 5.6). In wild-type cells, Smt3<sup>SUMO</sup> localises evenly along the length of pachytene chromosomes much like Zip1 (Hooker and Roeder 2006 and Figure 5.6 A). Analysis of this using 'ColoS' indeed revealed a similar localisation profile of Smt3<sup>SUMO</sup> to Zip1 at centromeres even though the Zip1 and Smt3<sup>SUMO</sup> analysis were not carried out on the same lot of nuclei (due to co-staining issues of Zip1 and Smt3<sup>SUMO</sup> antibodies being raised in the same species). There appeared to be marginally less Smt3<sup>SUMO</sup> than Zip1 at centromeres but nonetheless, the centromeric Smt3<sup>SUMO</sup> was similar in intensity to that present at arm regions (Figure 5.7 A-C).

Figure 5.6

In *zip2Δ* mutants the Smt3<sup>SUMO</sup> staining appeared more linear in structure than the Zip1 staining (Appendix Figure 6), suggesting that failure to extend SC in *zip2Δ* mutants is not due to a failure in forming short lines of Smt3<sup>SUMO</sup> that Zip1 may bind to. Moreover, Smt3<sup>SUMO</sup> did not appear to preferentially accumulate at centromeres as was observed for Zip1 (Figure 5.6 B). Quantification of this using 'ColoS' indeed revealed that Smt3<sup>SUMO</sup> did not accumulate to the same extent as Zip1 in *zip2Δ* mutants (Figure 5.7 E and F). None of the centromeres contained Smt3<sup>SUMO</sup> staining that was >2 brighter than Smt3<sup>SUMO</sup> present at arm regions which contrasts with the pattern observed for Zip1 which was frequently >2 and up to 4 times more intense than Zip1 at arm regions (Figure 5.7 E and F). Instead, the values for 'specific' intensities were tightly clustered around 1, indicative that the Smt3 present at centromeres was similar in intensity to the Smt3<sup>SUMO</sup> present at arm regions.

For the *zip3Δ* mutant, Smt3<sup>SUMO</sup> staining was present along the chromosomes consistent with previous reports (Hooker and Roeder, 2006), but again appeared depleted at some centromeres as was observed for Zip1 (Figure 5.6 C and D). As for Zip1, a fairly even distribution between 0 and 1 was observed for the proportion of each centromere containing Smt3<sup>SUMO</sup>, suggesting some level of heterogeneity in the amount of each centromere covered by Smt3<sup>SUMO</sup> (Figure 5.7 G). Moreover, similar to Zip1, the distributions of normalised centromeric Smt3<sup>SUMO</sup> intensities were slightly decreased relative to wild type (Figure 5.7 C and I).

In summary, these findings suggest that Smt3<sup>SUMO</sup> does not accumulate at centromeres in *zip2Δ* mutants like Zip1 does. Moreover, unlike Zip1 which appears as foci in *zip2Δ* mutants, Smt3<sup>SUMO</sup> forms numerous short 'stretches'

Figure 5.7

along pachytene chromosomes suggesting that failure to extend SC in *zip2Δ* mutants is not due to failure to extend Smt3<sup>SUMO</sup> along the chromosomes. In *zip3Δ* mutants, Smt3<sup>SUMO</sup> is depleted from some, but not all centromeres (as was Zip1), suggesting that the centromeric localisation of Smt3<sup>SUMO</sup> is defective in *zip3Δ* mutants.

#### **5.2.4. Zip3 acts upstream of Zip2 in both synapsis and in the localisation of Zip1 to centromeres.**

Previous models have placed Zip3 upstream of Zip2 in the 'ZMM' ensemble (Agarwal and Roeder, 2000; Shinohara et al., 2008), which predicts that Zip2 should be dispensable for Zip3-independent synapsis. To this end, the *zip2Δ zip3Δ* double mutant was made and immuno-stained surface spread nuclei were prepared. In nuclei where the DNA appeared highly condensed ('worm-like'), linear stretches of Zip1 and PCs were visible in the *zip2Δ zip3Δ* double mutant, analogous to that observed for the *zip3Δ* single mutant. This sharply contrasts with the *zip2Δ* mutant in which stretches of Zip1 are very rarely observed (Figure 5.8 A-C). Indeed, both the number and length of Zip1 stretches appeared indistinguishable for the *zip3Δ* and *zip2Δ zip3Δ* double mutant (Figure 5.8 D and E), suggesting that Zip2 is dispensable for Zip3-independent synapsis. This is consistent with data published subsequently (Macqueen and Roeder, 2009) and further reinforces the model that Zip3 acts upstream of Zip2 in synapsis initiation.

Given the model that Zip3 acts upstream of Zip2, this predicts that the increased accumulation of Zip1 at centromeres in *zip2Δ* mutants must be Zip3-dependent. In order to investigate this, the association of Zip1 with Ctf19-13Myc

Figure 5.8

foci was quantified both ‘classically’ and computationally for the *zip2Δ zip3Δ* mutant. The classical co-localisation analysis revealed that, as for *zip3Δ*, the *zip2Δ zip3Δ* double mutant had only ~half as many centromeres with Zip1 directly co-localised as compared to the wild type and *zip2Δ* mutant and instead had an increased proportion of centromeres with no Zip1 co-localised (41 %, Figure 5.9 B). Interestingly, the class of centromeres with ‘Zip1 juxtaposed’ was decreased in the *zip2Δ zip3Δ* mutant (21 %) relative to the *zip3Δ* mutant (41 %), suggesting that there may be some subtle differences between these two mutants. When this was quantified computationally, Zip1-Ctf19 co-localisation appeared very similar for the *zip3Δ* and *zip2Δ zip3Δ* mutants (Figure 5.9 C-E). However, there is marginally less Zip1 associated with centromeres in the *zip2Δ zip3Δ* double mutant than for the *zip3Δ* single mutant (Figure 5.9 C-E). Whether this marginal difference between *zip3Δ* and the double mutant is significant or not would require further biological repeats and many more nuclei to be examined. However, as the Zip1 stretch length and number appeared indistinguishable for *zip3Δ* and *zip2Δ zip3Δ* mutants, it is likely that the subtle differences in centromeric Zip1 localisation are merely due to chance.

Nevertheless, *zip2Δ zip3Δ* mutants appear much more like *zip3Δ* mutants both in the extent of synapsis and the association of Zip1 with centromeres. This suggests that the localisation, and in some cases the accumulation, of Zip1 at centromeres in *zip2Δ* mutants is dependent upon Zip3 and that Zip2 is dispensable for Zip3-independent “synapsis”.

**Figure 5.9**

#### **5.2.5. Zip2- and Zip3-independent centromere ‘coupling’ persists to mid-prophase in *spo11Δ* cells.**

Zip1 has been shown to ‘couple’ centromeres together during early meiotic prophase, prior to the onset of recombination. This ‘centromere coupling’ is independent of chromosomal homology with centromeres coupled together, seemingly at random. Importantly, this process is independent of Zip2 and Zip3 proteins (Tsubouchi and Roeder, 2005), which is intriguing because the Zip1-mediated ‘centromere pairing’ that holds together non-exchange chromosomes during pachytene is dependent upon both Zip2 and Zip3 (Chapter 4 and (Gladstone et al., 2009). This suggests that temporal differences exist in the regulation of centromeric Zip1 by the synapsis initiation proteins.

What is responsible for the switch in Zip1 function from Zip2- and Zip3-independent centromere ‘coupling’ to centromere ‘pairing’, which is dependent upon Zip2 and Zip3? A likely candidate for this switch is Spo11, the topoisomerase that initiates recombination and thus the process that ‘locks’ homologous chromosomes together (Keeney et al., 1997). In order to investigate this, *SPO11* was deleted in Ctf19-13Myc strains and the association of centromeres was examined in pachytene nuclei in which DNA appeared highly condensed and a brush-like structure of tubulin was visible (Note: this is not ‘true’ pachytene as homologous chromosomes do not pair in *spo11Δ* cells). Diploid *S. cerevisiae* cells contain 32 chromosomes, so when all 32 centromeres are “paired”, 16 Ctf19-13Myc foci are visible whereas 32 are visible when all centromeres are unpaired (Tsubouchi and Roeder, 2005). In pachytene nuclei in which the chromosomes appeared highly condensed and a single brush-like structure of tubulin was visible, *spo11Δ* mutants contained an

average of 15.2 Ctf19-13Myc foci consistent with the centromeres being paired (Figure 5.10 A and B). This was Zip1-dependent as the *spo11Δ zip1Δ* mutant contained an average of 28 Ctf19-13Myc foci, indicative of the majority of the centromeres being unpaired (Figure 5.10 C and D). Crucially though, the *spo11Δ zip2Δ* and the *spo11Δ zip3Δ* mutants contained an average of 16.3 and 17.1 Ctf19-13Myc foci, respectively (Figure 5.10 E-H). This suggests that the pair-wise centromeric associations observed in *spo11Δ* mutants at pachytene are independent of synapsis initiation proteins Zip2 and Zip3. So in the absence of Spo11, Zip1-mediated centromere ‘coupling’, which does not require Zip3 or Zip2, persists to pachytene.

The fact that the centromere associations present during pachytene in *spo11Δ*, *spo11Δ zip2Δ* and *spo11Δ zip3Δ* mutants are Zip1-dependent suggests that Zip1 should co-localise with Ctf19-13Myc foci in these cells. To this end, the association of Zip1 was quantified in these mutants. Indeed, Zip1 appeared as foci in these nuclei that frequently overlapped with Ctf19-13Myc foci (Figure 5.11). In the *spo11Δ* mutant, 77 % and 18 % of Ctf19-13Myc were co-localised with and juxtaposed to a Zip1 focus, respectively (Figure 5.11 A and D). This was similar to the *spo11Δ zip2Δ* mutant, in which 86 % and 14 % of Ctf19-13Myc foci were directly co-localised or juxtaposed to a Zip1 focus, respectively (Figure 5.11 B and D). There was a decreased proportion of Ctf19-13Myc foci that directly co-localised with Zip1 in the *spo11Δ zip3Δ* mutant (53 %), but the proportion of Ctf19-13Myc foci juxtaposed to Zip1 was increased (36 %, Figure 5.11 C and D). This suggests that deposition of Zip1 directly at centromeres may be marginally less efficient in cells deleted for *ZIP3*, but centromeres are presumably still coupled together by the Zip1 adjacent to the centromeres.

Figure 5.10

Figure 5.11

To conclude, Zip1-dependent centromere 'coupling' that occurs early during meiotic prophase does not require Zip2 or Zip3, whereas centromere 'pairing' that occurs during pachytene does. In the absence of *SPO11*, Zip1 continues to hold centromeres together in pairs through to pachytene. The fact that this is independent of Zip2 and Zip3, suggests that it reflects a continuation of 'centromere coupling'. Spo11 therefore controls the 'switch' in Zip1 function from homology-independent 'centromere coupling' to 'centromere pairing' between homologous partner chromosomes, the latter of which requires Zip2 and Zip3 (Figure 5.12).

Figure 5.12

### 5.3. Discussion

The results presented in this chapter demonstrate that Zip1 present at centromeres may be subject to distinct regulation to that at chromosome arm regions. That is, Zip1 can polymerise extensively along the chromosome arms in the absence of Zip3, but the deposition or continued association of Zip1 with centromeres during pachytene is defective. Moreover, Zip3-dependent accumulation of Zip1 is observed at centromeres in cells lacking Zip2. These findings are analogous to those described for the centromeres of non-exchange chromosomes (Chapter 4) and so suggest that centromeric Zip1 is regulated in the same way for exchange and non-exchange chromosomes.

How may Zip3 regulate the centromeric association of Zip1 at pachytene? Zip3 is a SUMO E3 ligase with known roles in synapsis initiation (Agarwal and Roeder, 2000; Cheng et al., 2006). Sumoylation is also known to play a pivotal role in the assembly of the synaptonemal complex in yeast (Cheng et al., 2006; Hooker and Roeder, 2006; Lin et al., 2009) and possibly mammals (Brown et al., 2008; Tarsounas et al., 1997). In yeast, it is thought that Zip3 may sumoylate target proteins at the leading edge of synapsis to which the SUMO binding motif present in the C-terminus of Zip1 can then bind. The target proteins for such sumoylation are unknown although several possible candidates exist. These include Pds5, which is required for the maintenance of the cohesin complex and has been shown to be sumoylated in vegetative cells (Stead et al., 2003). Moreover, a recent study has shown that Pds5 is present along the chromosome axes during meiosis where it regulates synapsis ensuring that it occurs between homologous chromosomes rather than sister chromatids (Jin et al., 2009). Another candidate is Top2, a type II

topoisomerase, which has been shown to localise to the chromosome axes during meiosis (Klein et al., 1992). Top2 is also known to be sumoylated in vegetative cells where it also regulates centromeric sister chromatid cohesion (Bachant et al., 2002). An alternative model suggests that no such target protein exists and the Smt3<sup>SUMO</sup> species observed along the chromosomes at pachytene are in fact polymeric Smt3<sup>SUMO</sup> chains that are 'sandwiched' by the axial element protein Red1 and the central element protein Zip1 (Lin et al., 2009). However, this is largely based on the evidence that Smt3<sup>SUMO</sup> chains form in meiotic cells but there is no evidence proving that these Smt3<sup>SUMO</sup> chains correspond to the stretches of Smt3 that co-localise with Zip1 on zygotene and pachytene chromosomes. These stretches could just as equally correspond to Smt3<sup>SUMO</sup>-conjugated proteins. In fact, earlier work by the same group showed that Zip1 polymerisation occurs even in *smt3-allR* mutant backgrounds where all nine lysine residues in Smt3<sup>SUMO</sup> were mutated so Smt3<sup>SUMO</sup> chains cannot form (Cheng et al., 2006). Therefore, further work is needed before the precise nature of the Smt3<sup>SUMO</sup> species that co-localise with Zip1 on pachytene chromosomes is known.

Smt3<sup>SUMO</sup> chains not only form in the absence of Zip3, but tend to accumulate (Cheng et al., 2006). These may correspond to the Smt3<sup>SUMO</sup> staining observed along the chromosomes in *zip3Δ* mutants (this work and (Hooker and Roeder, 2006). However, Smt3<sup>SUMO</sup> staining is depleted specifically from centromeres in *zip3Δ* mutants suggesting that these Zip3-independent Smt3<sup>SUMO</sup> conjugates may not extend into centromeric regions and rather, the Smt3<sup>SUMO</sup> observed at centromeres in wild type cells may be Zip3-dependent Smt3<sup>SUMO</sup> conjugates of an unknown centromeric target protein.

Chromatin immunoprecipitation (ChIP) analyses shows that the lateral element proteins, Red1 and Hop1 are present all along the chromosome arms but are depleted from centromeres (Blat et al., 2002). The absence of Red1 at the centromeres may mean that the Smt3<sup>SUMO</sup> chains cannot be stabilised and so an alternative, centromere-specific protein is sumoylated and this depends upon Zip3. This model may also account for how Zip1 disassembly is differentially regulated at the centromeres and arm regions. Furthermore, the requirement for Zip3 in the association of Zip1 with centromeres may explain why Zip3 foci co-localise with centromeres (Tsubouchi et al., 2008).

Whatever Zip3 activity is responsible for the association of Smt3<sup>SUMO</sup> and Zip1 at centromeres during pachytene, it is clear that Zip3 is dispensable for the Smt3<sup>SUMO</sup> and Zip1 stretches present along arm regions. It is possible that in the absence of Zip3, sumoylation can occur either from some other E3 ligase or directly from the E2 conjugating enzyme, Ubc9, which then permits Zip1 binding. However, Ubc9 fails to localise to meiotic chromosomes in *zip3Δ* mutants (Hooker and Roeder, 2006), which implies that Ubc9 is capable of forming cytologically detectable Smt3<sup>SUMO</sup> 'stretches' without itself becoming associated with the chromosomes.

Zip1 is clearly capable of localising at (or near to) centromeres in the absence of Zip3 at earlier stages of meiotic prophase. For example, Zip3 is dispensable for Zip1-dependent centromere coupling that occurs between non-homologous chromosomes during the leptotene stage (Tsubouchi and Roeder, 2005). Furthermore, Zip3 is dispensable for centromere-associated synapsis that occurs during early zygotene (Tsubouchi et al., 2008) and in *spo11Δ fpr3Δ* mutants (Macqueen and Roeder, 2009). These findings suggest that Zip3 is

required for the continued association/re-loading of Zip1 at centromeres by pachytene. In the context of sumoylation, it is possible that alternative SUMO E3 ligases (Siz1, Siz2, Nse2) are responsible for the 'early' association of Zip1 with centromeres whereas Zip3 is required 'later'. Alternatively, Zip3 may be the 'normal' E3 ligase, but in its absence other ligases are capable of carrying out sumoylation, but this may not be stable at centromeres.

SUMO modifications have been implicated in synaptonemal complex dynamics in several organisms. For example, in *C. elegans* SUMO appears to be important for synaptonemal complex disassembly (Bhalla et al., 2008). In Hamsters, the lateral element protein Cor1 and the central element protein Syn1 both interact with the Ubc9 homolog (Tarsounas et al., 1997). Homologs of both Cor1 (Sycp3) and Syn1 (Sycp1) are retained at centromeres following SC disassembly in other mammals (de la Fuente et al., 2007; Page et al., 2006; Parra et al., 2004), which raises the interesting possibility of whether SUMO modifications control the centromeric retention of SC proteins in mammals. In addition, the human synaptonemal complex proteins SCP1 and SCP2 are SUMO-modified during spermatogenesis, which is proposed to be important for stabilisation of the SC (Brown et al., 2008). Moreover, as well as localising along the lengths of chromosomes in pachytene spermatocytes, SUMO staining is also present as foci at autosomal centromeres (Brown et al., 2008).

Curiously, however, SUMO often appeared as denser staining regions at the centromeres of chromosomes 9 and 1, which are also the chromosomes with the largest regions of centric heterochromatin suggesting a link between centric heterochromatin and the SUMO modifications present on pachytene chromosomes (Brown et al., 2008). Finally, this study highlights a possible link

between SUMO modifications and human fertility with one patient showing severe azospermia also exhibiting a pattern of hypo-sumoylation (Brown et al., 2008). However, the authors point out that although the two are correlated there is no evidence for a direct causal link. Finally, the mammalian Zip3 homolog has been recently identified as Rnf212 in a study looking for single nucleotide polymorphisms (SNPs) that influence recombination rates in humans (Kong et al., 2008). Both male and female *RNF212*<sup>-/-</sup> knock out mice are infertile and synapsis is delayed and incomplete in these animals (Neil Hunter). Further characterisation of Rnf212 may provide insight into a possible role for SUMO in mammalian synapsis. In summary, these observations suggest that SUMO modifications are central to the regulation of the synaptonemal complex and this appears to be conserved from yeast, through to worms and mammals.

How is the SC extended in *zip3Δ* mutants? In an otherwise wild type meiosis, Zip2 is absolutely required to extend Zip1 along the chromosomes (Chua and Roeder, 1998), however in the absence of Zip3, Zip2 is seemingly dispensable in SC extension. These data are consistent with the model presented in Chapter 3 that suggested Zip3 is the 'primary regulator' for the 'ZMM' ensemble so that in the absence of Zip3, the synapsis that occurs is ZMM-independent. Zip2 being a downstream member of the 'ZMM' is therefore redundant in *zip3Δ* cells. What proteins are responsible for extending the SC in the absence of any of the known synapsis initiation proteins is a mystery open to further investigation.

The association of Zip1 with centromeres in *zip2Δ* mutants showed heterogeneity with some centromeres accumulating Zip1 up to four times as intense as Zip1 present at the arm regions whilst a few centromeres did not

contain any Zip1 signal. This heterogeneity may be explained by inter-chromosomal differences in the timing of Zip1 deposition at centromeres. It is possible that the homologous chromosomes that pair first are the first to receive Zip3-mediated deposition of Zip1 at centromeres and whilst the remaining chromosomes are searching for their homologous partner, this Zip3-mediated deposition of Zip1 continues at the original set of centromeres to the effect that it accumulates there. Alternatively, there may be some *cis*-acting factor that renders a specific pair of chromosomes more susceptible to accumulating Zip1 at their centromeres than others. Chromosome 5 may be such a chromosome pair, which would explain the consistently high accumulation of Zip1 at *neCEN5s* in *zip2Δ* mutants (Chapter 4, Appendix Figure 7). The heterogeneity of Zip1 signal between centromeres does not show any correlation to the Ctf19 signal intensities, suggesting that this heterogeneity is not an artefact of centromeres being in different focal planes or staining with different efficacy (Appendix Figure 8).

What is the basis for the accumulation of Zip1 at centromeres? The accumulation of Zip1 as bright foci in *zip2Δ* mutants may be explained in one of two ways. Zip1 may accumulate simply by virtue of the fact that absence of Zip2 results in a failure to propagate Zip1 along the chromosome. The result being that Zip1 is not dissipated from the synapsis initiation site. Alternatively, Zip2 may provide negative feedback on Zip3 so as to prevent 'over-loading' of Zip1. Perhaps a combination of the two culminates in the accumulation seen in *zip2Δ* mutants. Either way, it does not appear to be due to over-loading of Smt3<sup>SUMO</sup> at centromeres.

In summary, centromeric Zip1 is regulated differentially throughout meiotic prophase to match its different functions (Figure 5.12). Early in meiotic prophase, Zip1 'couples' centromeres and this process is independent of Zip2 and Zip3. Later in meiotic prophase at the pachytene stage, homologous chromosomes become paired and fully synapsed along their lengths. Chromosome pairs that fail to experience a cross over are paired by Zip1 at their centromeres, but unlike 'centromere coupling', this is dependent on Zip2 and Zip3. Moreover, the association of Zip1 with centromeres of exchange chromosomes at pachytene appears to be regulated in the same way as for non-exchange chromosomes. Following exit from pachytene, Zip1 remains associated with the centromeres of exchange and non-exchange chromosomes. How Zip1 is selectively retained at centromeres is unknown, but it may involve centromere-specific sumoylated proteins to which Zip1 is bound.

# **Chapter 6. The role of spindle checkpoint proteins in non-exchange chromosome segregation.**

## **6.1. Introduction.**

The spindle checkpoint delays anaphase onset until all chromosomes are correctly positioned on the metaphase spindle, attached to microtubules emanating from opposite spindle poles (Li and Murray, 1991). The checkpoint consists of a highly conserved group of proteins that are active during both mitosis and meiosis. There is evidence, however, to suggest that meiotic cells rely more heavily on the spindle checkpoint for accurate chromosome segregation, at least in budding yeast. This is based on the observations that spindle checkpoint mutants do not have much of a phenotype in an unperturbed mitotic cell cycle (i.e. in the absence of microtubule de-polymerising drugs), but they experience elevated chromosome missegregation at the first meiotic division during an otherwise wild-type meiosis (Li and Murray, 1991; Shonn et al., 2000). This may be due to the fact that homologous chromosomes are the segregating partners during meiosis I, rather than sister chromatids during mitosis. It has been suggested that the latter may be better able to adopt a correct spindle attachment owing to the presence of sister chromatid cohesion that geometrically constrains sister kinetochores to face in opposite directions, whereas the connections between homologous chromosomes may be more 'floppy' and so they require further attempts to correctly attach to the spindle.

The position of chromosomes is signalled to the spindle checkpoint by tension on the metaphase spindle. When chromosomes are correctly bi-oriented, the resulting tension silences the spindle checkpoint, which as a result triggers anaphase onset (Li and Nicklas, 1997).

In budding yeast, the spindle checkpoint proteins Mad1, Mad2, Mad3, Bub1 and Bub3 (Hoyt et al., 1991; Li and Murray, 1991) cooperate to mediate a metaphase delay in response to incorrectly attached and/or unattached kinetochores. Consistent with this, neither *mad2Δ* or *mad3Δ* mutants can delay the meiotic divisions in response to the microtubule depolymerising drug, benomyl. Despite this similarity, these mutants exhibit other meiotic phenotypes that differ hugely. For example, although *mad2Δ* mutants suffer reduced spore viability indicative of chromosome non-disjunction, the spore viability of *mad3Δ* mutants is indistinguishable from wild type (Shonn et al., 2003). This suggests that Mad2 and Mad3 have distinct roles in meiotic chromosome segregation and has led to the suggestion that Mad2 directly promotes homolog bi-orientation in addition to its canonical spindle checkpoint role (Shonn et al., 2003). Interestingly, longer chromosomes preferentially non-disjoin during meiosis I in *mad2Δ* mutants (Shonn et al., 2000). This is because longer chromosomes are less likely to have centromere-proximal crossovers that promote homolog bi-orientation. Such chromosomes presumably require Mad2 activity to allow them multiple chances at spindle attachment. The segregation of these chromosome pairs in *mad2Δ* mutants can be rescued by placement of an artificial 'tether' near the centromeres of long chromosomes that substitutes for a centromere-proximal crossover (Lacefield and Murray, 2007). Consistent with the notion that the spindle checkpoint proteins may have distinct roles, is

the finding that deletion of *MAD2* influences the segregation of both exchange and non-exchange chromosome pairs, whereas deletion of *MAD3* only influences the segregation of non-exchange chromosomes (Cheslock et al., 2005). The authors attribute this difference to the finding that Mad2 (and Mad1) mediate a metaphase I delay in response to incorrectly attached and/or unattached kinetochores, whereas Mad3 mediates a prophase I delay during prophase I of every meiosis.

Much is known regarding the mechanism by which spindle checkpoint proteins delay anaphase onset in response to incorrectly attached kinetochores. The lack of spindle tension results in Mad2 binding to Cdc20 and in doing so prevents Cdc20 from activating the anaphase-promoting complex (APC). When tension is achieved, Mad2 is believed to undergo a conformational change that liberates Cdc20, (Luo et al., 2000; Luo et al., 2002; Luo et al., 2004) that then activates the APC, triggering anaphase onset (Zachariae and Nasmyth, 1999).

The sensing of spindle tension by the spindle checkpoint is achieved by the chromosomal passenger proteins, Aurora B kinase, INCENP, Survivin and Borealin (reviewed in (Ruchaud et al., 2007)). These comprise a highly conserved protein complex that assembles at kinetochores by metaphase and responds to the absence of spindle tension. The lack of kinetochore tension causes Ipl1/Aurora B kinase to sever microtubule-kinetochore attachments (Cheeseman et al., 2002; Pinsky et al., 2006). Unattached kinetochores then activate the spindle checkpoint to mediate a metaphase delay (Pinsky et al., 2006; Wassmann et al., 2003). Presumably, this allows several cycles of spindle attachment until a bipolar spindle attachment is achieved. Several models exist for precisely how this protein complex responds to spindle tension

(Kelly and Funabiki, 2009; Sandall et al., 2006). Amongst these are the models that suggest tension results in a conformational change in the complex that either renders Aurora B kinase inactive (Sandall et al., 2006), or spatially removes Aurora B kinase from its target substrates (Mendoza et al., 2009). Substrates of Ipl1/Aurora B kinase in yeast include the kinetochore protein Dam1, whose phosphorylation by Ipl1 causes microtubule-kinetochore attachments to be severed (Cheeseman et al., 2002; Courtwright and He, 2002). Ipl1 is also known to phosphorylate Mad3, which is important for activation of the spindle checkpoint. Mutation of these phosphorylation sites within Mad3 results in an abolition of a metaphase delay in response to microtubule depolymerising drugs (King et al., 2007). In addition to regulating kinetochore – microtubule attachments and activating the spindle checkpoint, Aurora B kinase also promotes kinetochore mono-orientation during meiosis I (Monje-Casas et al., 2007) as well as protection of centromeric cohesin in yeast (Yu and Koshland, 2007) and *Drosophila* (Resnick et al., 2006).

Most of what is known about the spindle checkpoint during meiosis concerns crossover-proficient chromosome pairs. However, recent studies have revealed a role for the spindle checkpoint proteins in the segregation of non-exchange chromosome pairs as well (Cheslock et al., 2005; Shonn et al., 2003). Therefore, it was investigated how tension-mediated spindle checkpoint activity collaborates with Zip1 to ensure non-exchange chromosome segregation.

## 6.2. Results.

### 6.2.1. Mad3 promotes centromere pairing, but also acts in a parallel pathway to Zip1 in promoting NECS.

The segregation of non-exchange chromosomes at meiosis I is promoted by Zip1-mediated centromere pairing during pachytene (Gladstone et al., 2009; Newnham et al.). However, when centromere pairing frequencies are used to predict the segregation outcome of the non-exchange chromosome pair, the observed non-disjunction frequencies deviate from the expected. For example, non-exchange chromosomes are 'paired' in 14% of *zip1Δ* cells. Assuming that the remaining 86% of unpaired non-exchange chromosomes segregate at random, one would expect ~43% non-disjunction. However, the observed non-disjunction frequency is just 27%, which differs significantly ( $p < 0.01$ ) from the expected 43%. The same is true of wild type cells (Figure 6.1 B and C). This suggests that an alternative, Zip1-independent pathway assists in the segregation of non-exchange chromosomes.

A good candidate for this alternative pathway is the spindle checkpoint protein, Mad3. Deletion of *MAD3* specifically influences the segregation of non-exchange chromosomes, whilst the segregation of exchange chromosomes is unaffected (Cheslock et al., 2005). In order to investigate how Mad3 promotes non-exchange chromosome segregation (NECS), the behaviour of the homeologous non-exchange chromosome V pair was analysed in *mad3Δ* mutants. Centromere (*neCEN5*) pairing frequencies were decreased from 56% in wild type to 27% in *mad3Δ* mutants (Figure 6.1. A and B). This centromere pairing defect may be due to the shortened meiotic prophase experienced by *mad3Δ* mutants (Cheslock et al., 2005). In order to determine whether the

Figure 6.1

centromere pairing observed in *mad3Δ* mutants was Zip1-dependent, the double mutant was examined. The *neCEN5* pairing frequencies of the *mad3Δzip1Δ* double mutant (13 %) was indistinguishable from the *zip1Δ* single mutant (14 %, Figure 6.1 B), suggesting that the *neCEN5* pairing in *mad3Δ* mutants is Zip1-dependent. Crucially, however, the observed non-disjunction frequencies in cells deleted for *MAD3* (34 %) showed good correspondence with those expected from the centromere pairing frequencies (37 %), unlike the wild type and *zip1Δ* mutants (Figure 6.1 C). Furthermore, the non-disjunction frequencies showed an additive increase when both *ZIP1* and *MAD3* were deleted, resulting in random segregation of the non-exchange pair (50 % non-disjunction, Figure 6.1 C). This suggests that Zip1 and Mad3 act independently in the segregation of non-exchange chromosomes. Furthermore, as was the case with the *mad3Δ* mutant, the observed non-disjunction frequency (50 %) of the non-exchange pair were very similar to those predicted from the centromere pairing frequencies (44 %) in the *mad3Δzip1Δ* double mutant (Figure 6.1 C). They are even more similar if one assumes that the *neCEN5* 'pairing' observed in *zip1Δ* mutants (14 %) is in fact the lowest limit of detection in this assay and actually represents 0 % (see discussion of Chapter 4). These findings suggest that Mad3 aids the segregation of non-exchange chromosomes that are not paired by Zip1 at pachytene.

To summarise, these findings confirm a role for Mad3 in NECS. Mad3 not only promotes centromere pairing of non-exchange chromosomes, but also acts in an independent pathway to Zip1 in promoting NECS. While Zip1 promotes NECS through directly 'tethering' centromeres together so they

appear to be 'paired', Mad3 appears to aid the segregation of chromosome pairs that are not paired by Zip1, as well as assisting in centromere pairing.

### **6.2.2. Mad2 is also involved in NECS.**

The spindle checkpoint proteins, Mad1 and Mad2 are distinct from Mad3 in that they mediate a metaphase delay in response to incorrectly positioned chromosomes on the spindle, whereas Mad3 mediates a prophase delay in every meiosis (Cheslock et al., 2005). Moreover, Mad1 and Mad2 influence the segregation of both non-exchange and exchange chromosomes (Cheslock et al., 2005; Lacefield and Murray, 2007; Shonn et al., 2000; Shonn et al., 2003). However, studies on the role of Mad2 in NECS during meiosis have yielded conflicting results. For example, Lacefield and Murray (2007) reported non-disjunction frequencies of 48% for the homeologous chromosome V pair whereas Cheslock *et al.* (2003) reported 35% non-disjunction for the same chromosome pair. It is possible that these differences may be due to the mitotic *mad2Δ* phenotype (Li and Murray, 1991). For example, deletion of *MAD2* may compromise the fidelity of mitotic chromosome segregation and so cells may enter meiosis with a single copy of one of the chromosomes (this was shown to occur at a rate of 1.6 % for a single chromosome, ERASMUS student Andrea Haerzschel). It is known that addition of a centromere-containing plasmid or artificial chromosome disrupts disjunction of non-exchange chromosomes at meiosis I, presumably by interfering with centromere pairing (Kemp et al., 2004). Therefore, the resulting meiosis I non-disjunction frequencies may be an indirect result of mitotically-derived aneuploidy rather than a direct result of *MAD2* deletion. To circumvent this potential problem, a meiosis-specific *mad2* mutant was made in the diploid strain harbouring the GFP-labelled

homeologous chromosome V pair (made by ERASMUS student Andrea Haerzschel under supervision of LN). This was done by replacing the native *MAD2* promoter by that of *CLB2*, whose expression is shut off during meiosis (Chu and Herskowitz, 1998; Lee and Amon, 2003), Figure 6.2 A). In order to verify the *mad2-meiotic null* (*mad2-mn*) strain, Mad2 protein levels were assessed by western blot at various time points following transfer to sporulation media (Figure 6.2 B). Mad2 protein levels were vastly diminished by 12 hours and absent by 24 hours. Interestingly, there appeared to be a meiosis-specific slower migrating band that may represent meiosis-specific modification of Mad2. Cells were harvested at 20 hours and spread meiotic nuclei were prepared. Pachytene nuclei, defined by linear Zip1 staining and condensed DNA, were scored as having 'paired' or 'unpaired' *neCEN5s* (Figure 6.2 C). As for *mad3Δ*, there was no apparent SC defect in *mad2-mn* mutants. The pairing frequency in *mad20-mn* mutants was decreased relative to wild type (23%, compared to 56 % for the wild type, Figure 6.2 D). Consistent with a decrease in *neCEN5* pairing, the non-disjunction of the non-exchange chromosomes was elevated from 11 % in wild type to 37 % in *mad2-mn* mutants (Andrea Haerzschel, Figure 6.2 E and F). As was the case for *mad3Δ* mutants, *mad2-mn* mutants show good correspondence between the expected non-disjunction frequencies based on *neCEN5* pairing frequencies (39 %) and the observed non-disjunction frequency (37 %). This suggests that Mad2 may fulfil a similar function to Mad3 in promoting the segregation of non-exchange chromosomes not paired by Zip1 (see discussion).

These findings reveal an unexpected role for Mad2 in centromere pairing of non-exchange chromosomes during pachytene and verified a role for Mad2

Figure 6.2

in NECS. The use of the *mad2-mn* allele allowed the non-disjunction frequencies of non-exchange chromosome pairs to be attributed specifically to Mad2's meiotic function.

### **6.2.3. Ipl1/Aurora B kinase activity is required for NECS.**

Aurora B kinase (Ipl1 in *S. cerevisiae*) is a serine/threonine protein kinase that regulates microtubule-kinetochore attachments in response to spindle tension (Cheeseman et al., 2002). In the absence of tension, Ipl1 severs microtubule-kinetochore interactions (Courtwright and He, 2002) and the resulting unattached kinetochores activate the spindle checkpoint, which mediates a metaphase delay allowing the kinetochores another chance to attempt a bipolar spindle attachment (Pinsky et al., 2006).

As Ipl1/Aurora B kinase is required for the segregation of exchange chromosomes, it was investigated whether the same was true of non-exchange chromosomes. To this end, *neCEN5* pairing and segregation was assessed in an *ipl1-meiotic null* mutant (made by Phil Jordan). In pachytene nuclei, the *neCEN5*s were paired with similar frequencies to wild type (Figure 6.3 A and B). This finding suggests that Ipl1 is not involved in centromere pairing of non-exchange chromosomes and so does not act alongside the spindle checkpoint proteins Mad2 and Mad3 in this process. Owing to the low sporulation efficiency of *ipl1-mn* mutants, meiosis I non-disjunction of the non-exchange pair was assessed by immuno-fluorescence from anaphase I spindles (Figure 6.3 C). This revealed high levels of non-disjunction of the non-exchange chromosome pair (~80%, Figure 6.3 D), suggesting that non-exchange chromosomes are indeed dependent upon Ipl1/Aurora B kinase for their disjunction. In mutants

Figure 6.3

lacking Ipl1 activity, chromosome pairs cannot undergo repeated rounds of spindle attachment that are necessary to achieve bi-orientation. Therefore, having 'paired' chromosomes may actually be a disadvantage in *ipl1-mn* mutants. That is, paired chromosome pairs might be more prone to segregate together than unpaired chromosomes in mutants that cannot correct erroneous spindle attachments. To test this hypothesis, the *ipl1-mn zip1Δ* double mutant was analysed. The double mutant displayed *zip1Δ*-like *neCEN5* pairing frequencies, in the majority of cells the centromeres of non-exchange chromosomes were unpaired (Figure 6.3 B). Despite this, the double mutant experienced similar levels of non-disjunction as the *ipl1-mn* mutant (Figure 6.3 D). These findings show that regardless of chromosomes being paired or unpaired, they segregate towards the same spindle pole in 80% of nuclei. Thus *ipl1-mn* is epistatic to *zip1Δ* in NECS.

The meiotic non-disjunction frequencies are much higher than expected from random segregation (50%) and are likely to be due to the segregation of both chromosomes to the old spindle pole (Pereira et al., 2001; Tanaka et al., 2002); (Monje-Casas et al., 2007). Therefore, Ipl1 activity must be required to sever the initial kinetochore attachments from microtubules associated with the old spindle pole. Furthermore, this seems to be the case regardless of whether chromosomes are paired or not (see discussion).

#### **6.2.4. *ipl1-mn* mutants exhibit an SC disassembly defect.**

Whilst assessing *neCEN5* pairing in *ipl1-mn* mutants (above) it was noticed that nuclei frequently contained linear Zip1 staining, but had tubulin staining that was characteristic of cells that had progressed to later stages in

Figure 6.4

meiotic prophase (Figure 6.4). This was very unlike the Zip1 staining in wild type cells that appeared faint and dotted at these stages (Figure 4.14, 4.15 and Appendix Figure 4). Further investigation by the Hoffmann laboratory found that Ipl1 kinase activity is required for synaptonemal complex disassembly (Jordan et al., 2009). During this study, the disassembly of several candidate Zip1 binding proteins was also studied. These included Red1, Hop1, Smt3<sup>SUMO</sup> and Rec8. Of these, Hop1 is retained in both wild type and *ipl1-mn* but appears diffuse and not linear like the Zip1 staining present in the *ipl1-mn* mutant. Only Smt3<sup>SUMO</sup> staining appeared to closely match that of Zip1 (Jordan et al., 2009). In the wild type, Smt3<sup>SUMO</sup> staining became more faint and diffuse in diplotene nuclei and remained so through to subsequent stages where it did not appear to co-localise with residual Zip1 staining (Figure 6.5 A, C and E). In contrast, in *ipl1-mn* mutants, Smt3<sup>SUMO</sup> appeared as dense, linear structures during later stages of meiotic prophase that co-localised extensively with Zip1 (Figure 6.5 B, D and F). These findings are consistent with models that suggest Smt3<sup>SUMO</sup> is the binding partner of Zip1 (Cheng et al., 2006; Hooker and Roeder, 2006).

#### **6.2.5. Exploiting the *ipl-mn* SC disassembly phenotype to identify the Smt3<sup>SUMO</sup> species that co-localise with Zip1 on synapsed chromosomes.**

The SC disassembly phenotype of *ipl1-mn* mutants provided new insight into the lateral element proteins that are potential binding partners of Zip1. Retention of Zip1 as full-length synaptonemal complexes whilst other lateral element proteins were disassembled or reorganised provides clues as to which proteins are necessary for the retention of the synaptonemal complex. The only protein whose appearance closely matched that of Zip1 in *ipl1-mn* mutants, at

Figure 6.5

later stages, was Smt3<sup>SUMO</sup> (Hop1, although abundant, did not appear linear like Zip1). After pachytene exit, Smt3<sup>SUMO</sup> appeared to be less abundant and more diffuse in wild-type cells as compared to the linear stretches frequently observed in the *ipl1-mn* mutant that co-localised with Zip1 (Figure 6.5). It was therefore wondered whether the identity of these Smt3<sup>SUMO</sup> species could be revealed by comparison of Smt3 immuno-precipitation profiles between wild type and *ipl1-mn* cells (following exit from pachytene). In theory, this could have been done by comparing the Smt3 profiles during and after pachytene in wild-type cells. However, there may be many other changes in sumoylation patterns between these two cell stages that would complicate the identification of the band(s) of interest. To this end, an experiment was designed in which both wild type and *ipl1-mn* mutants were arrested in pachytene and then released so that they would exit pachytene synchronously. Cells would then be harvested at a time point with the maximal proportion of cells in metaphase I and anaphase I stages (1 hour after release, Jordan *et al.* 2009). Protein extracts of these cells would then be immuno-precipitated with an Smt3 antibody and the Smt3 profiles would be compared for wild type and *ipl1-mn* cells by western blotting (shown schematically in Figure 6.6).

Preliminary experiments probing whole cell extracts for Smt3 showed a complex mixture of proteins that are sumoylated at these time points, resulting in poor resolution of individual bands on a western blot for Smt3 (Appendix Figure 9 A). Therefore, in order to reduce the complexity of the sample and narrow the search to just chromatin-bound proteins, crude chromatin extracts were chosen to do the IP from (protocol adapted from Kee and Keeney 2002 and Kee *et al.* 2004).

Figure 6.6

The proteins present in the different fractions are shown in the ponceau-stained blot in appendix figure 9 B. The S2 fractions correspond to the crude chromatin extracts (note the abundance of low molecular weight proteins in this fraction that are likely to represent histone proteins). Consistent with this fraction being primarily chromatin-bound proteins, tubulin (which is found in the cytoplasm and nucleus) is not present in this fraction (Appendix Figure 9). When these fractions for both wild type and *ipl1-mn* were run out on a large-format 10% gel, transferred to a nitrocellulose filter and probed for Smt3, a ladder of proteins was revealed. However, there was one band that appeared enriched in the *ipl1-mn* mutant over wild type that was ~65 kDa in size (yellow arrow, Figure 6.7). This difference was observed in two out of three independent experiments (however, in the one where the band was not seen, no proteins larger than 55 kDa were transferred). This band may well correspond to the sumoylated species that co-localises with Zip1 at later stages in *ipl1-mn*. Regrettably, due to a combination of time constraints and the publication of a paper claiming that these SUMO species are SUMO chains (Lin et al., 2009) this band was not identified. However, this work is still ongoing and so may yet reveal further information in the future.

#### **6.2.6. Preliminary work on TAP-tagged Zip1**

In addition to using the *ipl1-mn* phenotype to probe the nature of the Smt3<sup>SUMO</sup> species on meiotic chromosomes, another approach would have been to purify Zip1 protein from meiotic cell extracts and see what other proteins co-purify. To this end, Zip1 was TAP-tagged in the SK1 strain

Figure 6.7

background that is capable of highly synchronous meiosis. In order to determine whether the Zip1-TAP strains behaved 'normally' a meiotic time course was performed for the Zip1-TAP and wild type strains (Figure 6.8). The wild type cells started entering the first meiotic division at ~6 hours and ~70 % of cells had completed both nuclear divisions by 10 hours (Figure 6.8 C). The relative abundance of Zip1 protein in wild type cells peaked at ~ 6 hours after which it decreased until Zip1 was barely detectable at 10 hours (Figure 6.8 A). In contrast, the Zip1-TAP strains were severely delayed in entering the meiotic divisions with virtually no bi-nucleates present, even at 10 hours (Figure 6.8 D). Similarly, the appearance of Zip1-TAP protein (which migrated at ~25 kDa higher than wild-type Zip1) was delayed with much less protein detectable at 6 hours compared to the wild type (Figure 6.8 B). It also appeared to accumulate to higher levels than wild type Zip1 (10 hours, Figure 6.8 B). However, >50% of cells eventually sporulated and spore viability was high (Figure 6.8 E), suggesting that of those cells that progressed through the nuclear divisions chromosome segregation occurred fairly normally. Regrettably, samples for immunocytology were only taken up until the 8-hour time point and so SC formation could not be assessed at 10 hours when the amount of Zip1-TAP protein peaked. However, at 8 hours no extensive linear Zip1-TAP staining was observed and Zip1-TAP appeared more diffuse than wild type Zip1. It is therefore unclear whether SC does not form normally in Zip1-TAP strains or whether it was just severely delayed. Due to time constraints, the TAP purification was never performed, but this work is ongoing in the Hoffmann lab.

Figure 6.8

### 6.3. Discussion.

The findings discussed in this chapter demonstrate a role for spindle checkpoint proteins in non-exchange chromosome segregation (NECS). Specifically, mutations that eliminate Mad2 and Mad3 proteins reduce the centromere pairing frequencies of non-exchange chromosomes and lead to corresponding increases in meiosis I non-disjunction. Furthermore, simultaneous deletion of *MAD3* and *ZIP1* had an additive effect on NECS, resulting in random segregation of non-exchange chromosome pairs at meiosis I. These findings suggest that spindle checkpoint proteins, Mad2 and Mad3 are important for centromere pairing, but Mad3 can also act independently of Zip1 in promoting the segregation of non-exchange chromosomes that are not 'tethered' by Zip1 (Figure 6.9).

Why is centromere pairing in pachytene nuclei perturbed in *mad3Δ* mutants? One possible explanation is that Mad3 is responsible for mediating a 2-3hr prophase delay during every meiosis (Cheslock et al., 2005). Therefore, in *mad3Δ* mutants in which prophase is shortened, non-exchange chromosomes may have less time to become 'paired'. This hypothesis could be tested by allowing the cells more time in pachytene and assaying whether the centromere pairing defect is rescued.

The Mad3-mediated prophase I delay is highly conserved from yeast (Cheslock et al., 2005) through to flies (Malmanche et al., 2007) and mammals (Homer et al., 2009). A recent study showed that the mammalian Mad3 ortholog BubR1 is responsible for the prophase I arrest of oocytes that initiates before birth and is sustained until ovulation. In the absence of BubR1 activity, mouse oocytes undergo germinal vesicle breakdown and enter pro-metaphase

Figure 6.9

without arresting (Homer et al., 2009). This study also showed that BubR1 is important for completion of anaphase I by limiting the accumulation of securin and in establishing kinetochore-microtubule attachments (Homer et al., 2009). These findings carry important implications, as inability of oocytes to engage in a prophase I arrest would deplete the pool of oocytes available in the adult ovary, rendering the female infertile. Similarly, inability to complete anaphase I or properly attach kinetochores to the spindle would also lead to fertility problems. These findings highlight the importance of BubR1/Mad3 in three distinct meiotic processes that are highly applicable to human fertility.

How might Mad3 assist in the segregation of non-exchange chromosome pairs that are not 'paired' by Zip1? It is difficult to envisage how 'unpaired' chromosomes are recognised by the meiotic spindle as segregating partners. Mad3 is thought to assemble at kinetochores prior to spindle attachment (Jablonski *et al.* 1998). Perhaps Mad3 mediates some transient interaction between non-exchange chromosomes prior to the division that is sufficient to direct them in opposite pole-ward directions. Alternatively, perhaps limited kinetochore attachment sites exist within the spindle once all of the other chromosome pairs have attached. The resulting 'crowded spindle' may force the non-exchange pair to adopt positions on opposite halves of the spindle, thus ensuring their correct segregation. It is possible that Mad3 may participate in this process. Whatever the mechanism, Mad3 fully accounts for the higher-than-expected frequency of unpaired non-exchange chromosomes managing to segregate correctly at meiosis I in wild type and *zip1* $\Delta$  cells (discussed in chapter 4).

The non-disjunction frequencies reported here (34 %) for the *mad3Δ* mutant differed substantially from the 50 % reported by Cheslock *et al.* (2005). In the latter case, meiosis I non-disjunction was measured by following the genetic markers present on each chromosome of the non-exchange pair in the viable spores of each tetrad dissected. In contrast, the work described here used GFP to visualise the non-exchange chromosomes directly from tetrads. Cheslock *et al.* examined 96 tetrads, whereas 340 were examined cytologically in this work. In order to investigate whether the discrepancy could be explained by differences in sample size, a bootstrapping analysis was carried out. Briefly, this involves sampling 96 of our 340 tetrads at random and seeing what the non-disjunction frequency was from this random sample. This is repeated 10,000 times for a single bootstrap analysis and the results are plotted in a histogram (a typical example is given in Appendix Figure 10). This revealed that the discrepancies cannot be accounted for by differences in sample size. This is not the first time, however that the two assessment methods have yielded different non-disjunction frequencies as similar discrepancies have been reported for the *mad2Δ* mutant (Cheslock *et al.*, 2005; Lacefield and Murray, 2007).

The work described here uncovers an unexpected role for Mad2 in centromere pairing of non-exchange chromosomes during pachytene. Mad2 is an extensively studied protein whose activity was previously thought as being confined to metaphase (Cheslock *et al.*, 2005; Gladstone *et al.*, 2009; Li and Murray, 1991; Shonn *et al.*, 2000; Shonn *et al.*, 2003). However the fact that centromere pairing of the non-exchange chromosomes was reduced during pachytene in *mad2-mn* cells suggests that Mad2 may play an earlier role in

meiotic prophase. It is possible that in the absence of Mad2, the kinetochore architecture is altered in a way that makes centromere pairing less efficient or less stable. As was the case for *mad3Δ* mutants, *mad2-mn* mutants show good correspondence in the expected (39%) and observed (37%) non-disjunction frequencies, suggesting that the mechanism that promotes the segregation of 'unpaired' non-exchange chromosomes is abolished in this mutant. This implies that Mad2 may act in the same pathway as Mad3 in promoting the segregation of non-exchange chromosomes that are not 'paired' by Zip1 (Figure 6.9). However, the *mad3Δ mad2-mn* double mutant would have to be analysed to investigate this possibility.

In addition to non-exchange chromosomes, Mad2 is known to assist the segregation of chromosome pairs that lack crossovers within 180 kb of their centromeres (Lacefield and Murray, 2007). Whether it does so by affording the chromosome pair more time to achieve a bipolar spindle attachment or by directly assisting in biorientation of the chromosome pair (Shonn et al., 2003), or both is unclear.

The finding that non-exchange chromosomes non-disjoin at a similar frequency as exchange chromosomes (Monje-Casas et al., 2007) in *ipl1-mn* mutants (~80%) suggests that both types of chromosome pair are dependent on Ipl1 activity to ensure their correct segregation at meiosis I. This non-disjunction is much higher than expected from random segregation (50%) and is likely to be due to the segregation of both chromosomes to the old spindle pole (Pereira et al., 2001; Tanaka et al., 2002) as treatment with the microtubule-depolymerising drug, benomyl in *ipl1-mn* cell randomises chromosome segregation (~ 50% non-disjunction, (Monje-Casas et al., 2007). Thus, Ipl1

activity is required to sever initial kinetochore -microtubule attachments that form before maturation of the new spindle pole body to allow kinetochores a chance to attach to microtubules emanating from the new spindle pole. Thus, more insight may have been gained from treating the *ipl1-mn* cells with a single benomyl treatment and then assaying segregation of the non-exchange chromosomes in these cells. If Zip1 geometrically constrains the kinetochores of non-exchange chromosomes to adopt a bipolar orientation, then the pair should non-disjoin with high frequencies following a single benomyl treatment. Alternatively, if the non-exchange pair require several rounds of attachment before achieving bi-orientation, a single benomyl treatment is unlikely to yield high disjunction frequencies of the non-exchange pair.

Nevertheless, undertaking these experiments led to the discovery that *ipl1-mn* mutants have a synaptonemal complex (SC) disassembly defect. Nuclei were frequently observed with linear Zip1 staining and anaphase I spindles. Further investigation of this phenotype revealed that the defect is specifically in SC disassembly with other meiotic landmark events (crossover formation, cyclin control) occurring normally (Jordan et al., 2009). This mechanism may be conserved in mammals as SYCP3, is retained at the centromeres following SC disassembly in an analogous fashion to Zip1 (Parra et al., 2004; Wojtasz et al., 2009). Furthermore, inhibition of Aurora B kinase during the G2-M transition in mouse spermatocytes results in a failure to disassemble the lateral element protein SYCP3, although the central element protein SYCP1 disassembles normally (Sun and Handel, 2008). This may provide clues into the mode of aurora B kinase action in SC disassembly, in controlling the removal of axial element proteins. It may be that in mammals, there exists a parallel Aurora B

kinase-independent pathway for SC disassembly that is sufficient to remove central element proteins from the chromosomes.

This SC disassembly phenotype of *ipl1-mn* mutants provides new insight into the protein architecture of the SC in yeast. Whilst the lateral element proteins Hop1 and Red1 disassembled or became more faint and diffuse following pachytene exit in *ipl1-mn* cells, Smt3<sup>SUMO</sup> staining showed high levels of co-localisation with Zip1. This suggests that full-length synaptonemal complexes can be maintained in the absence of both Hop1 and Red1 (at least at the level detectable cytologically). However, the retention of linear stretches of Smt3<sup>SUMO</sup> is consistent with Zip1 binding Smt3<sup>SUMO</sup> on the chromosome axes. Perhaps SC disassembly is triggered by degradation of Smt3-conjugates. Attempts to identify this sumoylated protein species revealed a band between 52 and 76 kDa in size that remains to be identified, although some possible candidates exist. It could merely represent a polymeric chain of ~ five Smt3 monomers (12 kDa each) that have previously been implicated as being involved with the synaptonemal complex (Cheng et al., 2006; Lin et al., 2009). Alternatively, this band may represent a sumoylated protein that is present along the chromosome axes. A good candidate may be Nse4 (46 kDa), a member of the Smc5-6 complex that is present along pachytene chromosomes (Phil Jordan, personal communication). Nse4 has also been shown to interact with Zip1 by yeast two-hybrid (Eva Hoffmann, personal communication) and is part of a protein complex that includes the SUMO E3 ligase, Nse2 (Zhao and Blobel, 2005). However, before this band can be identified, the experiment needs to be scaled-up in order to obtain sufficient protein to gain an ID by mass spectrometry. This work is ongoing in the Hoffmann laboratory.

To summarise, the highly conserved spindle assembly checkpoint plays several important roles during meiosis. Namely, in mediating prophase I and metaphase delays that assist in chromosome pairing and segregation, respectively. The recent finding that BubR1 is required for prophase I arrest in mouse oocytes (Homer et al., 2009) and in preventing premature SC disassembly in *Drosophila* oocytes (Malmanche et al., 2007), suggest that these mechanisms are well conserved and are highly relevant to human fertility. In fact, aberrations in the spindle checkpoint are thought to underpin age-related female infertility in humans (Mailhes, 2008). One popular model is that the age-related increase in incidence of aneuploidy is a result of ‘two-hits’ that compromise meiotic chromosome segregation (Hassold and Hunt, 2001; Lamb et al., 1996). This model posits that the ‘first hit’ is a chromosome pair with a crossover configuration that does not support high levels of disjunction. For example, a chromosome pair with crossovers located distally to the centromere. The model suggests that in ‘young’ oocytes, the spindle checkpoint is intact and can ‘deal’ with these error-prone chromosome pairs and promote their correct segregation at the first meiotic division. However, in ageing oocytes the ‘second hit’ comes from aberrations in the spindle checkpoint. The spindle checkpoint is suggested to be less efficient over time and so is unable to ‘cope’ with the error-prone chromosome pairs, which consequently non-disjoin at higher frequencies. Support for this model comes from the observation that in many of the maternally derived cases of trisomy 21, which cause Down’s syndrome, the non-disjoining chromosome 21 pair frequently contained distally located crossovers, or no crossovers at all (Lamb et al., 1996). Furthermore, *MAD2* and *BUB1* transcript levels decrease with increasing maternal age in human oocytes

(Steuerwald et al., 2001) and Mad2 depletion results in elevated aneuploidy in mouse oocytes (Homer et al., 2005). These findings are consistent with the notion that the increased frequency of aneuploidy that accompanies increasing maternal age may in part be due to reduced spindle checkpoint activity in ageing oocytes.

# Chapter 7. Discussion.

## 7.1. Discussion

The work outlined here describes a novel role for the synaptonemal complex protein, Zip1 and its regulatory proteins Zip2, Zip3 and Zip4 in the segregation of non-exchange chromosome pairs during meiosis I (Chapter 4). It also confirms a role for the spindle checkpoint proteins Mad3 and Mad2 in non-exchange chromosome segregation, which act in a parallel pathway to Zip1 in this process (Chapter 6). Furthermore, this work has provided new insight into how Zip1 is regulated throughout meiotic prophase by the synapsis initiation proteins, Zip2 and Zip3 (Chapter 5). In addition, this work has ascribed a novel function for the mismatch repair paralogue, Msh4 in regulating synapsis (Chapter 3).

What is the functional relevance of these findings? Zip1 is a structurally conserved protein that is central to many crucial processes in meiotic prophase. These include the synapsis of homologs, crossover formation, regulation of crossover position and chromosome segregation (references throughout). Consequently, mutation of the genes encoding synaptonemal complex proteins culminate in meiotic arrest and/or errors in chromosome segregation in the model organisms studied. The genes encoding SC proteins have been knocked out (individually) in mice and result in infertility or reduced fertility due to meiotic arrest and errors in meiotic chromosome segregation, respectively (Bolcun-Filas et al., 2007; Bolcun-Filas et al., 2009; de Vries et al., 2005; Hamer et al., 2008; Yuan et al., 2002; Yuan et al., 2000). This implies that mutations in the genes encoding SC proteins may cause similar fertility problems in humans. Indeed,

two independent mutations in the *SYCP3* gene (encoding a lateral element protein) have been mapped in females suffering recurrent pregnancy loss (Bolor et al., 2009) and also in male patients experiencing non-obstructive azospermia (Miyamoto et al., 2003). Given these findings and the mouse phenotypes, it seems reasonable to suppose that mutations in any of the genes encoding SC proteins, or the proteins that regulate the SC, may compromise fertility in humans.

The finding that the synaptonemal complex proteins (Zip1, Zip2, Zip3 and Zip4) are involved in non-exchange chromosome segregation in budding yeast is analogous to findings in many other organisms. For example, *Bombyx mori* females do not experience crossing over, but instead use a modified form of the SC to segregate homologous chromosomes at the first meiotic division (Rasmussen, 1977). There is also evidence to suggest that the SC may be involved in NECS in *Arabidopsis thaliana* as well (Pradillo et al., 2007). Similarly, in marsupial males, the lateral element protein SCP3 forms a 'folded sheet' between the ends of sex chromosomes that, together with the central element protein SCP1, holds the supposedly 'non-exchange' chromosomes together until they segregate at meiosis I (Page et al., 2006). Similar observations have been made for the sex chromosomes of eutherian mammals (de la Fuente et al., 2007). However, whether these studies have provided sufficient evidence that the X-Y pair are in fact lacking a crossover remains controversial.

Nevertheless, the lateral element protein SYCP3 is present at the centromeres of the autosomes following SC disassembly, through to the first meiotic division in mice (Parra et al., 2004; Wojtasz et al., 2009). Furthermore,

in marsupial spermatocytes, the central element protein SCP1 is also associated with the centromeres of the autosomes following SC disassembly through to diakinesis (Page et al., 2006). These findings in mammals are strikingly similar to the localisation pattern of Zip1 described in this work. This suggests that SYCP3 (and SYCP1?) may act in an analogous fashion to promote the segregation of chromosome pairs that fail to cross over in mammals. However, the rarity of naturally occurring non-exchange chromosomes in mice makes this a difficult area of study. It will be interesting to determine whether SC proteins are retained at centromeres following SC disassembly during human meiosis where non-exchange chromosomes are relatively frequent (25 % of chromosomes lack Mlh1 foci in human oocytes) (Cheng et al., 2009).

It is possible that the maintenance of SC proteins at the centromeres, following SC disassembly, may be important for NECS. On the other hand, the retention/re-loading of SC proteins following SC disassembly may simply reflect morphological changes to the chromosomes that accompany this transition. However, based on the examples where SC proteins are thought to be involved in NECS (mammalian XY chromosomes, *Bombyx mori* females, budding yeast), it is tempting to speculate that they may have stemmed from a common ancestral mechanism, rather than arising independently in these organisms. These mechanisms may even represent evolutionary relics that arose before crossover recombination to segregate chromosomes at meiosis I. If so, in those organisms where crossing over became the predominant mode by which chromosomes were segregated at meiosis I, the NECS mechanism may have been demoted to becoming a 'back-up' mechanism should chromosomes fail to

cross over (e.g. yeast and possibly mammals). In contrast, in those organisms where NECS was kept as the primary mode by which chromosomes are segregated at meiosis I, the NECS mechanism was kept in place (e.g. *Bombyx mori* females, *Drosophila* males).

How significant is non-exchange chromosome segregation to human fertility? It would appear that it is very significant. An estimated 40% of maternally derived cases of trisomy 21 involved a non-exchange chromosome pair and similar values (20-40 %) are estimated for the other common trisomies (Hassold et al., 2000; Lamb et al., 1996). A recent study also suggested that ~25% of all chromosomes lack a crossover in human oocytes (Cheng et al., 2009). This, coupled with the fact that aneuploidy increases sharply with increasing maternal age, implies that non-exchange chromosome segregation may be less efficient in ageing mothers. Therefore, faulty NECS mechanisms could pose the “second hit” in the two hit model for age-related aneuploidy (Hassold and Hunt, 2001) with a non-exchange chromosome pair comprising the “first hit”. Alternatively, it is possible that the incidence of non-exchange chromosomes increases with increasing maternal age, although this seems unlikely given that recombination is completed in the fetal ovary, prior to oocyte arrest (Cheng et al., 2009). In any case, a mechanism for segregating non-exchange chromosomes is clearly important for meiotic chromosome segregation in humans. It is possible that such a mechanism may become eroded with age, which may help explain why the incidence of aneuploidy increases with increasing maternal age. For example, SYCP3 may be lost from the centromeres over decades of meiotic arrest in ageing females.

## 7.2. Conclusions and Future Work

There are still many questions that remain to be answered regarding the regulation and function of Zip1 described in this work. For example, how is Zip1 removed from the chromosome arms following exit from pachytene but retained (or reloaded) at the centromeres? Do changes in sumoylation control this transition? Is Smt3 sufficient to bind Zip1? These questions could be addressed by targeting Smt3<sup>SUMO</sup> to the arm regions and examining whether Zip1 remained at these sites following SC disassembly. Alternatively, immunoprecipitation (IP) experiments could be done with Zip1 at different stages of meiotic prophase. By comparing which proteins co-immunoprecipitate with Zip1 at pachytene and later stages of meiotic prophase may provide insight into Zip1 binding partners at centromeres and arm regions. Another outstanding question remains regarding the precise nature of the SUMO species that are present with Zip1 on meiotic chromosomes. This could be addressed by scaling up the Smt3<sup>SUMO</sup> IP experiment (described in Chapter 6) to try and gain a protein ID by mass spectrometry. There also exists a 'destruction box' motif within Zip1 that could mean Zip1 it is targeted for degradation by the APC. If so, mutation of these residues should influence Zip1 protein levels in meiotic cell extracts. It would also be interesting to introduce a TEV-cleavage site within Zip1 and to assay whether non-exchange chromosomes come apart when the TEV protease is added. This would provide evidence that Zip1 acts as a 'tether' between non-exchange chromosomes.

Further work is also needed to understand the role(s) of spindle checkpoint proteins in non-exchange chromosome segregation. Do these

proteins aid NECS by affording the chromosomes more time to associate with one another before they segregate at meiosis I? Or are these proteins vital to the underlying kinetochore structure that is important for centromere pairing? One way of distinguishing between these possibilities would be to allow cells more time in a particular stage of meiotic prophase and observing whether this could rescue the deletion phenotypes. This could be done using an inducible *NTD80* system that arrests cells in pachytene.

The more we learn about the mechanisms underlying meiotic chromosome segregation, the more we understand about why errors in meiotic chromosome segregation occur and why, in the case of humans these errors increase with increasing maternal age. With continued advances in genome sequencing and personalised medicine, it may be possible in the future to construct genetic profiles that could be used to forecast an individuals' fertility, or provide much needed explanations for otherwise unexplained infertility in couples trying to conceive. Finally, with the recent development of *in vitro* derived spermatocytes from embryonic stem cells (Nayernia et al., 2009), the future promises to bring exciting new discoveries to the field of human meiosis research.

# Bibliography

Agarwal, S., and Roeder, G.S. (2000). Zip3 provides a link between recombination enzymes and synaptonemal complex proteins. *Cell* 102, 245-255.

Allers, T., and Lichten, M. (2001). Differential timing and control of noncrossover and crossover recombination during meiosis. *Cell* 106, 47-57.

Anderson, L.K., Royer, S.M., Page, S.L., McKim, K.S., Lai, A., Lilly, M.A., and Hawley, R.S. (2005). Juxtaposition of C(2)M and the transverse filament protein C(3)G within the central region of *Drosophila* synaptonemal complex. *Proceedings of the National Academy of Sciences of the United States of America* 102, 4482-4487.

Aravind, L., and Koonin, E.V. (1998). The HORMA domain: a common structural denominator in mitotic checkpoints, chromosome synapsis and DNA repair. *Trends Biochem Sci* 23, 284-286.

Arora, C., Kee, K., Maleki, S., and Keeney, S. (2004). Antiviral protein Ski8 is a direct partner of Spo11 in meiotic DNA break formation, independent of its cytoplasmic role in RNA metabolism. *Molecular cell* 13, 549-559.

Bachant, J., Alcasabas, A., Blat, Y., Kleckner, N., and Elledge, S.J. (2002). The SUMO-1 isopeptidase Smt4 is linked to centromeric cohesion through SUMO-1 modification of DNA topoisomerase II. *Molecular cell* 9, 1169-1182.

Baudat, F., Buard, J., Grey, C., Fledel-Alon, A., Ober, C., Przeworski, M., Coop, G., and de Massy, B. (2010) PRDM9 Is a Major Determinant of Meiotic Recombination Hotspots in Humans and Mice. *Science* 327, 836-840.

Baudat, F., Manova, K., Yuen, J.P., Jasin, M., and Keeney, S. (2000). Chromosome synapsis defects and sexually dimorphic meiotic progression in mice lacking Spo11. *Molecular cell* 6, 989-998.

Baumann, C., Korner, R., Hofmann, K., and Nigg, E.A. (2007). PICH, a centromere-associated SNF2 family ATPase, is regulated by Plk1 and required for the spindle checkpoint. *Cell* 128, 101-114.

Bhalla, N., Wynne, D.J., Jantsch, V., and Dernburg, A.F. (2008). ZHP-3 acts at crossovers to couple meiotic recombination with synaptonemal complex disassembly and bivalent formation in *C. elegans*. *PLoS genetics* 4, e1000235.

Bishop, D.K., Park, D., Xu, L., and Kleckner, N. (1992). DMC1: a meiosis-specific yeast homolog of *E. coli* recA required for recombination, synaptonemal complex formation, and cell cycle progression. *Cell* 69, 439-456.

Blat, Y., Protacio, R.U., Hunter, N., and Kleckner, N. (2002). Physical and functional interactions among basic chromosome organizational features govern early steps of meiotic chiasma formation. *Cell* 111, 791-802.

Bolcun-Filas, E., Costa, Y., Speed, R., Taggart, M., Benavente, R., De Rooij, D.G., and Cooke, H.J. (2007). SYCE2 is required for synaptonemal complex assembly, double strand break repair, and homologous recombination. *The Journal of cell biology* 176, 741-747.

Bolcun-Filas, E., Hall, E., Speed, R., Taggart, M., Grey, C., de Massy, B., Benavente, R., and Cooke, H.J. (2009). Mutation of the mouse Syce1 gene disrupts synapsis and suggests a link between synaptonemal complex structural components and DNA repair. *PLoS genetics* 5, e1000393.

Bolor, H., Mori, T., Nishiyama, S., Ito, Y., Hosoba, E., Inagaki, H., Kogo, H., Ohye, T., Tsutsumi, M., Kato, T., *et al.* (2009). Mutations of the SYCP3 gene in women with recurrent pregnancy loss. *Am J Hum Genet* 84, 14-20.

Borde, V., Goldman, A.S., and Lichten, M. (2000). Direct coupling between meiotic DNA replication and recombination initiation. *Science* 290, 806-809.

Borde, V., Robine, N., Lin, W., Bonfils, S., Geli, V., and Nicolas, A. (2008). Histone H3 lysine 4 trimethylation marks meiotic recombination initiation sites. *EMBO J.* 28, 99-111.

Borner, G.V., Barot, A., and Kleckner, N. (2008). Yeast Pch2 promotes domainal axis organization, timely recombination progression, and arrest of defective recombinosomes during meiosis. *Proceedings of the National Academy of Sciences of the United States of America* 105, 3327-3332.

Borner, G.V., Kleckner, N., and Hunter, N. (2004). Crossover/noncrossover differentiation, synaptonemal complex formation, and regulatory surveillance at the leptotene/zygotene transition of meiosis. *Cell* 117, 29-45.

Brar, G.A., and Amon, A. (2008). Emerging roles for centromeres in meiosis I chromosome segregation. *Nat Rev Genet.* 9, 899-910.

Brar, G.A., Hochwagen, A., Ee, L., and Amon, A. (2008). Sister Chromatid Cohesion Independent Roles of Cohesin in Meiotic Chromosome Morphogenesis and Pairing. *Molecular biology of the cell.* 20, 1030-1047.

Brar, G.A., Kiburz, B.M., Zhang, Y., Kim, J.E., White, F., and Amon, A. (2006). Rec8 phosphorylation and recombination promote the step-wise loss of cohesins in meiosis. *Nature* 441, 532-536.

Brown, P.W., Hwang, K., Schlegel, P.N., and Morris, P.L. (2008). Small ubiquitin-related modifier (SUMO)-1, SUMO-2/3 and SUMOylation are involved with centromeric heterochromatin of chromosomes 9 and 1 and proteins of the synaptonemal complex during meiosis in men. *Hum Reprod.* 23, 2850-2857.

Buffin, E., Emre, D., and Karess, R.E. (2007). Flies without a spindle checkpoint. *Nature cell biology* 9, 565-572.

Buonomo, S.B., Clyne, R.K., Fuchs, J., Loidl, J., Uhlmann, F., and Nasmyth, K. (2000). Disjunction of homologous chromosomes in meiosis I depends on proteolytic cleavage of the meiotic cohesin Rec8 by separin. *Cell* 103, 387-398.

Burgoyne, P.S. (1982). Genetic homology and crossing over in the X and Y chromosomes of Mammals. *Hum Genet* 61, 85-90.

Busygina, V., Sehorn, M.G., Shi, I.Y., Tsubouchi, H., Roeder, G.S., and Sung, P. (2008). Hed1 regulates Rad51-mediated recombination via a novel mechanism. *Genes & development* 22, 786-795.

Carballo, J.A., Johnson, A.L., Sedgwick, S.G., and Cha, R.S. (2008). Phosphorylation of the axial element protein Hop1 by Mec1/Tel1 ensures meiotic interhomolog recombination. *Cell* 132, 758-770.

Carpenter, A.T. (1973). A meiotic mutant defective in distributive disjunction in *Drosophila melanogaster*. *Genetics* 73, 393-428.

Cha, R.S., Weiner, B.M., Keeney, S., Dekker, J., and Kleckner, N. (2000). Progression of meiotic DNA replication is modulated by interchromosomal interaction proteins, negatively by Spo11p and positively by Rec8p. *Genes & development* 14, 493-503.

- Chambers, S.R., Hunter, N., Louis, E.J., and Borts, R.H. (1996). The mismatch repair system reduces meiotic homeologous recombination and stimulates recombination-dependent chromosome loss. *Mol Cell Biol* 16, 6110-6120.
- Chan, A.C., Borts, R.H., and Hoffmann, E. (2009). Temperature-Dependent Modulation of Chromosome Segregation in *msh4* Mutants of Budding Yeast. *PLoS One* 4, e7284.
- Chang, C.R., Wu, C.S., Hom, Y., and Gartenberg, M.R. (2005). Targeting of cohesin by transcriptionally silent chromatin. *Genes & development* 19, 3031-3042.
- Cheeseman, I.M., Anderson, S., Jwa, M., Green, E.M., Kang, J., Yates, J.R., 3rd, Chan, C.S., Drubin, D.G., and Barnes, G. (2002). Phospho-regulation of kinetochore-microtubule attachments by the Aurora kinase Ipl1p. *Cell* 111, 163-172.
- Chen, R.H., Brady, D.M., Smith, D., Murray, A.W., and Hardwick, K.G. (1999). The spindle checkpoint of budding yeast depends on a tight complex between the Mad1 and Mad2 proteins. *Molecular biology of the cell* 10, 2607-2618.
- Chen, S.Y., Tsubouchi, T., Rockmill, B., Sandler, J.S., Richards, D.R., Vader, G., Hochwagen, A., Roeder, G.S., and Fung, J.C. (2008). Global Analysis of the Meiotic Crossover Landscape. *Developmental cell* 15, 331-332.
- Cheng, C.H., Lo, Y.H., Liang, S.S., Ti, S.C., Lin, F.M., Yeh, C.H., Huang, H.Y., and Wang, T.F. (2006). SUMO modifications control assembly of synaptonemal complex and polycomplex in meiosis of *Saccharomyces cerevisiae*. *Genes & development* 20, 2067-2081.
- Cheng, E.Y., Hunt, P.A., Nalwai-Cecchini, T.A., Fligner, C.L., Fujimoto, V.Y., Pasternack, T.L., Schwartz, J.M., Steinauer, J.E., Woodruff, T.J., Cherry, S.M., *et al.* (2009). Meiotic recombination in human oocytes. *PLoS genetics* 5, e1000661.
- Cheslock, P.S., Kemp, B.J., Boumil, R.M., and Dawson, D.S. (2005). The roles of MAD1, MAD2 and MAD3 in meiotic progression and the segregation of nonexchange chromosomes. *Nature genetics* 37, 756-760.
- Chikashige, Y., Ding, D.Q., Funabiki, H., Haraguchi, T., Mashiko, S., Yanagida, M., and Hiraoka, Y. (1994). Telomere-led premeiotic chromosome movement in fission yeast. *Science* 264, 270-273.
- Chu, S., and Herskowitz, I. (1998). Gametogenesis in yeast is regulated by a transcriptional cascade dependent on Ndt80. *Molecular cell* 1, 685-696.
- Chua, P.R., and Roeder, G.S. (1997). Tam1, a telomere-associated meiotic protein, functions in chromosome synapsis and crossover interference. *Genes & development* 11, 1786-1800.
- Chua, P.R., and Roeder, G.S. (1998). Zip2, a meiosis-specific protein required for the initiation of chromosome synapsis. *Cell* 93, 349-359.
- Ciosk, R., Shirayama, M., Shevchenko, A., Tanaka, T., Toth, A., and Nasmyth, K. (2000). Cohesin's binding to chromosomes depends on a separate complex consisting of Scc2 and Scc4 proteins. *Molecular cell* 5, 243-254.
- Ciosk, R., Zachariae, W., Michaelis, C., Shevchenko, A., Mann, M., and Nasmyth, K. (1998). An ESP1/PDS1 complex regulates loss of sister chromatid cohesion at the metaphase to anaphase transition in yeast. *Cell* 93, 1067-1076.

- Clift, D., Bizzari, F., and Marston, A.L. (2009). Shugoshin prevents cohesin cleavage by PP2A(Cdc55)-dependent inhibition of separase. *Genes & development* 23, 766-780.
- Clyne, R.K., Katis, V.L., Jessop, L., Benjamin, K.R., Herskowitz, I., Lichten, M., and Nasmyth, K. (2003). Polo-like kinase Cdc5 promotes chiasmata formation and cosegregation of sister centromeres at meiosis I. *Nature cell biology* 5, 480-485.
- Cohen-Fix, O., Peters, J.M., Kirschner, M.W., and Koshland, D. (1996). Anaphase initiation in *Saccharomyces cerevisiae* is controlled by the APC-dependent degradation of the anaphase inhibitor Pds1p. *Genes & development* 10, 3081-3093.
- Colaiacovo, M.P., MacQueen, A.J., Martinez-Perez, E., McDonald, K., Adamo, A., La Volpe, A., and Villeneuve, A.M. (2003). Synaptonemal complex assembly in *C. elegans* is dispensable for loading strand-exchange proteins but critical for proper completion of recombination. *Developmental cell* 5, 463-474.
- Conrad, M.N., Dominguez, A.M., and Dresser, M.E. (1997). Ndj1p, a meiotic telomere protein required for normal chromosome synapsis and segregation in yeast. *Science* 276, 1252-1255.
- Conrad, M.N., Lee, C.Y., Chao, G., Shinohara, M., Kosaka, H., Shinohara, A., Conchello, J.A., and Dresser, M.E. (2008). Rapid telomere movement in meiotic prophase is promoted by NDJ1, MPS3, and CSM4 and is modulated by recombination. *Cell* 133, 1175-1187.
- Cooper, K.W. (1964). Meiotic Conjunctive Elements Not Involving Chiasmata. *Proceedings of the National Academy of Sciences of the United States of America* 52, 1248-1255.
- Costa, Y., Speed, R., Ollinger, R., Alsheimer, M., Semple, C.A., Gautier, P., Maratou, K., Novak, I., Hoog, C., Benavente, R., *et al.* (2005). Two novel proteins recruited by synaptonemal complex protein 1 (SYCP1) are at the centre of meiosis. *J Cell Sci* 118, 2755-2762.
- Courtwright, A.M., and He, X. (2002). Dam1 is the right one: phosphoregulation of kinetochore biorientation. *Developmental cell* 3, 610-611.
- Couteau, F., and Zetka, M. (2005). HTP-1 coordinates synaptonemal complex assembly with homolog alignment during meiosis in *C. elegans*. *Genes & development* 19, 2744-2756.
- Cromie, G.A., Hyppa, R.W., Taylor, A.F., Zakharyevich, K., Hunter, N., and Smith, G.R. (2006). Single Holliday junctions are intermediates of meiotic recombination. *Cell* 127, 1167-1178.
- Davis, L., and Smith, G.R. (2005). Dynein promotes achiasmate segregation in *Schizosaccharomyces pombe*. *Genetics* 170, 581-590.
- Dawson, D.S., Murray, A.W., and Szostak, J.W. (1986). An alternative pathway for meiotic chromosome segregation in yeast. *Science* 234, 713-717.
- de la Fuente, R., Parra, M.T., Viera, A., Calvente, A., Gomez, R., Suja, J.A., Rufas, J.S., and Page, J. (2007). Meiotic Pairing and Segregation of Achiasmate Sex Chromosomes in Eutherian Mammals: The Role of SYCP3 Protein. *PLoS genetics* 3, e198.
- de los Santos, T., Hunter, N., Lee, C., Larkin, B., Loidl, J., and Hollingsworth, N.M. (2003). The Mus81/Mms4 endonuclease acts independently of double-Holliday junction resolution to promote a distinct subset of crossovers during meiosis in budding yeast. *Genetics* 164, 81-94.

- de los Santos, T., Loidl, J., Larkin, B., and Hollingsworth, N.M. (2001). A role for MMS4 in the processing of recombination intermediates during meiosis in *Saccharomyces cerevisiae*. *Genetics* 159, 1511-1525.
- de Vries, F.A., de Boer, E., van den Bosch, M., Baarends, W.M., Ooms, M., Yuan, L., Liu, J.G., van Zeeland, A.A., Heyting, C., and Pastink, A. (2005). Mouse Sycp1 functions in synaptonemal complex assembly, meiotic recombination, and XY body formation. *Genes & development* 19, 1376-1389.
- Dernburg, A.F., McDonald, K., Moulder, G., Barstead, R., Dresser, M., and Villeneuve, A.M. (1998). Meiotic recombination in *C. elegans* initiates by a conserved mechanism and is dispensable for homologous chromosome synapsis. *Cell* 94, 387-398.
- Dernburg, A.F., Sedat, J.W., and Hawley, R.S. (1996). Direct evidence of a role for heterochromatin in meiotic chromosome segregation. *Cell* 86, 135-146.
- Ding, D.Q., Yamamoto, A., Haraguchi, T., and Hiraoka, Y. (2004). Dynamics of homologous chromosome pairing during meiotic prophase in fission yeast. *Developmental cell* 6, 329-341.
- Ding, R., McDonald, K.L., and McIntosh, J.R. (1993). Three-dimensional reconstruction and analysis of mitotic spindles from the yeast, *Schizosaccharomyces pombe*. *The Journal of cell biology* 120, 141-151.
- Dobson, M.J., Pearlman, R.E., Karaiskakis, A., Spyropoulos, B., and Moens, P.B. (1994). Synaptonemal complex proteins: occurrence, epitope mapping and chromosome disjunction. *J Cell Sci* 107 ( Pt 10), 2749-2760.
- Dong, H., and Roeder, G.S. (2000). Organization of the yeast Zip1 protein within the central region of the synaptonemal complex. *The Journal of cell biology* 148, 417-426.
- Du, P., Kibbe, W.A., and Lin, S.M. (2006). Improved peak detection in mass spectrum by incorporating continuous wavelet transform-based pattern matching. *Bioinformatics* 22, 2059-2065.
- Egel, R. (1978). Synaptonemal complex and crossing-over: structural support or interference? *Heredity* 41, 233-237.
- Engbrecht, J., Masse, S., Davis, L., Rose, K., and Kessel, T. (1998). Yeast meiotic mutants proficient for the induction of ectopic recombination. *Genetics* 148, 581-598.
- Franklin, F.C., Higgins, J.D., Sanchez-Moran, E., Armstrong, S.J., Osman, K.E., Jackson, N., and Jones, G.H. (2006). Control of meiotic recombination in *Arabidopsis*: role of the MutL and MutS homologues. *Biochem Soc Trans* 34, 542-544.
- Fung, J.C., Rockmill, B., Odell, M., and Roeder, G.S. (2004). Imposition of crossover interference through the nonrandom distribution of synapsis initiation complexes. *Cell* 116, 795-802.
- Gerton, J.L., DeRisi, J., Shroff, R., Lichten, M., Brown, P.O., and Petes, T.D. (2000). Inaugural article: global mapping of meiotic recombination hotspots and coldspots in the yeast *Saccharomyces cerevisiae*. *Proceedings of the National Academy of Sciences of the United States of America* 97, 11383-11390.
- Gietz, R.D., and Schiestl, R.H. (2007). High-efficiency yeast transformation using the LiAc/SS carrier DNA/PEG method. *Nat Protoc* 2, 31-34.

- Gietz, R.D., Schiestl, R.H., Willems, A.R., and Woods, R.A. (1995). Studies on the transformation of intact yeast cells by the LiAc/SS-DNA/PEG procedure. *Yeast* 11, 355-360.
- Gilliland, W.D., Hughes, S.F., Vietti, D.R., and Hawley, R.S. (2009). Congression of achiasmate chromosomes to the metaphase plate in *Drosophila melanogaster* oocytes. *Dev Biol* 325, 122-128.
- Gladstone, M.N., Obeso, D., Chuong, H., and Dawson, D.S. (2009). The synaptonemal complex protein Zip1 promotes bi-orientation of centromeres at meiosis I. *PLoS genetics* 5, e1000771.
- Goodyer, W., Kaitna, S., Couteau, F., Ward, J.D., Boulton, S.J., and Zetka, M. (2008). HTP-3 links DSB formation with homolog pairing and crossing over during *C. elegans* meiosis. *Developmental cell* 14, 263-274.
- Grelon, M., Vezon, D., Gendrot, G., and Pelletier, G. (2001). AtSPO11-1 is necessary for efficient meiotic recombination in plants. *EMBO J* 20, 589-600.
- Guacci, V., and Kaback, D.B. (1991). Distributive disjunction of authentic chromosomes in *Saccharomyces cerevisiae*. *Genetics* 127, 475-488.
- Haering, C.H., Lowe, J., Hochwagen, A., and Nasmyth, K. (2002). Molecular architecture of SMC proteins and the yeast cohesin complex. *Molecular cell* 9, 773-788.
- Hamer, G., Gell, K., Kouznetsova, A., Novak, I., Benavente, R., and Hoog, C. (2006). Characterization of a novel meiosis-specific protein within the central element of the synaptonemal complex. *J Cell Sci* 119, 4025-4032.
- Hamer, G., Wang, H., Bolcun-Filas, E., Cooke, H.J., Benavente, R., and Hoog, C. (2008). Progression of meiotic recombination requires structural maturation of the central element of the synaptonemal complex. *J Cell Sci* 121, 2445-2451.
- Hardwick, K.G., Johnston, R.C., Smith, D.L., and Murray, A.W. (2000). MAD3 encodes a novel component of the spindle checkpoint which interacts with Bub3p, Cdc20p, and Mad2p. *The Journal of cell biology* 148, 871-882.
- Hardy, C.F., Dryga, O., Seematter, S., Pahl, P.M., and Sclafani, R.A. (1997). mcm5/cdc46-bob1 bypasses the requirement for the S phase activator Cdc7p. *Proceedings of the National Academy of Sciences of the United States of America* 94, 3151-3155.
- Hassold, T., and Hunt, P. (2001). To err (meiotically) is human: the genesis of human aneuploidy. *Nat Rev Genet* 2, 280-291.
- Hassold, T., Sherman, S., and Hunt, P. (2000). Counting cross-overs: characterizing meiotic recombination in mammals. *Human molecular genetics* 9, 2409-2419.
- Hauf, S., Biswas, A., Langeegger, M., Kawashima, S.A., Tsukahara, T., and Watanabe, Y. (2007). Aurora controls sister kinetochore mono-orientation and homolog bi-orientation in meiosis-I. *Embo J* 26, 4475-4486.
- Hawley, R.S. (2002). Meiosis: how male flies do meiosis. *Curr Biol* 12, R660-662.
- Hawley, R.S., and Theurkauf, W.E. (1993). Requiem for distributive segregation: achiasmate segregation in *Drosophila* females. *Trends Genet* 9, 310-317.
- Hayase, A., Takagi, M., Miyazaki, T., Oshiumi, H., Shinohara, M., and Shinohara, A. (2004). A protein complex containing Mei5 and Sae3 promotes the assembly of the meiosis-specific RecA homolog Dmc1. *Cell* 119, 927-940.

Hayashi, K., Yoshida, K., and Matsui, Y. (2005). A histone H3 methyltransferase controls epigenetic events required for meiotic prophase. *Nature* 438, 374-378.

Heidinger-Pauli, J.M., Unal, E., Guacci, V., and Koshland, D. (2008). The kleisin subunit of cohesin dictates damage-induced cohesion. *Molecular cell* 31, 47-56.

Henderson, K.A., Kee, K., Maleki, S., Santini, P.A., and Keeney, S. (2006). Cyclin-dependent kinase directly regulates initiation of meiotic recombination. *Cell* 125, 1321-1332.

Henderson, K.A., and Keeney, S. (2004). Tying synaptonemal complex initiation to the formation and programmed repair of DNA double-strand breaks. *Proceedings of the National Academy of Sciences of the United States of America* 101, 4519-4524.

Henderson, K.A., and Keeney, S. (2005). Synaptonemal complex formation: where does it start? *Bioessays* 27, 995-998.

Hepworth, S.R., Friesen, H., and Segall, J. (1998). NDT80 and the meiotic recombination checkpoint regulate expression of middle sporulation-specific genes in *Saccharomyces cerevisiae*. *Mol Cell Biol* 18, 5750-5761.

Hochwagen, A., and Marais, G.A. Meiosis: A PRDM9 Guide to the Hotspots of Recombination. *Curr Biol* 20, R271-R274.

Hochwagen, A., Tham, W.H., Brar, G.A., and Amon, A. (2005). The FK506 binding protein Fpr3 counteracts protein phosphatase 1 to maintain meiotic recombination checkpoint activity. *Cell* 122, 861-873.

Hollingsworth, N.M., and Brill, S.J. (2004). The Mus81 solution to resolution: generating meiotic crossovers without Holliday junctions. *Genes & development* 18, 117-125.

Holloway, J.K., Booth, J., Edelmann, W., McGowan, C.H., and Cohen, P.E. (2008). MUS81 generates a subset of MLH1-MLH3-independent crossovers in mammalian meiosis. *PLoS genetics* 4, e1000186.

Homer, H., Gui, L., and Carroll, J. (2009). A spindle assembly checkpoint protein functions in prophase I arrest and prometaphase progression. *Science* 326, 991-994.

Homer, H.A., McDougall, A., Levasseur, M., Yallop, K., Murdoch, A.P., and Herbert, M. (2005). Mad2 prevents aneuploidy and premature proteolysis of cyclin B and securin during meiosis I in mouse oocytes. *Genes & development* 19, 202-207.

Hooker, G.W., and Roeder, G.S. (2006). A Role for SUMO in meiotic chromosome synapsis. *Curr Biol* 16, 1238-1243.

Hoyt, M.A., Totis, L., and Roberts, B.T. (1991). *S. cerevisiae* genes required for cell cycle arrest in response to loss of microtubule function. *Cell* 66, 507-517.

Huang, C.E., Milutinovich, M., and Koshland, D. (2005). Rings, bracelet or snaps: fashionable alternatives for Smc complexes. *Philos Trans R Soc Lond B Biol Sci* 360, 537-542.

Hughes, S.E., Gilliland, W.D., Cotitta, J.L., Takeo, S., Collins, K.A., and Hawley, R.S. (2009). Heterochromatic threads connect oscillating chromosomes during prometaphase I in *Drosophila* oocytes. *PLoS genetics* 5, e1000348.

Hunt, P.A., and Hassold, T.J. (2002). Sex matters in meiosis. *Science* 296, 2181-2183.

Hunter, N., and Borts, R.H. (1997). Mlh1 is unique among mismatch repair proteins in its ability to promote crossing-over during meiosis. *Genes & development* 11, 1573-1582.

Hunter, N., and Kleckner, N. (2001). The single-end invasion: an asymmetric intermediate at the double-strand break to double-holliday junction transition of meiotic recombination. *Cell* 106, 59-70.

Hwang, L.H., Lau, L.F., Smith, D.L., Mistrot, C.A., Hardwick, K.G., Hwang, E.S., Amon, A., and Murray, A.W. (1998). Budding yeast Cdc20: a target of the spindle checkpoint. *Science* 279, 1041-1044.

Ip, S.C., Rass, U., Blanco, M.G., Flynn, H.R., Skehel, J.M., and West, S.C. (2008). Identification of Holliday junction resolvases from humans and yeast. *Nature* 456, 357-361.

Ivanov, D., and Nasmyth, K. (2005). A topological interaction between cohesin rings and a circular minichromosome. *Cell* 122, 849-860.

Ivanovska, I., Khandan, T., Ito, T., and Orr-Weaver, T.L. (2005). A histone code in meiosis: the histone kinase, NHK-1, is required for proper chromosomal architecture in *Drosophila* oocytes. *Genes & development* 19, 2571-2582.

Ivanovska, I., and Orr-Weaver, T.L. (2006). Histone modifications and the chromatin scaffold for meiotic chromosome architecture. *Cell Cycle* 5, 2064-2071.

Jessop, L., Rockmill, B., Roeder, G.S., and Lichten, M. (2006). Meiotic chromosome synapsis-promoting proteins antagonize the anti-crossover activity of sgs1. *PLoS genetics* 2, e155.

Jiao, K., Salem, L., and Malone, R. (2003). Support for a meiotic recombination initiation complex: interactions among Rec102p, Rec104p, and Spo11p. *Mol Cell Biol* 23, 5928-5938.

Jin, H., Guacci, V., and Yu, H.G. (2009). Pds5 is required for homologue pairing and inhibits synapsis of sister chromatids during yeast meiosis. *The Journal of cell biology* 186, 713-725.

Johzuka, K., and Ogawa, H. (1995). Interaction of Mre11 and Rad50: two proteins required for DNA repair and meiosis-specific double-strand break formation in *Saccharomyces cerevisiae*. *Genetics* 139, 1521-1532.

Jordan, P., Copsey, A., Newnham, L., Kolar, E., Lichten, M., and Hoffmann, E. (2009). Ipl1/Aurora B kinase coordinates synaptonemal complex disassembly with cell cycle progression and crossover formation in budding yeast meiosis. *Genes & development* 23, 2237-2251.

Joshi, N., Barot, A., Jamison, C., and Borner, G.V. (2009). Pch2 links chromosome axis remodeling at future crossover sites and crossover distribution during yeast meiosis. *PLoS genetics* 5, e1000557.

Katis, V.L., Lipp, J.J., Imre, R., Bogdanova, A., Okaz, E., Habermann, B., Mechtler, K., Nasmyth, K., and Zachariae, W. Rec8 phosphorylation by casein kinase 1 and Cdc7-Dbf4 kinase regulates cohesin cleavage by separase during meiosis. *Developmental cell* 18, 397-409.

Katis, V.L., Matos, J., Mori, S., Shirahige, K., Zachariae, W., and Nasmyth, K. (2004). Spo13 facilitates monopolin recruitment to kinetochores and regulates maintenance of centromeric cohesion during yeast meiosis. *Curr Biol* 14, 2183-2196.

- Kee, K., and Keeney, S. (2002). Functional interactions between SPO11 and REC102 during initiation of meiotic recombination in *Saccharomyces cerevisiae*. *Genetics* 160, 111-122.
- Kee, K., Protacio, R.U., Arora, C., and Keeney, S. (2004). Spatial organization and dynamics of the association of Rec102 and Rec104 with meiotic chromosomes. *EMBO J* 23, 1815-1824.
- Keeney, S., Giroux, C.N., and Kleckner, N. (1997). Meiosis-specific DNA double-strand breaks are catalyzed by Spo11, a member of a widely conserved protein family. *Cell* 88, 375-384.
- Kelly, A.E., and Funabiki, H. (2009). Correcting aberrant kinetochore microtubule attachments: an Aurora B-centric view. *Curr Opin Cell Biol.* 21, 51-58.
- Kemmler, S., Stach, M., Knapp, M., Ortiz, J., Pfannstiel, J., Ruppert, T., and Lechner, J. (2009). Mimicking Ndc80 phosphorylation triggers spindle assembly checkpoint signalling. *EMBO J* 28, 1099-1110.
- Kemp, B., Boumil, R.M., Stewart, M.N., and Dawson, D.S. (2004). A role for centromere pairing in meiotic chromosome segregation. *Genes & development* 18, 1946-1951.
- Kiburz, B.M., Reynolds, D.B., Megee, P.C., Marston, A.L., Lee, B.H., Lee, T.I., Levine, S.S., Young, R.A., and Amon, A. (2005). The core centromere and Sgo1 establish a 50-kb cohesin-protected domain around centromeres during meiosis I. *Genes & development* 19, 3017-3030.
- King, E.M., Rachidi, N., Morrice, N., Hardwick, K.G., and Stark, M.J. (2007). Ipl1p-dependent phosphorylation of Mad3p is required for the spindle checkpoint response to lack of tension at kinetochores. *Genes & development* 21, 1163-1168.
- Kitagawa, R., and Rose, A.M. (1999). Components of the spindle-assembly checkpoint are essential in *Caenorhabditis elegans*. *Nat Cell Biol* 1, 514-521.
- Kitajima, T.S., Kawashima, S.A., and Watanabe, Y. (2004). The conserved kinetochore protein shugoshin protects centromeric cohesion during meiosis. *Nature* 427, 510-517.
- Kitajima, T.S., Sakuno, T., Ishiguro, K., Iemura, S., Natsume, T., Kawashima, S.A., and Watanabe, Y. (2006). Shugoshin collaborates with protein phosphatase 2A to protect cohesin. *Nature* 441, 46-52.
- Klein, F., Laroche, T., Cardenas, M.E., Hofmann, J.F., Schweizer, D., and Gasser, S.M. (1992). Localization of RAP1 and topoisomerase II in nuclei and meiotic chromosomes of yeast. *The Journal of cell biology* 117, 935-948.
- Klein, F., Mahr, P., Galova, M., Buonomo, S.B., Michaelis, C., Nairz, K., and Nasmyth, K. (1999). A central role for cohesins in sister chromatid cohesion, formation of axial elements, and recombination during yeast meiosis. *Cell* 98, 91-103.
- Kneitz, B., Cohen, P.E., Avdievich, E., Zhu, L., Kane, M.F., Hou, H., Jr., Kolodner, R.D., Kucherlapati, R., Pollard, J.W., and Edelmann, W. (2000). MutS homolog 4 localization to meiotic chromosomes is required for chromosome pairing during meiosis in male and female mice. *Genes & development* 14, 1085-1097.
- Kong, A., Thorleifsson, G., Stefansson, H., Masson, G., Helgason, A., Gudbjartsson, D.F., Jonsdottir, G.M., Gudjonsson, S.A., Sverrisson, S.,

- Thorlacius, T., *et al.* (2008). Sequence variants in the RNF212 gene associate with genome-wide recombination rate. *Science* 319, 1398-1401.
- Koszul, R., Kim, K.P., Prentiss, M., Kleckner, N., and Kameoka, S. (2008). Meiotic chromosomes move by linkage to dynamic actin cables with transduction of force through the nuclear envelope. *Cell* 133, 1188-1201.
- Kouznetsova, A., Lister, L., Nordenskjold, M., Herbert, M., and Hoog, C. (2007). Bi-orientation of achiasmatic chromosomes in meiosis I oocytes contributes to aneuploidy in mice. *Nature genetics* 39, 966-968.
- Kraft, C., Vodermaier, H.C., Maurer-Stroh, S., Eisenhaber, F., and Peters, J.M. (2005). The WD40 propeller domain of Cdh1 functions as a destruction box receptor for APC/C substrates. *Molecular cell* 18, 543-553.
- Kudo, N.R., Anger, M., Peters, A.H., Stemmann, O., Theussl, H.C., Helmhart, W., Kudo, H., Heyting, C., and Nasmyth, K. (2009). Role of cleavage by separase of the Rec8 kleisin subunit of cohesin during mammalian meiosis I. *J Cell Sci* 122, 2686-2698.
- Kudo, N.R., Wassmann, K., Anger, M., Schuh, M., Wirth, K.G., Xu, H., Helmhart, W., Kudo, H., McKay, M., Maro, B., *et al.* (2006). Resolution of chiasmata in oocytes requires separase-mediated proteolysis. *Cell* 126, 135-146.
- Lacefield, S., and Murray, A.W. (2007). The spindle checkpoint rescues the meiotic segregation of chromosomes whose crossovers are far from the centromere. *Nature genetics* 39, 1273-1277.
- Lamb, N.E., Freeman, S.B., Savage-Austin, A., Pettay, D., Taft, L., Hersey, J., Gu, Y., Shen, J., Saker, D., May, K.M., *et al.* (1996). Susceptible chiasmate configurations of chromosome 21 predispose to non-disjunction in both maternal meiosis I and meiosis II. *Nature genetics* 14, 400-405.
- Lambie, E.J., and Roeder, G.S. (1988). A yeast centromere acts in cis to inhibit meiotic gene conversion of adjacent sequences. *Cell* 52, 863-873.
- Lao, J.P., Oh, S.D., Shinohara, M., Shinohara, A., and Hunter, N. (2008). Rad52 promotes postinvasion steps of meiotic double-strand-break repair. *Molecular cell* 29, 517-524.
- Lee, B.H., and Amon, A. (2003). Role of Polo-like kinase CDC5 in programming meiosis I chromosome segregation. *Science* 300, 482-486.
- Lee, J., Kitajima, T.S., Tanno, Y., Yoshida, K., Morita, T., Miyano, T., Miyake, M., and Watanabe, Y. (2008). Unified mode of centromeric protection by shugoshin in mammalian oocytes and somatic cells. *Nature cell biology* 10, 42-52.
- LeMaire-Adkins, R., Radke, K., and Hunt, P.A. (1997). Lack of checkpoint control at the metaphase/anaphase transition: a mechanism of meiotic nondisjunction in mammalian females. *The Journal of cell biology* 139, 1611-1619.
- Lengsfeld, B.M., Rattray, A.J., Bhaskara, V., Ghirlando, R., and Paull, T.T. (2007). Sae2 is an endonuclease that processes hairpin DNA cooperatively with the Mre11/Rad50/Xrs2 complex. *Molecular cell* 28, 638-651.
- Leu, J.Y., Chua, P.R., and Roeder, G.S. (1998). The meiosis-specific Hop2 protein of *S. cerevisiae* ensures synapsis between homologous chromosomes. *Cell* 94, 375-386.
- Li, J., Hooker, G.W., and Roeder, G.S. (2006). *Saccharomyces cerevisiae* Mer2, Mei4 and Rec114 form a complex required for meiotic double-strand break formation. *Genetics* 173, 1969-1981.

- Li, R., and Murray, A.W. (1991). Feedback control of mitosis in budding yeast. *Cell* 66, 519-531.
- Li, X., and Dawe, R.K. (2009). Fused sister kinetochores initiate the reductional division in meiosis I. *Nature cell biology* 11, 1103-1108.
- Li, X., and Nicklas, R.B. (1997). Tension-sensitive kinetochore phosphorylation and the chromosome distribution checkpoint in praying mantid spermatocytes. *J Cell Sci* 110 ( Pt 5), 537-545.
- Li, Y., and Benezra, R. (1996). Identification of a human mitotic checkpoint gene: hsMAD2. *Science* 274, 246-248.
- Lichten, M., and Goldman, A.S. (1995). Meiotic recombination hotspots. *Annual review of genetics* 29, 423-444.
- Lin, F.M., Lai, Y.J., Shen, H.J., Cheng, Y.H., and Wang, T.F. (2009). Yeast axial-element protein, Red1, binds SUMO chains to promote meiotic interhomologue recombination and chromosome synapsis. *EMBO J.* 29, 586-596.
- Lin, Y., and Smith, G.R. (1994). Transient, meiosis-induced expression of the *rec6* and *rec12* genes of *Schizosaccharomyces pombe*. *Genetics* 136, 769-779.
- Liu, J.G., Yuan, L., Brundell, E., Bjorkroth, B., Daneholt, B., and Hoog, C. (1996). Localization of the N-terminus of SCP1 to the central element of the synaptonemal complex and evidence for direct interactions between the N-termini of SCP1 molecules organized head-to-head. *Exp Cell Res* 226, 11-19.
- Loidl, J., Scherthan, H., and Kaback, D.B. (1994). Physical association between nonhomologous chromosomes precedes distributive disjunction in yeast. *Proceedings of the National Academy of Sciences of the United States of America* 91, 331-334.
- Longtine, M.S., McKenzie, A., 3rd, Demarini, D.J., Shah, N.G., Wach, A., Brachat, A., Philippsen, P., and Pringle, J.R. (1998). Additional modules for versatile and economical PCR-based gene deletion and modification in *Saccharomyces cerevisiae*. *Yeast* 14, 953-961.
- Lowe, J., Cordell, S.C., and van den Ent, F. (2001). Crystal structure of the SMC head domain: an ABC ATPase with 900 residues antiparallel coiled-coil inserted. *J Mol Biol* 306, 25-35.
- Luo, X., Fang, G., Coldiron, M., Lin, Y., Yu, H., Kirschner, M.W., and Wagner, G. (2000). Structure of the Mad2 spindle assembly checkpoint protein and its interaction with Cdc20. *Nature structural biology* 7, 224-229.
- Luo, X., Tang, Z., Rizo, J., and Yu, H. (2002). The Mad2 spindle checkpoint protein undergoes similar major conformational changes upon binding to either Mad1 or Cdc20. *Molecular cell* 9, 59-71.
- Luo, X., Tang, Z., Xia, G., Wassmann, K., Matsumoto, T., Rizo, J., and Yu, H. (2004). The Mad2 spindle checkpoint protein has two distinct natively folded states. *Nature structural & molecular biology* 11, 338-345.
- MacQueen, A.J., Colaiacovo, M.P., McDonald, K., and Villeneuve, A.M. (2002). Synapsis-dependent and -independent mechanisms stabilize homolog pairing during meiotic prophase in *C. elegans*. *Genes & development* 16, 2428-2442.
- MacQueen, A.J., Phillips, C.M., Bhalla, N., Weiser, P., Villeneuve, A.M., and Dernburg, A.F. (2005). Chromosome sites play dual roles to establish homologous synapsis during meiosis in *C. elegans*. *Cell* 123, 1037-1050.

Macqueen, A.J., and Roeder, G.S. (2009). Fpr3 and Zip3 Ensure that Initiation of Meiotic Recombination Precedes Chromosome Synapsis in Budding Yeast. *Curr Biol.* 19, 1519-1526.

Maguire, M.P. (1995). Is the synaptonemal complex a disjunction machine? *J Hered* 86, 330-340.

Mailhes, J.B. (2008). Faulty spindle checkpoint and cohesion protein activities predispose oocytes to premature chromosome separation and aneuploidy. *Environ Mol Mutagen* 49, 642-658.

Maleki, S., Neale, M.J., Arora, C., Henderson, K.A., and Keeney, S. (2007). Interactions between Mei4, Rec114, and other proteins required for meiotic DNA double-strand break formation in *Saccharomyces cerevisiae*. *Chromosoma* 116, 471-486.

Malmanche, N., Owen, S., Gegick, S., Steffensen, S., Tomkiel, J.E., and Sunkel, C.E. (2007). *Drosophila* BubR1 Is Essential for Meiotic Sister-Chromatid Cohesion and Maintenance of Synaptonemal Complex. *Curr Biol.* 17, 1489-97

Manfrini, N., Guerini, I., Citterio, A., Lucchini, G., and Longhese, M.P. Processing of meiotic DNA double-strand breaks requires cyclin-dependent kinase and multiple nucleases. *J Biol Chem.* 285, 11628-37.

Manheim, E.A., and McKim, K.S. (2003). The Synaptonemal complex component C(2)M regulates meiotic crossing over in *Drosophila*. *Curr Biol* 13, 276-285.

Mapelli, M., Filipp, F.V., Rancati, G., Massimiliano, L., Nezi, L., Stier, G., Hagan, R.S., Confalonieri, S., Piatti, S., Sattler, M., *et al.* (2006). Determinants of conformational dimerization of Mad2 and its inhibition by p31comet. *EMBO J* 25, 1273-1284.

Marston, A.L., Tham, W.H., Shah, H., and Amon, A. (2004). A genome-wide screen identifies genes required for centromeric cohesion. *Science* 303, 1367-1370.

Martini, E., Diaz, R.L., Hunter, N., and Keeney, S. (2006). Crossover homeostasis in yeast meiosis. *Cell* 126, 285-295.

Matos, J., Lipp, J.J., Bogdanova, A., Guillot, S., Okaz, E., Junqueira, M., Shevchenko, A., and Zachariae, W. (2008). Dbf4-dependent cdc7 kinase links DNA replication to the segregation of homologous chromosomes in meiosis I. *Cell* 135, 662-678.

Maure, J.F., Kitamura, E., and Tanaka, T.U. (2007). Mps1 kinase promotes sister-kinetochore bi-orientation by a tension-dependent mechanism. *Curr Biol* 17, 2175-2182.

Maxfield Boumil, R., Kemp, B., Angelichio, M., Nilsson-Tillgren, T., and Dawson, D.S. (2003). Meiotic segregation of a homeologous chromosome pair. *Mol Genet Genomics* 268, 750-760.

McGuinness, B.E., Anger, M., Kouznetsova, A., Gil-Bernabe, A.M., Helmhart, W., Kudo, N.R., Wuensche, A., Taylor, S., Hoog, C., Novak, B., *et al.* (2009). Regulation of APC/C activity in oocytes by a Bub1-dependent spindle assembly checkpoint. *Curr Biol* 19, 369-380.

McKim, K.S., and Hayashi-Hagihara, A. (1998). mei-W68 in *Drosophila melanogaster* encodes a Spo11 homolog: evidence that the mechanism for initiating meiotic recombination is conserved. *Genes & development* 12, 2932-2942.

- Mendoza, M., Norden, C., Durrer, K., Rauter, H., Uhlmann, F., and Barral, Y. (2009). A mechanism for chromosome segregation sensing by the NoCut checkpoint. *Nature cell biology* 11, 477-483.
- Meuwissen, R.L., Offenberg, H.H., Dietrich, A.J., Riesewijk, A., van Iersel, M., and Heyting, C. (1992). A coiled-coil related protein specific for synapsed regions of meiotic prophase chromosomes. *EMBO J* 11, 5091-5100.
- Michaelis, C., Ciosk, R., and Nasmyth, K. (1997). Cohesins: chromosomal proteins that prevent premature separation of sister chromatids. *Cell* 91, 35-45.
- Milutinovich, M., and Koshland, D.E. (2003). Molecular biology. SMC complexes--wrapped up in controversy. *Science* 300, 1101-1102.
- Mimitou, E.P., and Symington, L.S. (2008). Sae2, Exo1 and Sgs1 collaborate in DNA double-strand break processing. *Nature* 455, 770-774.
- Miyamoto, T., Hasuike, S., Yogev, L., Maduro, M.R., Ishikawa, M., Westphal, H., and Lamb, D.J. (2003). Azoospermia in patients heterozygous for a mutation in SYCP3. *Lancet* 362, 1714-1719.
- Moldovan, G.L., Pfander, B., and Jentsch, S. (2006). PCNA controls establishment of sister chromatid cohesion during S phase. *Molecular cell* 23, 723-732.
- Monje-Casas, F., Prabhu, V.R., Lee, B.H., Boselli, M., and Amon, A. (2007). Kinetochore orientation during meiosis is controlled by Aurora B and the monopolin complex. *Cell* 128, 477-490.
- Myers, S., Bowden, R., Tumian, A., Bontrop, R.E., Freeman, C., Macfie, T.S., McVean, G., and Donnelly, P. (2010) Drive Against Hotspot Motifs in Primates Implicates the PRDM9 Gene in Meiotic Recombination. *Science* 327, 876-879.
- Nasmyth, K. (2005). How do so few control so many? *Cell* 120, 739-746.
- Nayernia, K., Lee, J.H., Lako, M., Armstrong, L., Herbert, M., Li, M., Engel, W., Elliott, D., Stojkovic, M., Parrington, J., *et al.* (2009). In Vitro Derivation of Human Sperm from Embryonic Stem Cells. *Stem Cells Dev.*
- Neale, M.J., Pan, J., and Keeney, S. (2005). Endonucleolytic processing of covalent protein-linked DNA double-strand breaks. *Nature* 436, 1053-1057.
- Newnham, L., Jordan, P., Rockmill, B., Roeder, G.S., and Hoffmann, E. The synaptonemal complex protein, Zip1, promotes the segregation of nonexchange chromosomes at meiosis I. *Proceedings of the National Academy of Sciences of the United States of America* 107, 781-785.
- Nezi, L., Rancati, G., De Antoni, A., Pasqualato, S., Piatti, S., and Musacchio, A. (2006). Accumulation of Mad2-Cdc20 complex during spindle checkpoint activation requires binding of open and closed conformers of Mad2 in *Saccharomyces cerevisiae*. *The Journal of cell biology* 174, 39-51.
- Niu, H., Li, X., Job, E., Park, C., Moazed, D., Gygi, S.P., and Hollingsworth, N.M. (2007). Mek1 kinase is regulated to suppress double-strand break repair between sister chromatids during budding yeast meiosis. *Mol Cell Biol* 27, 5456-5467.
- Niu, H., Wan, L., Busygina, V., Kwon, Y., Allen, J.A., Li, X., Kunz, R.C., Kubota, K., Wang, B., Sung, P., *et al.* (2009). Regulation of meiotic recombination via Mek1-mediated Rad54 phosphorylation. *Molecular cell* 36, 393-404.

Novak, J.E., Ross-Macdonald, P.B., and Roeder, G.S. (2001). The budding yeast Msh4 protein functions in chromosome synapsis and the regulation of crossover distribution. *Genetics* 158, 1013-1025.

Offenberg, H.H., Schalk, J.A., Meuwissen, R.L., van Aalderen, M., Kester, H.A., Dietrich, A.J., and Heyting, C. (1998). SCP2: a major protein component of the axial elements of synaptonemal complexes of the rat. *Nucleic Acids Res* 26, 2572-2579.

Oh, S.D., Lao, J.P., Hwang, P.Y., Taylor, A.F., Smith, G.R., and Hunter, N. (2007). BLM Ortholog, Sgs1, Prevents Aberrant Crossing-over by Suppressing Formation of Multichromatid Joint Molecules. *Cell* 130, 259-272.

Ohta, K., Nicolas, A., Furuse, M., Nabetani, A., Ogawa, H., and Shibata, T. (1998). Mutations in the MRE11, RAD50, XRS2, and MRE2 genes alter chromatin configuration at meiotic DNA double-stranded break sites in premeiotic and meiotic cells. *Proceedings of the National Academy of Sciences of the United States of America* 95, 646-651.

Orr-Weaver, T.L. (1995). Meiosis in *Drosophila*: seeing is believing. *Proceedings of the National Academy of Sciences of the United States of America* 92, 10443-10449.

Page, J., Berrios, S., Rufas, J.S., Parra, M.T., Suja, J.A., Heyting, C., and Fernandez-Donoso, R. (2003). The pairing of X and Y chromosomes during meiotic prophase in the marsupial species *Thylamys elegans* is maintained by a dense plate developed from their axial elements. *J Cell Sci* 116, 551-560.

Page, J., Viera, A., Parra, M.T., de la Fuente, R., Suja, J.A., Prieto, I., Barbero, J.L., Rufas, J.S., Berrios, S., and Fernandez-Donoso, R. (2006). Involvement of synaptonemal complex proteins in sex chromosome segregation during marsupial male meiosis. *PLoS genetics* 2, e136.

Page, S.L., and Hawley, R.S. (2001). c(3)G encodes a *Drosophila* synaptonemal complex protein. *Genes & development* 15, 3130-3143.

Page, S.L., and Hawley, R.S. (2004). The genetics and molecular biology of the synaptonemal complex. *Annual review of cell and developmental biology* 20, 525-558.

Page, S.L., Khetani, R.S., Lake, C.M., Nielsen, R.J., Jeffress, J.K., Warren, W.D., Bickel, S.E., and Hawley, R.S. (2008). Corona is required for higher-order assembly of transverse filaments into full-length synaptonemal complex in *Drosophila* oocytes. *PLoS genetics* 4, e1000194.

Paques, F., and Haber, J.E. (1999). Multiple pathways of recombination induced by double-strand breaks in *Saccharomyces cerevisiae*. *Microbiol Mol Biol Rev* 63, 349-404.

Parra, M.T., Viera, A., Gomez, R., Page, J., Benavente, R., Santos, J.L., Rufas, J.S., and Suja, J.A. (2004). Involvement of the cohesin Rad21 and SCP3 in monopolar attachment of sister kinetochores during mouse meiosis I. *J Cell Sci* 117, 1221-1234.

Parvanov, E.D., Petkov, P.M., and Paigen, K. Prdm9 controls activation of Mammalian recombination hotspots. (2010) *Science* 327, 835.

Penkner, A.M., Fridkin, A., Gloggnitzer, J., Baudrimont, A., Machacek, T., Woglar, A., Csaszar, E., Pasierbek, P., Ammerer, G., Gruenbaum, Y., *et al.* (2009). Meiotic chromosome homology search involves modifications of the nuclear envelope protein Matefin/SUN-1. *Cell* 139, 920-933.

- Pereira, G., Tanaka, T.U., Nasmyth, K., and Schiebel, E. (2001). Modes of spindle pole body inheritance and segregation of the Bfa1p-Bub2p checkpoint protein complex. *Embo J* 20, 6359-6370.
- Perry, J., Kleckner, N., and Borner, G.V. (2005). Bioinformatic analyses implicate the collaborating meiotic crossover/chiasma proteins Zip2, Zip3, and Spo22/Zip4 in ubiquitin labeling. *Proceedings of the National Academy of Sciences of the United States of America* 102, 17594-17599.
- Petronczki, M., Matos, J., Mori, S., Gregan, J., Bogdanova, A., Schwickart, M., Mechtler, K., Shirahige, K., Zachariae, W., and Nasmyth, K. (2006). Monopolar attachment of sister kinetochores at meiosis I requires casein kinase 1. *Cell* 126, 1049-1064.
- Phillips, C.M., and Dernburg, A.F. (2006). A family of zinc-finger proteins is required for chromosome-specific pairing and synapsis during meiosis in *C. elegans*. *Developmental cell* 11, 817-829.
- Pinsky, B.A., Kung, C., Shokat, K.M., and Biggins, S. (2006). The Ipl1-Aurora protein kinase activates the spindle checkpoint by creating unattached kinetochores. *Nature cell biology* 8, 78-83.
- Pradillo, M., Lopez, E., Romero, C., Sanchez-Moran, E., Cunado, N., and Santos, J.L. (2007). An analysis of univalent segregation in meiotic mutants of *Arabidopsis thaliana*: a possible role for synaptonemal complex. *Genetics* 175, 505-511.
- Prieto, I., Suja, J.A., Pezzi, N., Kremer, L., Martinez, A.C., Rufas, J.S., and Barbero, J.L. (2001). Mammalian STAG3 is a cohesin specific to sister chromatid arms in meiosis I. *Nature cell biology* 3, 761-766.
- Prinz, S., Amon, A., and Klein, F. (1997). Isolation of COM1, a new gene required to complete meiotic double-strand break-induced recombination in *Saccharomyces cerevisiae*. *Genetics* 146, 781-795.
- Rabitsch, K.P., Petronczki, M., Javerzat, J.P., Genier, S., Chwalla, B., Schleiffer, A., Tanaka, T.U., and Nasmyth, K. (2003). Kinetochores recruitment of two nucleolar proteins is required for homolog segregation in meiosis I. *Developmental cell* 4, 535-548.
- Rasmussen, S.W. (1977). The transformation of the Synaptonemal Complex into the 'elimination chromatin' in *Bombyx mori* oocytes. *Chromosoma* 60, 205-221.
- Resnick, T.D., Satinover, D.L., MacIsaac, F., Stukenberg, P.T., Earnshaw, W.C., Orr-Weaver, T.L., and Carmena, M. (2006). INCENP and Aurora B promote meiotic sister chromatid cohesion through localization of the Shugoshin MEI-S332 in *Drosophila*. *Developmental cell* 11, 57-68.
- Revenkova, E., Eijpe, M., Heyting, C., Hodges, C.A., Hunt, P.A., Liebe, B., Scherthan, H., and Jessberger, R. (2004). Cohesin SMC1 beta is required for meiotic chromosome dynamics, sister chromatid cohesion and DNA recombination. *Nature cell biology* 6, 555-562.
- Riedel, C.G., Katis, V.L., Katou, Y., Mori, S., Itoh, T., Helmhart, W., Galova, M., Petronczki, M., Gregan, J., Cetin, B., *et al.* (2006). Protein phosphatase 2A protects centromeric sister chromatid cohesion during meiosis I. *Nature* 441, 53-61.
- Rockmill, B., Sym, M., Scherthan, H., and Roeder, G.S. (1995). Roles for two RecA homologs in promoting meiotic chromosome synapsis. *Genes & development* 9, 2684-2695.

Rockmill, B., Voelkel-Meiman, K., and Roeder, G.S. (2006). Centromere-proximal crossovers are associated with precocious separation of sister chromatids during meiosis in *Saccharomyces cerevisiae*. *Genetics* 174, 1745-1754.

Romanienko, P.J., and Camerini-Otero, R.D. (2000). The mouse Spo11 gene is required for meiotic chromosome synapsis. *Molecular cell* 6, 975-987.

Ross-Macdonald, P., and Roeder, G.S. (1994). Mutation of a meiosis-specific MutS homolog decreases crossing over but not mismatch correction. *Cell* 79, 1069-1080.

Ross, L.O., Rankin, S., Shuster, M.F., and Dawson, D.S. (1996). Effects of homology, size and exchange of the meiotic segregation of model chromosomes in *Saccharomyces cerevisiae*. *Genetics* 142, 79-89.

Ruchaud, S., Carmenta, M., and Earnshaw, W.C. (2007). Chromosomal passengers: conducting cell division. *Nature reviews* 8, 798-812.

Sakuno, T., Tada, K., and Watanabe, Y. (2009). Kinetochore geometry defined by cohesion within the centromere. *Nature* 458, 852-858.

Sakuno, T., and Watanabe, Y. (2009). Studies of meiosis disclose distinct roles of cohesion in the core centromere and pericentromeric regions. *Chromosome Res* 17, 239-249.

Sanchez Moran, E., Armstrong, S.J., Santos, J.L., Franklin, F.C., and Jones, G.H. (2001). Chiasma formation in *Arabidopsis thaliana* accession Wassileskija and in two meiotic mutants. *Chromosome Res* 9, 121-128.

Sandall, S., Severin, F., McLeod, I.X., Yates, J.R., 3rd, Oegema, K., Hyman, A., and Desai, A. (2006). A Bir1-Sli15 complex connects centromeres to microtubules and is required to sense kinetochore tension. *Cell* 127, 1179-1191.

Sato, A., Isaac, B., Phillips, C.M., Rillo, R., Carlton, P.M., Wynne, D.J., Kasad, R.A., and Dernburg, A.F. (2009). Cytoskeletal forces span the nuclear envelope to coordinate meiotic chromosome pairing and synapsis. *Cell* 139, 907-919.

Schalk, J.A., Dietrich, A.J., Vink, A.C., Offenberg, H.H., van Aalderen, M., and Heyting, C. (1998). Localization of SCP2 and SCP3 protein molecules within synaptonemal complexes of the rat. *Chromosoma* 107, 540-548.

Schwacha, A., and Kleckner, N. (1997). Interhomolog bias during meiotic recombination: meiotic functions promote a highly differentiated interhomolog-only pathway. *Cell* 90, 1123-1135.

Seol, J.H., Shevchenko, A., Shevchenko, A., and Deshaies, R.J. (2001). Skp1 forms multiple protein complexes, including RAVE, a regulator of V-ATPase assembly. *Nature cell biology* 3, 384-391.

Severson, A.F., Ling, L., van Zuylen, V., and Meyer, B.J. (2009). The axial element protein HTP-3 promotes cohesin loading and meiotic axis assembly in *C. elegans* to implement the meiotic program of chromosome segregation. *Genes & development*. 23, 1763-78.

Shimogawa, M.M., Graczyk, B., Gardner, M.K., Francis, S.E., White, E.A., Ess, M., Molk, J.N., Ruse, C., Niessen, S., Yates, J.R., 3rd, *et al.* (2006). Mps1 phosphorylation of Dam1 couples kinetochores to microtubule plus ends at metaphase. *Curr Biol* 16, 1489-1501.

Shinohara, A., Gasior, S., Ogawa, T., Kleckner, N., and Bishop, D.K. (1997). *Saccharomyces cerevisiae* recA homologues RAD51 and DMC1 have

both distinct and overlapping roles in meiotic recombination. *Genes Cells* 2, 615-629.

Shinohara, A., and Ogawa, T. (1998). Stimulation by Rad52 of yeast Rad51-mediated recombination. *Nature* 391, 404-407.

Shinohara, M., Oh, S.D., Hunter, N., and Shinohara, A. (2008). Crossover assurance and crossover interference are distinctly regulated by the ZMM proteins during yeast meiosis. *Nature genetics*. 40, 299-309.

Shonn, M.A., McCarroll, R., and Murray, A.W. (2000). Requirement of the spindle checkpoint for proper chromosome segregation in budding yeast meiosis. *Science* 289, 300-303.

Shonn, M.A., McCarroll, R., and Murray, A.W. (2002). Spo13 protects meiotic cohesin at centromeres in meiosis I. *Genes & development* 16, 1659-1671.

Shonn, M.A., Murray, A.L., and Murray, A.W. (2003). Spindle checkpoint component Mad2 contributes to biorientation of homologous chromosomes. *Curr Biol* 13, 1979-1984.

Shubochkina, E.A., Nielsen, T.L., and Nilsson-Tillgren, T. (2001). Meiotic crossing-over in the regions of homology between homologous chromosomes V. *Yeast* 18, 1173-1183.

Smith, A.V., and Roeder, G.S. (1997). The yeast Red1 protein localizes to the cores of meiotic chromosomes. *The Journal of cell biology* 136, 957-967.

Snowden, T., Acharya, S., Butz, C., Berardini, M., and Fishel, R. (2004). hMSH4-hMSH5 recognizes Holliday Junctions and forms a meiosis-specific sliding clamp that embraces homologous chromosomes. *Molecular cell* 15, 437-451.

Sourirajan, A., and Lichten, M. (2008). Polo-like kinase Cdc5 drives exit from pachytene during budding yeast meiosis. *Genes & development* 22, 2627-2632.

Stead, K., Aguilar, C., Hartman, T., Drexel, M., Meluh, P., and Guacci, V. (2003). Pds5p regulates the maintenance of sister chromatid cohesion and is sumoylated to promote the dissolution of cohesion. *The Journal of cell biology* 163, 729-741.

Steuerwald, N., Cohen, J., Herrera, R.J., Sandalinas, M., and Brenner, C.A. (2001). Association between spindle assembly checkpoint expression and maternal age in human oocytes. *Mol Hum Reprod* 7, 49-55.

Storlazzi, A., Xu, L., Schwacha, A., and Kleckner, N. (1996). Synaptonemal complex (SC) component Zip1 plays a role in meiotic recombination independent of SC polymerization along the chromosomes. *Proceedings of the National Academy of Sciences of the United States of America* 93, 9043-9048.

Straight, P.D., Giddings, T.H., Jr., and Winey, M. (2000). Mps1p regulates meiotic spindle pole body duplication in addition to having novel roles during sporulation. *Molecular biology of the cell* 11, 3525-3537.

Strom, L., Karlsson, C., Lindroos, H.B., Wedahl, S., Katou, Y., Shirahige, K., and Sjogren, C. (2007). Postreplicative formation of cohesion is required for repair and induced by a single DNA break. *Science* 317, 242-245.

Strom, L., Lindroos, H.B., Shirahige, K., and Sjogren, C. (2004). Postreplicative recruitment of cohesin to double-strand breaks is required for DNA repair. *Mol Cell* 16, 1003-1015.

Sturtevant, A.H., and Beadle, G.W. (1936). The Relations of Inversions in the X Chromosome of *Drosophila Melanogaster* to Crossing over and Disjunction. *Genetics* 21, 554-604.

Sun, F., and Handel, M.A. (2008). Regulation of the meiotic prophase I to metaphase I transition in mouse spermatocytes. *Chromosoma* 117, 471-485.

Sym, M., Engebrecht, J.A., and Roeder, G.S. (1993). ZIP1 is a synaptonemal complex protein required for meiotic chromosome synapsis. *Cell* 72, 365-378.

Szostak, J.W., Orr-Weaver, T.L., Rothstein, R.J., and Stahl, F.W. (1983). The double-strand-break repair model for recombination. *Cell* 33, 25-35.

Tanaka, T.U., Rachidi, N., Janke, C., Pereira, G., Galova, M., Schiebel, E., Stark, M.J., and Nasmyth, K. (2002). Evidence that the Ipl1-Sli15 (Aurora kinase-INCENP) complex promotes chromosome bi-orientation by altering kinetochore-spindle pole connections. *Cell* 108, 317-329.

Tarsounas, M., Pearlman, R.E., Gasser, P.J., Park, M.S., and Moens, P.B. (1997). Protein-protein interactions in the synaptonemal complex. *Molecular biology of the cell* 8, 1405-1414.

Thomas, S.E., Soltani-Bejnood, M., Roth, P., Dorn, R., Logsdon, J.M., Jr., and McKee, B.D. (2005). Identification of two proteins required for conjunction and regular segregation of achiasmate homologs in *Drosophila* male meiosis. *Cell* 123, 555-568.

Tinker-Kulberg, R.L., and Morgan, D.O. (1999). Pds1 and Esp1 control both anaphase and mitotic exit in normal cells and after DNA damage. *Genes & development* 13, 1936-1949.

Tomkiel, J.E., Wakimoto, B.T., and Briscoe, A., Jr. (2001). The teflon gene is required for maintenance of autosomal homolog pairing at meiosis I in male *Drosophila melanogaster*. *Genetics* 157, 273-281.

Toth, A., Ciosk, R., Uhlmann, F., Galova, M., Schleiffer, A., and Nasmyth, K. (1999). Yeast cohesin complex requires a conserved protein, Eco1p(Ctf7), to establish cohesion between sister chromatids during DNA replication. *Genes & development* 13, 320-333.

Toth, A., Rabitsch, K.P., Galova, M., Schleiffer, A., Buonomo, S.B., and Nasmyth, K. (2000). Functional genomics identifies monopolin: a kinetochore protein required for segregation of homologs during meiosis I. *Cell* 103, 1155-1168.

Tsubouchi, H., and Ogawa, H. (1998). A novel mre11 mutation impairs processing of double-strand breaks of DNA during both mitosis and meiosis. *Mol Cell Biol* 18, 260-268.

Tsubouchi, H., and Ogawa, H. (2000). Exo1 roles for repair of DNA double-strand breaks and meiotic crossing over in *Saccharomyces cerevisiae*. *Molecular biology of the cell* 11, 2221-2233.

Tsubouchi, H., and Roeder, G.S. (2002). The Mnd1 protein forms a complex with hop2 to promote homologous chromosome pairing and meiotic double-strand break repair. *Mol Cell Biol* 22, 3078-3088.

Tsubouchi, T., Macqueen, A.J., and Roeder, G.S. (2008). Initiation of meiotic chromosome synapsis at centromeres in budding yeast. *Genes & development* 22, 3217-3226.

Tsubouchi, T., and Roeder, G.S. (2005). A synaptonemal complex protein promotes homology-independent centromere coupling. *Science* 308, 870-873.

- Tsubouchi, T., Zhao, H., and Roeder, G.S. (2006). The meiosis-specific zip4 protein regulates crossover distribution by promoting synaptonemal complex formation together with zip2. *Developmental cell* 10, 809-819.
- Tung, K.S., and Roeder, G.S. (1998). Meiotic chromosome morphology and behavior in zip1 mutants of *Saccharomyces cerevisiae*. *Genetics* 149, 817-832.
- Uetz, P., Giot, L., Cagney, G., Mansfield, T.A., Judson, R.S., Knight, J.R., Lockshon, D., Narayan, V., Srinivasan, M., Pochart, P., *et al.* (2000). A comprehensive analysis of protein-protein interactions in *Saccharomyces cerevisiae*. *Nature* 403, 623-627.
- Uhlmann, F., and Nasmyth, K. (1998). Cohesion between sister chromatids must be established during DNA replication. *Curr Biol* 8, 1095-1101.
- Uhlmann, F., Wernic, D., Poupard, M.A., Koonin, E.V., and Nasmyth, K. (2000). Cleavage of cohesin by the CD clan protease separin triggers anaphase in yeast. *Cell* 103, 375-386.
- Usui, T., Ohta, T., Oshiumi, H., Tomizawa, J., Ogawa, H., and Ogawa, T. (1998). Complex formation and functional versatility of Mre11 of budding yeast in recombination. *Cell* 95, 705-716.
- Vazquez, J., Belmont, A.S., and Sedat, J.W. (2002). The dynamics of homologous chromosome pairing during male *Drosophila* meiosis. *Curr Biol* 12, 1473-1483.
- Wan, L., Niu, H., Fitcher, B., Zhang, C., Shokat, K.M., Boulton, S.J., and Hollingsworth, N.M. (2008). Cdc28-Clb5 (CDK-S) and Cdc7-Dbf4 (DDK) collaborate to initiate meiotic recombination in yeast. *Genes & development* 22, 386-397.
- Wanat, J.J., Kim, K.P., Koszul, R., Zanders, S., Weiner, B., Kleckner, N., and Alani, E. (2008). Csm4, in collaboration with Ndj1, mediates telomere-led chromosome dynamics and recombination during yeast meiosis. *PLoS genetics* 4, e1000188.
- Wang, T.F., Kleckner, N., and Hunter, N. (1999). Functional specificity of MutL homologs in yeast: evidence for three Mlh1-based heterocomplexes with distinct roles during meiosis in recombination and mismatch correction. *Proceedings of the National Academy of Sciences of the United States of America* 96, 13914-13919.
- Wassmann, K., Niaux, T., and Maro, B. (2003). Metaphase I arrest upon activation of the Mad2-dependent spindle checkpoint in mouse oocytes. *Curr Biol* 13, 1596-1608.
- Webber, H.A., Howard, L., and Bickel, S.E. (2004). The cohesion protein ORD is required for homologue bias during meiotic recombination. *The Journal of cell biology* 164, 819-829.
- Winey, M., Mamay, C.L., O'Toole, E.T., Mastroratte, D.N., Giddings, T.H., Jr., McDonald, K.L., and McIntosh, J.R. (1995). Three-dimensional ultrastructural analysis of the *Saccharomyces cerevisiae* mitotic spindle. *The Journal of cell biology* 129, 1601-1615.
- Winkel, K., Alsheimer, M., Ollinger, R., and Benavente, R. (2008). Protein SYCP2 provides a link between transverse filaments and lateral elements of mammalian synaptonemal complexes. *Chromosoma* 118, 259-67.
- Wojtasz, L., Daniel, K., Roig, I., Bolcun-Filas, E., Xu, H., Boonsanay, V., Eckmann, C.R., Cooke, H.J., Jasin, M., Keeney, S., *et al.* (2009). Mouse HORMAD1 and HORMAD2, two conserved meiotic chromosomal proteins, are

depleted from synapsed chromosome axes with the help of TRIP13 AAA-ATPase. *PLoS genetics* 5, e1000702.

Wolf, K.W. (1994). How meiotic cells deal with non-exchange chromosomes. *Bioessays* 16, 107-114.

Woltering, D., Baumgartner, B., Bagchi, S., Larkin, B., Loidl, J., de los Santos, T., and Hollingsworth, N.M. (2000). Meiotic segregation, synapsis, and recombination checkpoint functions require physical interaction between the chromosomal proteins Red1p and Hop1p. *Mol Cell Biol* 20, 6646-6658.

Wu, H.Y., and Burgess, S.M. (2006). Two distinct surveillance mechanisms monitor meiotic chromosome metabolism in budding yeast. *Curr Biol* 16, 2473-2479.

Wu, T.C., and Lichten, M. (1994). Meiosis-induced double-strand break sites determined by yeast chromatin structure. *Science* 263, 515-518.

Xu, H., Beasley, M.D., Warren, W.D., van der Horst, G.T., and McKay, M.J. (2005). Absence of mouse REC8 cohesin promotes synapsis of sister chromatids in meiosis. *Developmental cell* 8, 949-961.

Xu, L., Ajimura, M., Padmore, R., Klein, C., and Kleckner, N. (1995). NDT80, a meiosis-specific gene required for exit from pachytene in *Saccharomyces cerevisiae*. *Mol Cell Biol* 15, 6572-6581.

Yoo, S., and McKee, B.D. (2005). Functional analysis of the *Drosophila* Rad51 gene (*spn-A*) in repair of DNA damage and meiotic chromosome segregation. *DNA Repair (Amst)* 4, 231-242.

Yu, H.G., and Koshland, D. (2005). Chromosome morphogenesis: condensin-dependent cohesin removal during meiosis. *Cell* 123, 397-407.

Yu, H.G., and Koshland, D. (2007). The Aurora kinase Ipl1 maintains the centromeric localization of PP2A to protect cohesin during meiosis. *The Journal of cell biology* 176, 911-918.

Yuan, L., Liu, J.G., Hoja, M.R., Wilbertz, J., Nordqvist, K., and Hoog, C. (2002). Female germ cell aneuploidy and embryo death in mice lacking the meiosis-specific protein SCP3. *Science* 296, 1115-1118.

Yuan, L., Liu, J.G., Zhao, J., Brundell, E., Daneholt, B., and Hoog, C. (2000). The murine SCP3 gene is required for synaptonemal complex assembly, chromosome synapsis, and male fertility. *Molecular cell* 5, 73-83.

Zachariae, W., and Nasmyth, K. (1999). Whose end is destruction: cell division and the anaphase-promoting complex. *Genes & development* 13, 2039-2058.

Zetka, M.C., Kawasaki, I., Strome, S., and Muller, F. (1999). Synapsis and chiasma formation in *Caenorhabditis elegans* require HIM-3, a meiotic chromosome core component that functions in chromosome segregation. *Genes & development* 13, 2258-2270.

Zhao, X., and Blobel, G. (2005). A SUMO ligase is part of a nuclear multiprotein complex that affects DNA repair and chromosomal organization. *Proceedings of the National Academy of Sciences of the United States of America* 102, 4777-4782.

Zickler, D., and Kleckner, N. (1998). The leptotene-zygotene transition of meiosis. *Annual review of genetics* 32, 619-697.

Zickler, D., Moreau, P.J., Huynh, A.D., and Slezec, A.M. (1992). Correlation between pairing initiation sites, recombination nodules and meiotic recombination in *Sordaria macrospora*. *Genetics* 132, 135-148.

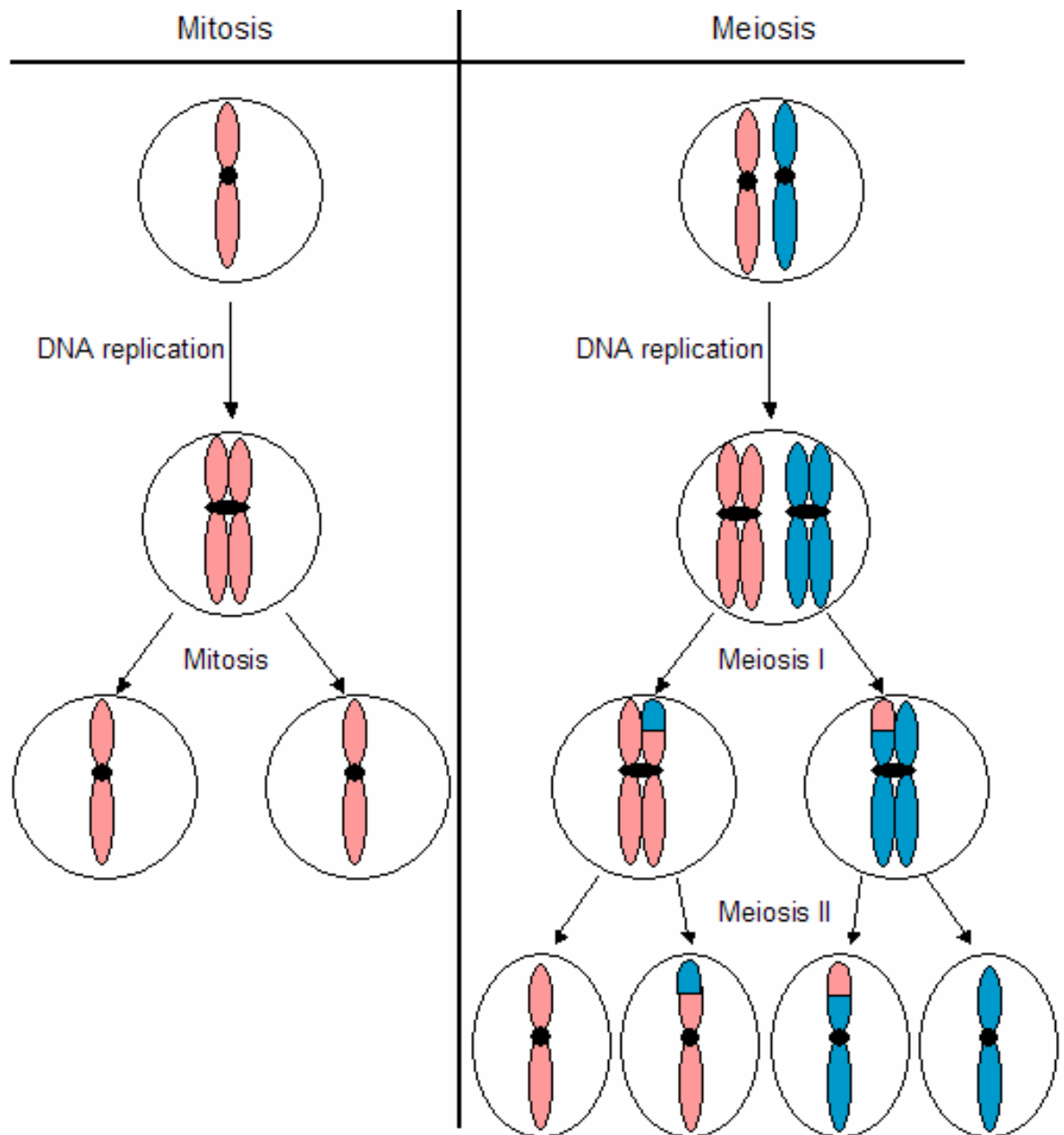


**Figure 1.1.** Diagram outlining the differences between mitotic and meiotic cell divisions. The mitotic cell division (left) involves DNA replication that generates sister chromatids, followed by a single cell division in which sister chromatids are partitioned to opposing daughter cells. A single chromosome is shown for clarity. The products of mitotic divisions are two daughter cells that are genetically identical to the original parent cell. The meiotic division (right) involves a single round of DNA replication, followed by two successive cell divisions. The first meiotic division segregates homologous chromosomes to opposite daughter cells ('reductional' division), whereas the second meiotic division is more like a mitotic division in which sister chromatids are segregated to opposite daughter cells ('equational' division). A single pair of homologous chromosomes is shown for clarity. The end product of a meiotic division is four daughter cells with half the number of chromosomes as the original parent cell.

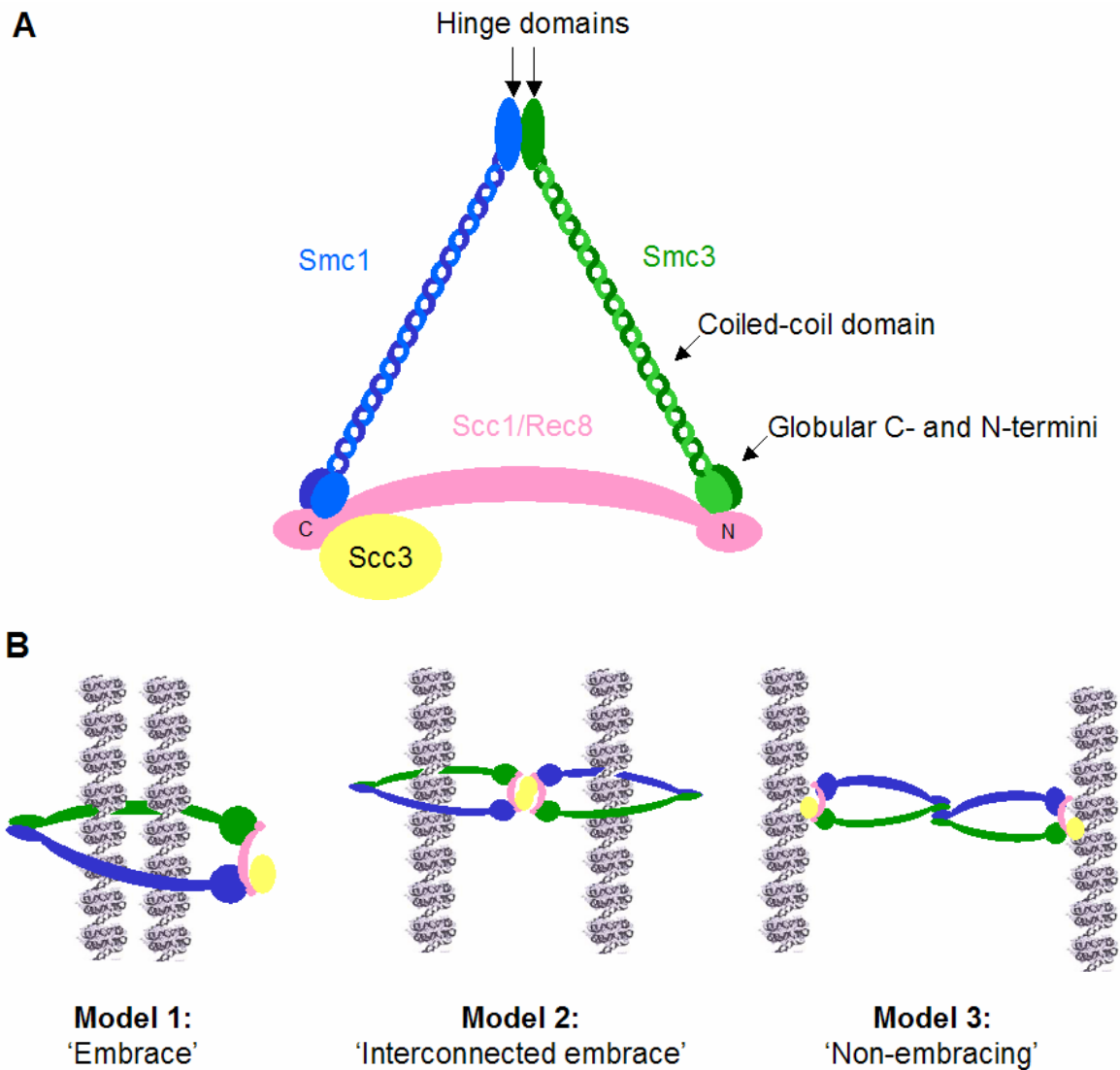


**Figure 1.2.** Proposed structure of the cohesin complex and models for how cohesin may mediate sister chromatid cohesion. (A) Smc1 and Smc3 contain two coiled-coil domains with an intervening 'hinge' domain. They are believed to fold back on themselves through the hinge domain to form intra-molecular coiled-coils, uniting the globular N- and C-termini into a putative ABC (ATP binding cassette) ATPase domain. Smc1 and Smc3 interact through their hinge domains. The globular 'heads' of Smc1 and Smc3 are connected by the kleisin subunit Scc1 or Rec8 in meiotic cells and Scc3 is thought to interact with the C-terminus of these proteins. The cohesin complex forms a ring-like structure, ~40 nm in diameter. (B) There are three main models for how cohesin may mediate sister chromatid cohesion. The most common of these is the 'embrace' model in which cohesin rings entrap both sister chromatids only allowing them to be liberated when the kleisin subunit is cleaved at anaphase (Model 1, Ivanov and Nasmyth 2005). An alternative possibility is the 'inter-connected embrace' model where cohesin rings entrap each sister chromatid and then interact with each other, thus mediating cohesion of the sister chromatids (Model 2, Chang 2005). The final model suggests that cohesin rings do not encircle the DNA at all ('non-embracing') and instead bind the DNA and interact with another cohesin molecule that is bound to the opposing sister chromatid (Huang 2005).

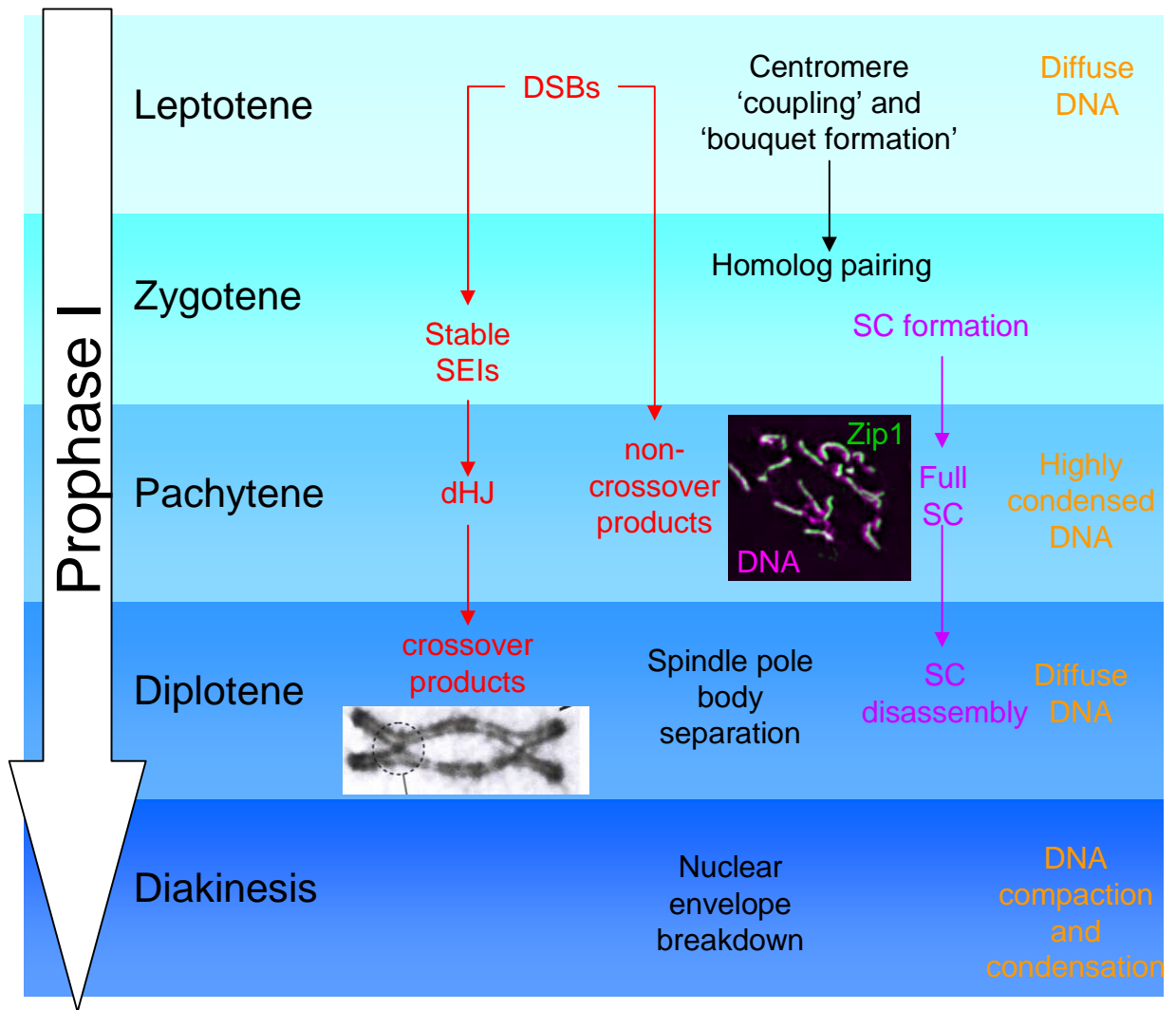


**Figure 1.3.** Stages of meiotic prophase I. The intermediates in the recombination pathway are given in red text. DSB: double-stranded break, SEI: single-end invasion, dHJ: double Holliday junction. The picture below 'crossover products' is of two chiasmata (one is circled) present upon a single bivalent from grasshopper spermatocytes (courtesy of Dr. Jasna Puizina, in Petronczki *et al.* 2003). Chromosomal interactions are shown in black text, pairing of homologous chromosomes is preceded by 'centromere coupling' and 'bouquet formation' in budding yeast. Synaptonemal Complex (SC) formation initiates in early zygotene and is complete by pachytene with homologous chromosomes connected lengthways by the central element of the SC. Image to the left of 'Full SC' is of a spread *S. cerevisiae* nucleus in pachytene with linear Zip1 (green) and condensed DNA (magenta). DNA condensation status is shown in orange text on the far right.

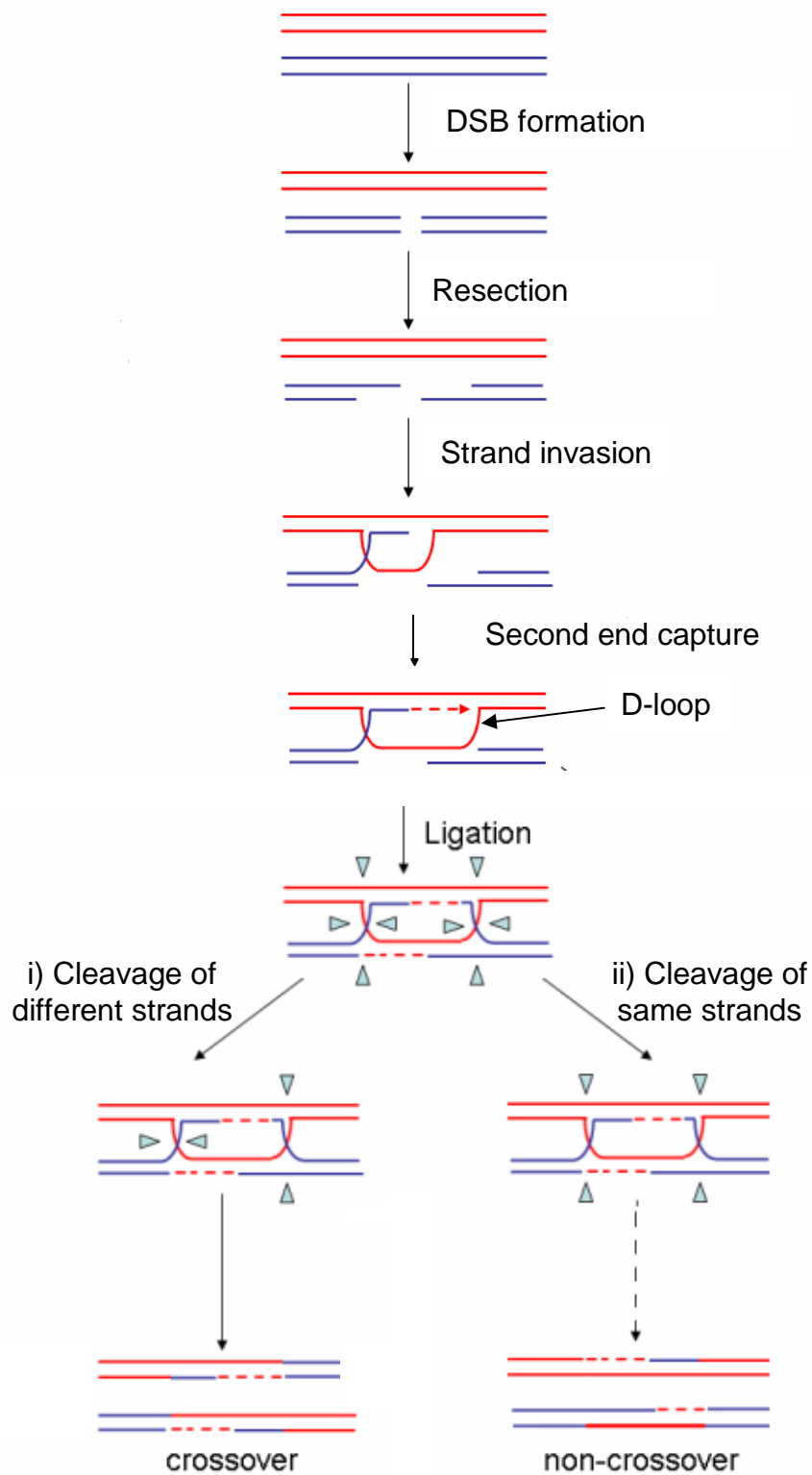
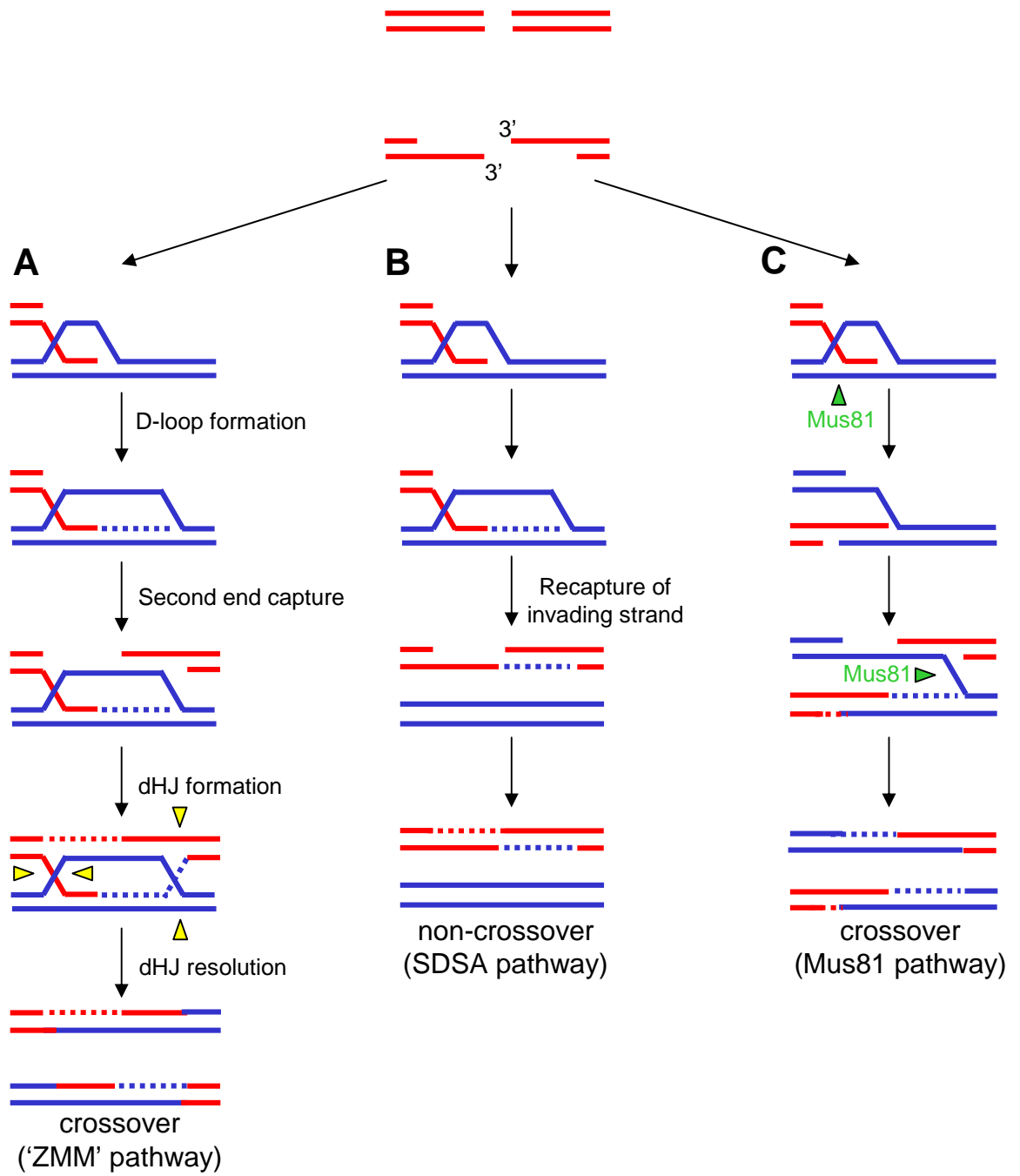


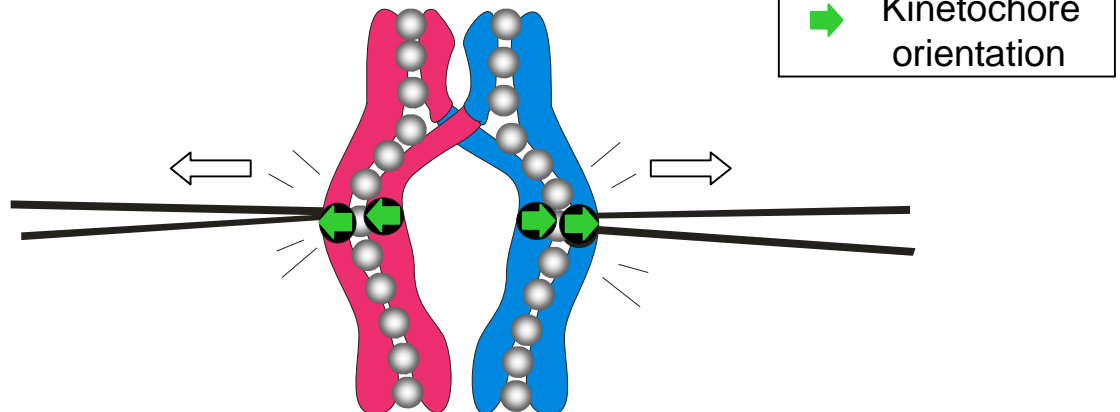
**Figure 1.4.** Original DNA double-strand break repair model. The model, first proposed by Szostak *et al.* 1983 proposes that crossovers and non-crossovers are generated by cleavage of opposing strands and the same strands of double Holliday junction, respectively. Experimental evidence now suggests that stable single-end invasions and double Holliday junctions are specific intermediates in the crossover pathway, whereas non-crossovers are generated through an independent pathway not involving these intermediates. See text for details of individual steps.

**Figure 1.5.** Pathways of meiotic DSB repair in *Saccharomyces cerevisiae*.

Following DSB formation (top, red lines) single stranded resection generates 3' overhangs that then invade a homologous DNA duplex (blue lines). This intermediate then has three possible fates. (A) Crossovers can be generated from the canonical DSB repair model proposed by Szostak *et al.* (1983). This is the 'ZMM'-dependent crossover pathway. The single end invasion (SEI) intermediate is promoted and stabilised by the Mer3 helicase and Msh4-Msh5 heterodimer, respectively. The invading 3' end primes DNA synthesis using the intact DNA duplex as a template, which through the formation of a 'Displacement loop' (D-loop) allows second end capture and repair synthesis of the other 3' end (dotted lines indicate new synthesis). Ligation of the newly synthesised strands to the resected 5' ends yields a double Holliday junction (dHJ) that through cleavage of opposing strands of the Holliday junction, generates crossovers. This may be carried out by the HJ resolvase Yen1. (B) The synthesis-dependent strand annealing (SDSA) pathway (middle) gives rise to non-crossovers with only a transient SEI intermediate (Hunter and Kleckner 2001). This differs from the DSB repair pathway in that second end capture does not occur and rather, following repair synthesis of the invading strand it is recaptured by the second end, which can then be repaired to yield non-crossovers. (C) The third pathway is dependent upon the endonuclease activity of Mus81/Mms4 which nicks branched DNA structures to generate crossovers without a dHJ intermediate. Red lines represent two DNA strands of one chromatid and blue lines represent DNA strands of a sister chromatid belonging to a homologous chromosome. Only a single chromatid for each chromosome is shown for clarity, but each chromosome actually consists of two sister chromatids at this stage. Diagram adapted from Whitby, M. C. (2005). "Making crossovers during meiosis." *Biochem Soc Trans* **33** (Pt 6): 1451-5.



**A** Reductional division:



**B** Equational division:

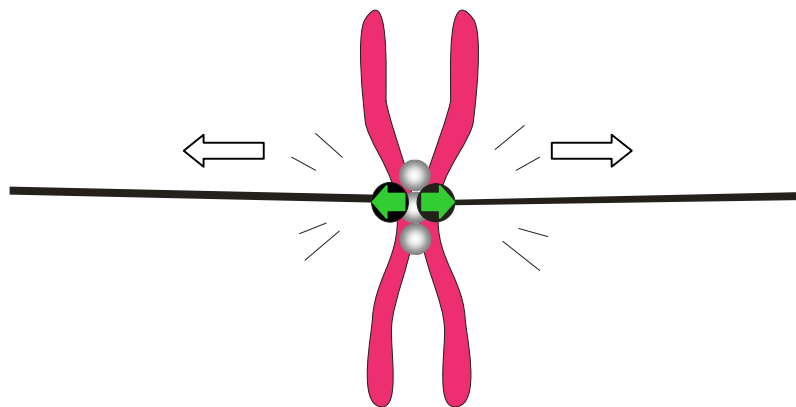
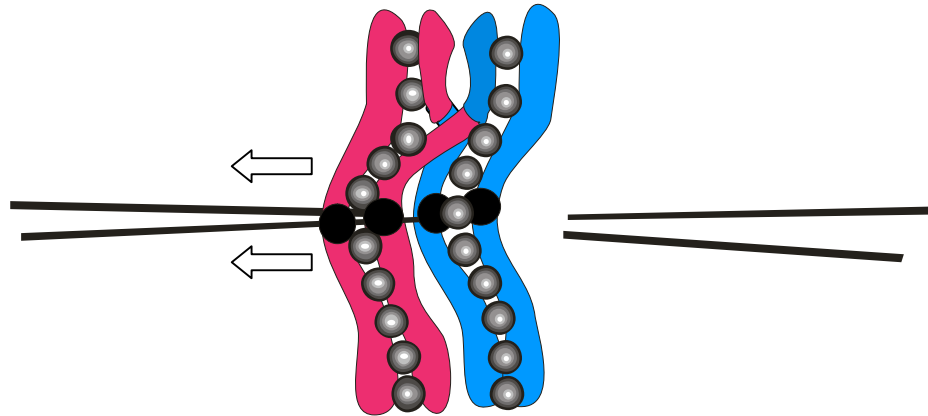


**Figure 1.6.** Sister kinetochore orientation in the first and second meiotic division. (A) During the first meiotic division, sister kinetochores must be attached to microtubules emanating from the same spindle pole (mono-orientation) in order for homologs to segregate. (B) During the second meiotic division, sister kinetochores must face in opposite directions to attach to microtubules emanating from opposite spindle poles. This is required to ensure sister chromatids segregate at meiosis II instead of meiosis I. Arrows indicate the pulling forces of the spindle. In *S. cerevisiae* each kinetochore binds a single microtubule (Winey *et al.* 1995)

**A** No tension (mono-orientation):

● Cohesin



**B** Tension (bi-orientation):

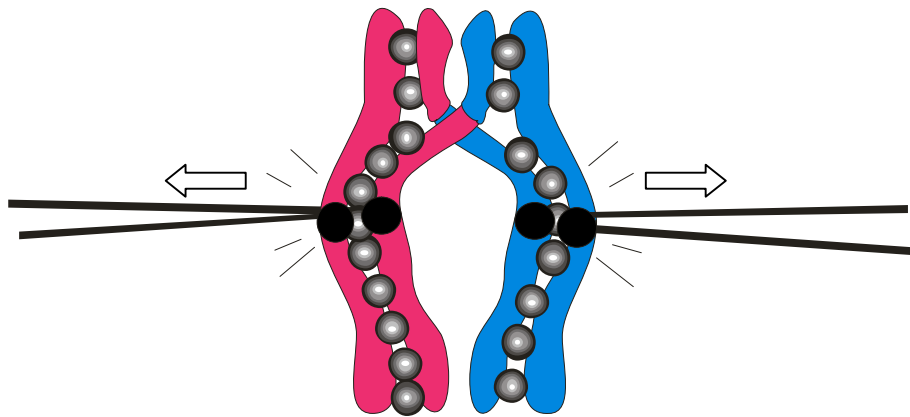
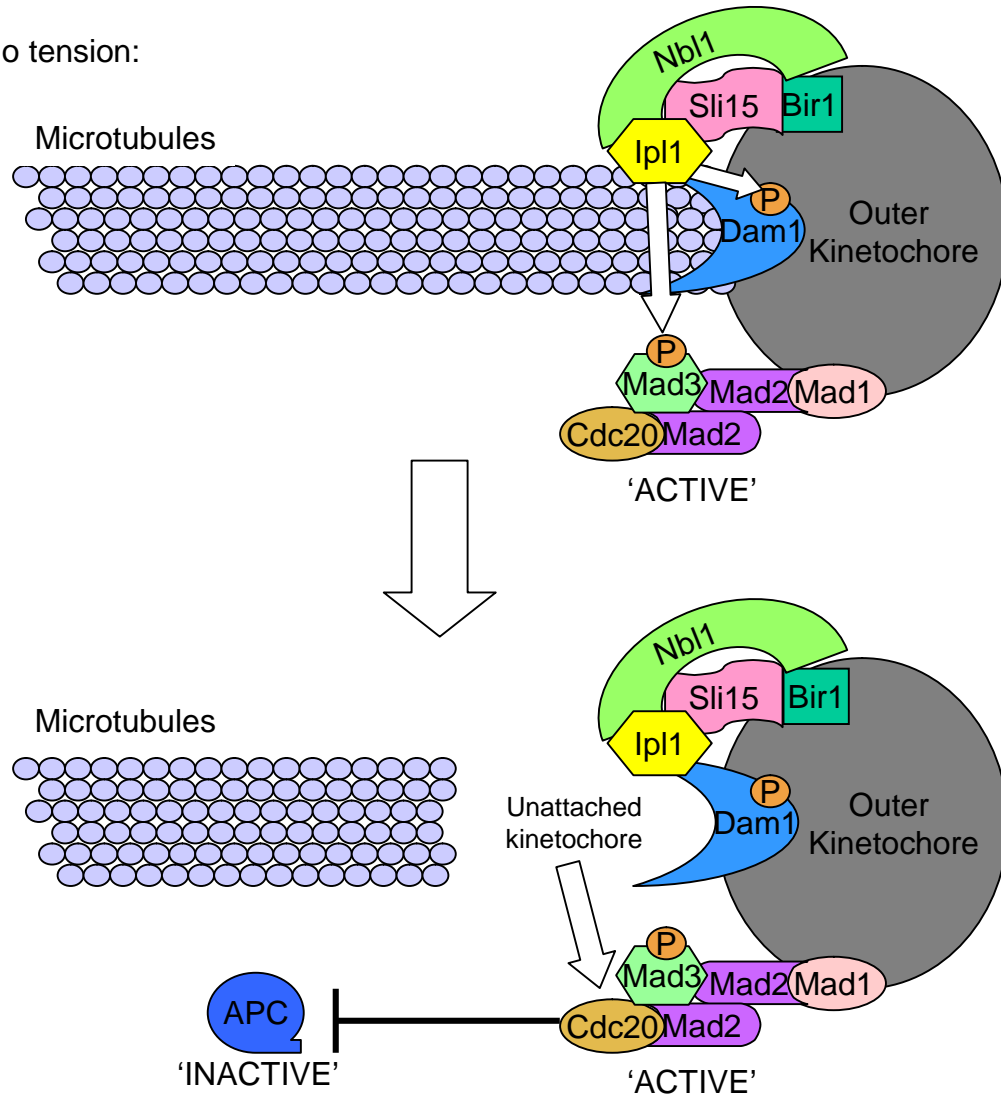


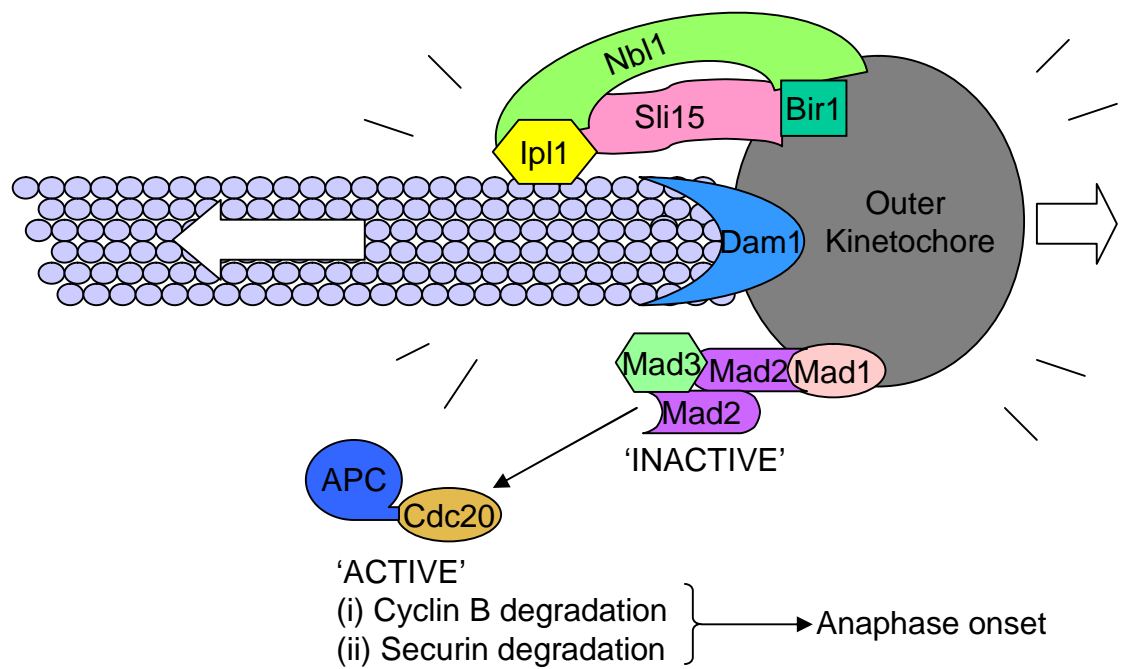
**Figure 1.7.** Homolog bi-orientation generates kinetochore-microtubule tension. (A) When homologs attach to microtubules emanating from the same spindle pole, no spindle tension is generated. However, when they attach to microtubules from opposite spindle poles as shown in (B), the cohesin distal to the crossover site antagonises the opposing pulling forces of the spindle and so generates spindle tension. This spindle tension is necessary to silence the spindle checkpoint.

**Figure 1.8.** Diagram outlining how the chromosomal passenger proteins regulate the spindle checkpoint in response to spindle tension. Microtubules are shown as small grey circles and the outer kinetochore is depicted by the large grey oval. The chromosomal passenger proteins (Aurora B kinase: Ipl1, INCENP: Sli15, Survivin: Bir1 and Borealin: Nbl1). (A) In the absence of spindle tension, Ipl1/Aurora B kinase phosphorylates the kinetochore protein Dam1 (Cheeseman *et al.* 2002) and the spindle checkpoint protein Mad3 (King *et al.* 2007). Phosphorylation of Dam1 severs kinetochore-microtubule attachments generating unattached kinetochores that activate the spindle checkpoint allowing the kinetochores a chance to reattempt spindle attachment. Phosphorylation of Mad3 directly activates the spindle checkpoint. When the spindle checkpoint is 'active' Mad2 is bound to the APC activator, Cdc20, keeping the APC inactive and blocking the onset of anaphase. Mad2 is known to dimerise (Mapelli *et al.* 2006) and exist in 'open' and 'closed' conformations when unbound and bound to Cdc20, respectively (Nezi *et al.* 2006). Mad2 also physically interacts with Mad1 and Mad3 (King *et al.* 2007; Nezi *et al.* 2006). (B) In the presence of spindle tension, the chromosomal passenger complex is believed to undergo conformational changes that either render Ipl1/Aurora B kinase inactive, or sequester it away from its target proteins. This prevents the spindle checkpoint from being active, resulting in a conformational change in Mad2 that liberates Cdc20. Cdc20, together with the APC can then trigger anaphase onset. The configuration of the chromosomal passenger proteins is based on Model proposed by Sandall *et al.* 2006.

**A** No tension:



**B** Tension:



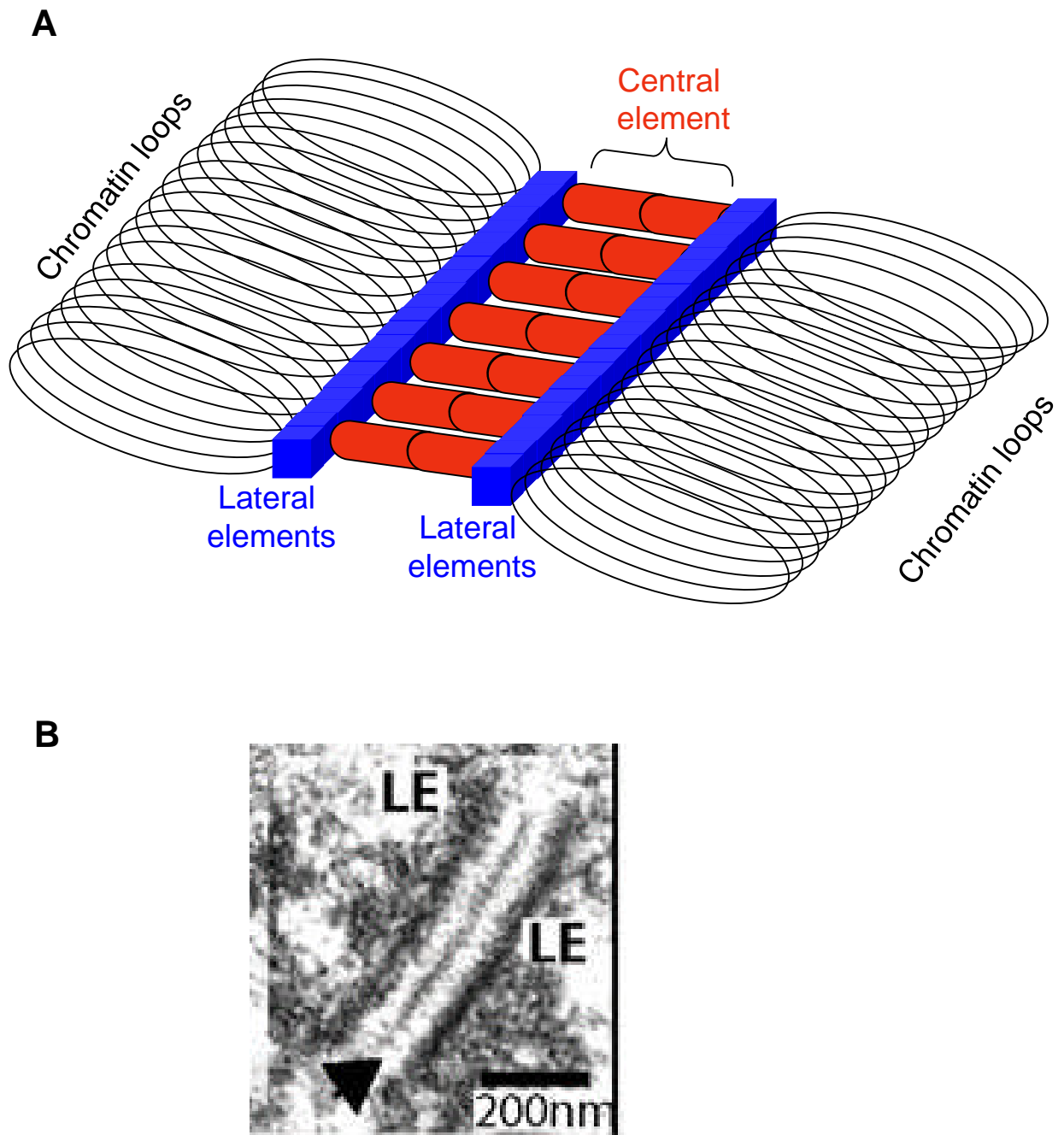


**Figure 1.9.** The structure of the Synaptonemal Complex. (A) Schematic representation of the Synaptonemal Complex. Chromatin belonging to two sister chromatids is looped onto a common axis so that each chromosome contains a single axis. The axes of homologous chromosomes are connected by the central element that traverses the gap between adjacent axes. The axes that are initially referred to as ‘axial elements’ mature into ‘lateral elements’ (blue) following the deposition of the central element (red). Central element proteins lie perpendicular to the lateral elements forming a zip-like structure between the lateral elements of homologous chromosomes. (B) Electron micrograph of the SC in wild-type mouse spermatocytes from Bolcun-Filas *et al.* 2009. The dense-staining lateral elements (LE) are connected along their lengths at a constant distance (~100-150 nm) by the central element as shown by the electron-dense region between the two axes (Arrow).

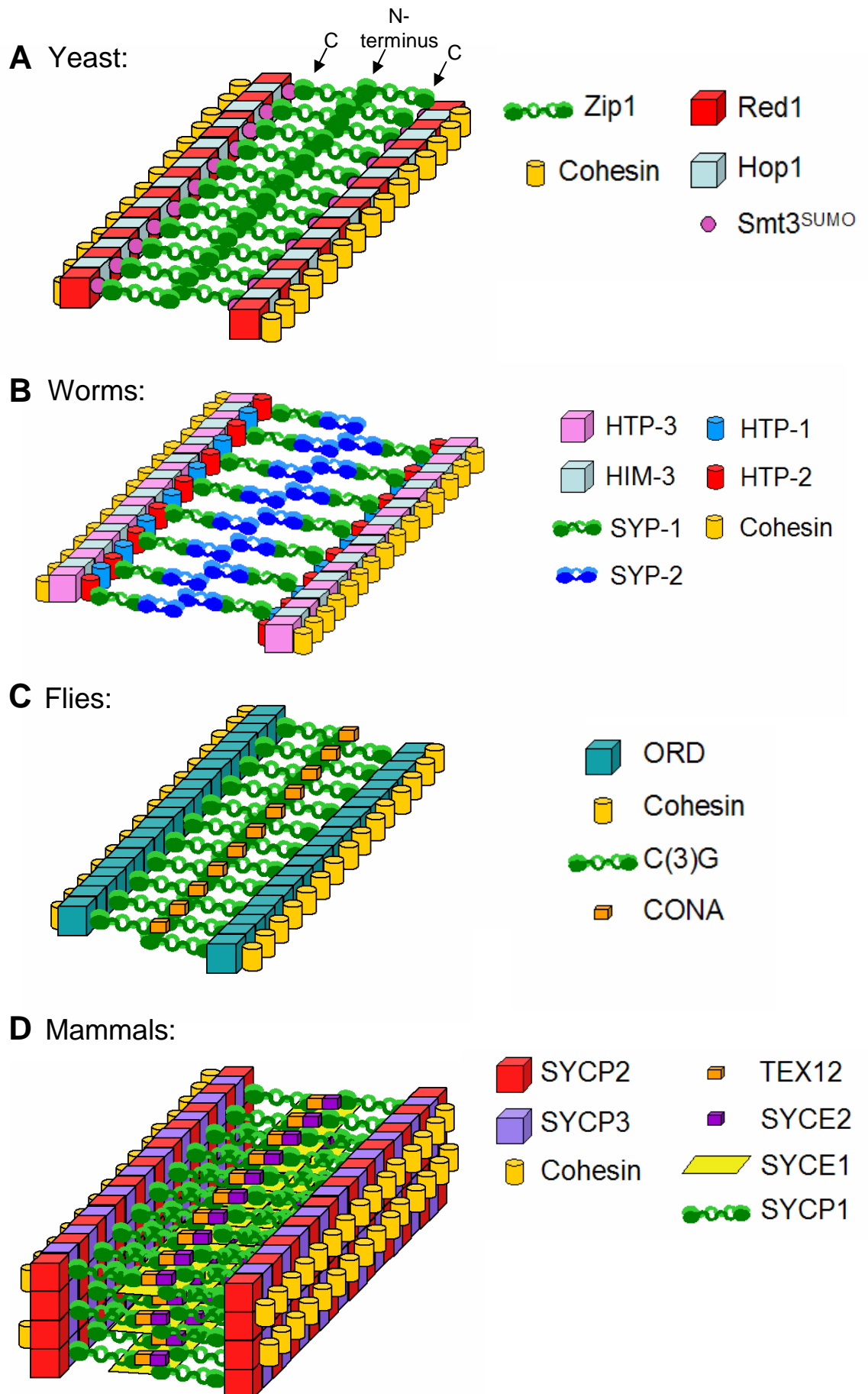
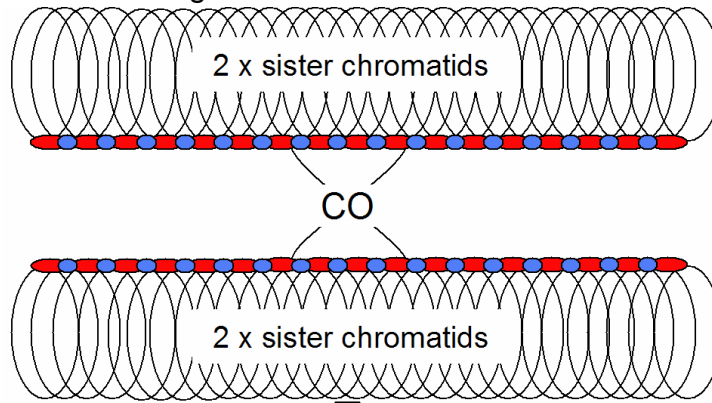


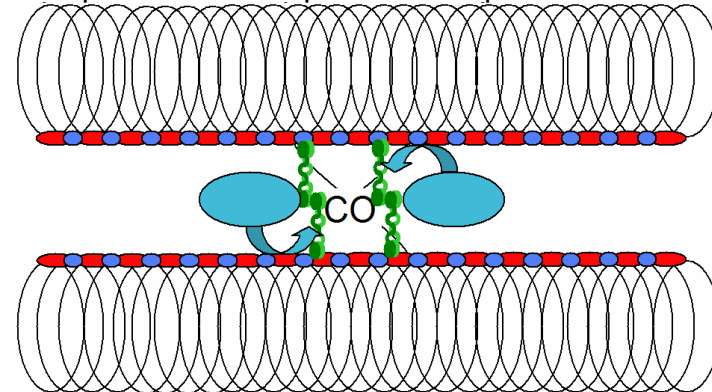
**Figure 1.10.** Structural models of the synaptonemal complex in yeast (*Saccharomyces cerevisiae*), worms (*Caenorhabditis elegans*), flies (*Drosophila melanogaster*) and mammals (*Mus musculus*). See text for details.

**Figure 1.11.** Model for the initiation of SC formation by the ‘ZMM’s. In the first step, a DSB is designated to become a crossover (CO). Then Zip3 mediates the deposition of Zip1 at the crossover-designated site. This recruits the ‘DNA transaction’ proteins Msh4-Msh5 and Mer3 as well as the SC extension proteins, Zip2-Zip4-Spo16 that polymerise Zip1 outwards from the synapsis initiation site. Concomitant with SC extension is the promotion of ZMM-dependent crossover formation. A key showing the different proteins is shown on the right. Model based on that of Shinohara *et al.* (2008).

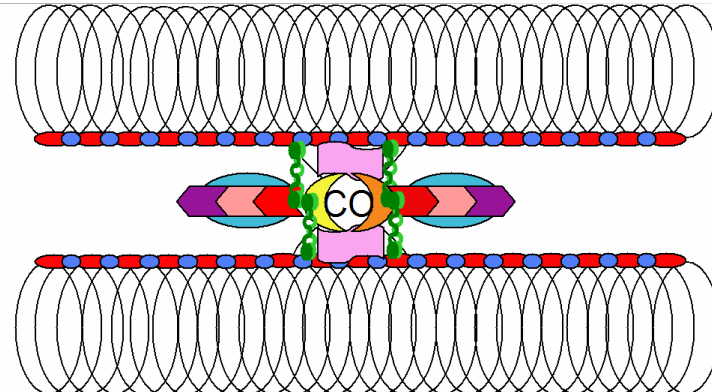
**Step 1: DSB designated to become crossover**



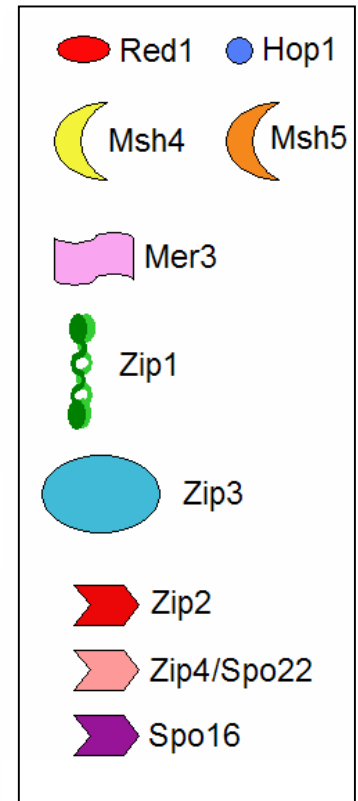
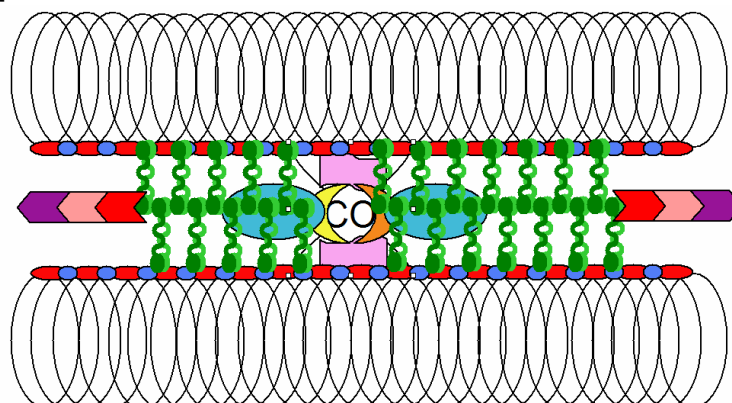
**Step 2: Zip3-mediated deposition of Zip1**

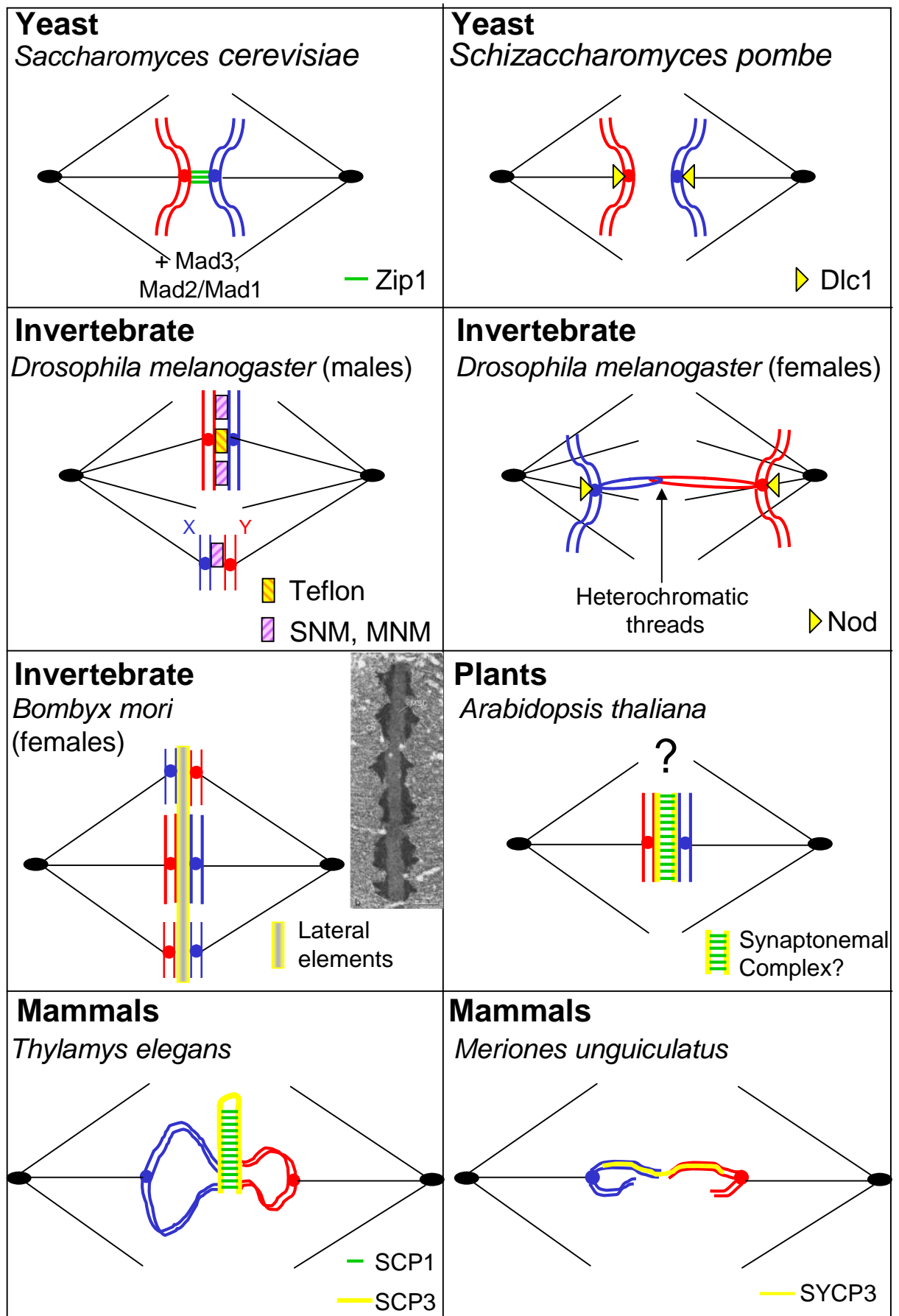


**Step 3: Recruitment of DNA transaction and SC extension proteins**



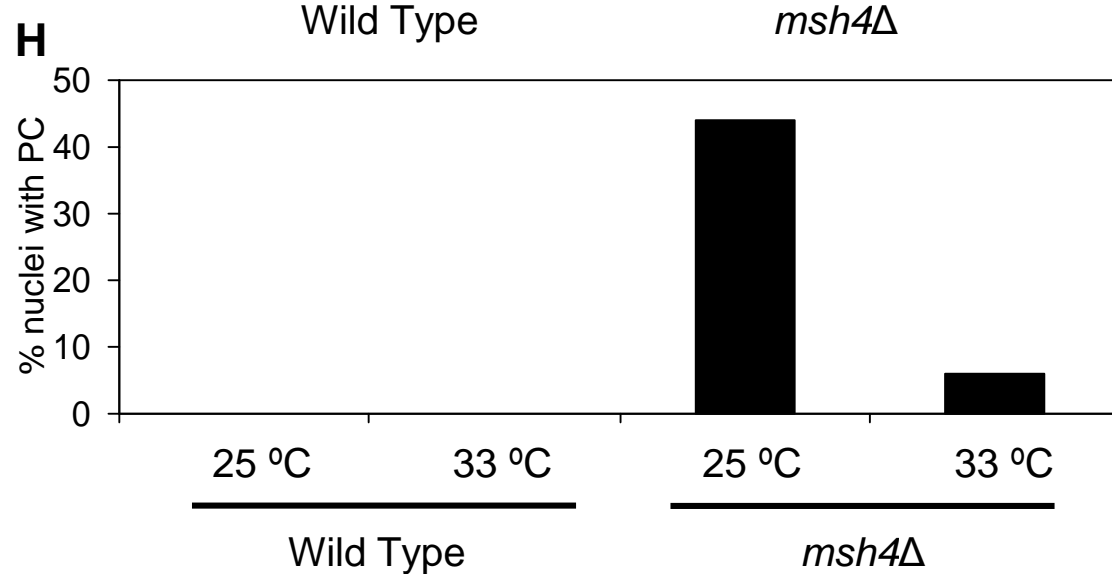
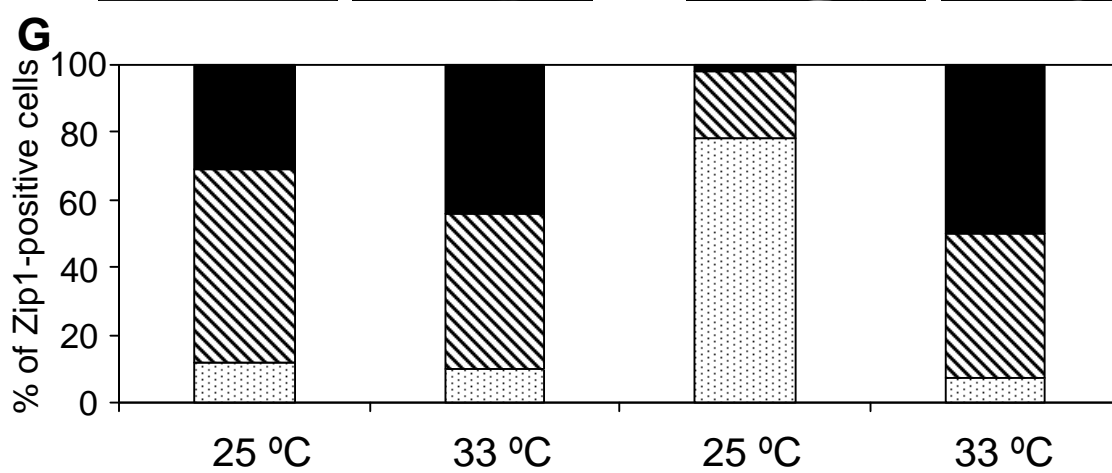
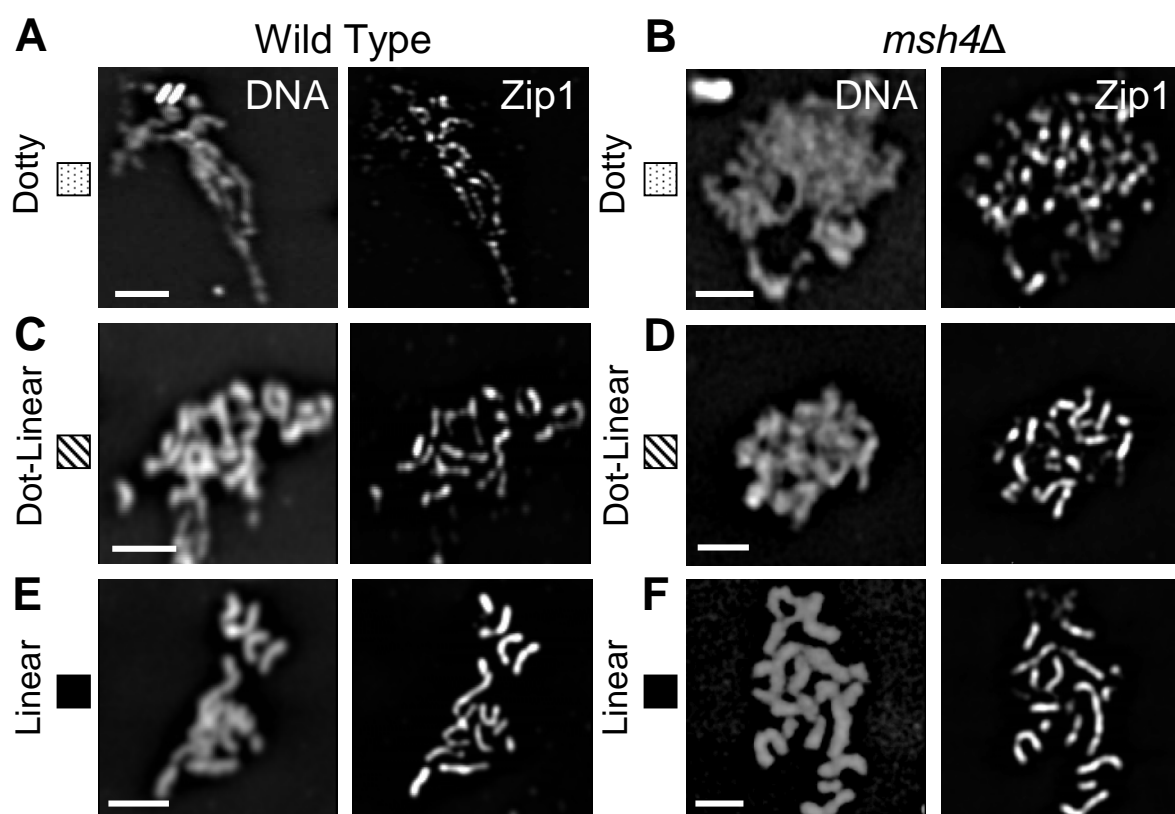
**Step 4: Bidirectional SC extension**



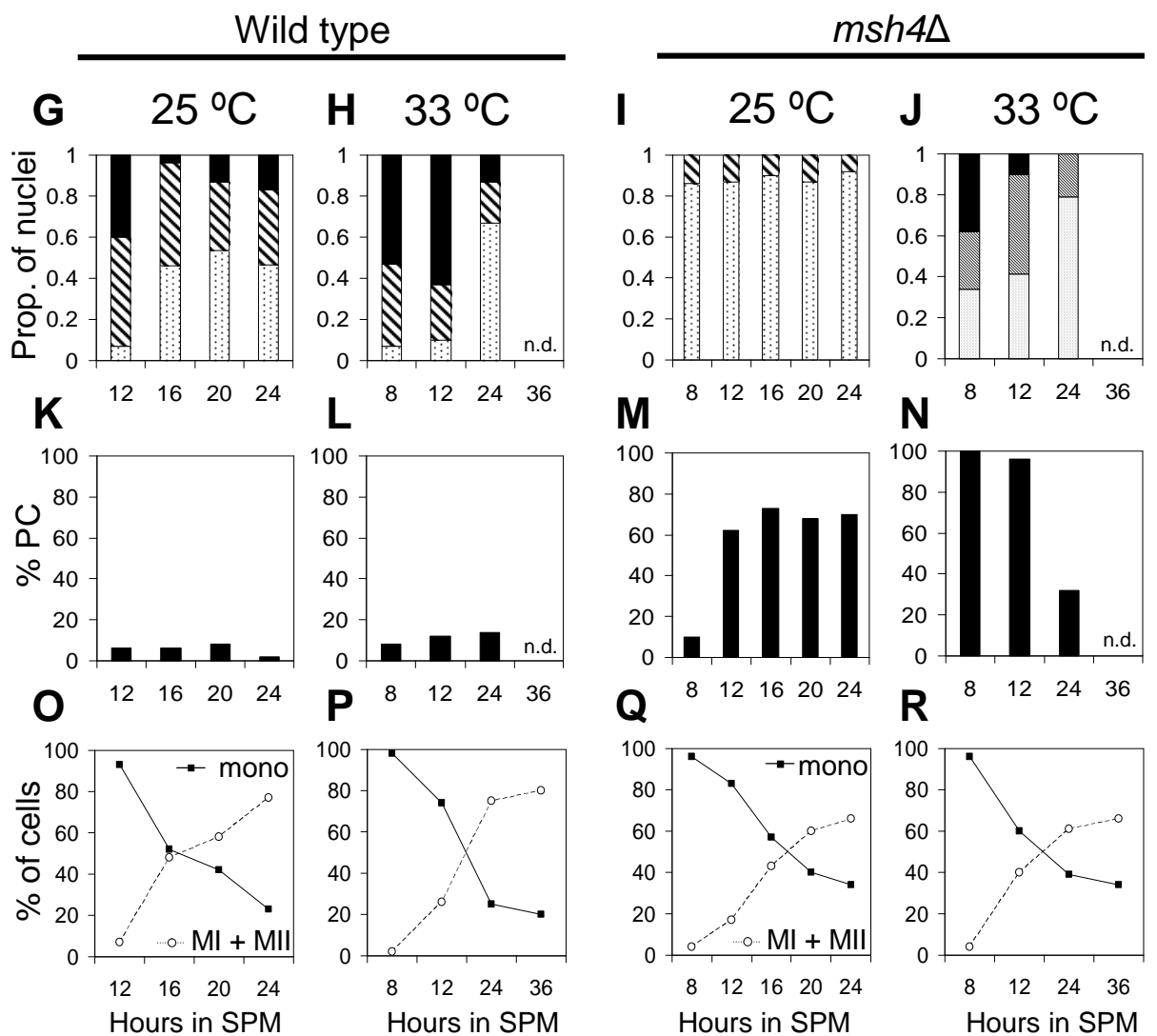
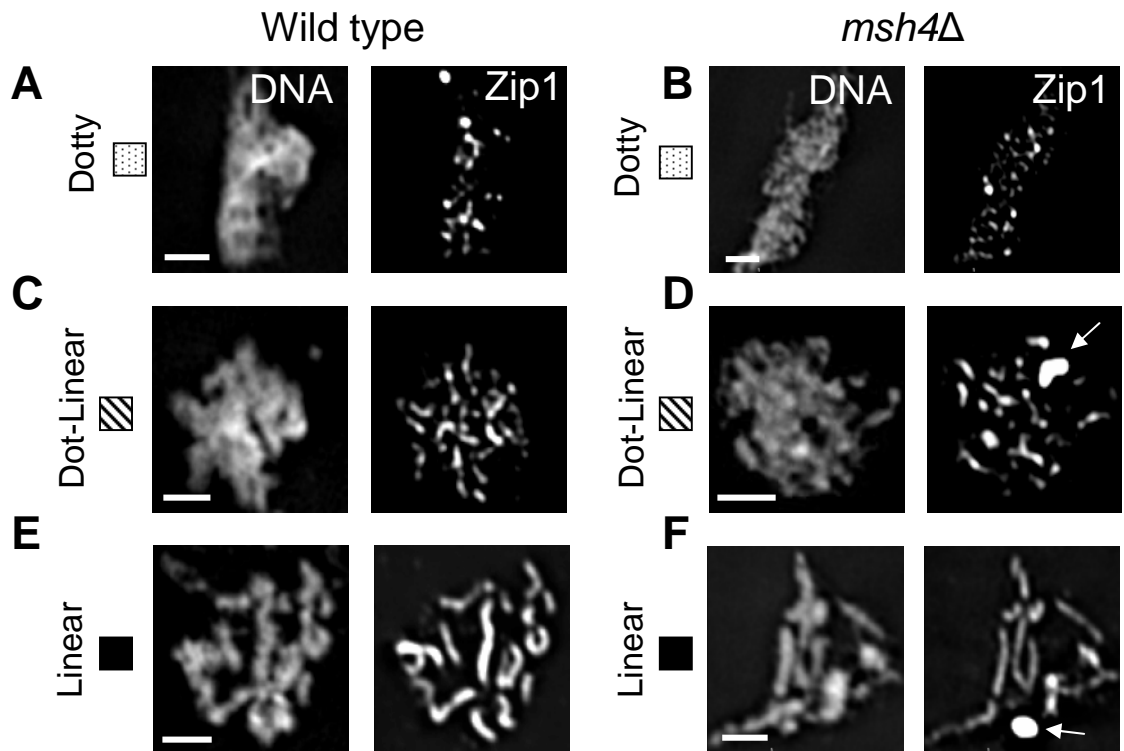


**Figure 1.12.** Summary of the mechanisms used by different organisms to segregate non-exchange chromosomes at meiosis I. A pair of non-exchange chromosomes are shown in red and blue. See text for detailed descriptions. In the *Bombyx mori* panel an electron micrograph of a metaphase I plate from *Bombyx mori* oocytes is shown (from Rasmussen 1997). Note the end-to-end association of the modified SC of each bivalent.

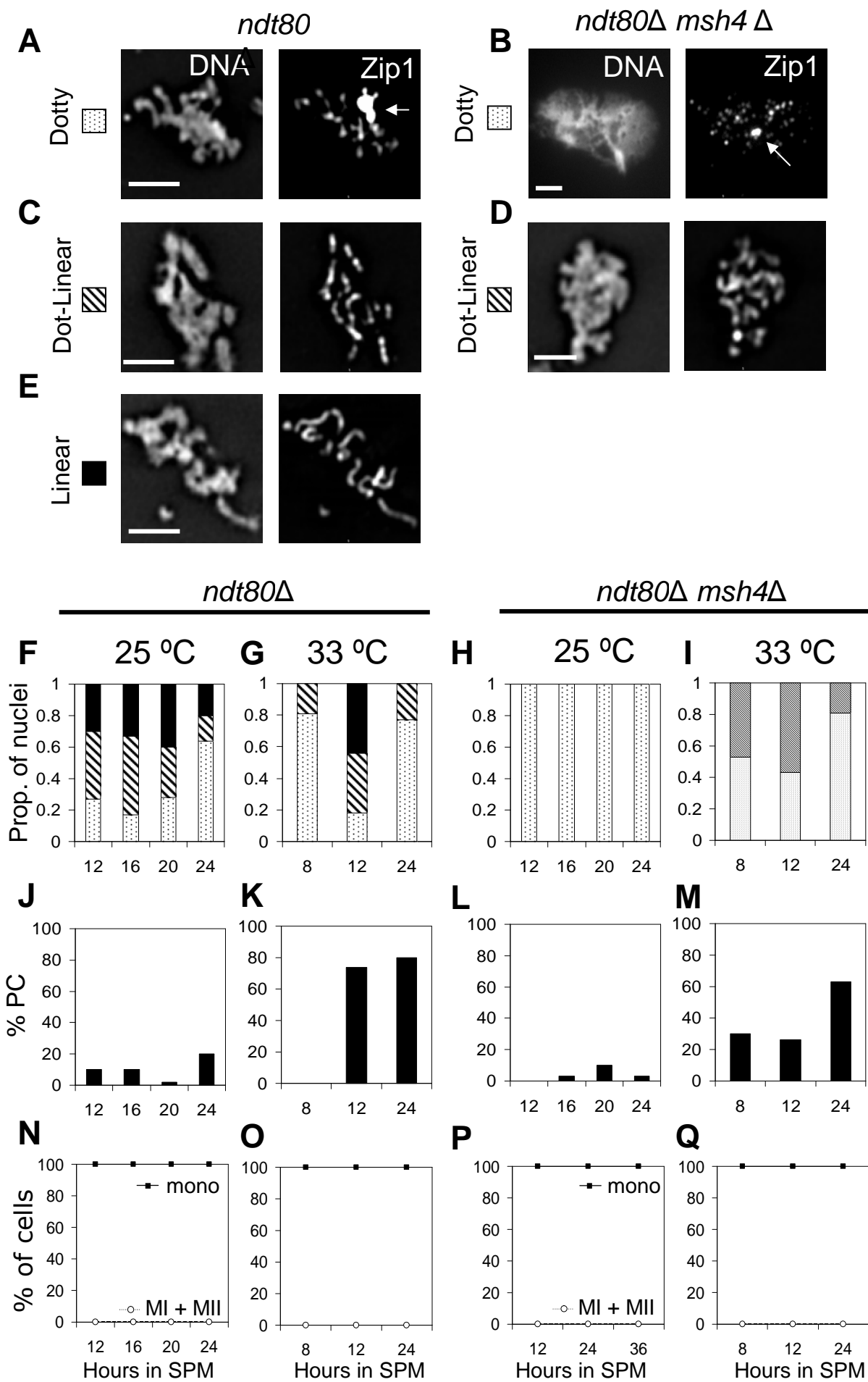
**Figure 3.1.** Improved synapsis in *msh4* $\Delta$  nuclei at 33 °C in the BR strain background. Wild type and *msh4* strains (BR) were sporulated in liquid potassium acetate medium (2%) for 16 hours and meiotic nuclear spreads were assessed for chromosome structure (DNA stained with DAPI) and Zip1. The proportion of nuclei with 'dotty' (A and B), 'dot-linear' (dotty Zip1 with some short stretches, C and D), and 'linear' Zip1 staining (E and F) were quantified in wild type and *msh4* $\Delta$  at 25 and 33 °C (G). The proportion of nuclei with a polycomplex (PC) is shown in (H). >50 nuclei were scored for each strain at each temperature. Bars: 2  $\mu$ m. Strains: Y1293 (wild type) and Y2251 (*msh4* $\Delta$ ).



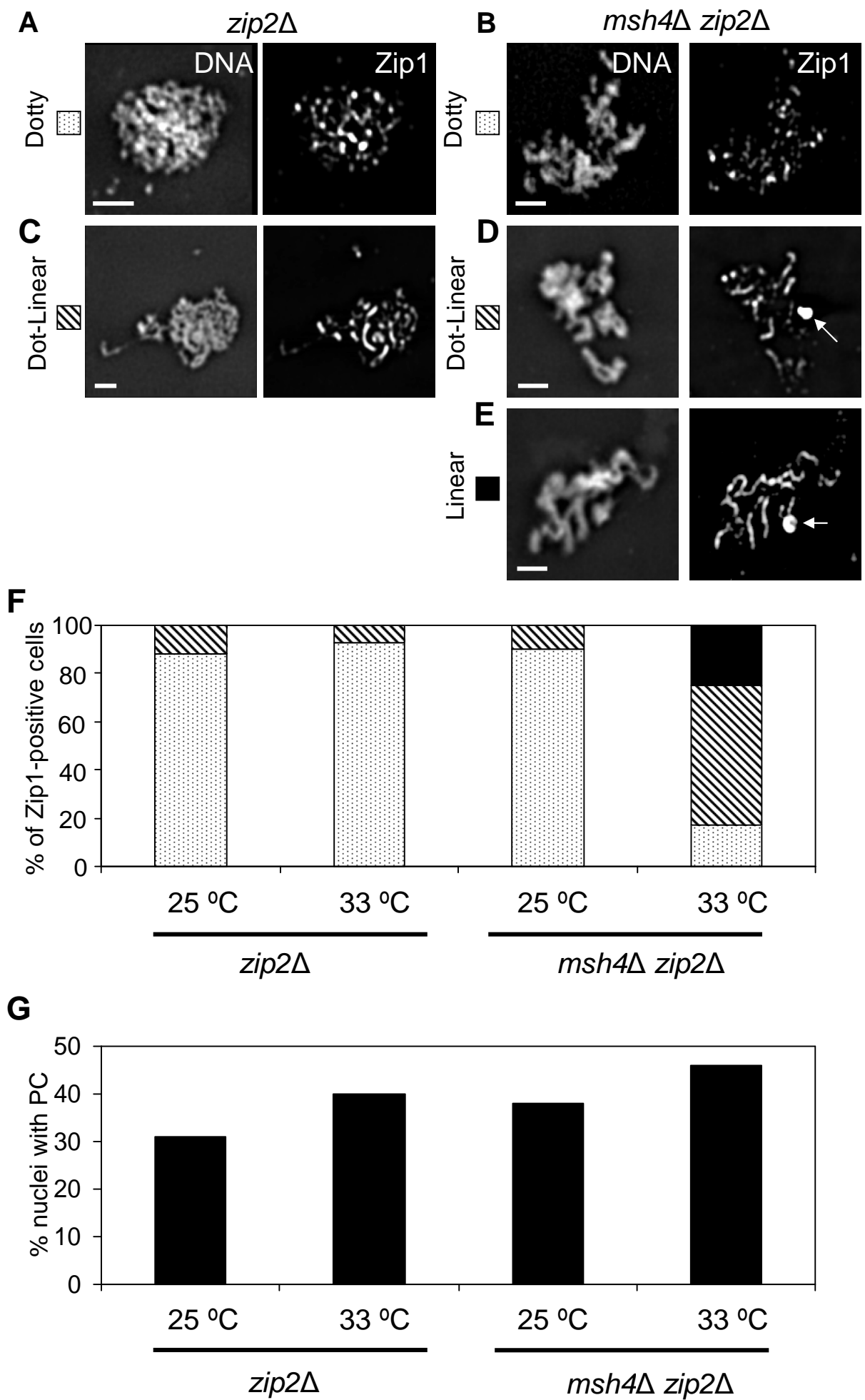
**Figure 3.2.** Improved synapsis in *msh4* $\Delta$  nuclei at 33 °C precedes meiotic nuclear divisions in Y55 strains. (A-F) Examples of surface-spread nuclei from a wild type (Y55; Y650) and an isogenic *msh4* $\Delta$  strain (Y55; Y1465) stained with DAPI (left) and an anti-Zip1 antibody (right). Nuclei were categorized as having 'dotty' (A and B), 'dot-linear' (C and D) or 'linear' (E and F) Zip1 staining. Arrows indicate polycomplexes (PCs). Bars: 2  $\mu$ m. (G-J) Bar plots depicting the relative proportions of each category of Zip1-positive nuclei. (K-N) Bar plots of the proportions of nuclei containing a polycomplex. > 50 surface-spread nuclei were scored for each time point. (O-R) Cumulative curves for the proportion of cells with one (undivided), two (completion of MI) or more (completion of MII) DAPI-stained nuclei as a function of time (hours in sporulation medium, SPM). > 200 nuclei were scored for each time point. n.d. –not determined.



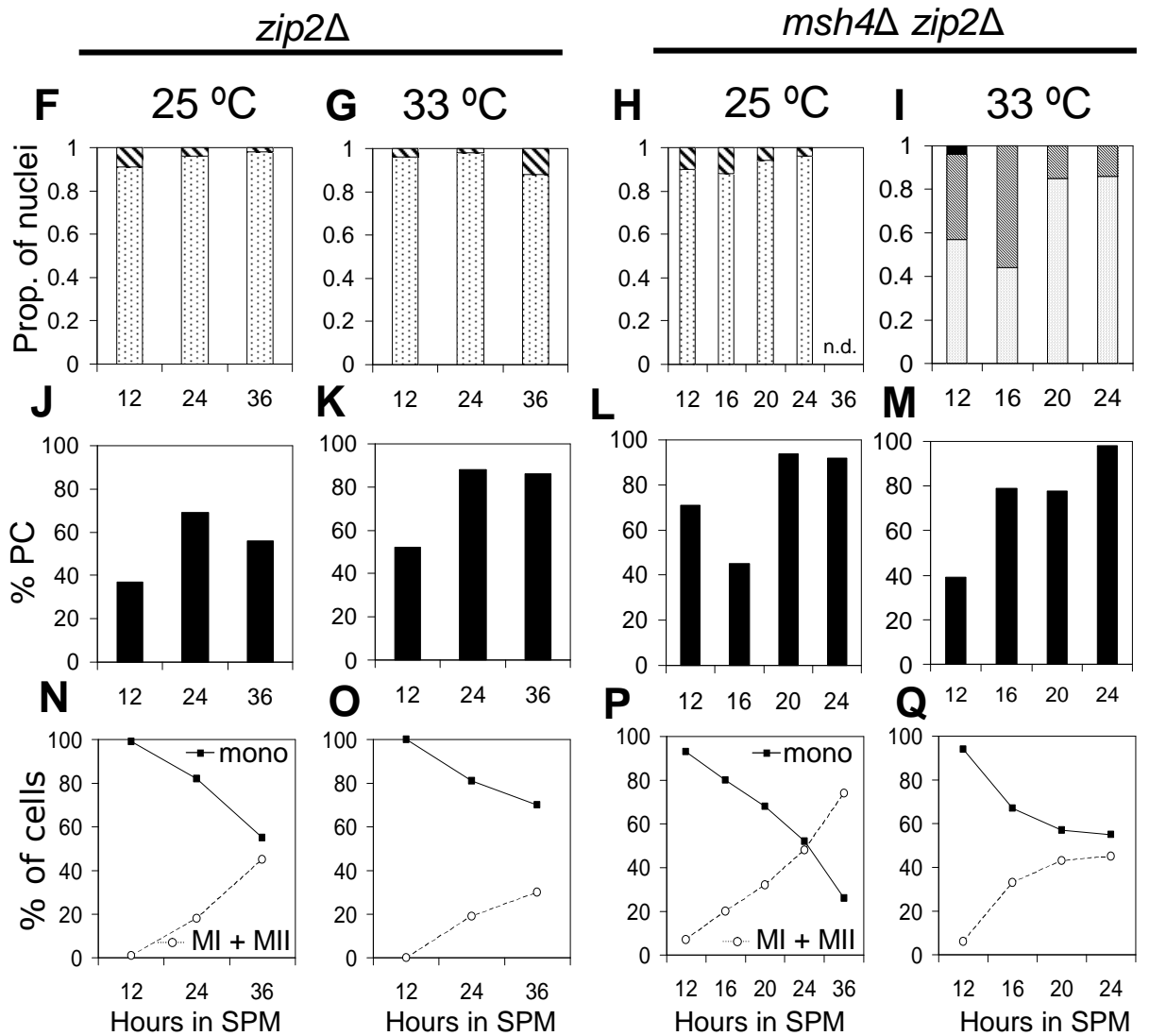
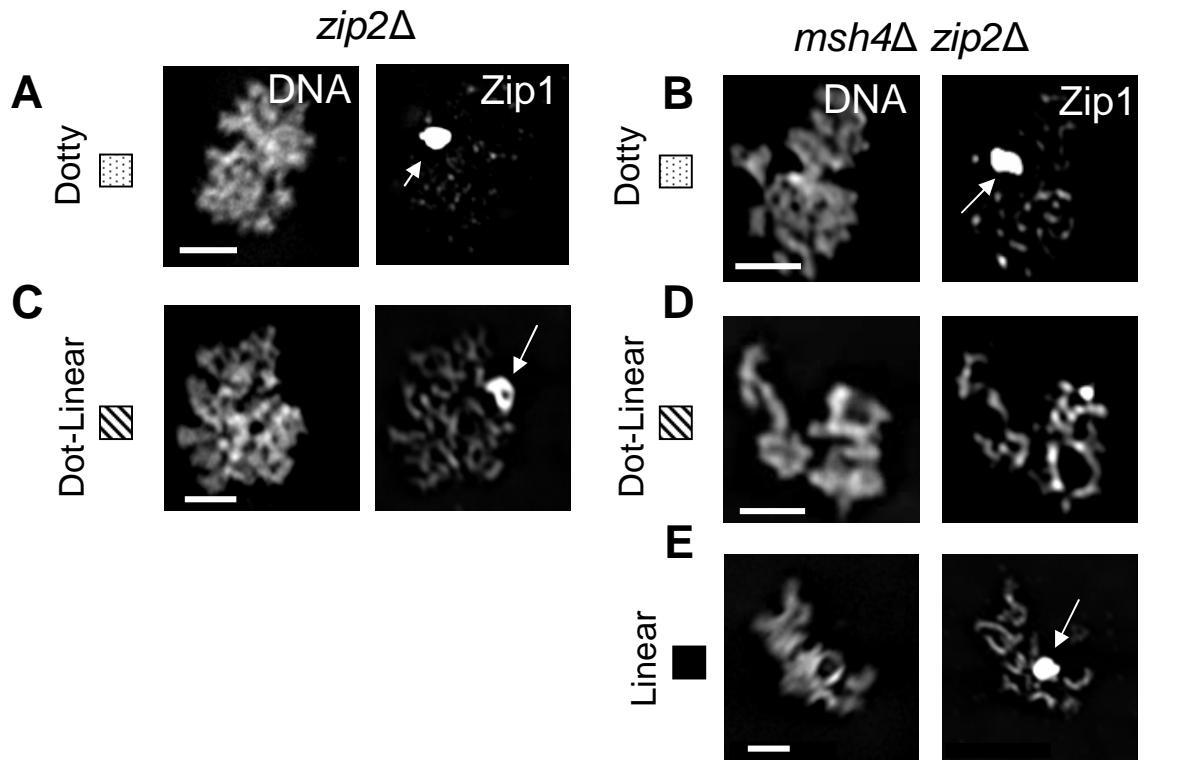
**Figure 3.3.** *msh4* $\Delta$  mutants do not form extensive SCs at 25 °C even when arrested in pachytene. (A-E) Zip1 staining patterns in *ndt80* $\Delta$  (Y1815) and *ndt80* $\Delta$  *msh4* $\Delta$  (Y1816) cells. Arrow indicates polycomplexes. Bars: 2  $\mu$ m. (F-I) Barplots displaying the relative proportions of the different classes of nuclei shown in A-E. (J-M) Barplot showing the proportion of nuclei that contained a polycomplex (PC). > 50 surface-spread nuclei were scored for each time point. (N-Q) Cumulative curves for the proportion of cells with two (completion of MI) or more (completion of MII) DAPI-stained nuclei as a function of time (hours in sporulation medium, SPM). > 200 nuclei were scored for each time point.



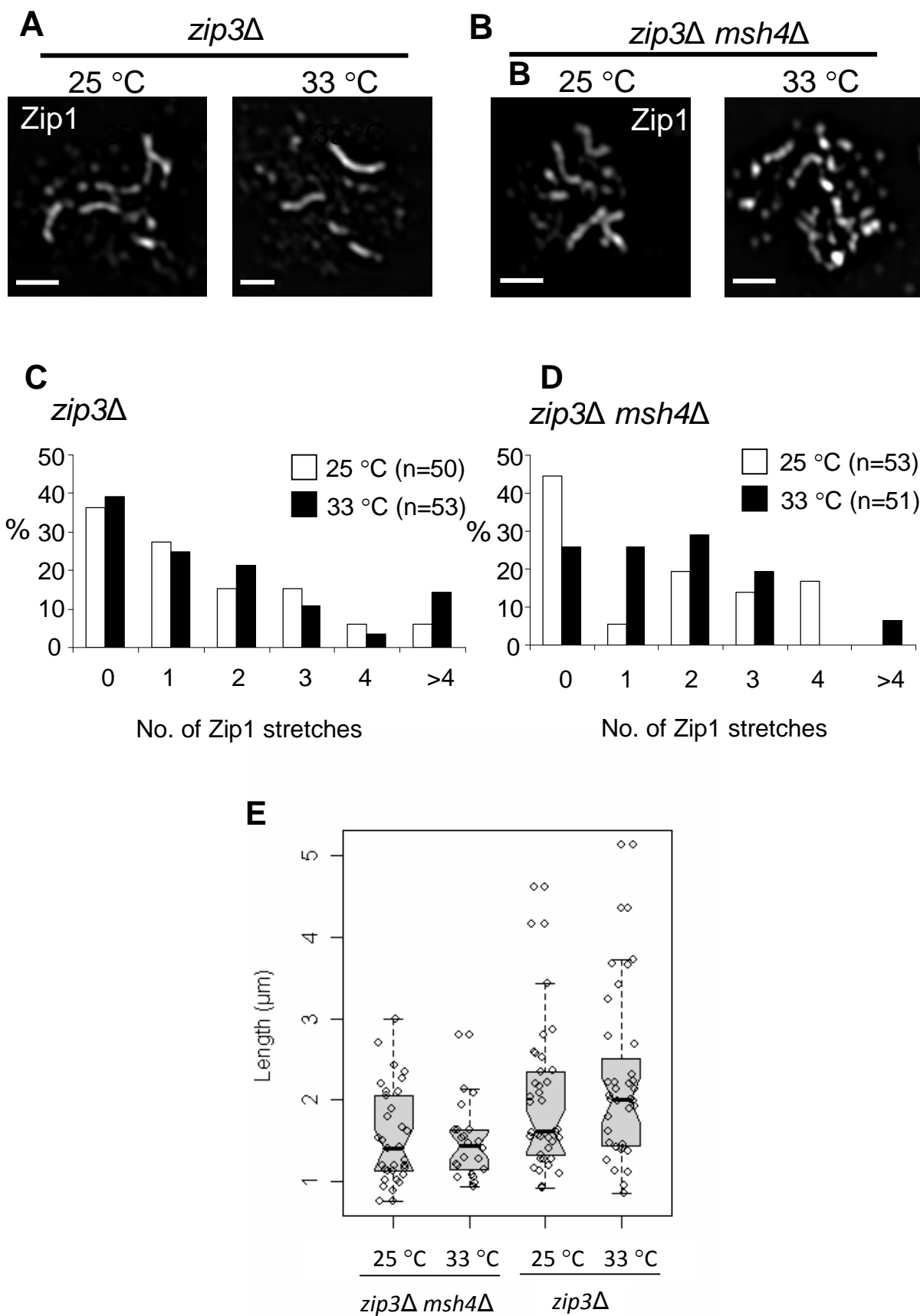
**Figure 3.4.** Deletion of *MSH4* improves Zip1 polymerization in *zip2Δ* mutants of the BR background, at 33 °C. Cells from meiotic cultures of *zip2Δ* (Y1269) and *msh4Δ zip2Δ* (Y2248) strains were collected at 16 hours, meiotic nuclear spreads were stained for Zip1 and categorised as 'dotty' (A and B), 'dot-linear' (C and D) or 'linear' (E). The arrow indicates polycomplexes. Bars: 2 μm. (F) Proportion of nuclei with staining patterns described in (A-E). (G) Proportion of nuclei with polycomplexes. > 50 nuclei were scored at each temperature.



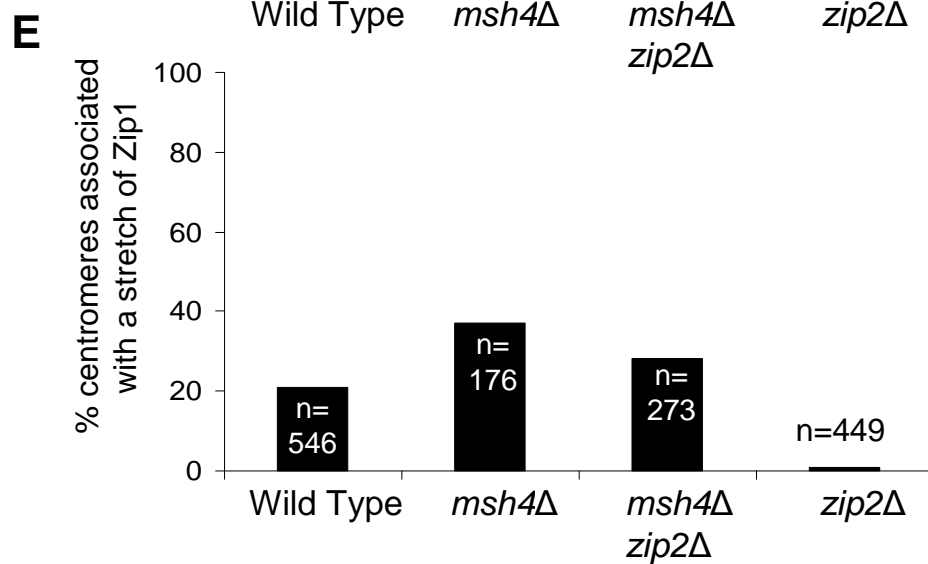
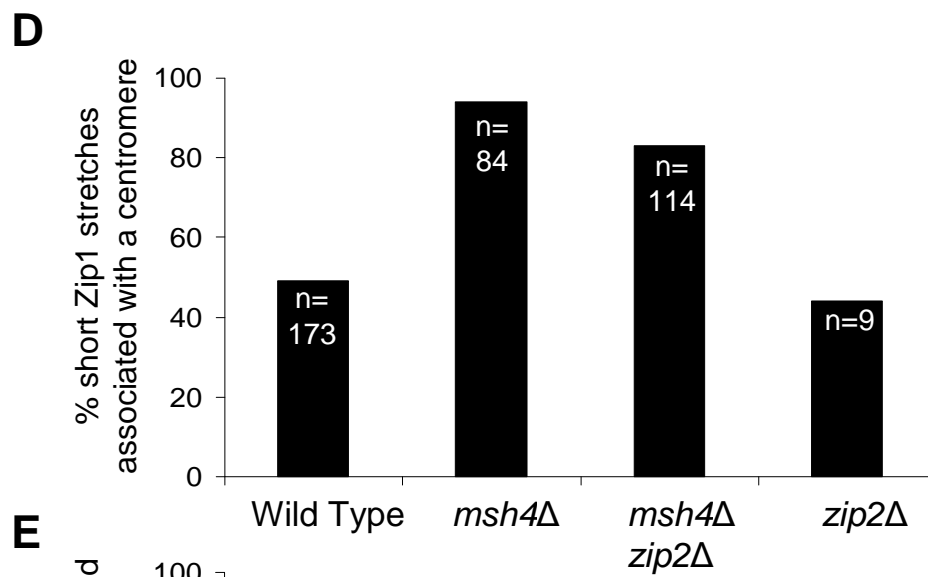
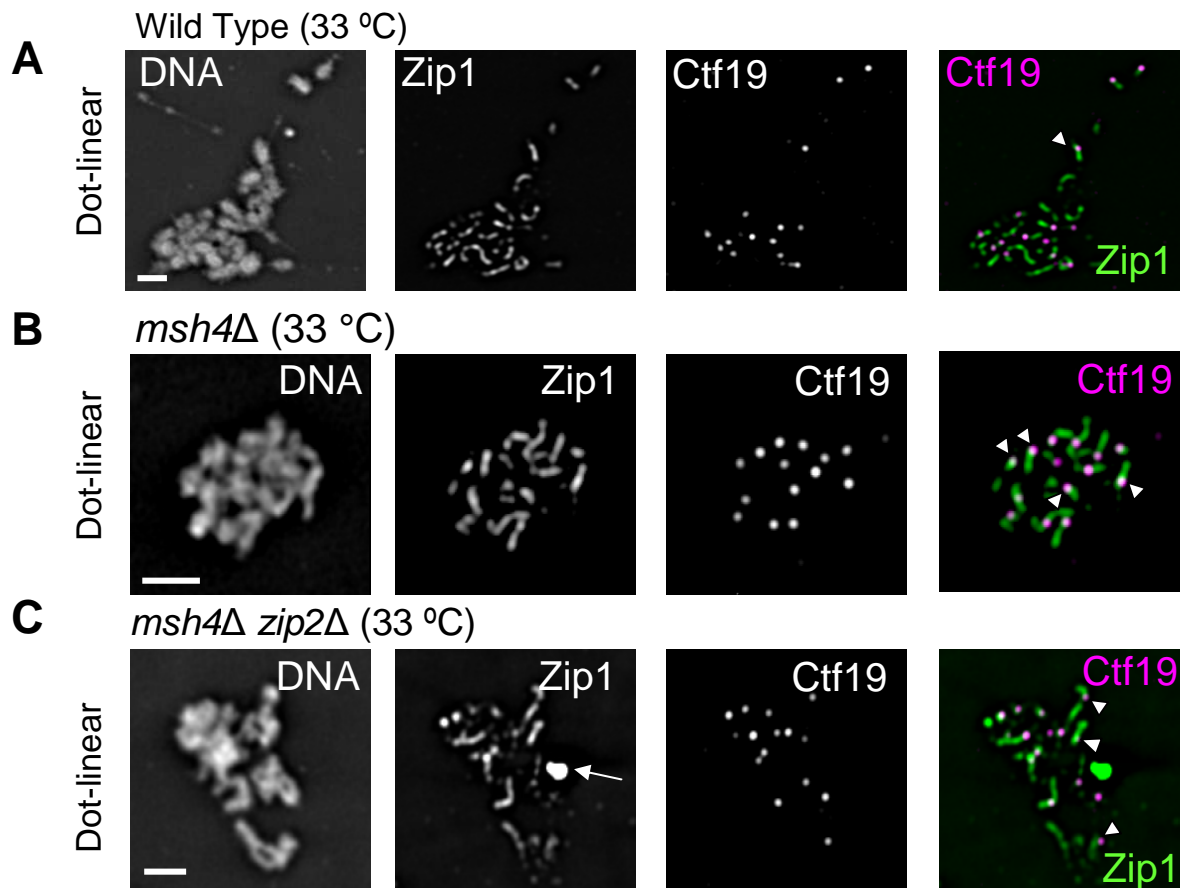
**Figure 3.5.** Improved synapsis precedes meiotic nuclear divisions in *msh4Δ zip2Δ* double mutants of the Y55 background, at 33 °C. (A-E) Examples of Zip1 staining in surface-spread nuclei from *zip2* (Y1571) and *msh4 zip2* (Y1465) strains in the Y55 background. The arrows indicate polycomplexes of Zip1. Bars: 2 μm. (F-I) Bar plots of the proportions of nuclei with dotted, dot-linear, or linear staining at the given time points after transfer to sporulation medium (SPM). (J-M) Bar plots of the proportions of nuclei with a polycomplex (PC). > 50 nuclei were assessed for each time point. (N-Q) Nuclei were stained with DAPI and cumulative curves generated for the proportion of cells that have completed MI (two nuclei) and MII (more than two nuclei). > 200 nuclei were scored for each time point. n.d. –not determined.

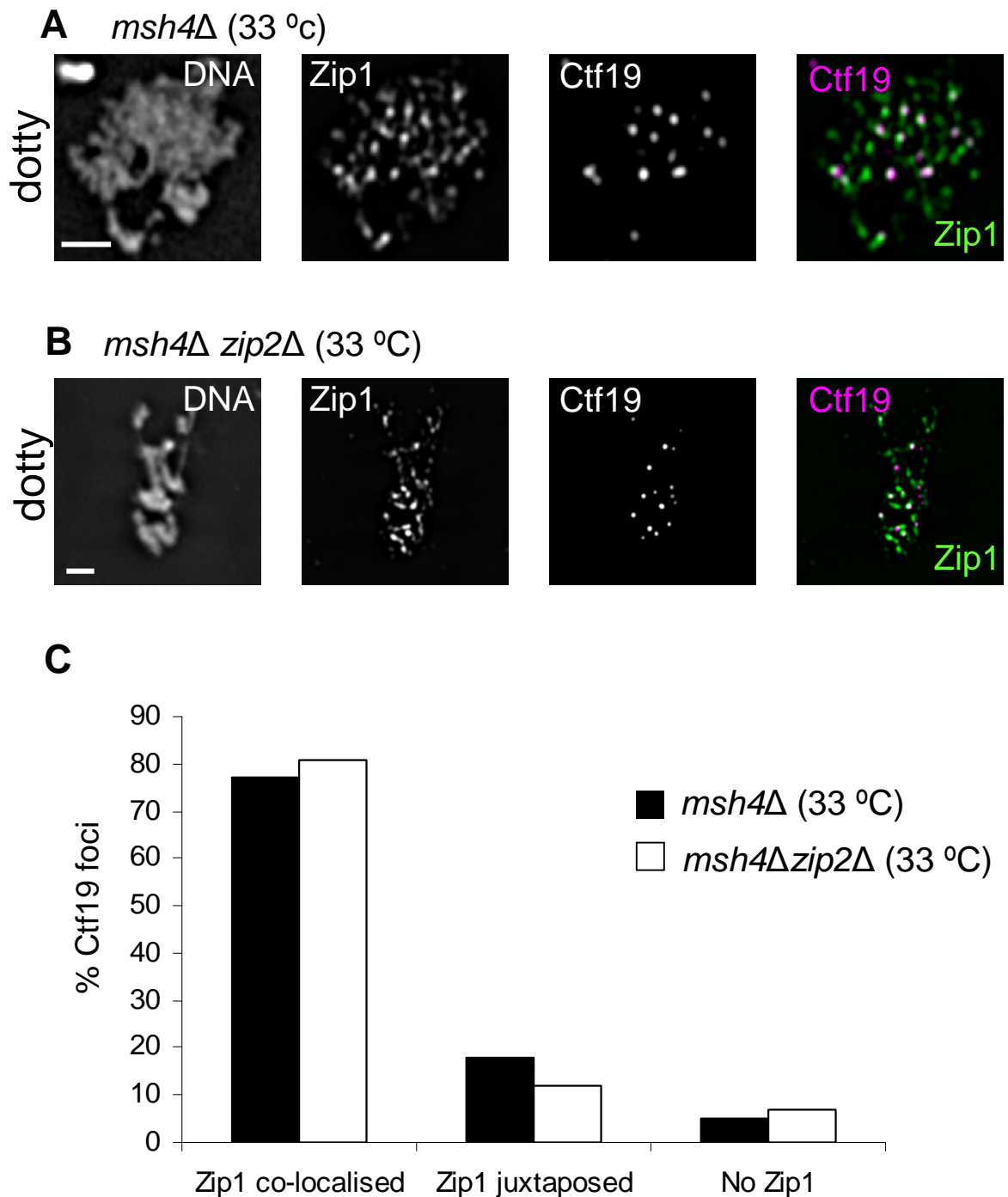


**Figure 3.6.** Synapsis is unaffected by both temperature and deletion of *MSH4* in *zip3Δ* mutants. (A and B) Representative images of Zip1 staining in *zip3Δ* (Y1274) and *msh4Δ zip3Δ* (Y1350) mutants of the BR strain background. Cells were harvested after 20 hours in sporulation medium and only spreads with highly condensed chromosomes were examined. Bars: 2  $\mu$ m. Histograms showing the number of Zip1 stretches *per* nucleus in the *zip3Δ* mutant at 25 °C and 33 °C (C) and for *zip3Δ msh4Δ* at 25 °C and 33 °C (D). 30 nuclei *per* strain and condition were examined. The number of stretches analysed is given in brackets. (E) Box plots displaying the lengths of Zip1 stretches for both mutants at 25 °C and 33 °C. The boxes represent the 25% range either side of the median and the whiskers represent  $1.5 \times$  the interquartile range. The horizontal black line indicates the median, which is surrounded by a notched area that approximates the 95% confidence interval. Individual data points are shown as empty circles.



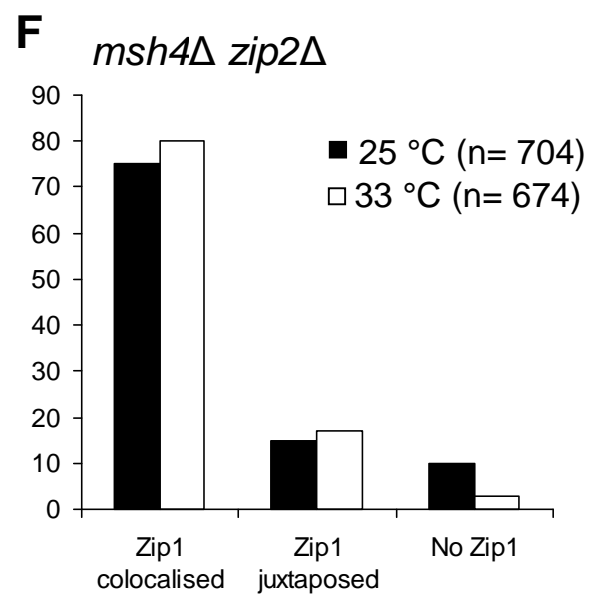
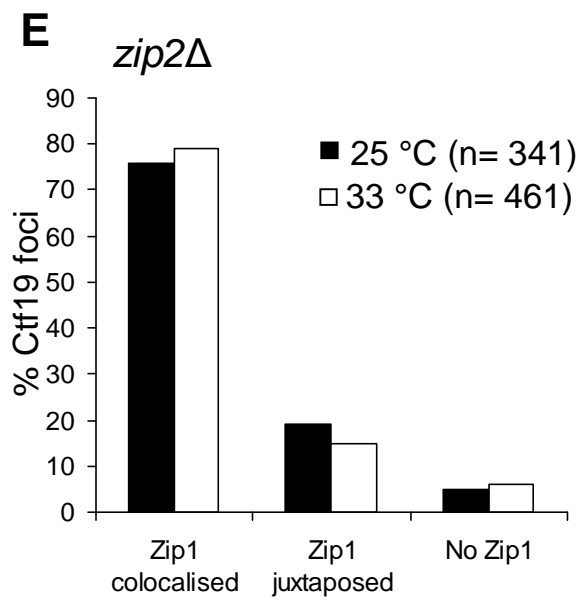
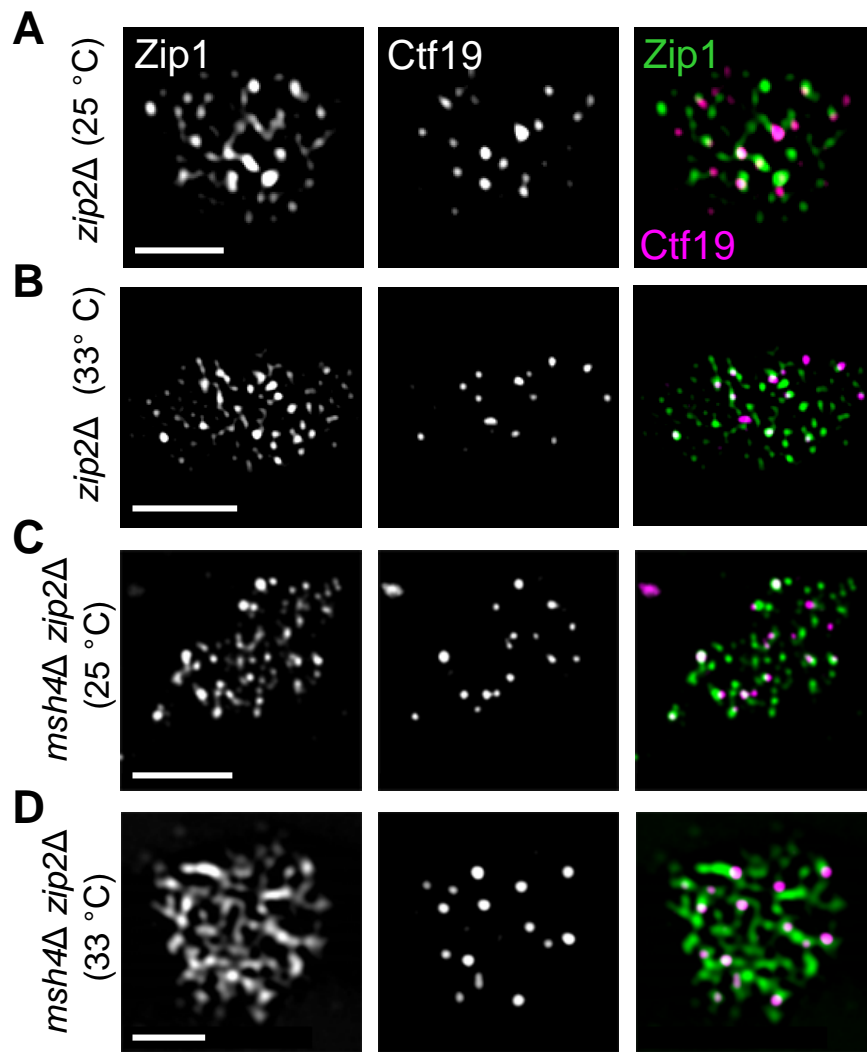
**Figure 3.7.** Zip1 stretches observed in *msh4Δ* and *msh4Δ zip2Δ* mutants at 33 °C are predominantly associated with centromeres (Ctf19-13Myc). Example images of zygotene nuclei with dot-linear Zip1 staining for wild type (A), *msh4Δ* mutants (B) and *msh4Δ zip2Δ* double mutants (C) at 33 °C. In the merged images, Zip1 is shown in green and Ctf19-13Myc in magenta. Arrows and arrowheads indicate polycomplexes and centromere-associated Zip1 stretches, respectively. Bars: 2 μm. (D) Quantification of short Zip1 stretches (~1 μm) that were associated with a Ctf19-13Myc focus. The number of zygotene nuclei scored: 40 for wild type, 12 for *msh4Δ*, 24 for *msh4Δzip2Δ* and 30 for *zip2Δ* mutants. The number of stretches scored is shown within the bars. (E) The proportion of centromeres associated with a stretch of Zip1 in the nuclei used in (D). Strains (BR): Y2064 (wild type), Y2251 (*msh4Δ*), Y1269 (*zip2Δ*), and Y2248 (*msh4Δ zip2Δ*).



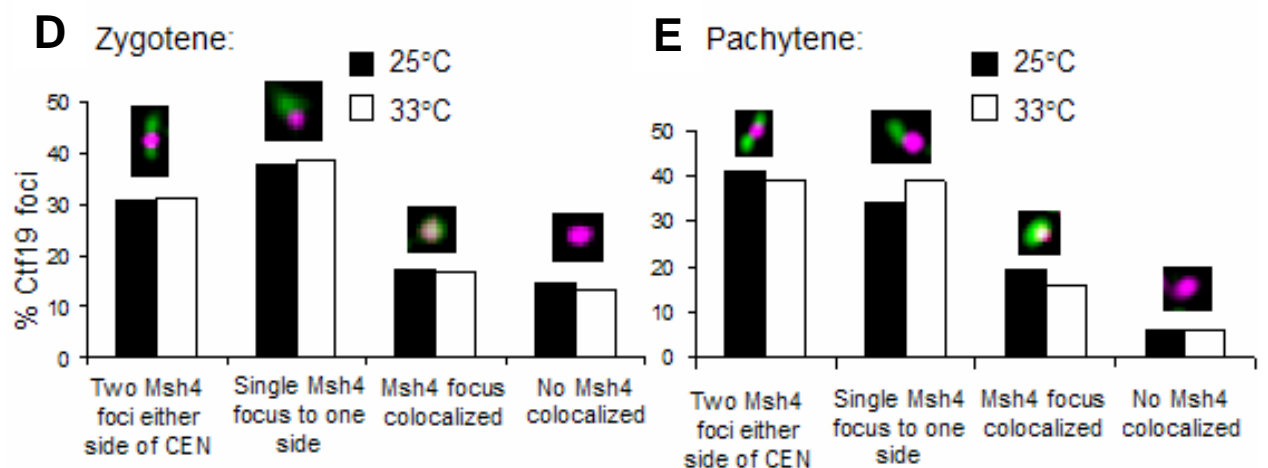
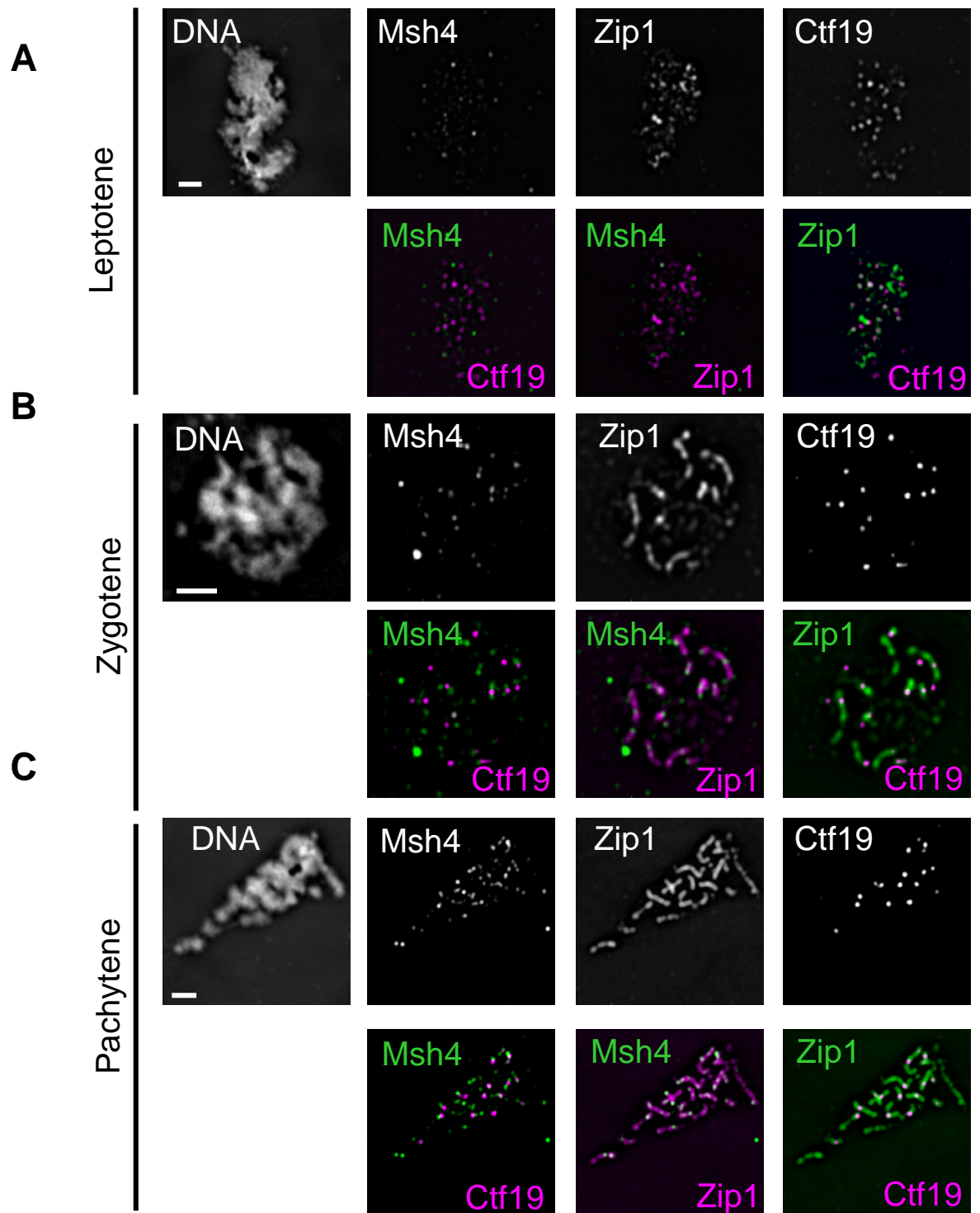


**Figure 3.8.** Centromeres frequently co-localise with Zip1 foci in early zygotene nuclei of *msh4* $\Delta$  and *msh4* $\Delta$ *zip2* $\Delta$  mutants. (A-B) Representative images showing Zip1-Ctf19 co-localisation in early zygotene nuclei of *msh4* $\Delta$  (A) and *msh4* $\Delta$ *zip2* $\Delta$  (B) mutants. In the merged images, Zip1 is shown in green and Ctf19 in magenta. Bars: 2  $\mu$ m. (C) Quantification of the percentage of centromeres (Ctf19 foci) directly co-localised with, or juxtaposed to a Zip1 focus or with no Zip1 in early zygotene nuclei at 33 °C. 312 and 389 Ctf19 foci were analysed for the *msh4* $\Delta$  mutant and the *msh4* $\Delta$ *zip2* $\Delta$  mutants, respectively. This was derived from analysis of 22 and 25 nuclei for the *msh4* $\Delta$  mutant and the *msh4* $\Delta$ *zip2* $\Delta$  mutants, respectively. Strains: Y2251 (*msh4* $\Delta$ ) and Y2248 (*msh4* $\Delta$  *zip2* $\Delta$ ).

**Figure 3.9.** Zip1 association with centromeres (Ctf19-13Myc) is similar in *zip2* $\Delta$  and *msh4* $\Delta$  *zip2* $\Delta$  strains and is irrespective of temperature. (A-D) Examples of Zip1 and Ctf19-13Myc co-localisation in *zip2* $\Delta$  (Y1269) and *msh4* $\Delta$  *zip2* $\Delta$  (Y2248) strains at 25 °C and 33 °C. Bars: 5  $\mu$ m. (E) Quantification of the percentage of Ctf19-13Myc foci with Zip1 directly co-localised, juxtaposed, or not associated at all. The number of Ctf19-13Myc foci assessed at each temperature is given in brackets. The number of *zip2* $\Delta$  nuclei analysed were 22 (25 °C) and 29 (33 °C). The number of *msh4* $\Delta$ *zip2* $\Delta$  nuclei analysed were 42 (25 °C) and 44 (33 °C).



**Figure 3.10.** Msh4-GFP foci are frequently juxtaposed to centromeres at both zygotene and pachytene. Meiotic nuclear spreads were stained with antibodies against GFP (Msh4-GFP), Zip1, and Myc (Ctf19-13Myc). DNA was stained with DAPI. Localisation of Msh4-GFP at leptotene (A), zygotene (B), and pachytene (C) stages. Individual proteins are shown in black and white with merged images of Msh4-GFP with Ctf19-13Myc, Msh4-GFP with Zip1, and Ctf19-13Myc with Zip1 shown in the second row. Bars: 2  $\mu$ m. (D-E) Co-localisation of Msh4-GFP and Ctf19-13Myc foci at zygotene (D) and pachytene (E). Strains: Y2064.





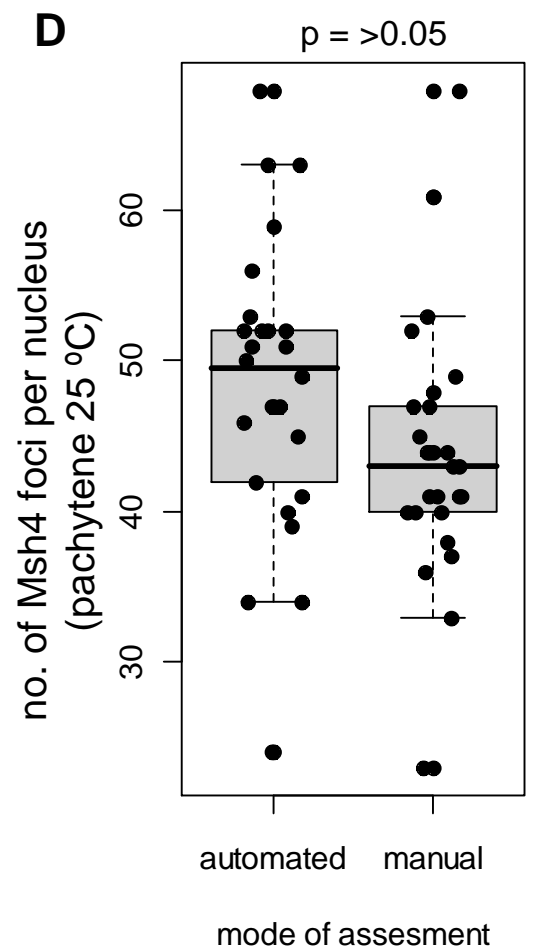
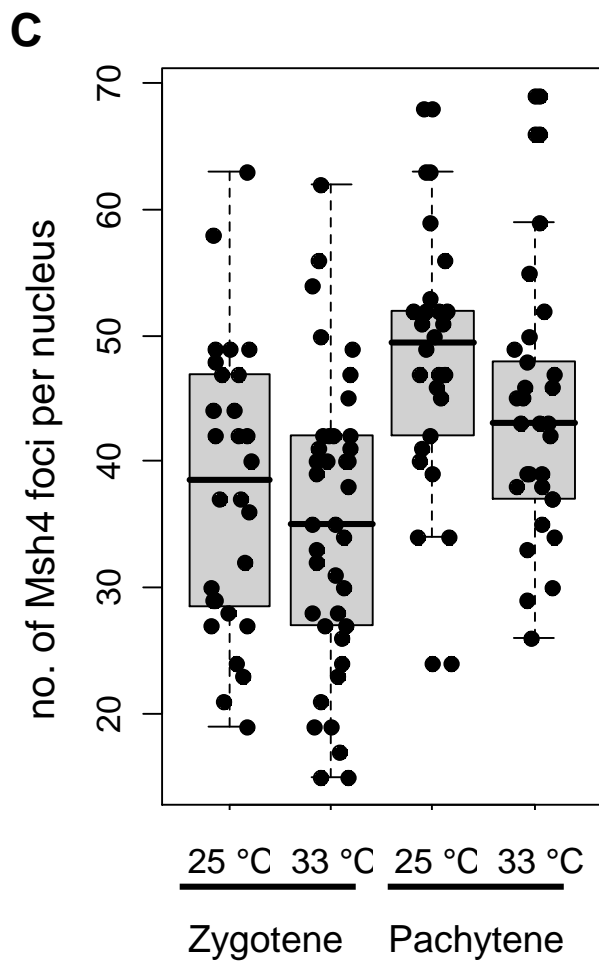
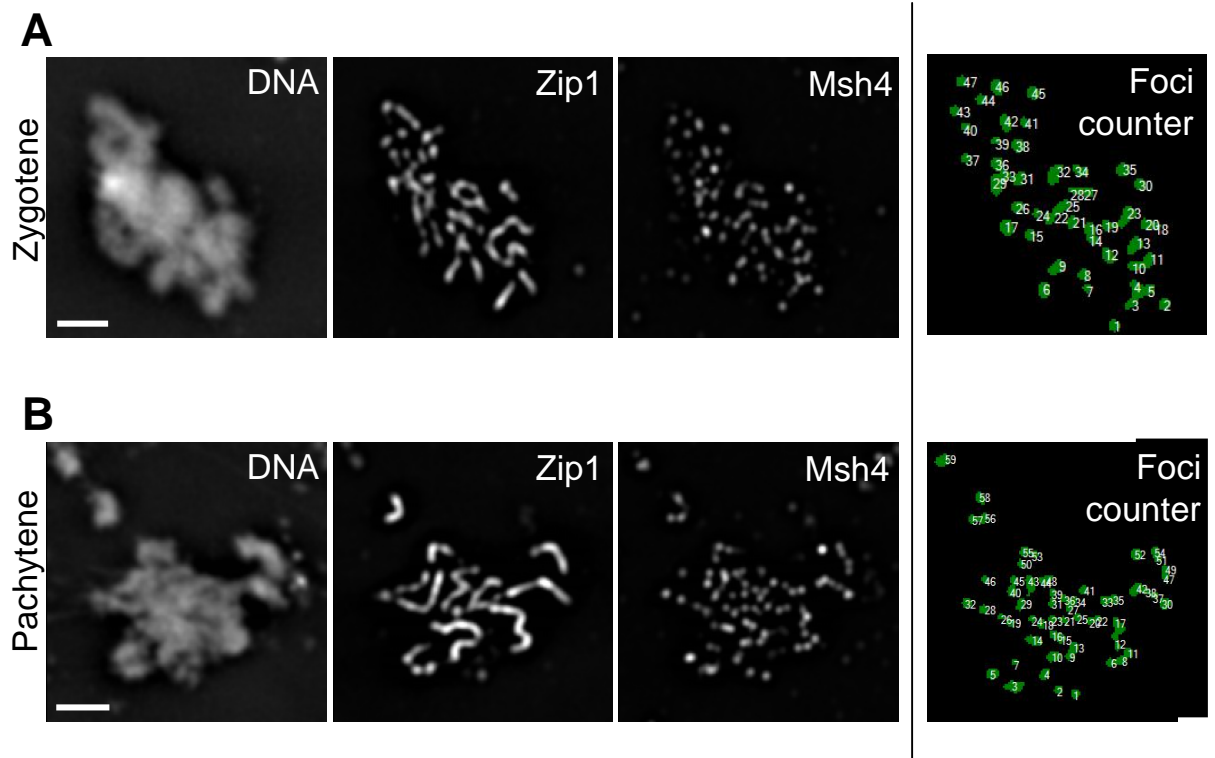



**Figure 3.11.** The number of Msh4-GFP foci *per* nucleus is unaffected by temperature. (A-B) Example of wild type (Y2064) zygotene (A) and pachytene (B) nuclei stained with anti-GFP and anti-Zip1 antibodies. Bars: 2  $\mu$ m. The panel to the right depicts the Msh4 foci detected using automated object detection. (C) Boxplot depicting the number of Msh4 foci detected *per* nucleus in zygotene and pachytene nuclei at both temperatures. 30 - 50 nuclei were analysed for each stage at each temperature. (D) Boxplot comparing the Msh4 foci counts from 'automated' or 'manual' modes of assessment. The pachytene (25 °C) images were used for this analysis. A paired t-test of these two sets of data gave a p-value < 0.05.














**Figure 3.12.** Zip1 stretches are found to one side or both sides of Msh4-GFP foci. (A) In wild type zygotene nuclei, short Zip1 stretches (~ 1  $\mu\text{m}$ ) that do not contain a centromere were assessed for the relative positions of Msh4-GFP foci. All Zip1 stretches examined contained at least one Msh4-GFP focus. Grey ovals represent Zip1 stretches and black circles indicate Msh4 foci. (B) Quantification of the Msh4-GFP foci that were not associated with a Zip1 stretch. Grey circles represent Zip1 foci, black circles represent Msh4 foci and circles with black and white diagonal stripes represent centromeres. Key is shown below tables. Numbers and percentages are given in the 2<sup>nd</sup> and 3<sup>rd</sup> columns of the tables, respectively. (C) Representative image of a wild type, zygotene nuclei with centromeres, Zip1 and Msh4-GFP, shown in red, green and blue, respectively. Bars: 2  $\mu\text{m}$ . Boxed regions of non-centromeric Zip1 stretches (S1 to S3) and Msh4 foci not associated with a Zip1 stretch (F1 to F3) are shown enlarged in (D) and (E), respectively. Magnification is given in the bottom left-hand corner of each merged image.

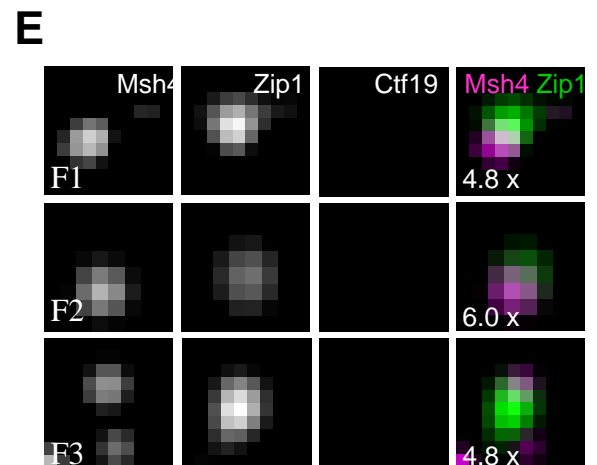
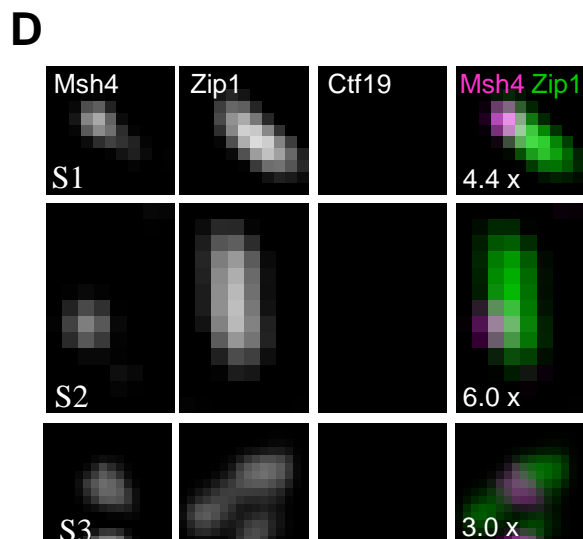
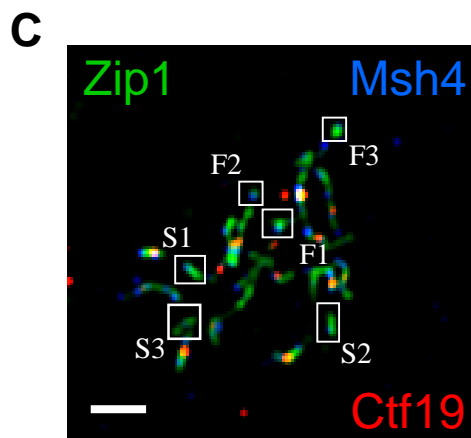
**A**

	Category	No.	%
1.		27	46
2.		16	28
3.		8	14
4.		5	9
5.		2	3

**B**

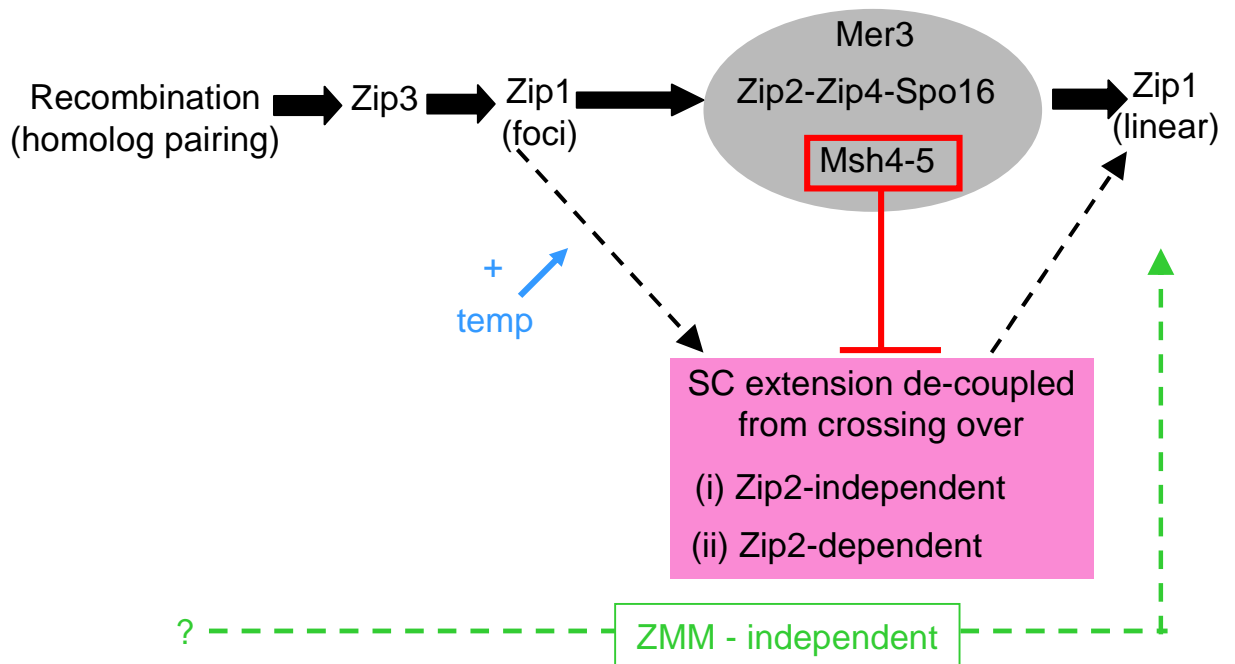
	Category	No.	%
1.		65	30
2.		14	6
3.		55	26
4.		5	2
5.		0	0
6.		4	2
7.		72	34

 Zip1 stretch     Msh4 focus     Centromere     Zip1 focus



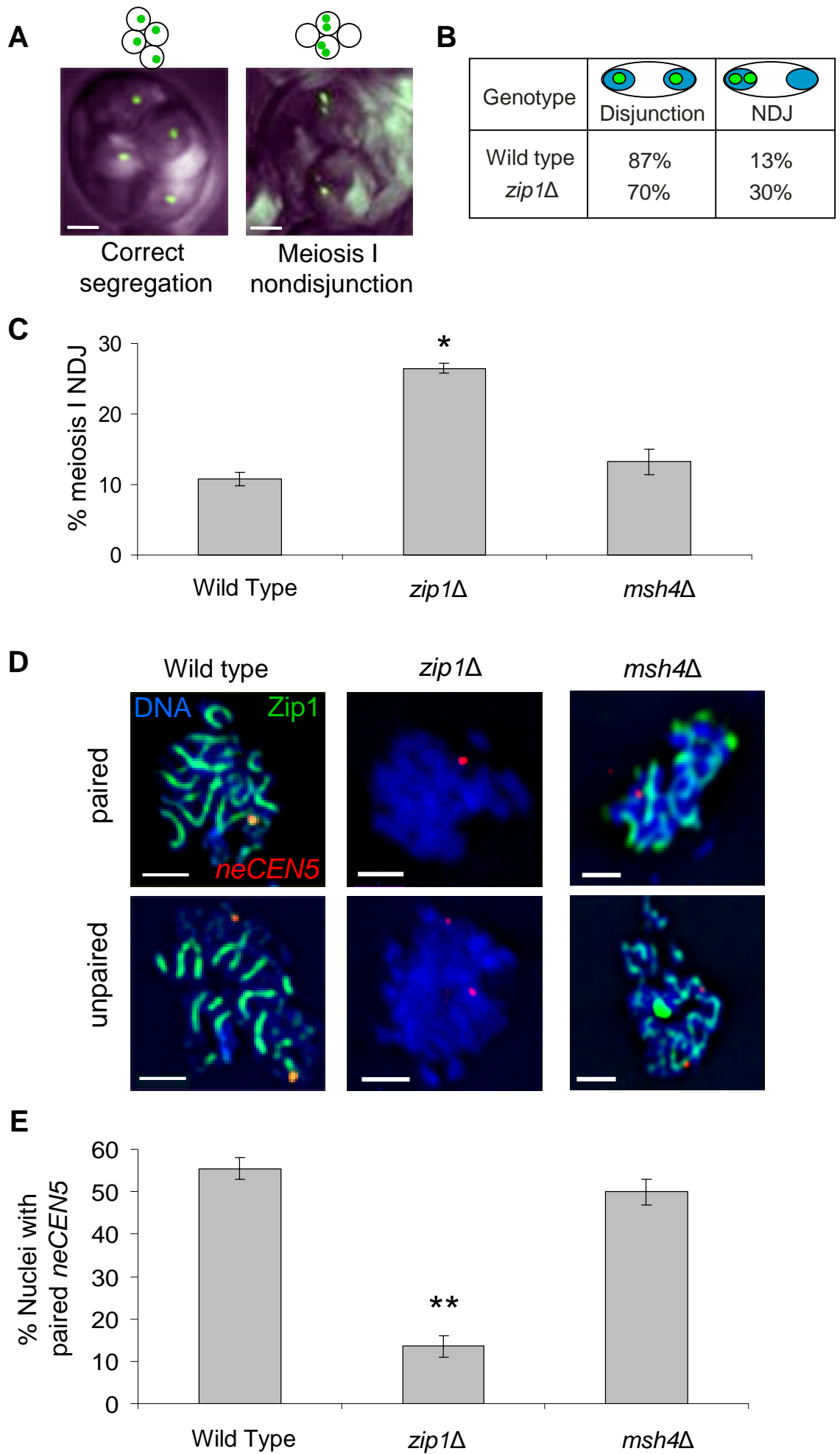
**Table 3.1.** Table summarising the synopsis phenotypes of the *zip2Δ*, *msh4Δ* and *msh4Δ zip2Δ* mutants. See discussion for more details.

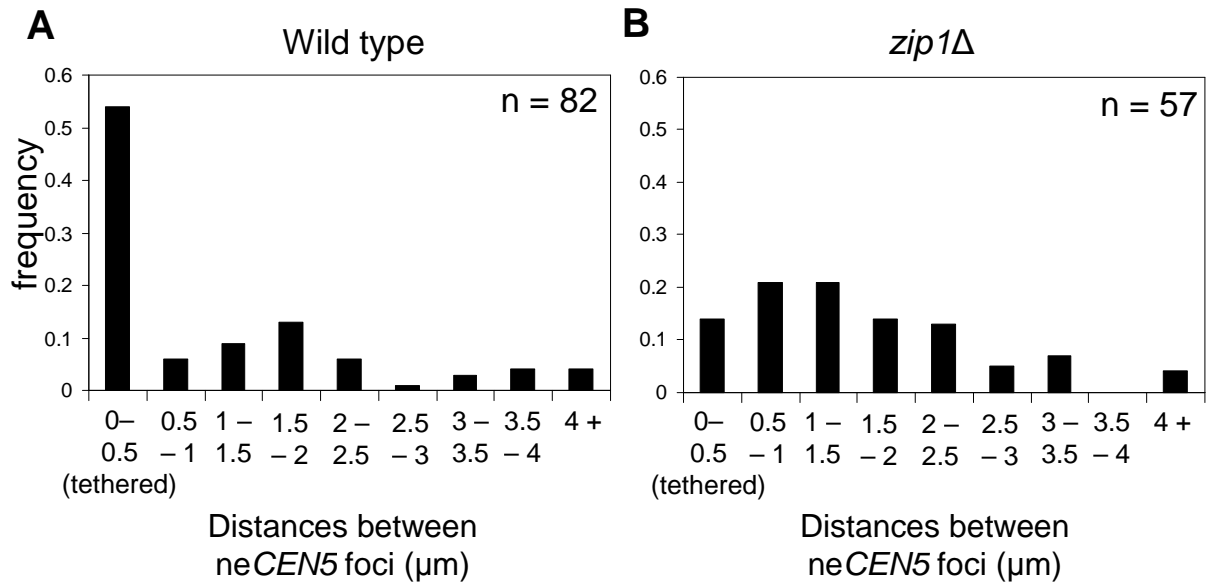
Synopsis	25 ° C	Interpretation	33 ° C	Interpretation
<i>zip2Δ</i>	bad	Zip2 is absent so SC cannot be extended.	bad	Zip2 is absent so SC cannot be extended.
<i>msh4Δ</i>	bad (= <i>zip2Δ</i> )	Msh4 is absent so crossing over (CO) is defective. As CO and SC extension are tightly coupled at 25°C, SC extension is also defective.	very good	Absence of Msh4 means CO is defective, but higher temperature allows SC extension that is de-coupled from crossing over. So SC can extend despite the CO defect.
<i>msh4Δ zip2Δ</i>	bad (= <i>zip2Δ</i> , = <i>msh4Δ</i> )	Zip2 is absent so SC cannot be extended.	good	As above, but in this case, only Zip2-independent synopsis can occur. As synopsis is more extensive in <i>msh4Δ</i> single mutants, it suggests both Zip2-dependent and Zip2-independent modes of SC extension exist.



**Figure 3.13.** Model outlining the regulation of Synaptonemal Complex (SC) formation by the ‘ZMM’ ensemble and temperature. Recombination initiates homologous pairing of chromosomes permitting the initiation of SC formation. Zip3 is the primary regulator committing SC formation to the ‘ZMM’ pathway (grey oval). In wild-type meiosis, Zip3 promotes initial loading of Zip1 at synapsis initiation sites and Zip2, together with Zip4 and Spo16, polymerize Zip1 along the chromosomal axes (thick black arrows). Concomitant with this process is the stabilisation of crossover-designated joint molecules by Msh4-Msh5 and Mer3 (grey oval). Alternative pathways, both dependent and independent of Zip2, can extend polymers of Zip1 along the chromosomal axes (pink box). However, these pathways are subject to opposing negative and positive regulation by Msh4 and increased temperature, respectively. These modes of Zip1 extension are likely to be de-coupled from crossover formation as crossovers are similar at both temperatures (Chan *et al.* 2009). Finally, in the absence of the primary regulator Zip3, SC formation occurs in a mode that is unaffected by temperature and/or Msh4 status (green dotted line).

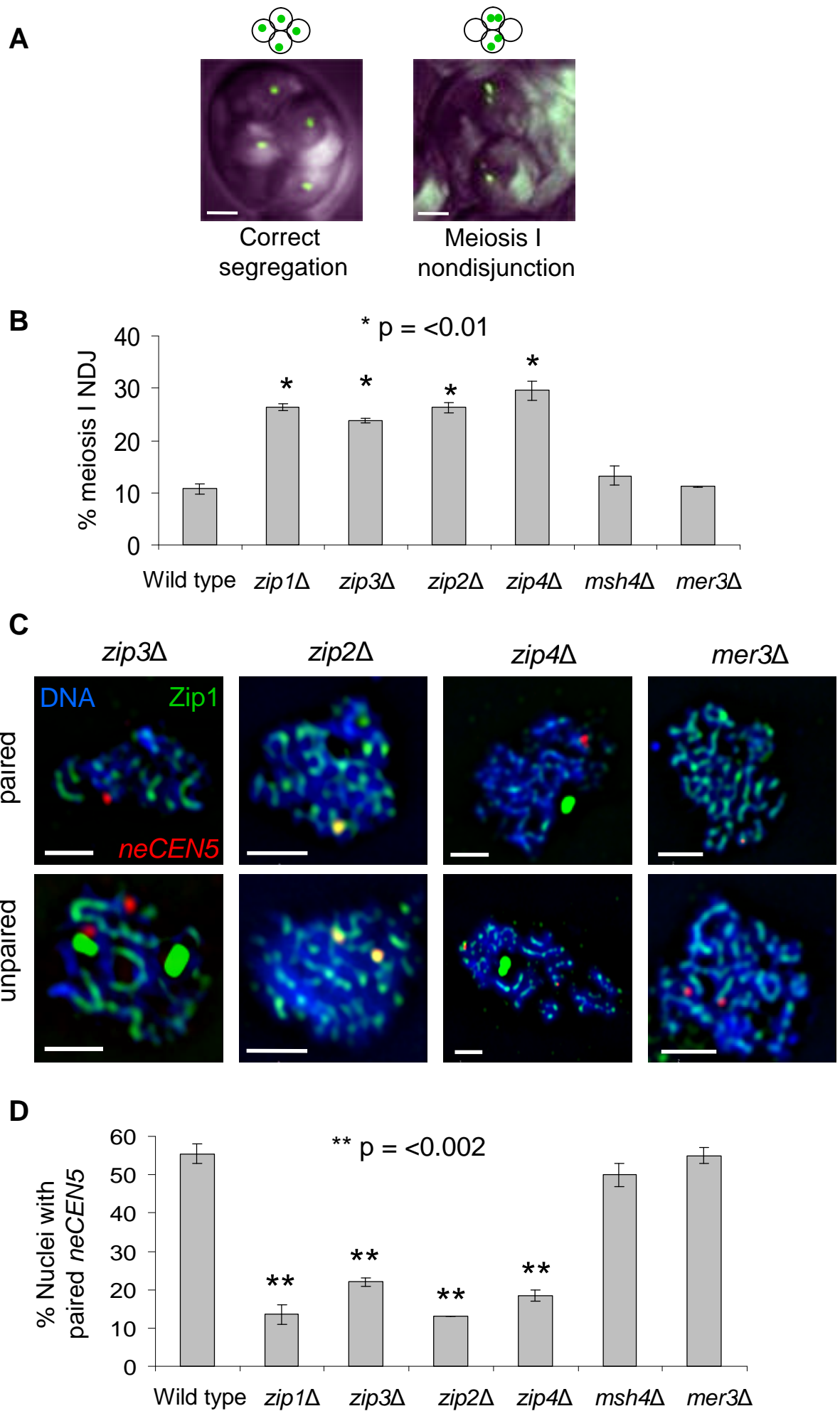
**Figure 4.1.** Decreased centromere pairing frequencies correlate with increased meiosis I non-disjunction of a non-exchange chromosome pair. Normal meiosis yields a tetrad containing a single GFP (*neCEN5*) focus in each spore (A, right), whereas a meiosis I non-disjunction results in two spores each containing two GFP foci and two containing none (A, left). (B) Quantification of meiosis I non-disjunction as assessed from the binucleate stage. (C) Quantification of meiosis I non-disjunction frequencies. >100 tetrads were examined for each strain. Error bars represent standard error between at least two independent experiments. (D) Representative images of pachytene nuclei containing 'paired' (top row) and 'unpaired' (bottom row) *neCEN5*s. Zip1 is shown in green, *neCEN5*s in red and DNA in blue. Bars: 2  $\mu$ m. (E) Quantification of the *neCEN5* pairing frequencies in pachytene nuclei. >60 nuclei were examined for each strain and the error bars represent the standard error between two independent experiments. Star (\*) depicts a significant ( $p = <0.01$ ) difference to wild type. Two stars (\*\*) depict a significant ( $p = <0.002$ ) difference to wild type. Strains: wild type (Y712), *zip1* $\Delta$  (Y787), and *msh4* $\Delta$  (Y790).





**Figure 4.2.** Histograms showing the distribution of distances between *neCEN5* foci in spread pachytene nuclei for the wild type (A) and *zip1Δ* mutant (B). Distances are grouped and shown on the x-axis and the frequencies shown on the y-axis. The number of nuclei analysed for each strain (n) are shown in the upper right-hand corner.

**Figure 4.3.** Differing *ZMM* mutant phenotypes for centromere pairing and meiosis I segregation of the non-exchange chromosome pair. Normal meiosis yields a tetrad containing a single GFP (*neCEN5*) focus in each spore (A, right), whereas a meiosis I non-disjunction results in two spores each containing two GFP foci and two containing none (A, left). (B) Quantification of meiosis I non-disjunction frequencies. >100 tetrads were examined for each strain. Error bars represent standard error between at least two independent experiments. Star (\*) depicts a significant ( $p = <0.01$ ) difference to wild type. (C) Representative images of pachytene nuclei containing 'paired' (top row) and 'unpaired' (bottom row) *neCEN5*s. Zip1 is shown in green, *neCEN5*s in red and DNA in blue. Bars: 2  $\mu$ m. (D) Quantification of the *neCEN5* pairing frequencies in pachytene nuclei. >60 nuclei were examined for each strain and the error bars represent the standard error between two independent experiments. Two stars (\*\*) depict a significant ( $p = <0.002$ ) difference to wild type. Strains: wild type (Y712), *zip1* $\Delta$  (Y787), *zip3* $\Delta$  (Y1010), *zip2* $\Delta$  (Y813), *zip4* $\Delta$  (Y1133), *mer3* $\Delta$  (Y2172) and *msh4* $\Delta$  (Y790).



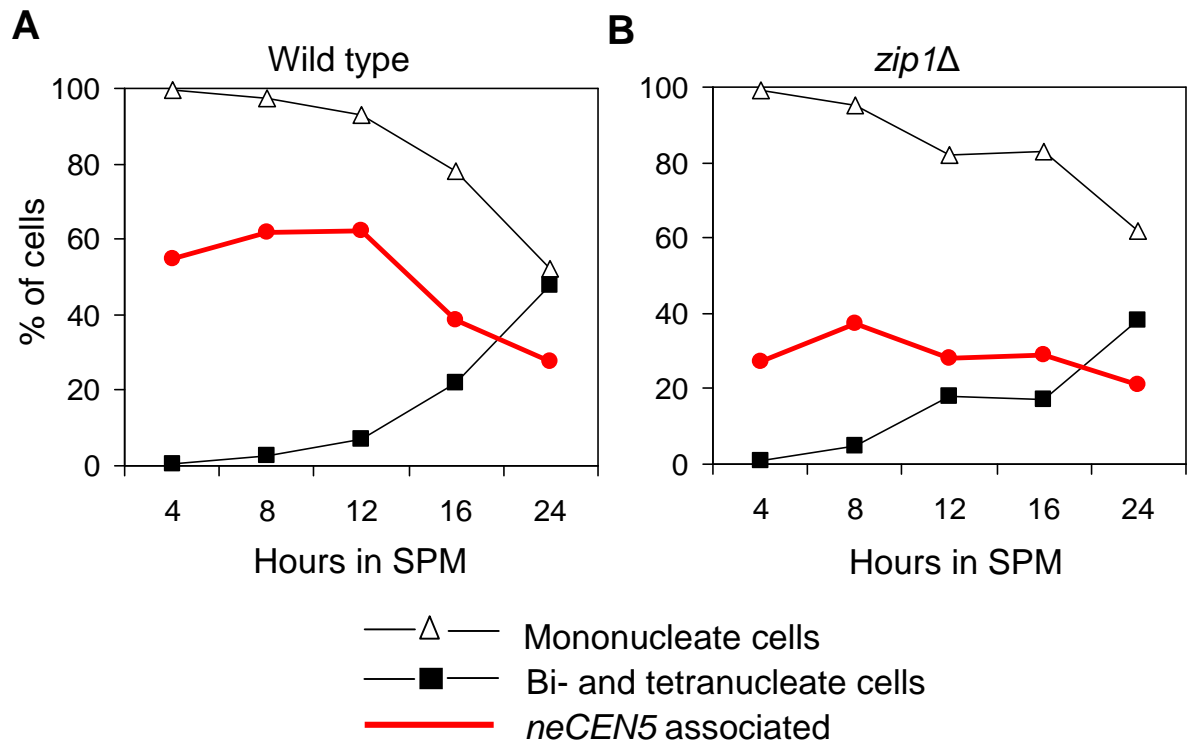


**Figure 4.4.** Time course analysis of *neCEN5* pairing frequencies for wild type and *zip1Δ* cells. Nuclear divisions (black lines) and *neCEN5* pairing (red line) is shown at the indicated time points after transfer into sporulation media for wild type (A) and *zip1Δ* (B) cells. Pairing of *neCEN5*s was inferred from the proportion of whole cells containing a single GFP focus.

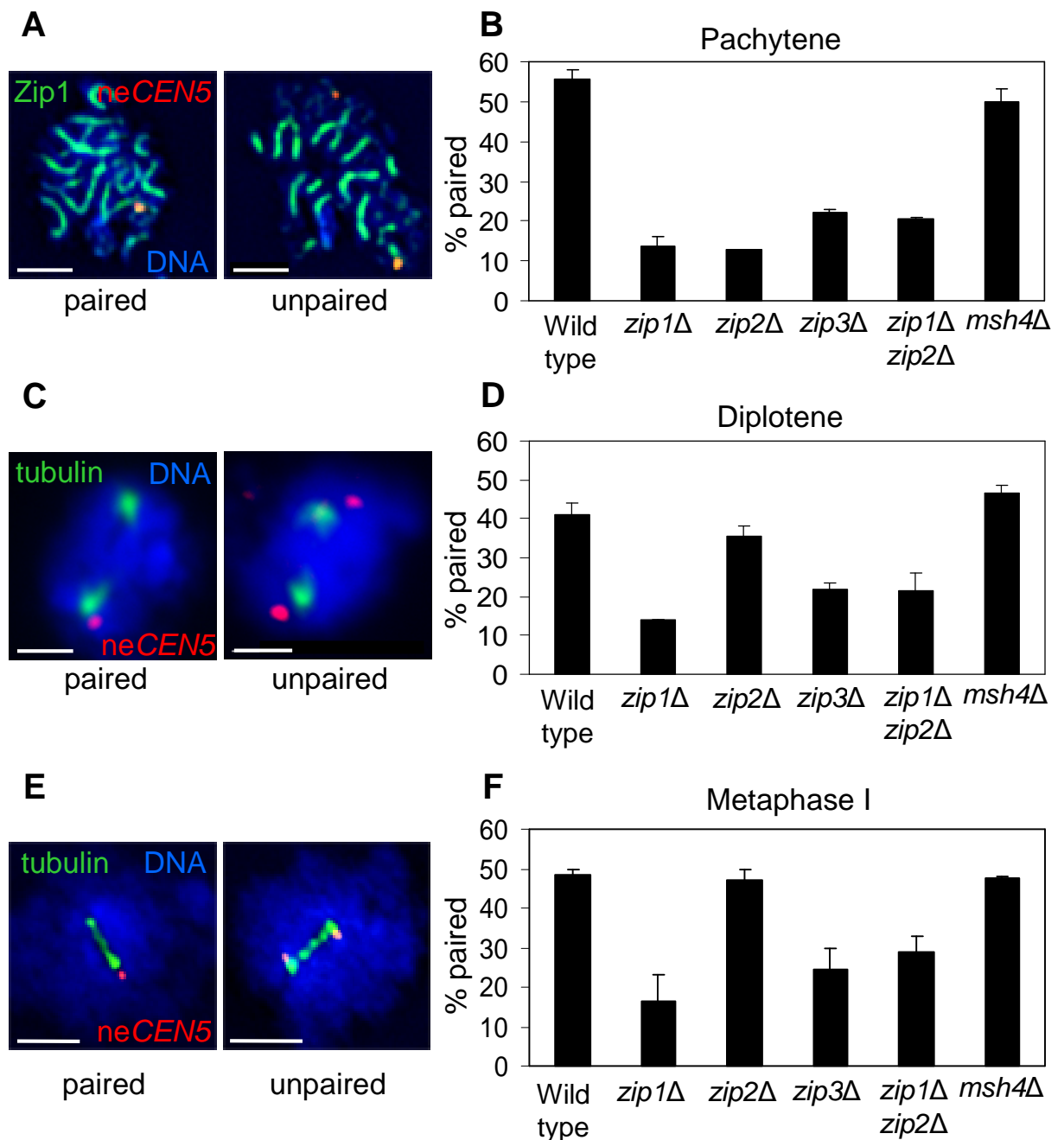


**Figure 4.5.** *neCEN5* pairing frequencies in pachytene, diplotene and metaphase I nuclei. Representative images of spread wild type nuclei with paired (left) and unpaired (right) *neCEN5*s for pachytene (A), diplotene (C) and metaphase I (E) stages. Zip1 is shown as green, *neCEN5*s in red and DNA in blue for A. Tubulin is shown in green, *neCEN5*s in red and DNA in blue for C and D. Bars: 2  $\mu$ m. Quantification of *neCEN5* pairing frequencies for pachytene (B), diplotene (D) and metaphase I (F) stages. >60 nuclei were examined for each strain at each stage and the error bars represent the standard error between two independent experiments. Strains: wild type (Y712), *zip1* $\Delta$  (Y787), *zip2* $\Delta$  (Y813), *zip3* $\Delta$  (Y1010), *zip1* $\Delta$  *zip2* $\Delta$  (Y983) and *msh4* $\Delta$  (Y790).

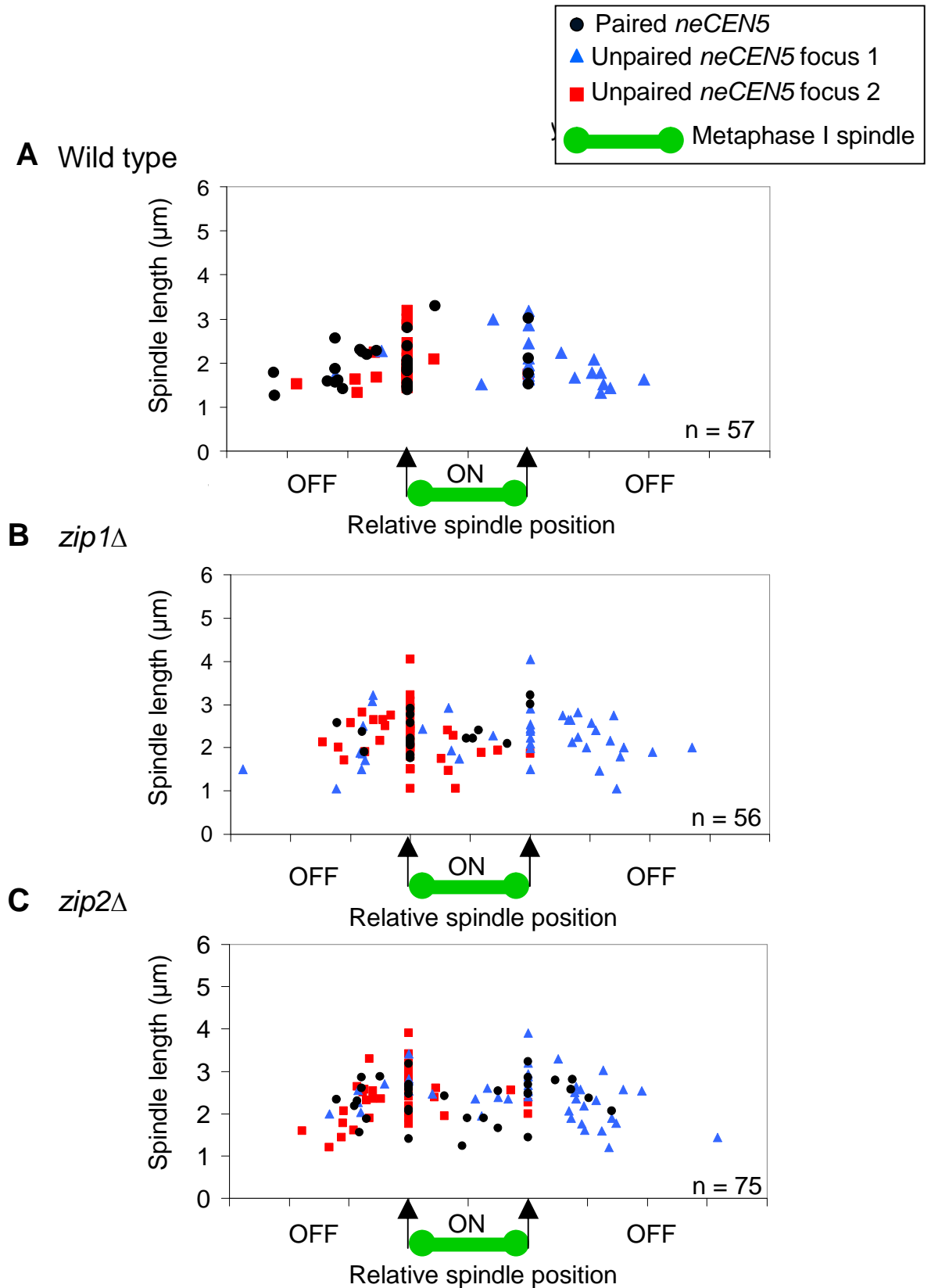
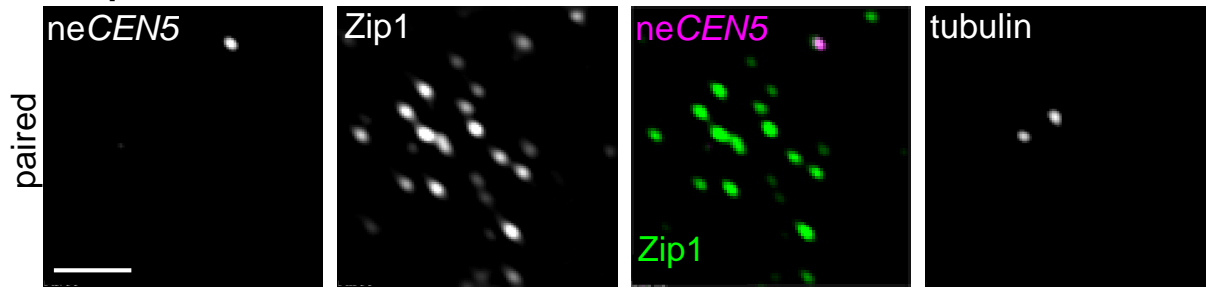


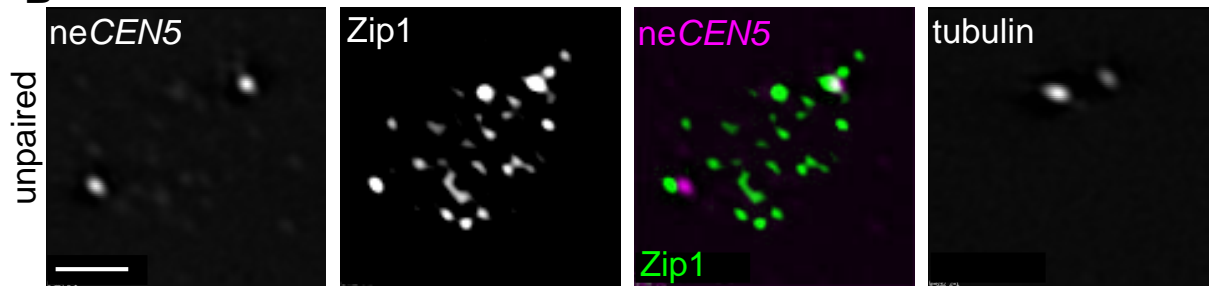
**Figure 4.6.** Analysis of *neCEN5* position relative to the metaphase I spindle for wild type, *zip1* $\Delta$  and *zip2* $\Delta$  cells. (A-C) Scatterplots showing the spindle length (y-axis) and the relative spindle position of the *neCEN5*s (x-axis), where data points between the two arrows on the x-axis represent the relative position of the *neCEN5* on the metaphase spindle. Values outside of this range represent the relative positions of *neCEN5*s that were not on the spindle. Black circles represent 'paired' *neCEN5*s, while blue triangles and red squares represent a pair of 'unpaired' *neCEN5*s. Strains: wild type (Y712), *zip1* $\Delta$  (Y787) and *zip2* $\Delta$  (Y813).

**Figure 4.7.** Zip1 co-localises with *neCEN5*s at diplotene and metaphase I. (A) Wild type nuclei in diplotene shown by separated spindle poles with Zip1 co-localised with the single 'paired' *neCEN5* focus. (B) Wild type diplotene nucleus with Zip1 co-localised with one of the two 'unpaired' *neCEN5*s. (C) Percent of wild-type diplotene nuclei with Zip1 co-localised to paired or unpaired *neCEN5*s. (D and E) Co-localisation of *neCEN5* and Zip1 at metaphase I. Zip1 is often found along the entire spindle (27/34 spindles examined). Zip1 is shown as green and *neCEN5* as magenta in merged images. Bars: 2  $\mu$ m. Strain: wild type (Y712).

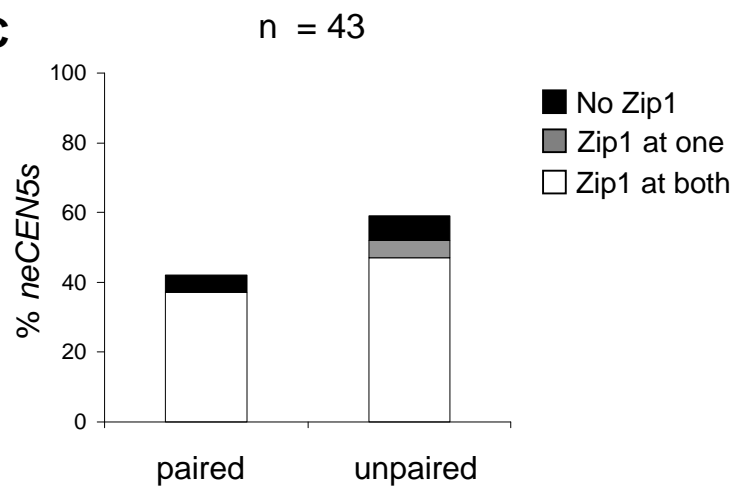
### A Diplotene



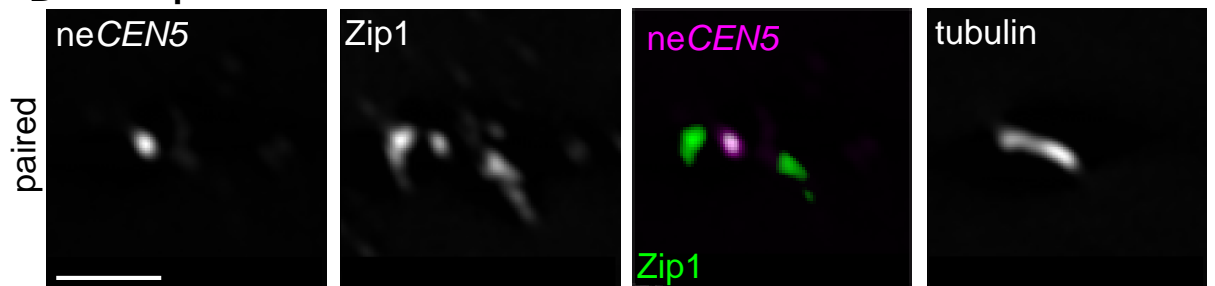
### B



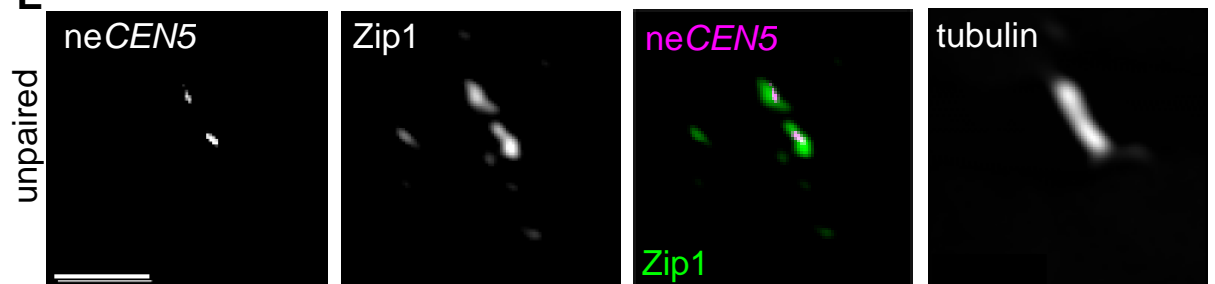
### C

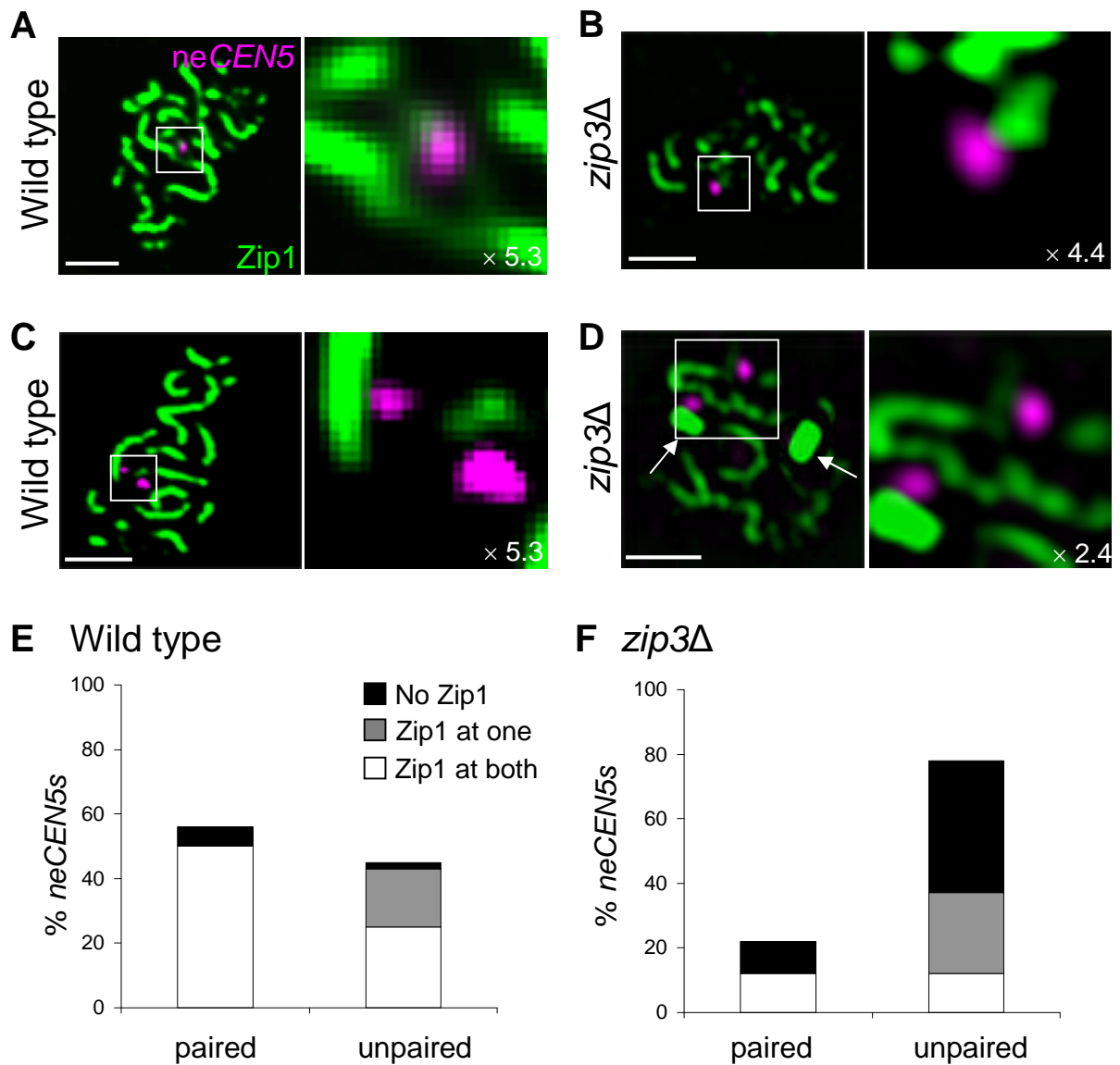


### D Metaphase I

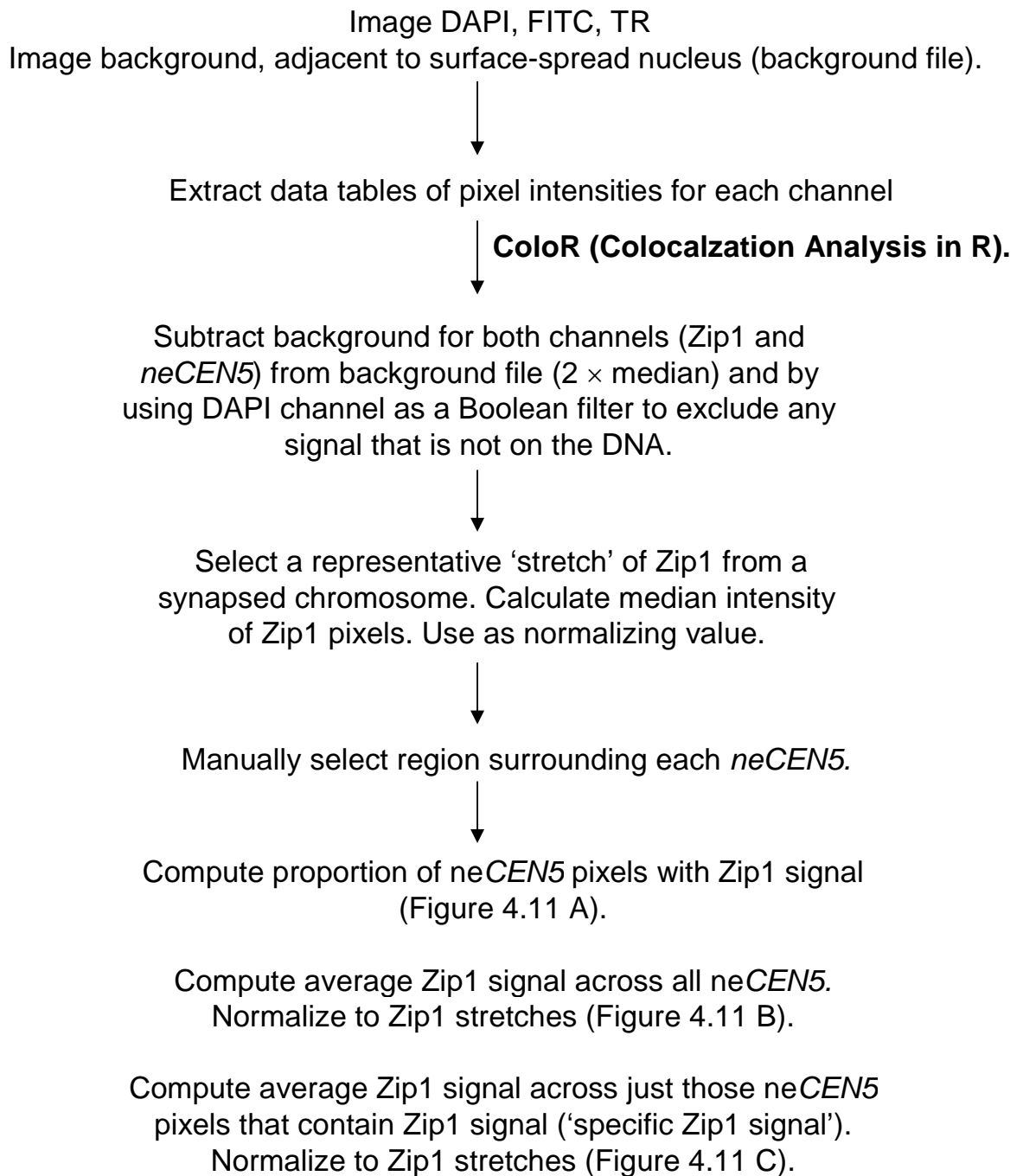


### E

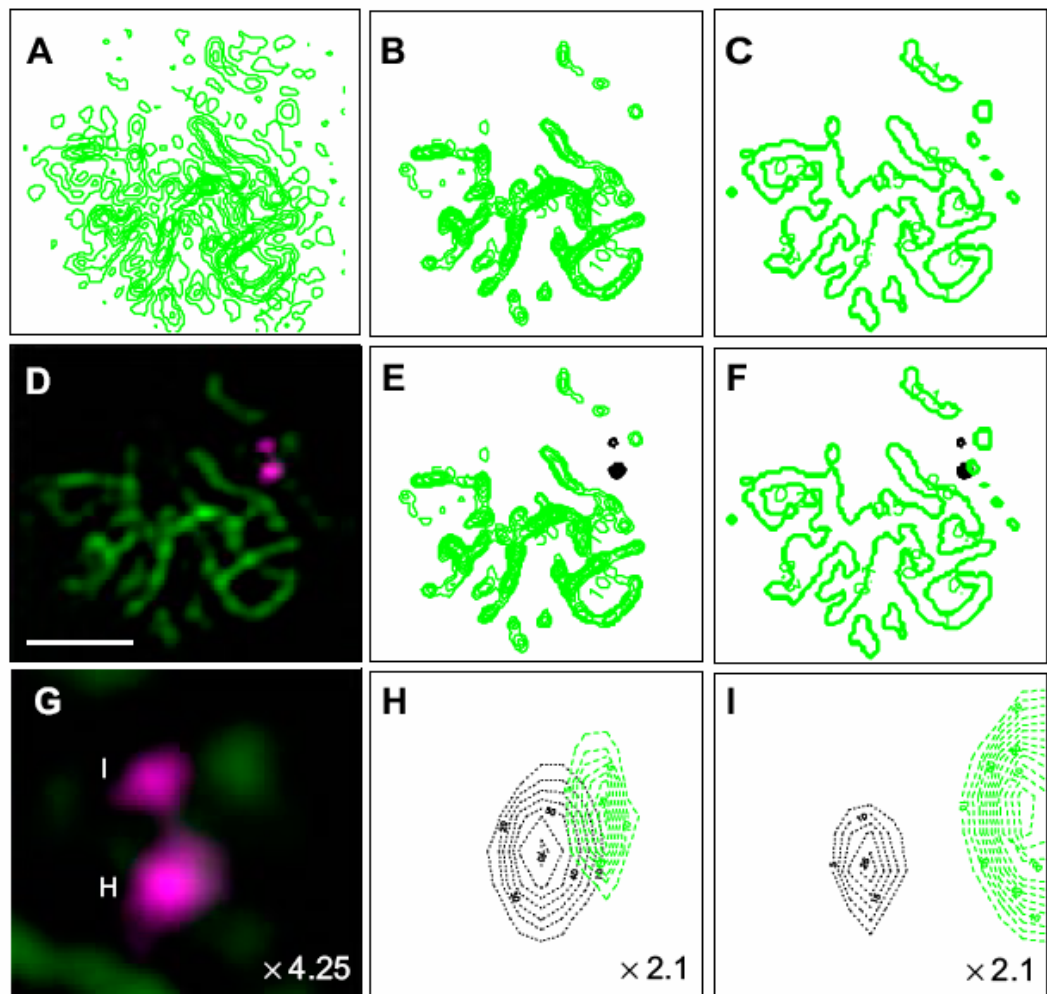




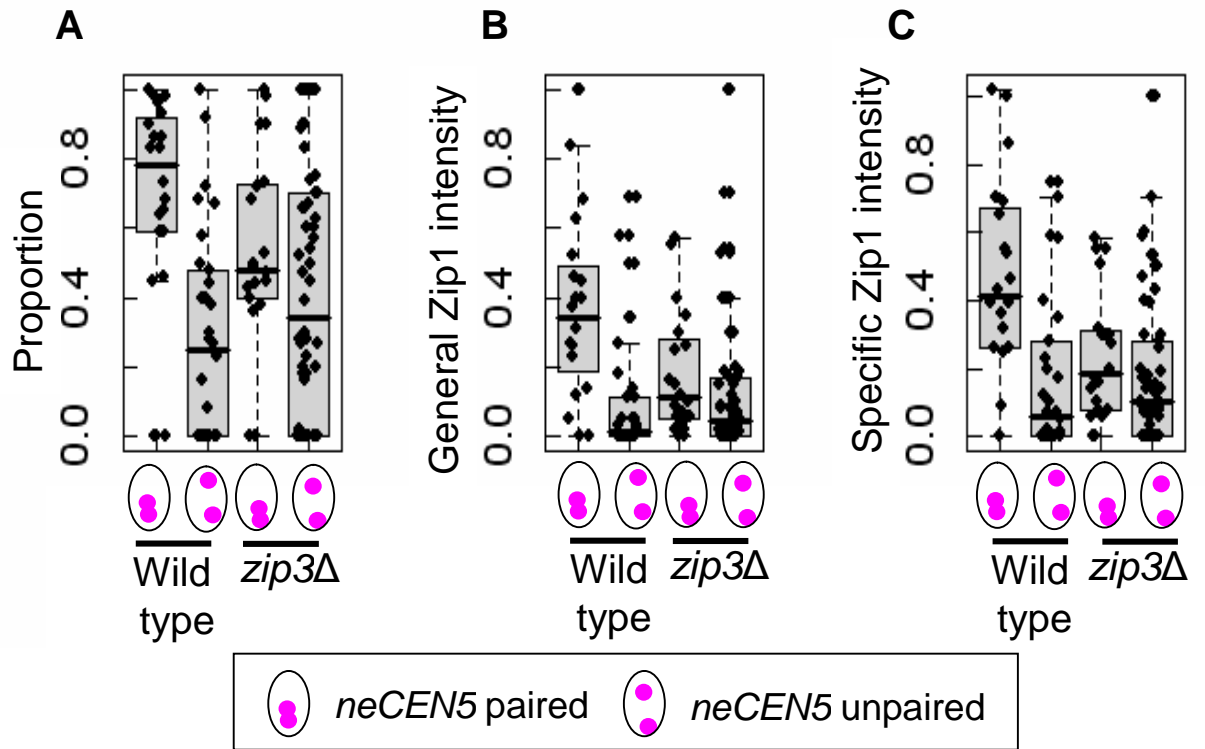
**Figure 4.8.** Zip1 co-localises with *neCEN5s* in pachytene nuclei in a Zip3-dependent manner. Example images of well-spread wild type pachytene nuclei with paired (A) and unpaired (C) *neCEN5s*. Example images of well-spread *zip3* $\Delta$  pachytene nuclei with paired (B) and unpaired (D) *neCEN5s*. Boxed regions containing *neCEN5s* are shown enlarged to the right of each image with the scale of magnification shown in the bottom right-hand corner. Bars: 2  $\mu\text{m}$ . Zip1 is shown as green and *neCEN5* as magenta. Proportions of paired and unpaired *neCEN5s* that have Zip1 co-localised in wild type (E) and *zip3* $\Delta$  (F) nuclei. > 60 nuclei were examined for each strain.



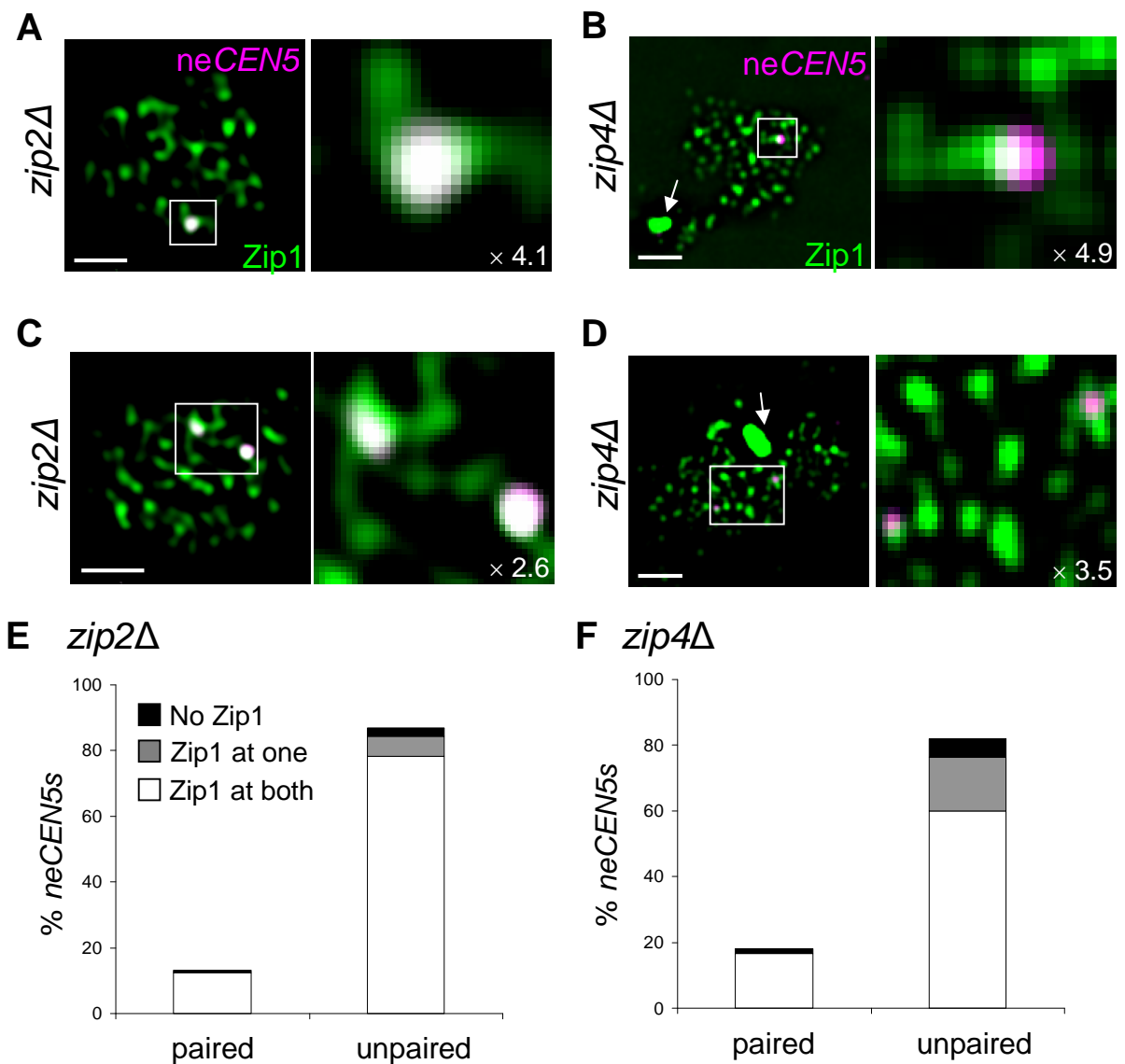
**Figure 4.9.** Flow diagram detailing the *neCEN5*-Zip1 co-localisation analysis using 'ColoR'. Following background subtraction, regions surrounding each *neCEN5* were manually selected and the proportion of Zip1-positive pixels as well as the relative intensity of Zip1 was calculated.



**Figure 4.10.** A representative image of a wild type pachytene nucleus used for the 'ColoR' analysis. Contour of Zip1 signal in the raw image (A), after background subtraction (B), and the total area included after background subtraction (Boolean, C). (D) Corresponding image from the Deltavision IX70, with Zip1 in green and *neCEN5* in magenta. Bar: 2 µm. (E) Contour image of *neCEN5* and Zip1, and co-localisation of *neCEN5* with Zip1 positive pixels (Boolean, F). (G) Enlargement of the area containing the two *neCEN5* foci compared to (D) followed by contour plots of the individual *neCEN5* (black) and Zip1 (green) signals (H and I). Scale of magnification is shown in the right hand corner.

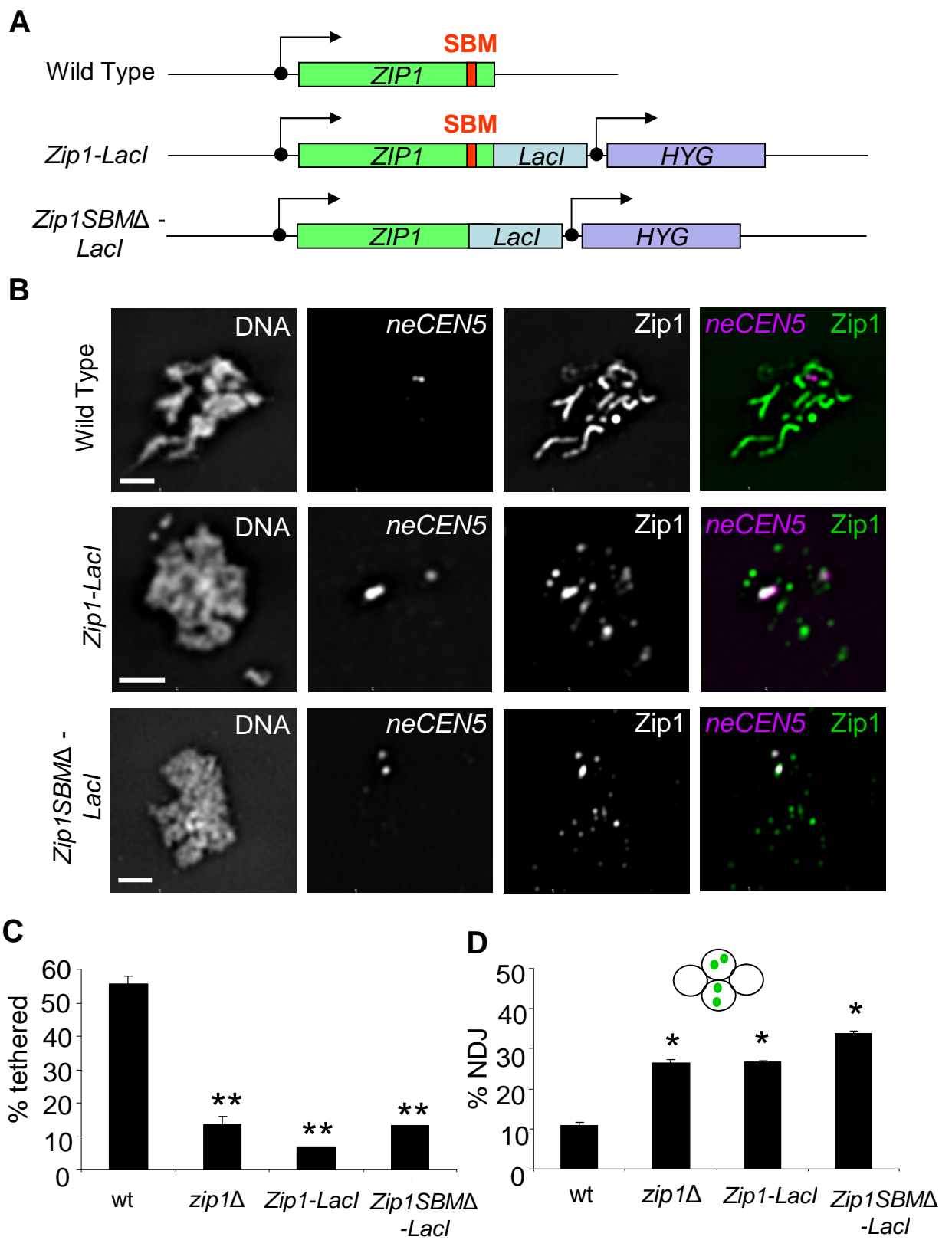


**Figure 4.11.** Analysis of Zip1-*neCEN5* co-localisation using ColoR. (A) Box-and-whisker plot showing the proportion of each *neCEN5* focus (paired and unpaired) that has Zip1 co-localised for wild type and *zip3Δ*. Each black dot represents a single *neCEN5* focus. The grey-shaded boxes denote the interquartile range (25th to 75th percentile) and the whiskers illustrate  $1.5 \times$  the interquartile range or the maximum or minimum value, whichever is lower. (B) General Zip1 intensity was calculated as the total overlapping Zip1 signal divided by the total area of each *neCEN5*. This was normalized against the mean Zip1 intensity of a synapsed pachytene chromosome. (C) Specific intensity of the Zip1 signal was calculated as the total overlapping Zip1 signal divided by the number of those Zip1-positive *neCEN5* pixels. This value was normalized as in (B).



**Figure 4.12.** Zip2 and Zip4 are dispensable for localisation of Zip1 to *neCEN5s* in pachytene nuclei. Example images of well-spread *zip2Δ* pachytene nuclei with paired (A) and unpaired (C) *neCEN5s*. Note that Zip1 appears to be accumulated at the *neCEN5s*. Example images of well-spread *zip4Δ* pachytene nuclei with paired (B) and unpaired (D) *neCEN5s*. Boxed regions containing *neCEN5s* are shown enlarged to the right of each image with the scale of magnification shown in the bottom right-hand corner. Bars: 2  $\mu$ m. Zip1 is shown as green and *neCEN5* as magenta. Proportions of paired and unpaired *neCEN5s* that have Zip1 co-localised in *zip2Δ* (E) and *zip4Δ* (F) nuclei. > 60 nuclei were examined for each strain. Strains: *zip2Δ* (Y813) and *zip4Δ* (Y1133).

**Figure 4.13.** Zip1-LacI fusion protein fails to ‘tether’ centromeres of the non-exchange chromosomes despite proficient localisation to *LacO* repeats. (A) Zip1-LacI fusion proteins were constructed with and without the C-terminus SUMO binding motif (SBM). This was done by placing the *LACI* coding region just before the stop codon of *ZIP1*, or in the case of the *Zip1-SBM $\Delta$ -LacI* allele the LacI sequence was placed 2562bp into the Zip1 coding region that corresponds to the start of Zip1’s SBM (854 amino acids into protein sequence). (B) Representative images of pachytene nuclei for wild type and Zip1-LacI strains with and without the SUMO binding motif (SBM). Zip1 is shown in green and *neCEN5*s in magenta in merged images. Bars: 2  $\mu$ m. (C) *neCEN5* pairing frequencies during pachytene for wild type, *zip1 $\Delta$*  and the Zip1-LacI strains with and without SBM. ~30 nuclei were examined for each strain. 96 % and 97 % of *neCEN5*s had Zip1 co-localised in the Zip1-LacI (no SBM) and the Zip1-LacI (with SBM) strains, respectively. (D) Meiosis I non-disjunction frequencies as assessed from visualization of GFP in tetrads for wild type, *zip1 $\Delta$*  and the Zip1-LacI strains with and without SBM. >100 tetrads were scored for each strain. Strains: wild type (Y712), *zip1 $\Delta$*  (Y787), *Zip1-LacI* (Y2117) and *Zip1SBM $\Delta$ -LacI* (Y2116).



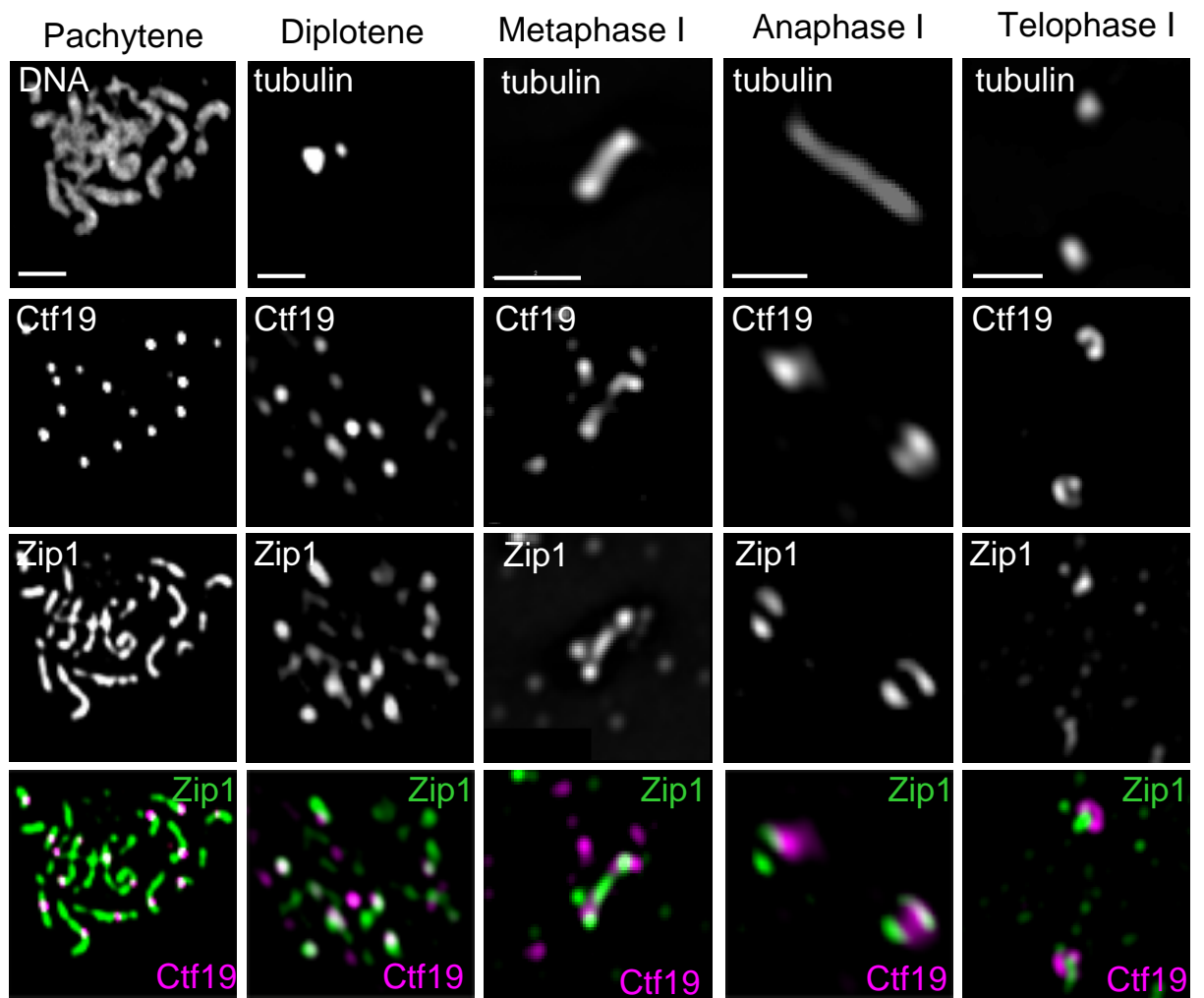


**Figure 4.14.** Zip1 remains associated with the centromeres of exchange chromosomes following SC disassembly. (A) Representative images of pachytene, diplotene, metaphase, anaphase, and telophase nuclei from wild type stained for DNA, tubulin, Zip1, and Myc-tagged Ctf19 (centromeres). At diplotene, 75 % of Ctf19 foci have Zip1 co-localised, 11 % have Zip1 juxtaposed and 14 % of centromeres are not associated with Zip1 (n =543 Ctf19 foci, 31 nuclei inspected). Diplotene nuclei displayed  $23 \pm 5$  (SD) Zip1 foci per nucleus, and 59 % of these co-localised with centromeres. Bars: 2  $\mu$ m. Strain: wild type (Y636).

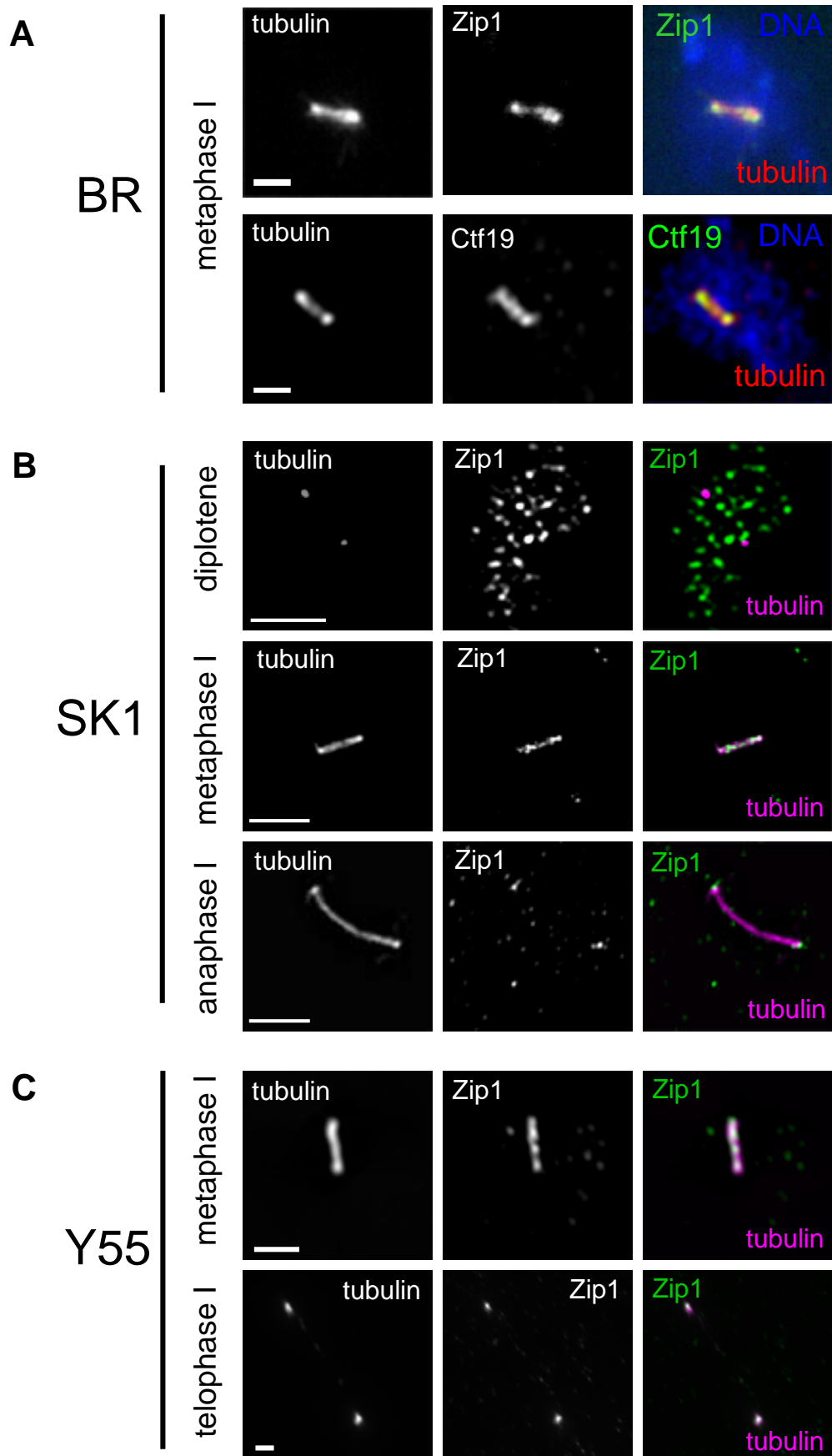


**Figure 4.15.** Zip1 is detected following SC disassembly in three different strain backgrounds. Example images of Zip1 staining in wild type nuclei in metaphase I, anaphase I or telophase for BR (A), SK1 (B) and Y55 (C) strain backgrounds. 40/40 metaphase I spindles observed in Y55 contained Zip1 staining. Bars: 2  $\mu$ m. Strains: BR (Y636), SK1 (Y1688) and Y55 (Y650) all are wild type.

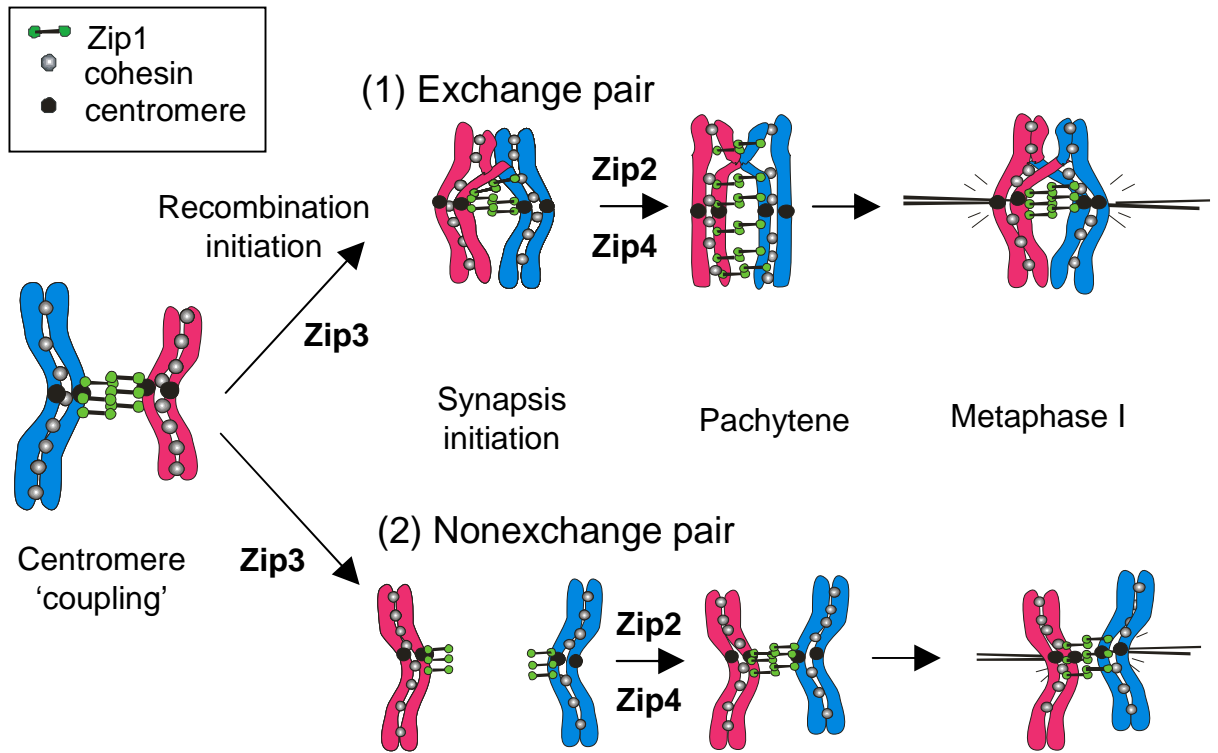


**Figure 4.16.** Model for how Zip1 promotes the segregation of both non-exchange and exchange chromosomes at meiosis I. Early on in meiotic prophase, prior to the onset of recombination Zip1 'couples' centromeres together independently of homology. Initiation of recombination signals homologous pairing of chromosomes. Exchange chromosomes become fully synapsed by Zip1 at pachytene. Chromosome pairs that fail to crossover are paired at the centromeres by Zip1. Zip3 is required for the localisation of Zip1 to the centromeres of exchange chromosomes whereas Zip2 and Zip4 are required to enable Zip1 to 'tether' centromeres. Following SC disassembly, Zip1 remains at the centromeres of all chromosome pairs where it assists in bi-polar spindle attachment that promotes their disjunction at the reductional division.

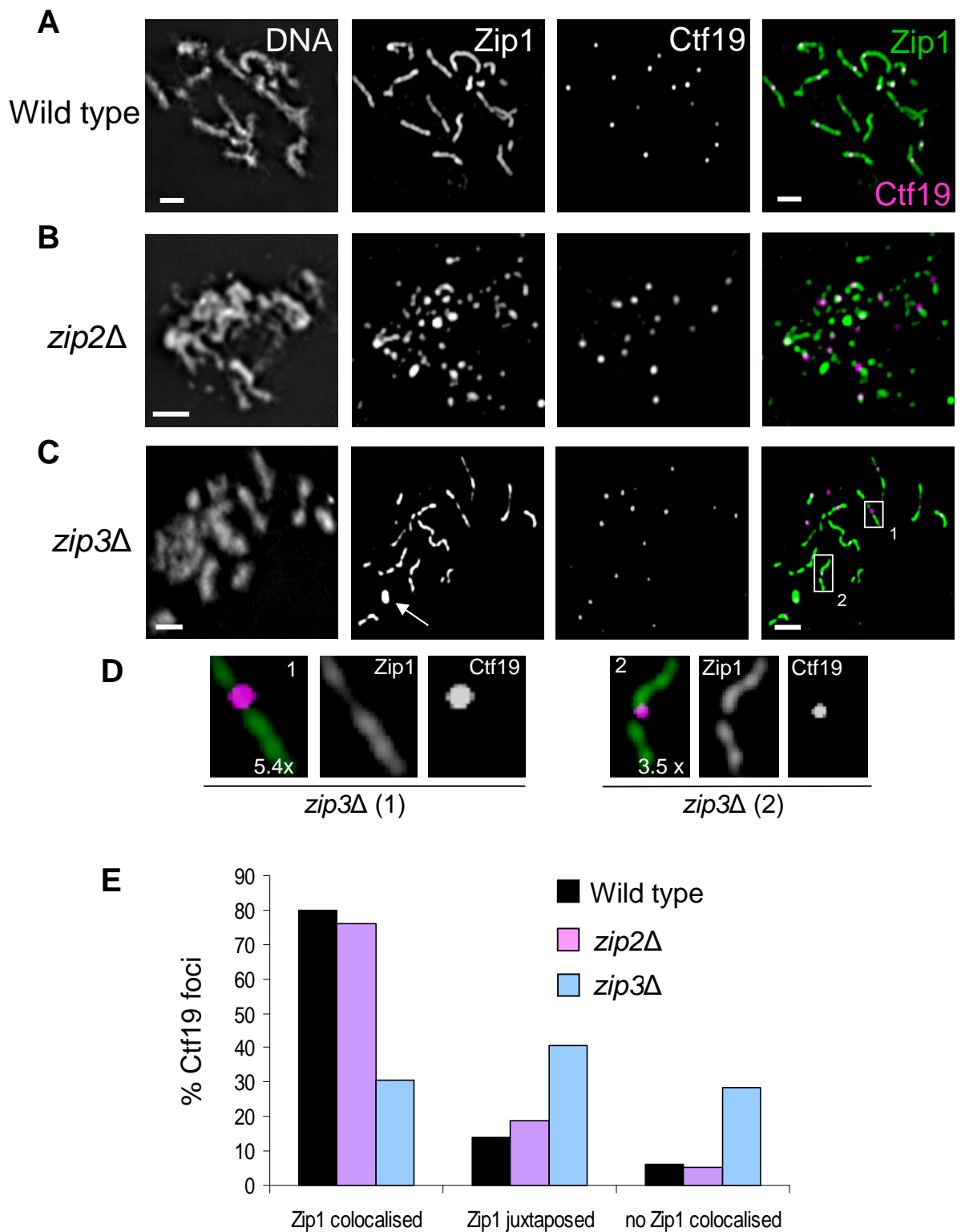


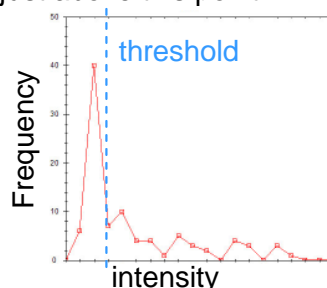
**Figure 5.1.** Zip1 localisation to centromeres during pachytene is different for *zip2* $\Delta$  and *zip3* $\Delta$  mutants. Representative images of a wild type (A), *zip2* $\Delta$  (B) and *zip3* $\Delta$  (C) pachytene nuclei. In the merged image, Zip1 is shown in green and Ctf19-13Myc in magenta. Bars: 2  $\mu$ m. Arrows indicate polycomplexes. (D) The boxed regions shown in (C) at a higher magnification. Scale of enlargement is shown in the bottom, right-hand corner. (E) Quantification of the number of Ctf19 foci that have Zip1 co-localised, Zip1 juxtaposed (touching, but not overlapping) or no Zip1 co-localised during pachytene for wild type, *zip2* $\Delta$  and *zip3* $\Delta$  mutants. The number of Ctf19 analysed were 213 (wild type), 341 (*zip2* $\Delta$ ) and 404 (*zip3* $\Delta$ ) from 15, 22 and 28 nuclei respectively. Strains: Y1293 (wild type), Y1269 (*zip2* $\Delta$ ) and Y1274 (*zip3* $\Delta$ ).

Capture image (DAPI, FITC, TR etc.) → Extract data matrix of pixel intensities for each channel

### 1. Background Subtraction

The program identifies all peaks within a file matrix and plots their frequency vs. intensity. The very frequent, low intensity peaks are identified as background 'noise' and the program sets the threshold just above this point.

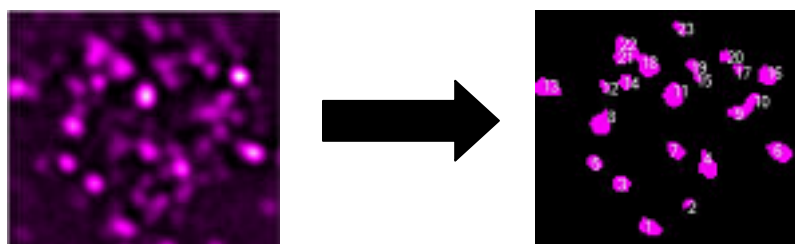
Typical frequency plot of the peaks in a Ctf19 channel:



### 2. Peak/Foci Identification

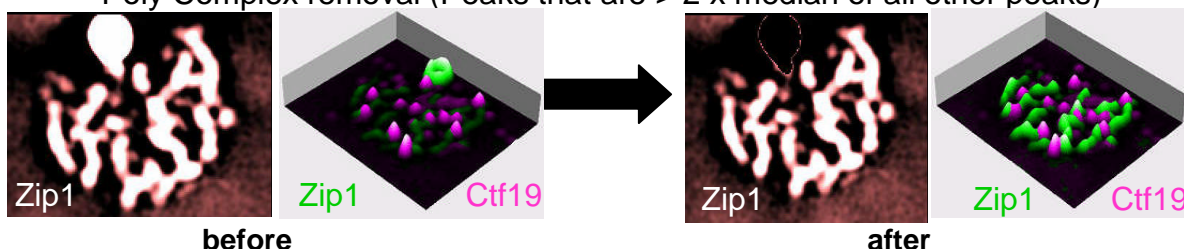
(i) All peaks above this threshold proceed for full identification. This is achieved by iteratively analysing each pixel at the perimeter of each peak ('edge-detection' algorithms). Pixels with lower intensity at the perimeter are added to the current peak, down to the point of the threshold defined in the previous step, or where two peaks converge (local minimum). This allows for resolution of two foci that are close together (Du *et al.* 2006).

(ii) Peaks are identified and assigned an ID.



### 3. Peak/Foci Validation

- Size exclusion (e.g. exclude Ctf19 foci that are <10 pixels)
- Poly Complex removal (Peaks that are > 2 x median of all other peaks)

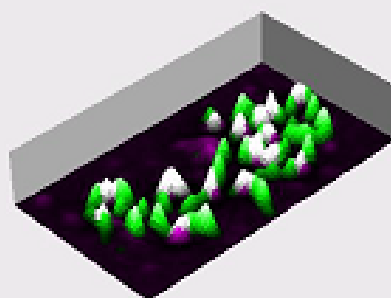
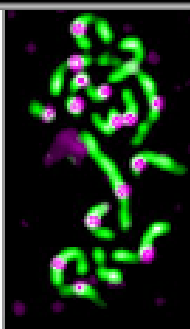
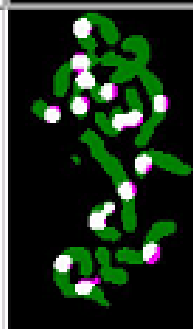
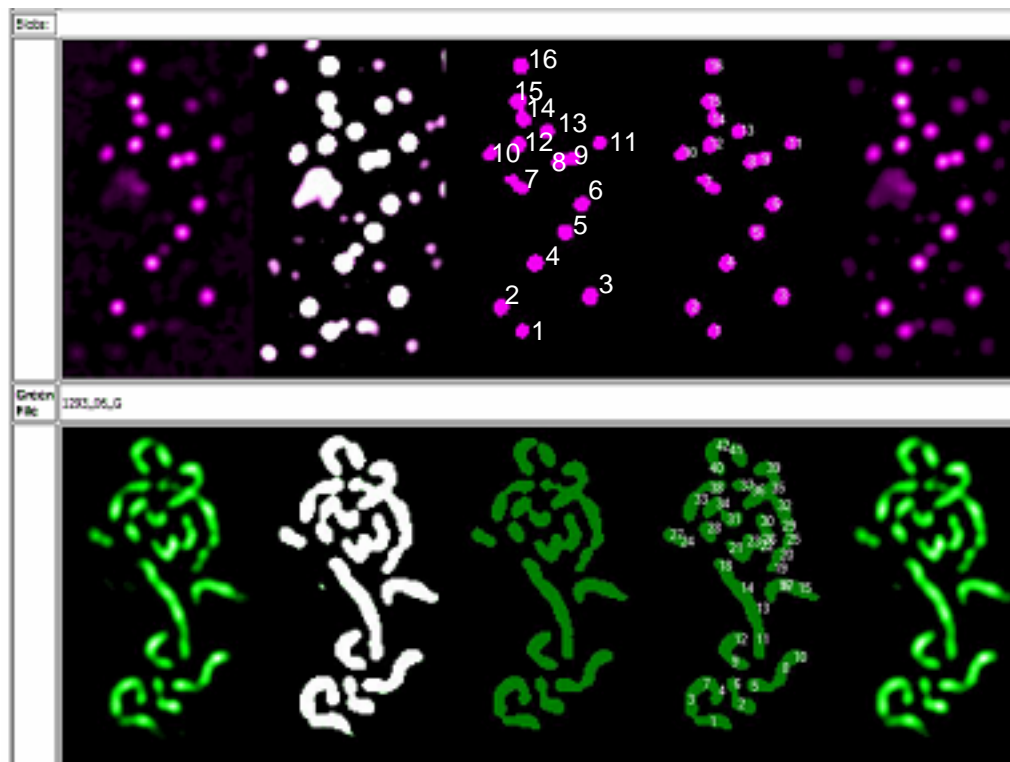


### 4. Analysis

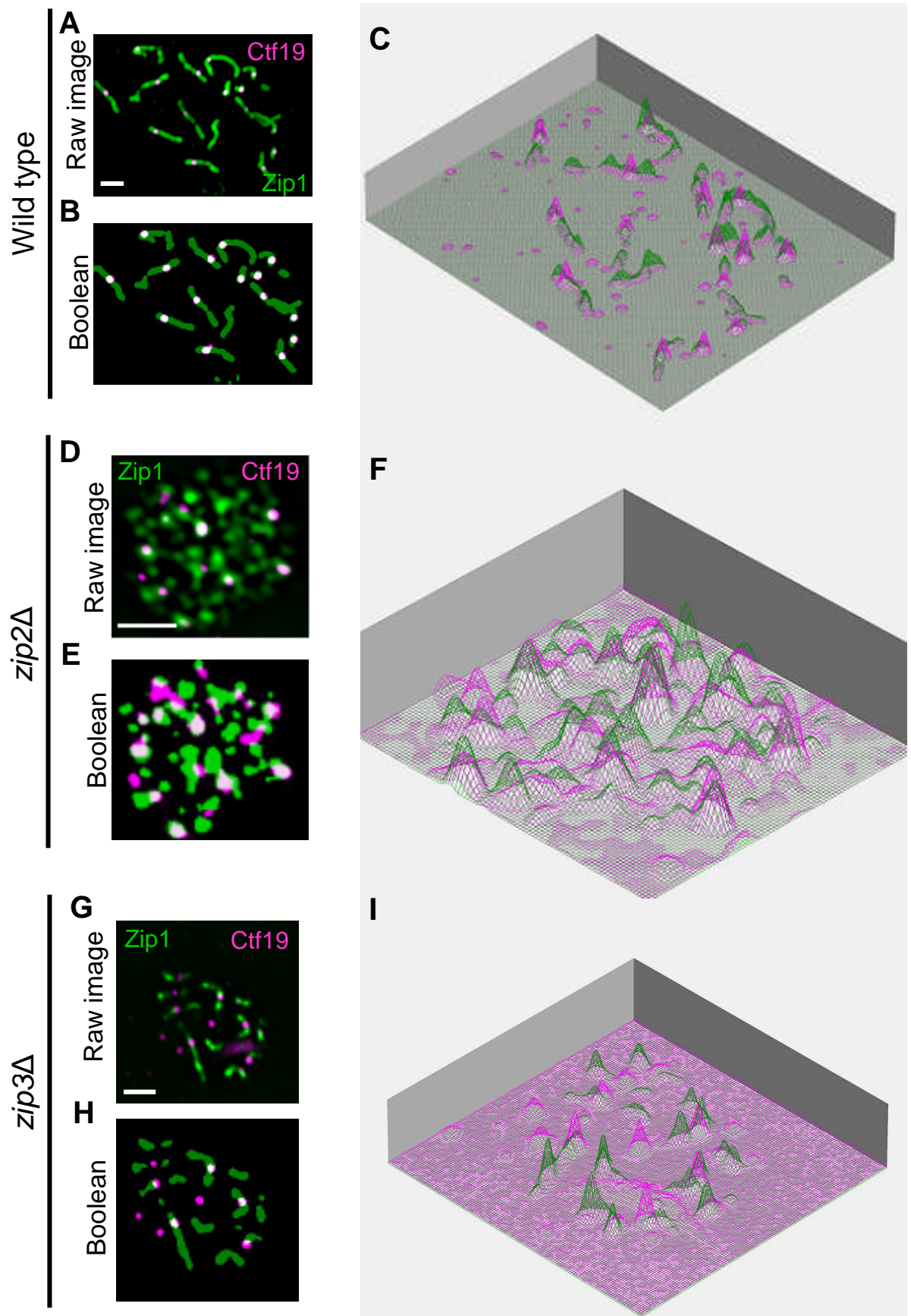
- The % area overlapping with green (Zip1)
- Of this overlapping region, the avg. intensity of green (Zip1) normalised to the avg. green of the entire image. (*i.e.* How the amount of Zip1 at centromeres compares to the arm regions)

**Figure 5.2.** Schematic flow diagram of how 'ColoS' performs automated object detection and quantifies protein co-localisation. See text for description.

**Figure 5.3.** Typical example of the output file generated for each image by 'ColoS'. Graphical outputs for each channel are shown with the raw image (far left) and processed image (right) with each object defined by the program assigned an ID number. The channels are overlaid in the graphics given in the third row. Below is a breakdown of the statistics calculated for each Ctf19 focus with the focus ID given on the left and the statistics (Size of focus, Mean Zip1 intensity, Proportion of Ctf19 containing Zip1 signal, normalised Zip1 intensity).

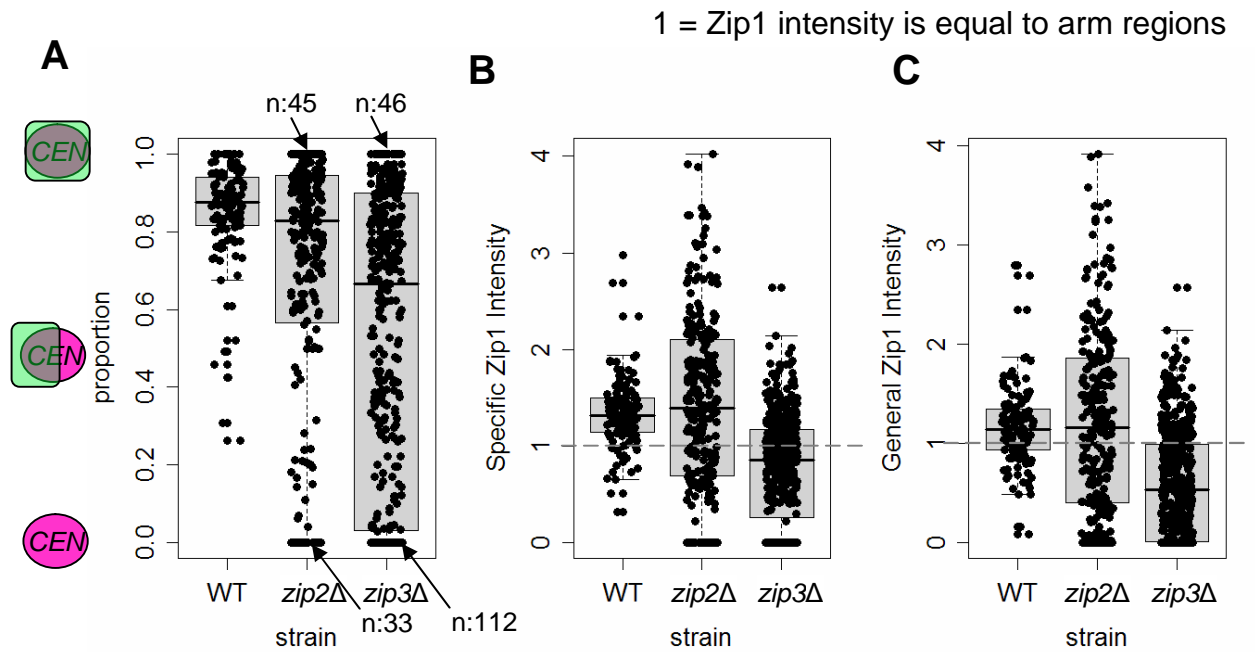


Total Green Mean:	4648.32235621521
Foci ID : 1	Mean Int. : 3049.8275862069
	Mean Green Int. : 5690.14285714286
	Overlap Coverage : 0.7241379
	Size : 58
	Normalised Green Overlap Int. : 1.2241282813647
Foci ID : 2	Mean Int. : 4366.37735849057
	Mean Green Int. : 5904.72549019608
	Overlap Coverage : 0.9622642
	Size : 53
	Normalised Green Overlap Int. : 1.2702917391908
Foci ID : 3	Mean Int. : 3838.46875
	Mean Green Int. : 5339.64102564103
	Overlap Coverage : 0.609375
	Size : 64
	Normalised Green Overlap Int. : 1.14872433890078
Foci ID : 4	Mean Int. : 3784.0843373494
	Mean Green Int. : 6498.67088607595
	Overlap Coverage : 0.9518072
	Size : 83
	Normalised Green Overlap Int. : 1.39806803144508
Foci ID : 5	Mean Int. : 4272.03448275862
	Mean Green Int. : 6224.78723404255
	Overlap Coverage : 0.8103448
	Size : 58
	Normalised Green Overlap Int. : 1.33914706361091
Foci ID : 6	Mean Int. : 3890.50909090909
	Mean Green Int. : 5733.10416666667
	Overlap Coverage : 0.8727273
	Size : 55
	Normalised Green Overlap Int. : 1.2333706071398
Foci ID : 7	Mean Int. : 4479.72043010753
	Mean Green Int. : 6992.10126582278
	Overlap Coverage : 0.8494624

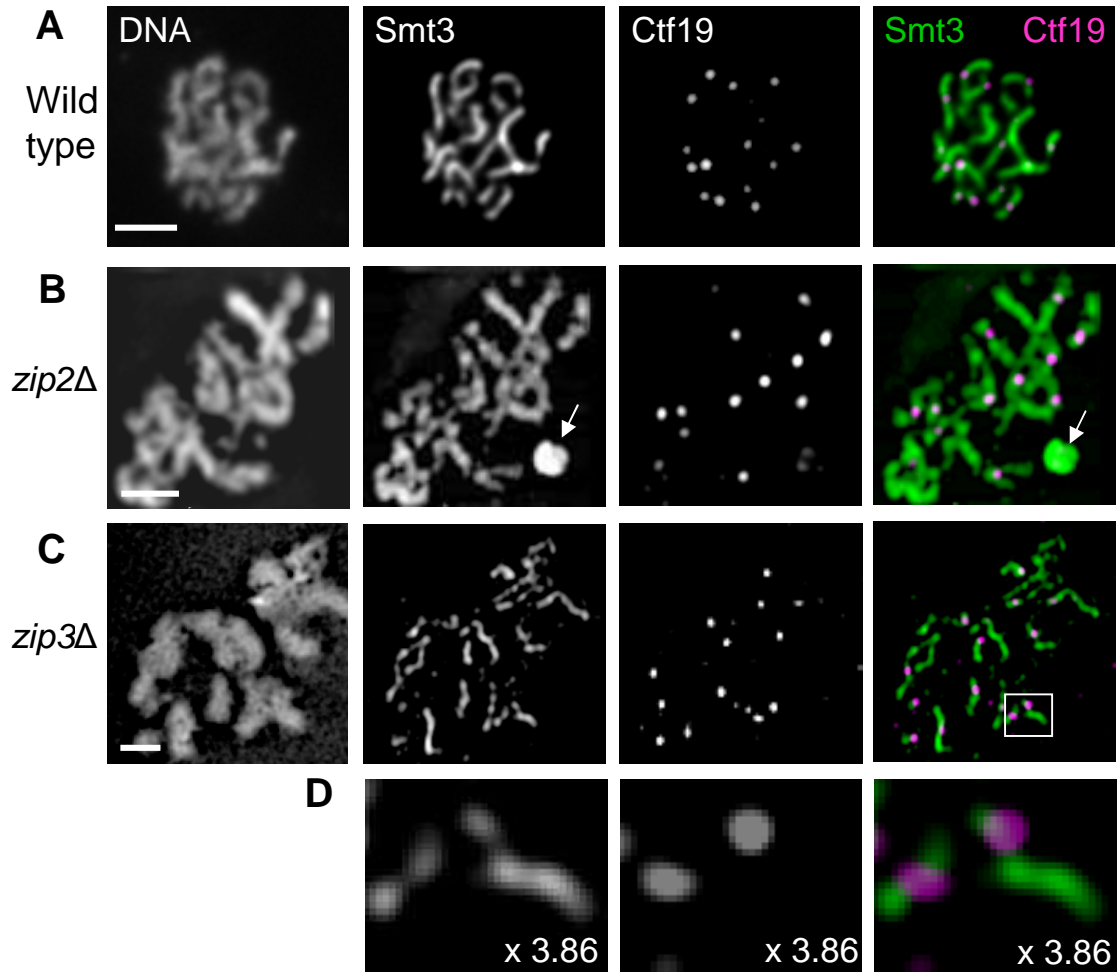


**Figure 5.4.** A comparison of the raw, unprocessed images with corresponding graphical outputs following automated object-detection. (A) Raw image of a wild type pachytene nucleus with Zip1 shown in green and Ctf19 in magenta. Bars: 2  $\mu\text{m}$ . (B) Processed image showing all pixels above the threshold in a Boolean plot. (C) 3D contour plot of the overlaid Zip1 (green) and Ctf19 (red) channels. (D-F) The equivalent images as A-C, but *zip2Δ* mutants. (G-I) The equivalent images as A-C, but *zip3Δ* mutants.

Figure 5.5

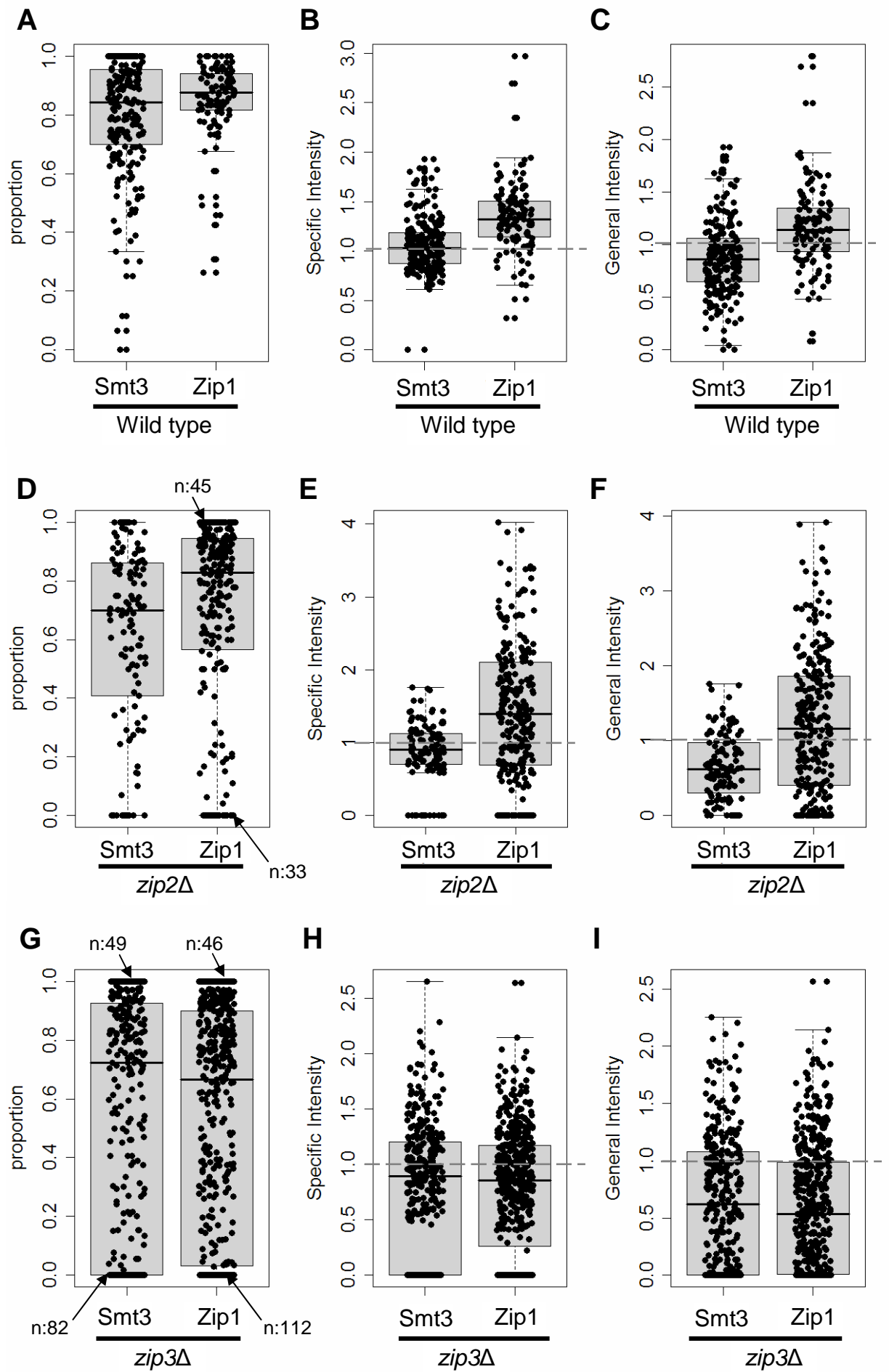


**Figure 5.5.** The results of Zip1-Ctf19 co-localisation analysis done using 'ColoS'. (A) Boxplot showing the proportion of each Ctf19 focus that contained Zip1 for wild type, *zip2Δ* and *zip3Δ* mutants. The values range from 0 to 1 corresponding with 0% to 100% of Ctf19 pixels containing Zip1. The grey-shaded boxes denote the interquartile range (25th to 75th percentile) and the whiskers illustrate 1.5 × the interquartile range or the maximum or minimum value, whichever is lower. Where the number of values saturates the width of the graph, actual numbers are given (arrows). (B) Boxplot showing the 'Specific' Zip1 intensity for each Ctf19 focus for wild type, *zip2Δ* and *zip3Δ* mutants. 'Specific' Zip1 intensities are derived by taking the mean Zip1 intensity of each Ctf19 focus and dividing it by the number of Zip1-positive Ctf19 pixels. This value is then normalised to the mean intensity of all Zip1 pixels in the image that do not overlap with Ctf19. (C) Boxplot showing the 'General' Zip1 intensity for each Ctf19 focus for wild type, *zip2Δ* and *zip3Δ* mutants. 'General' Zip1 intensities are derived by taking the mean Zip1 intensity of each Ctf19 focus and averaging it out across the whole Ctf19 focus. This value is then normalised to the mean intensity of all Zip1 pixels in the image that do not overlap with Ctf19. For both 'Specific' and 'General' Zip1 intensities, values of 1 (dotted line) indicate equal Zip1 intensity to that of arm regions. The number of Ctf19 foci analysed are 115 (wild type), 260 (*zip2Δ*) and 451 (*zip3Δ*).



**Figure 5.6. localisation of Smt3<sup>SUMO</sup> during pachytene in wild type, *zip2Δ* and *zip3Δ* nuclei.** Representative images of wild type (A), *zip2Δ* (B) and *zip3Δ* (C) pachytene nuclei. In the merged image, Smt3<sup>SUMO</sup> is shown in green and Ctf19-13Myc in magenta. Bars: 2  $\mu$ m. Arrows indicate polycomplexes. (D) The boxed regions shown in C at a higher magnification. Scale of enlargement is shown in the bottom, right-hand corner. Strains: Y1293 (wild type), Y1269 (*zip2Δ*) and Y1274 (*zip3Δ*).

**Figure 5.7.** Boxplots comparing the co-localisation of Zip1 and Smt3<sup>SUMO</sup> with centromeres, during pachytene. 'ColoS' was used to calculate the 'proportion' of Ctf19 foci containing Smt3<sup>SUMO</sup> signal and the relative intensity of centromeric Smt3<sup>SUMO</sup> signal compared to arm regions. For description see figure 5.5 or main text. Where the number of values saturates the width of the graph, actual numbers are given (arrows). Boxplots showing the proportion of each Ctf19 containing Zip1 and Smt3<sup>SUMO</sup> for wild type (A), *zip2Δ* (D) and *zip3Δ* (G) pachytene nuclei. Boxplots showing the 'Specific' intensities of centromeric Zip1 and Smt3<sup>SUMO</sup> in wild type (B), *zip2Δ* (E) and *zip3Δ* (H) pachytene nuclei. Boxplots showing the 'General' intensities of centromeric Zip1 and Smt3<sup>SUMO</sup> in wild type (C), *zip2Δ* (F) and *zip3Δ* (I) pachytene nuclei. A value of 1 indicates equal intensity to the arm regions (dotted lines). The same nuclei were not used for Zip1 and Smt3<sup>SUMO</sup> analyses. The number of Ctf19 analysed for Smt3<sup>SUMO</sup> co-localisation were 207 (wild type), 121 (*zip2Δ*) and 389 (*zip3Δ*). Strains: Y1293 (wild type), Y1269 (*zip2Δ*) and Y1274 (*zip3Δ*).



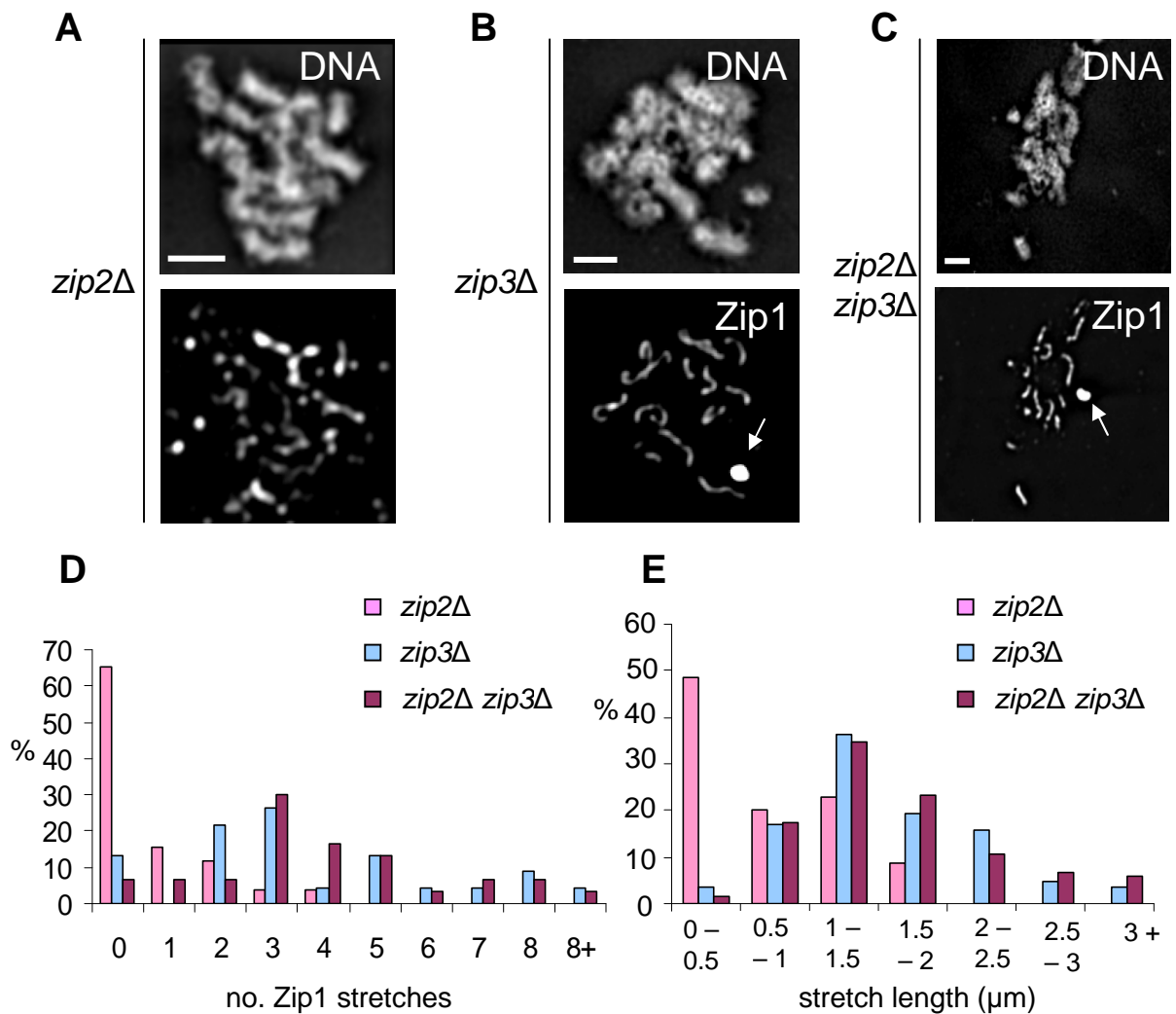
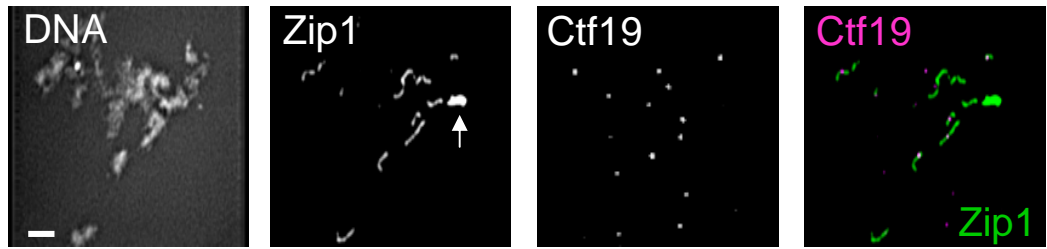


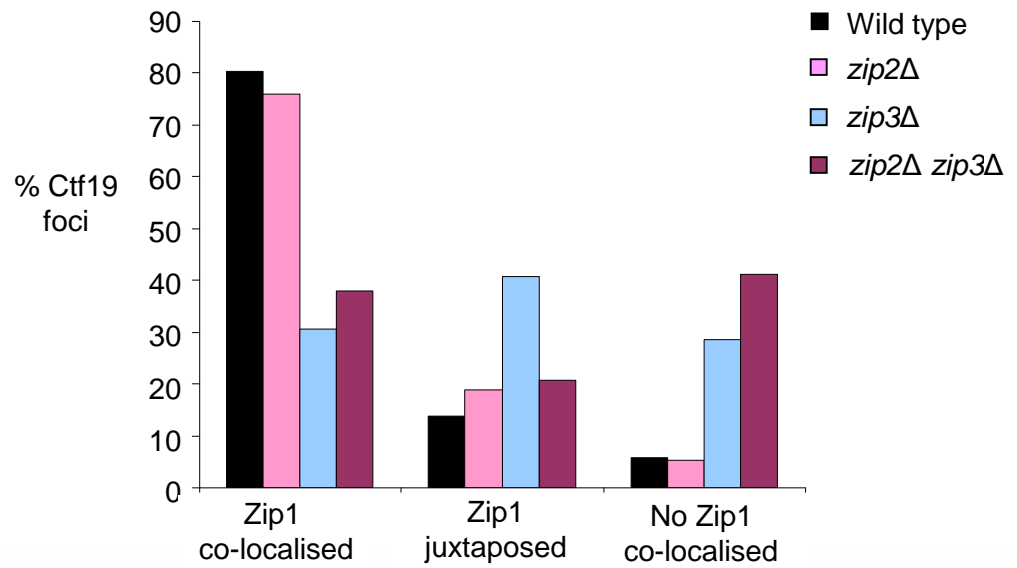
**Figure 5.8.** Synapsis is indistinguishable in *zip3Δ* and *zip2Δ zip3Δ* mutants. Example images of pachytene nuclei from *zip2Δ* (A), *zip3Δ* (B) and *zip2Δ zip3Δ* (C) mutants. (D) Histogram showing the number of Zip1 stretches in pachytene nuclei of *zip3Δ*, *zip2Δ* and *zip2Δ zip3Δ* mutants. (E) Histogram showing the length of Zip1 stretches in pachytene nuclei for *zip3Δ*, *zip2Δ* and *zip2Δ zip3Δ* mutants. The number of nuclei analysed was 26 for the *zip2Δ* mutant, 23 for the *zip3Δ* mutant and 30 for the *zip2Δ zip3Δ* mutant. Bars: 2 μm. Arrows indicate poly-complexes. Strains: Y1269 (*zip2Δ*), Y1274 (*zip3Δ*) and Y1907 (*zip2Δ zip3Δ*).

**Figure 5.9.** The association of Zip1 with centromeres in *zip2Δzip3Δ* pachytene nuclei. (A) Example image of a spread *zip2Δzip3Δ* pachytene nucleus. In the merged image, Zip1 is shown in green and Ctf19 in magenta. Arrows indicate polycomplexes. Bars: 2 μm. (B) Quantification of 'classical' co-localisation analysis of Zip1 and Ctf19 for wild type, *zip2Δ*, *zip3Δ* and *zip2Δzip3Δ*. The number of Ctf19 analysed were 213 (wild type), 341 (*zip2Δ*), 404 (*zip3Δ*) and 327 (*zip2Δzip3Δ*). (C) Boxplot showing the proportion of each Ctf19 focus that contained Zip1 for wild type, *zip2Δ*, *zip3Δ* and *zip2Δzip3Δ* mutants as measured using 'ColoS'. Boxplots showing the 'Specific' (D) and 'General' (E) Zip1 intensities for each Ctf19 focus in wild type, *zip2Δ*, *zip3Δ* and *zip2Δzip3Δ* mutants as assessed by 'ColoS'. The number of Ctf19 foci analysed using 'ColoS' are 115 (wild type), 260 (*zip2Δ*), 451 (*zip3Δ*) and 325 (*zip2Δzip3Δ*). Strains: Y1293 (wild type), Y1269 (*zip2Δ*), Y1274 (*zip3Δ*) and Y1907 (*zip2Δzip3Δ*).

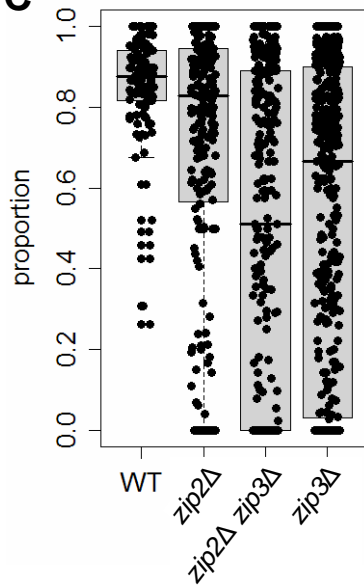
**A** *zip2Δ zip3Δ*



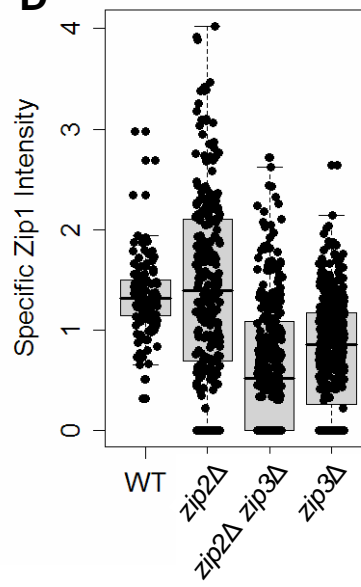
**B**



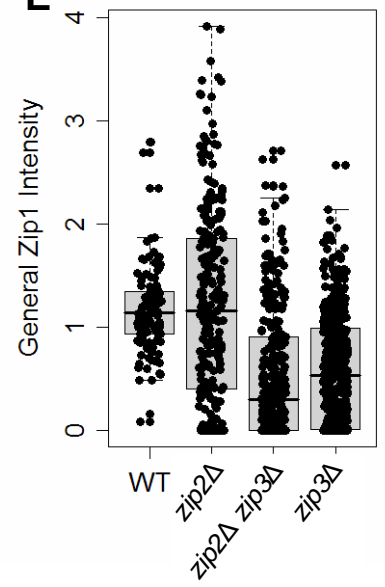
**C**



**D**



**E**



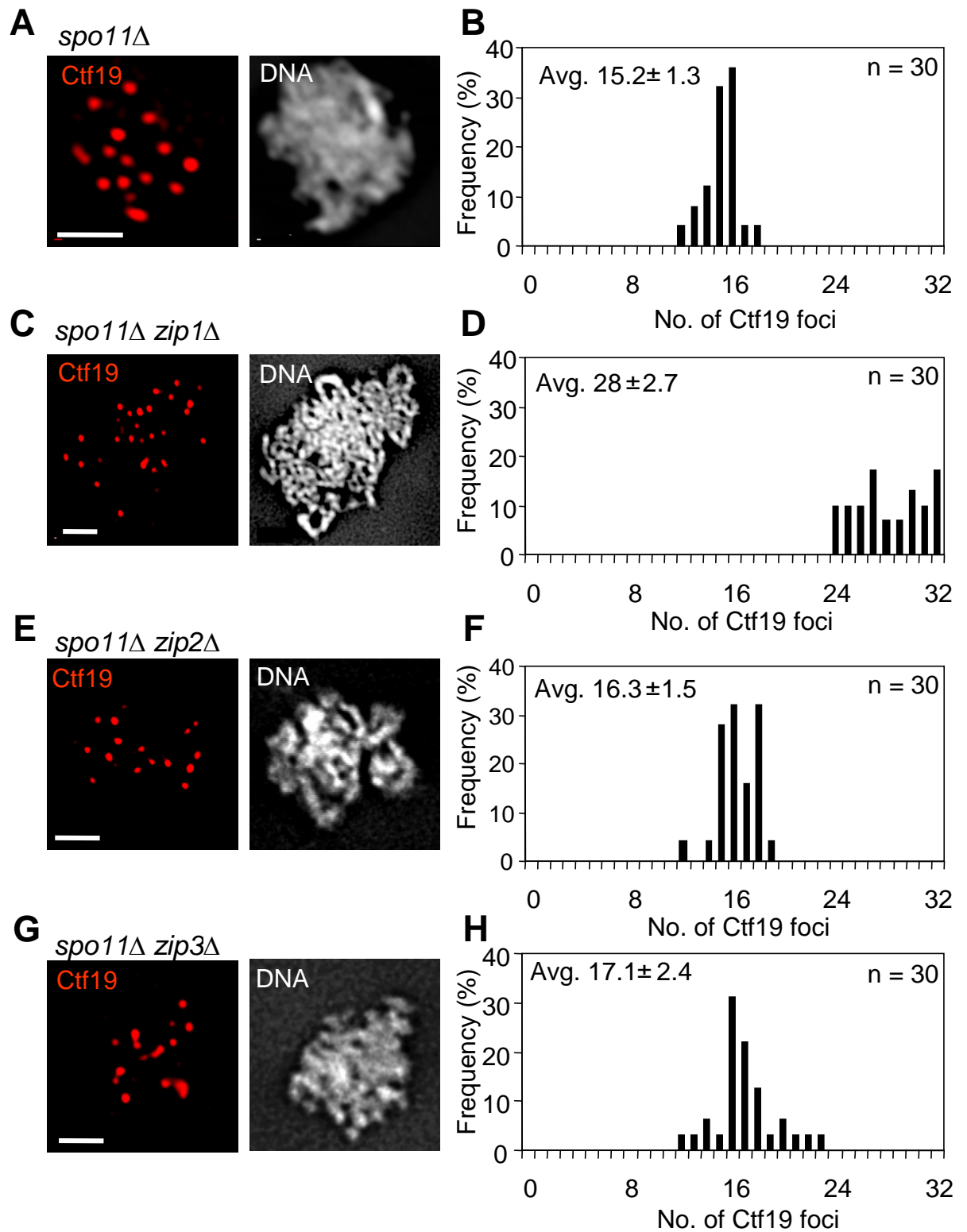
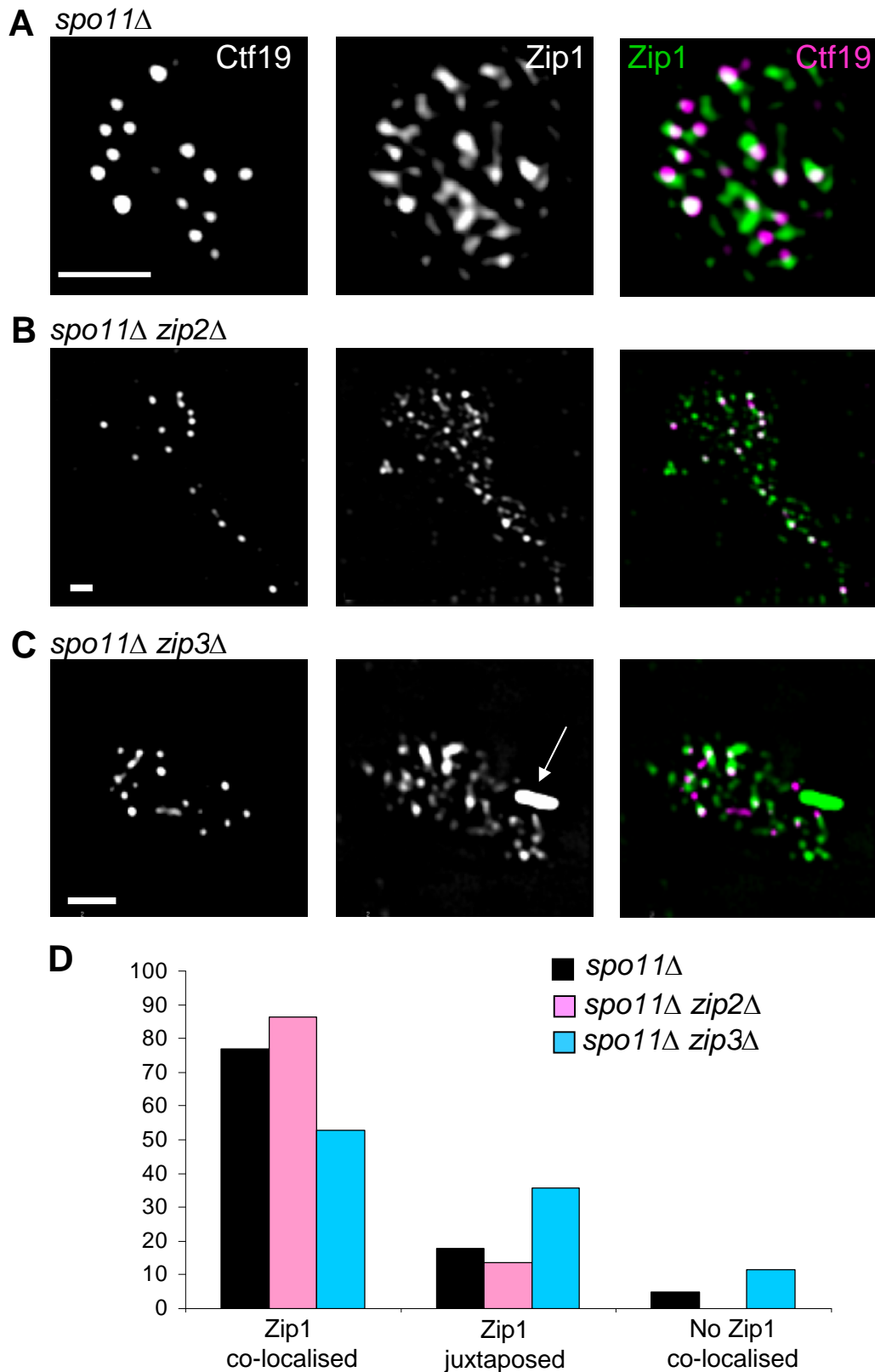
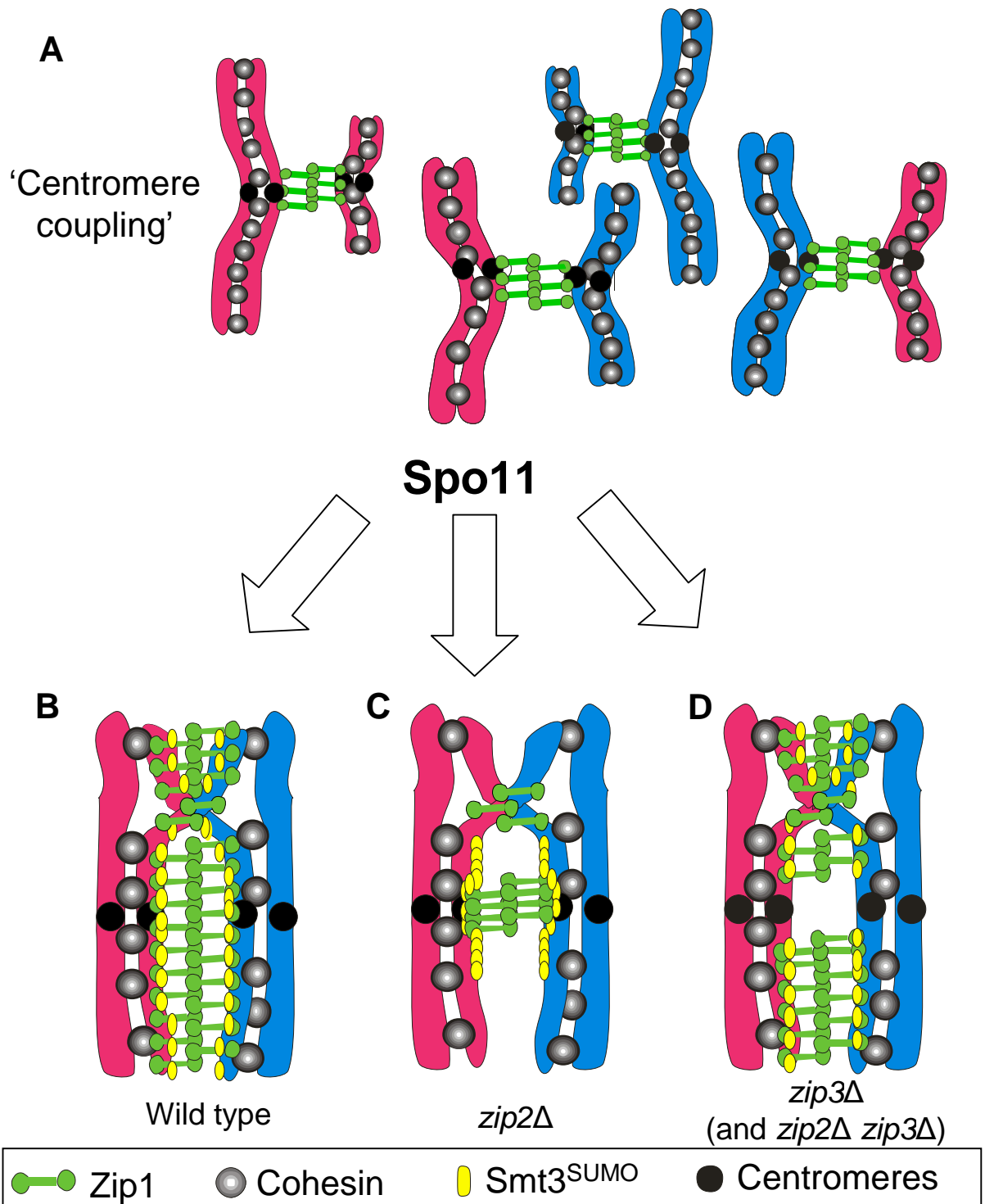


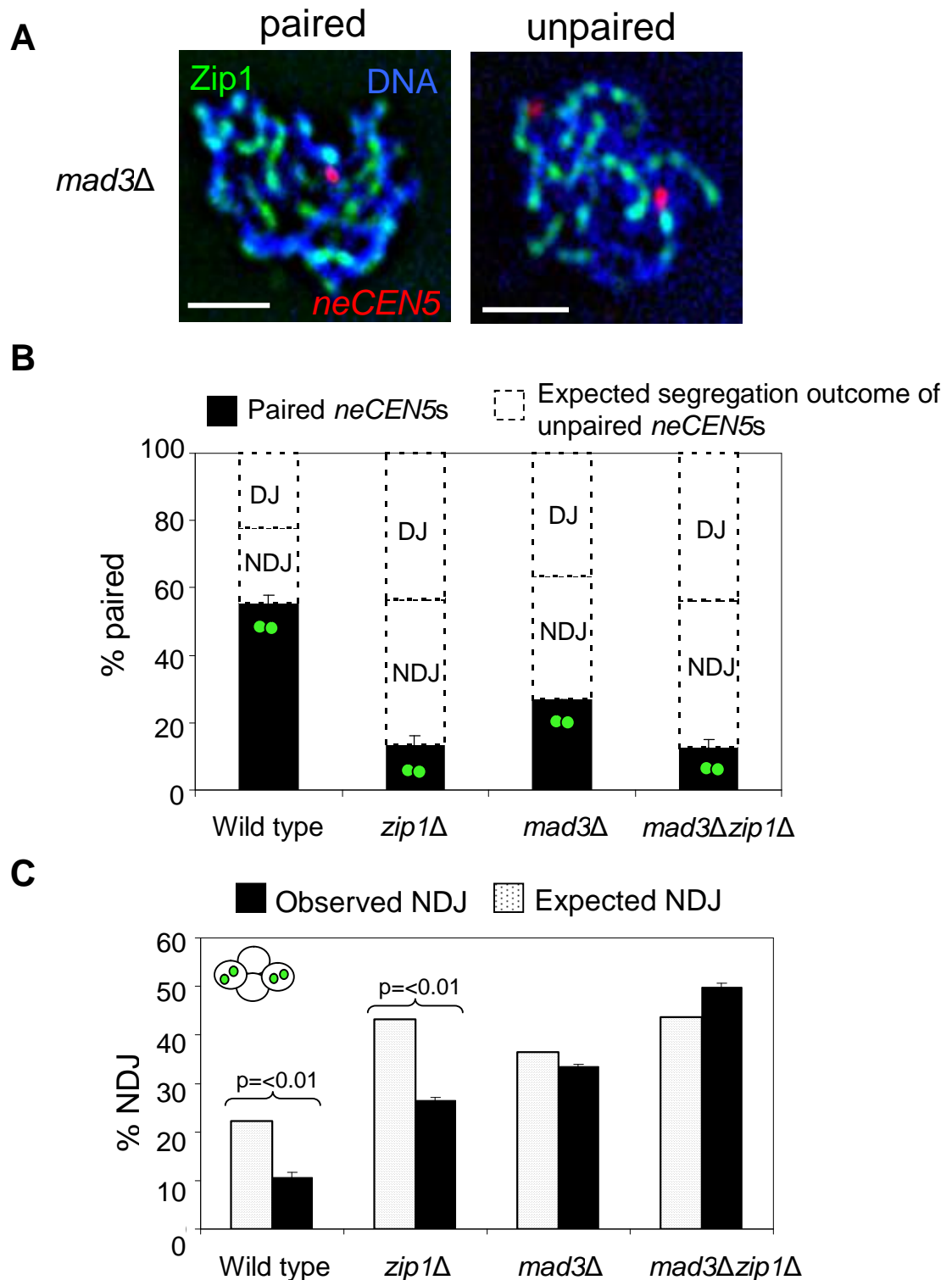
Figure 5.10. Pair-wise associations of centromeres in *spo11Δ* mutants during pachytene. Example images of *spo11Δ* (A), *spo11Δ zip1Δ* (C), *spo11Δ zip2Δ* (E) and *spo11Δ zip3Δ* (G) pachytene nuclei with condensed DNA and a single brush-like dot of tubulin (not shown). Bars: 2  $\mu$ m. Histograms showing the number of Ctf19 foci per pachytene nucleus for *spo11Δ* (B), *spo11Δ zip1Δ* (D), *spo11Δ zip2Δ* (F) and *spo11Δ zip3Δ* (H). The number of nuclei examined is shown in the top, right-hand corner. The mean and standard deviations are shown in the top, left-hand corner. Strains: Y1136 (*spo11Δ*), Y1188 (*spo11Δ zip2Δ*) and Y1266 (*spo11Δ zip3Δ*).



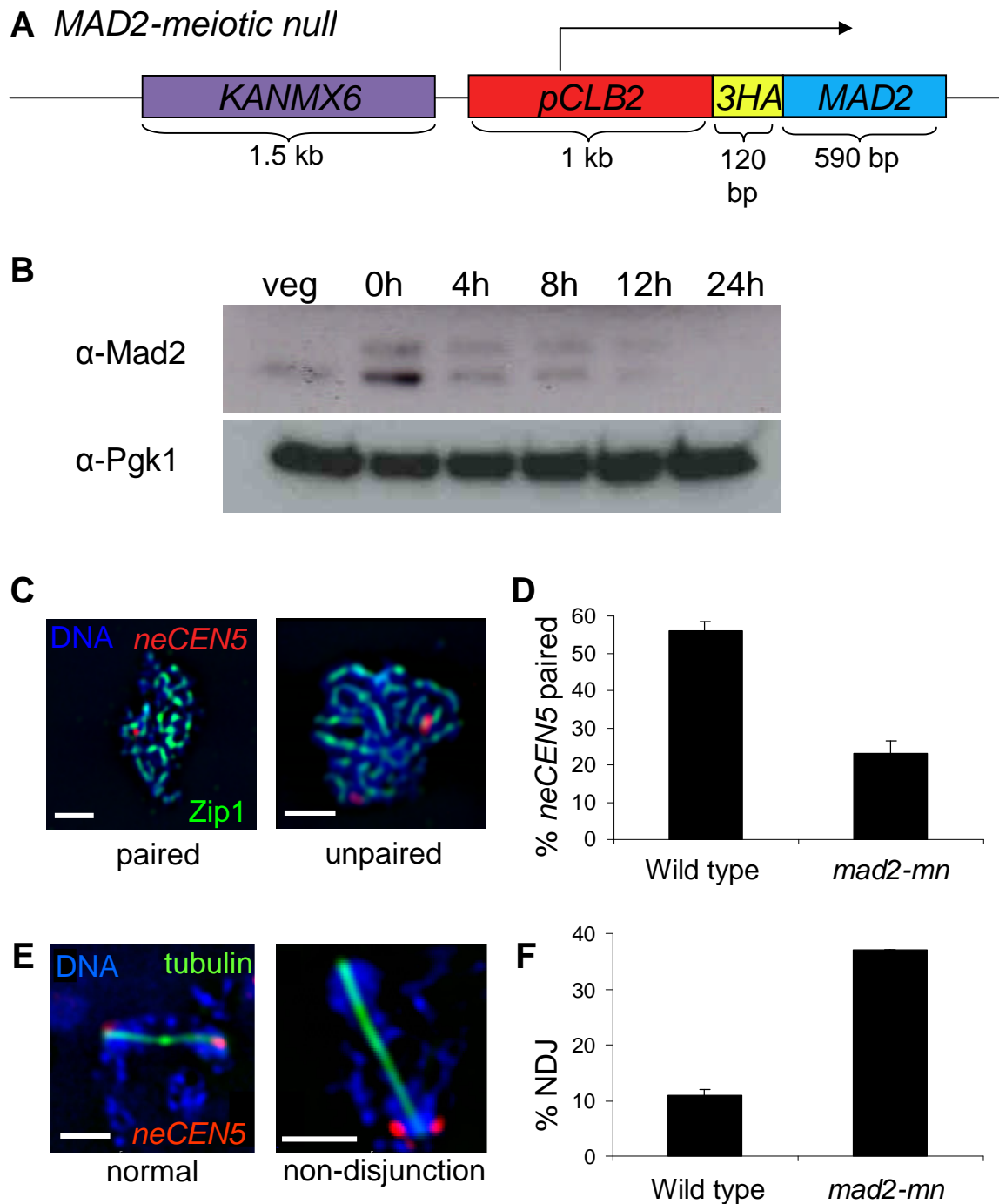
**Figure 5.11.** Co-localisation of Zip1 with Ctf19 foci during pachytene in *spo11Δ*, *spo11Δ zip2Δ* and *spo11Δ zip3Δ* mutants. Examples of Zip1 (green) and Ctf19 (magenta) in pachytene nuclei of *spo11Δ* (A), *spo11Δ zip2Δ* (B) and *spo11Δ zip3Δ* (C) mutants. Arrows indicate poly-complexes. Bars: 2  $\mu$ m. (D) Quantification of 'classic' co-localisation analysis of Ctf19 with Zip1. Shown are the percentages of Ctf19 foci with Zip1 directly co-localised, Zip1 juxtaposed (touching, but not overlapping) and not co-localised. The numbers of Ctf19 foci analysed are 380 (*spo11Δ*), 206 (*spo11Δ zip2Δ*) and 261 (*spo11Δ zip3Δ*). Strains: Y1136 (*spo11Δ*), Y1188 (*spo11Δ zip2Δ*) and Y1266 (*spo11Δ zip3Δ*).



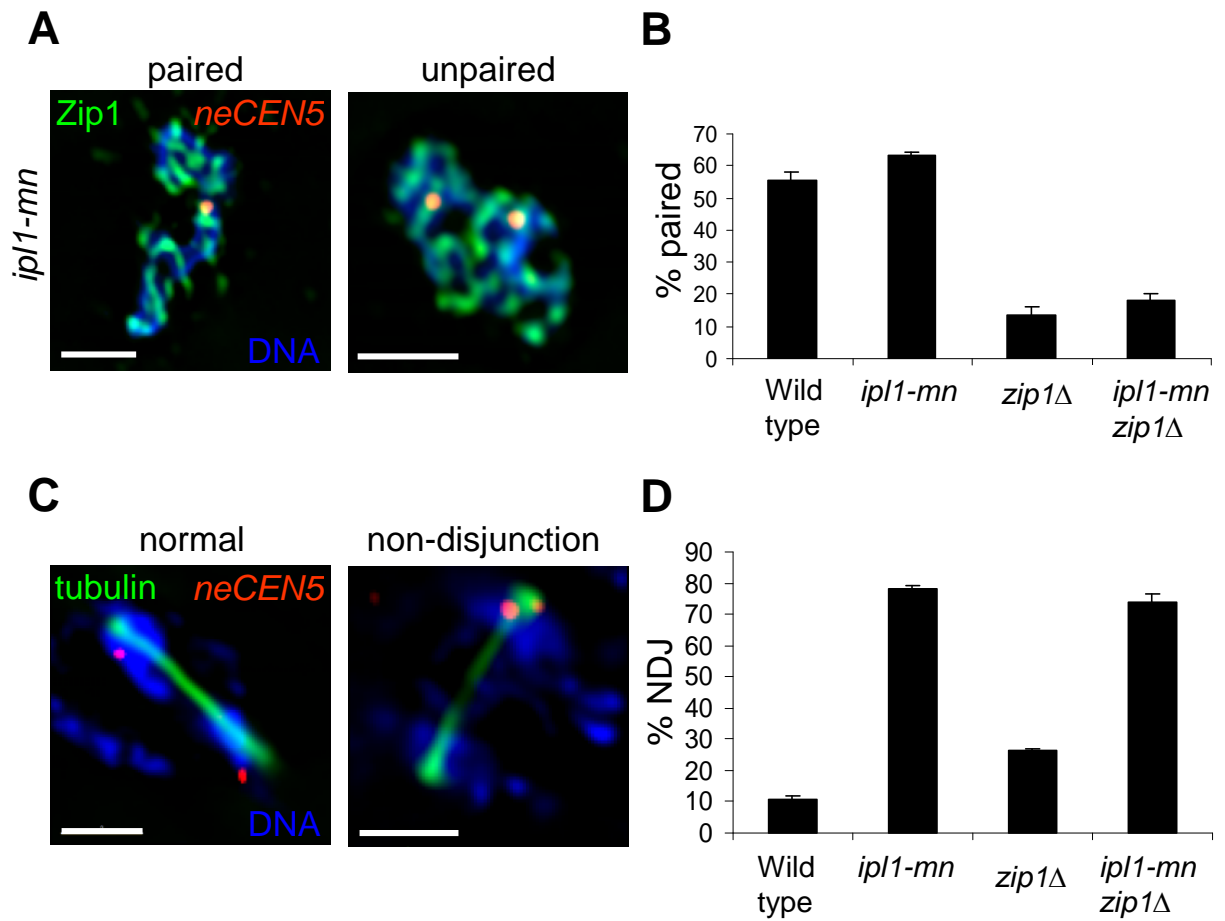
**Figure 5.12.** Diagram summarising the *zip2Δ* and *zip3Δ* synapsis phenotypes. (A) During early meiotic prophase, prior to recombination, centromeres are 'coupled' by Zip1. This occurs between non-homologous centromeres and is independent of Zip2 and Zip3. Spo11 triggers the 'switch' in centromeric Zip1 regulation. (B) In wild type pachytene nuclei, Zip1 connects homologous chromosomes along their lengths. It is thought that the C-terminus of Zip1 binds to Smt3<sup>SUMO</sup> present along the chromosome axes. (C) In *zip2Δ* pachytene nuclei, Zip1 localises and sometimes accumulates at centromeres, but this does not seem to be due to accumulation of Smt3<sup>SUMO</sup> conjugates. Rather, Smt3<sup>SUMO</sup> conjugates manage to extend into short stretches in *zip2Δ* mutants, which is not the case for Zip1. (D) In *zip3Δ* and *zip2Δ zip3Δ* pachytene nuclei, Zip1 and Smt3<sup>SUMO</sup> are present along the chromosome arms, but are often depleted at centromeres. This may be due to a failure to sumoylate a centromeric target protein in cells lacking Zip3.



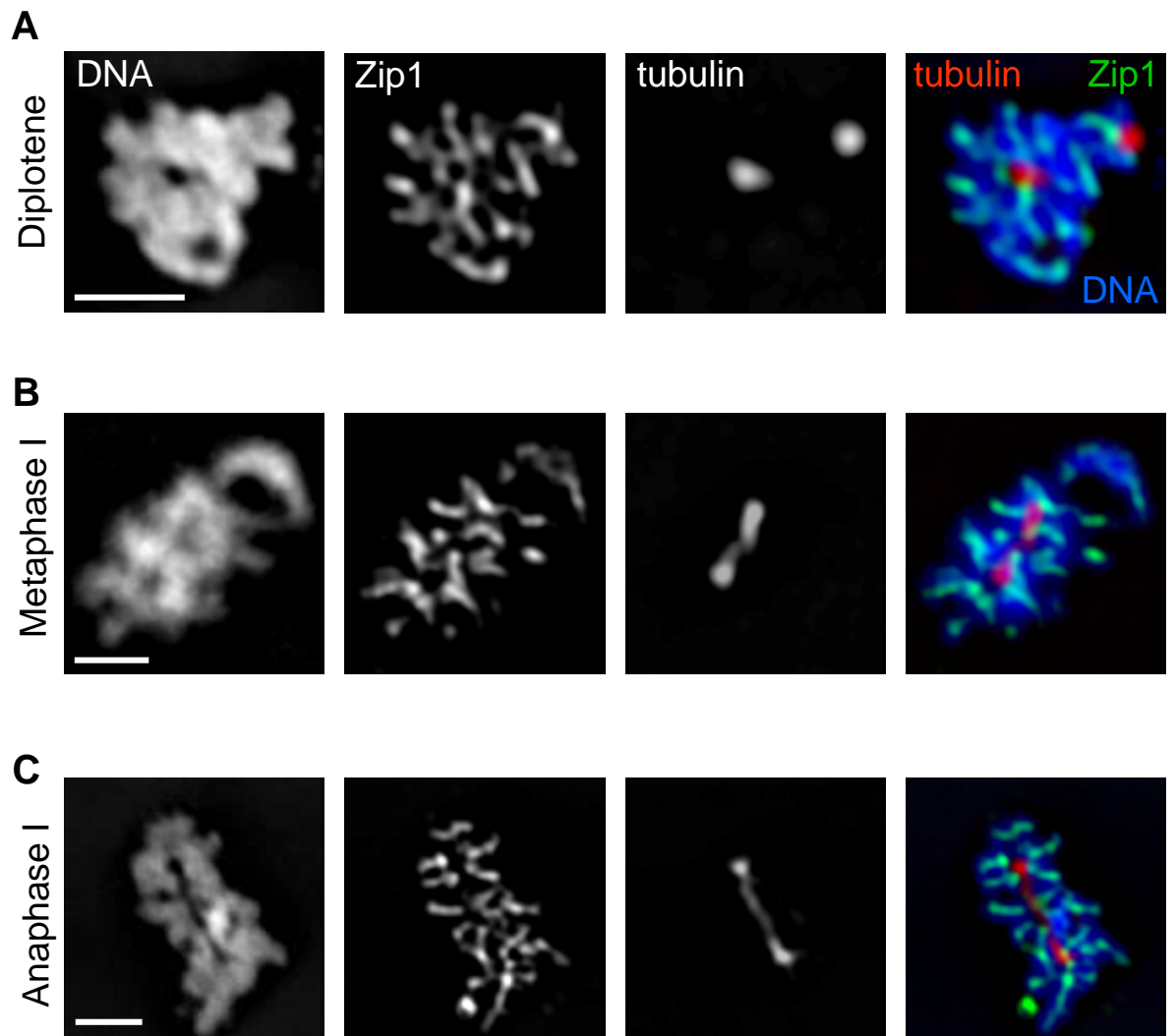
**Figure 6.1.** Mad3 promotes centromere pairing and the segregation of non-exchange chromosomes not 'paired' by Zip1. (A) Representative *mad3Δ* pachytene nuclei with 'paired' (left) and 'unpaired' *neCEN5*s. Bars: 2 μm. (B) Bar-chart showing *neCEN5* pairing frequencies for wild type, *zip1Δ*, *mad3Δ* and *mad3Δ zip1Δ* cells during pachytene (black bars). The expected non-disjunction frequencies are shown assuming that unpaired non-exchange chromosomes (*neCEN5*s) segregate at random and paired non-exchange chromosomes segregate correctly (dashed lines). (C) Bar-chart showing the observed and expected chromosome V non-disjunction frequencies for wild type, *zip1Δ*, *mad3Δ* and *zip1Δmad3Δ* mutants. Strains: Y712 (wild type), Y787 (*zip1Δ*), Y784 (*mad3Δ*), Y1155 (*mad3Δzip1Δ*).



**Figure 6.2.** Mad2 promotes centromere pairing and the segregation of non-exchange chromosomes not ‘paired’ by Zip1. (A) Schematic representation of how the *MAD2-meiotic null* strain was made. The native *MAD2* promoter was replaced by that of *CLB2*, whose expression is shut off during meiosis (mutant made by ERASMUS student Andrea Haerzschel). (B) Western blot showing the abundance of Mad2 protein at different time points during sporulation. (C) Representative images of *mad2-mn* pachytene nuclei with ‘paired’ (left) and ‘unpaired’ (right) *neCEN5*s. (D) *neCEN5* pairing frequencies in wild type and *mad2-mn* pachytene nuclei. >50 nuclei were examined for each strain. (E) Representative images of cells undergoing anaphase I in which the non-exchange pair segregated correctly (left) and non-disjoined (right). (F) Quantification of meiosis I non-disjunction frequencies as assessed by looking at cells that had completed anaphase I (Andrea Haerzschel). >100 nuclei were examined for each strain. Bars: 2  $\mu$ m. Strains: Y712 (wild type) and Y1476 (*mad2-mn*).

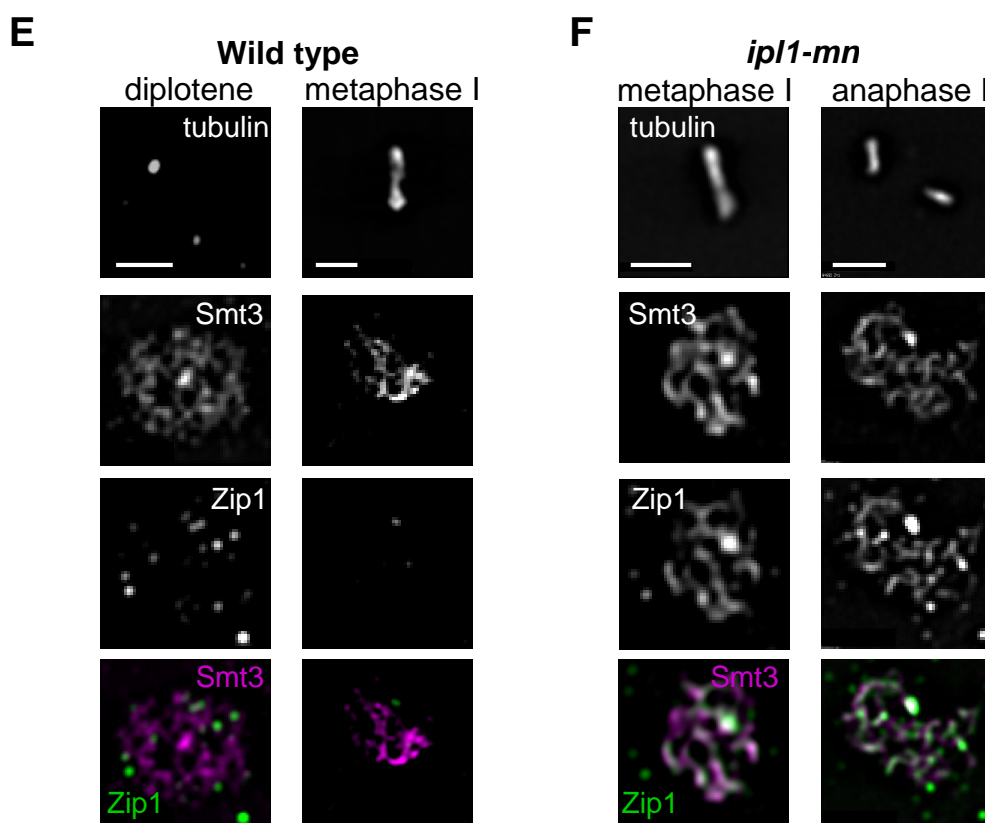
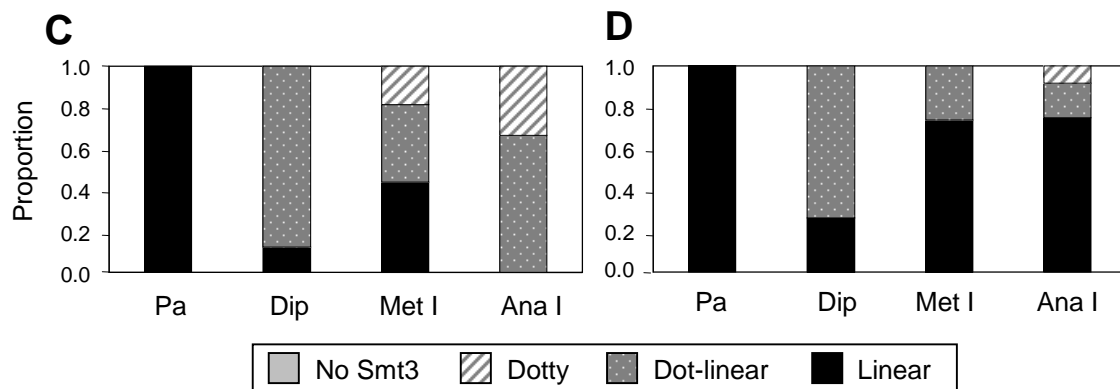
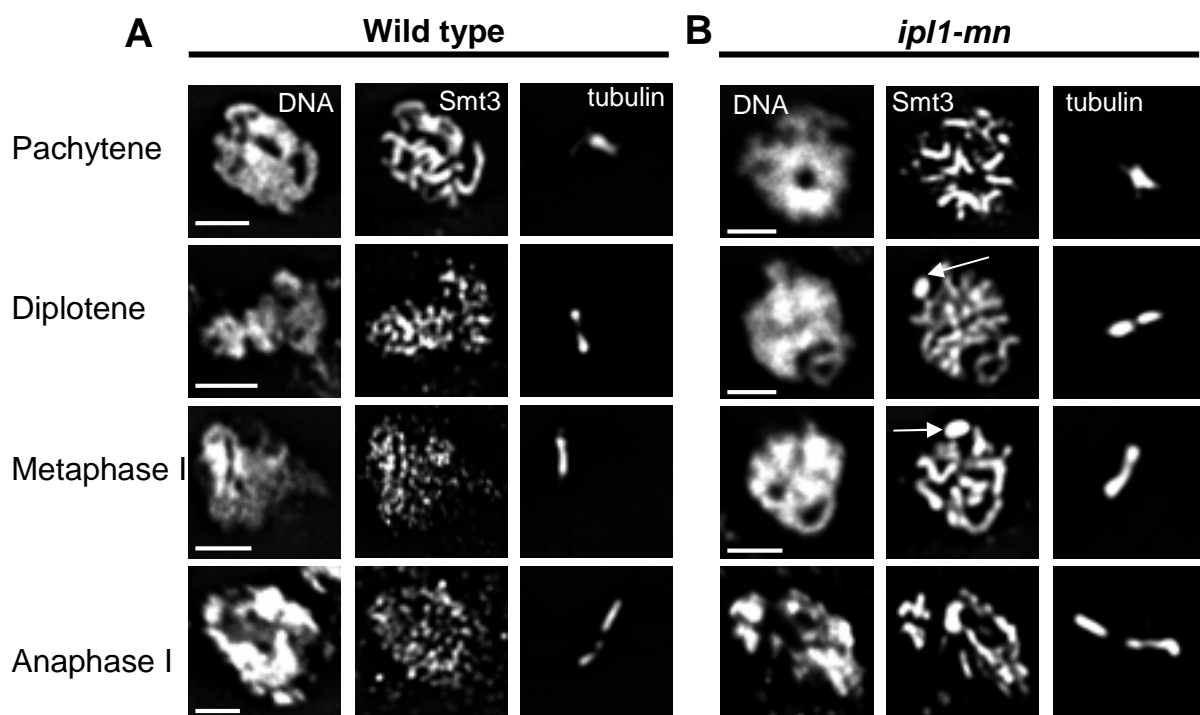


**Figure 6.3.** Ipl1/Aurora B kinase activity is required for non-exchange chromosome segregation. (A) Representative *ipl1-mn* pachytene nuclei with ‘paired’ (left) and ‘unpaired’ *neCEN5*s. (B) Quantification of *neCEN5* pairing frequencies during pachytene in wild type, *zip1Δ*, *ipl1-mn* and *ipl1-mn zip1Δ* mutants. >50 nuclei were examined for each strain. (C) Representative images of cells with anaphase I spindles in which the non-exchange pair segregated correctly (left) and non-disjoined (right). (D) Quantification of meiosis I non-disjunction frequencies as assessed by looking at cells containing anaphase I spindles. >100 nuclei were examined for each strain. Bars: 2  $\mu$ m. Strains: Y712 (wild type), Y787 (*zip1Δ*) Y991 (*ipl1-mn*) and Y1191 (*ipl1-mn zip1Δ*).



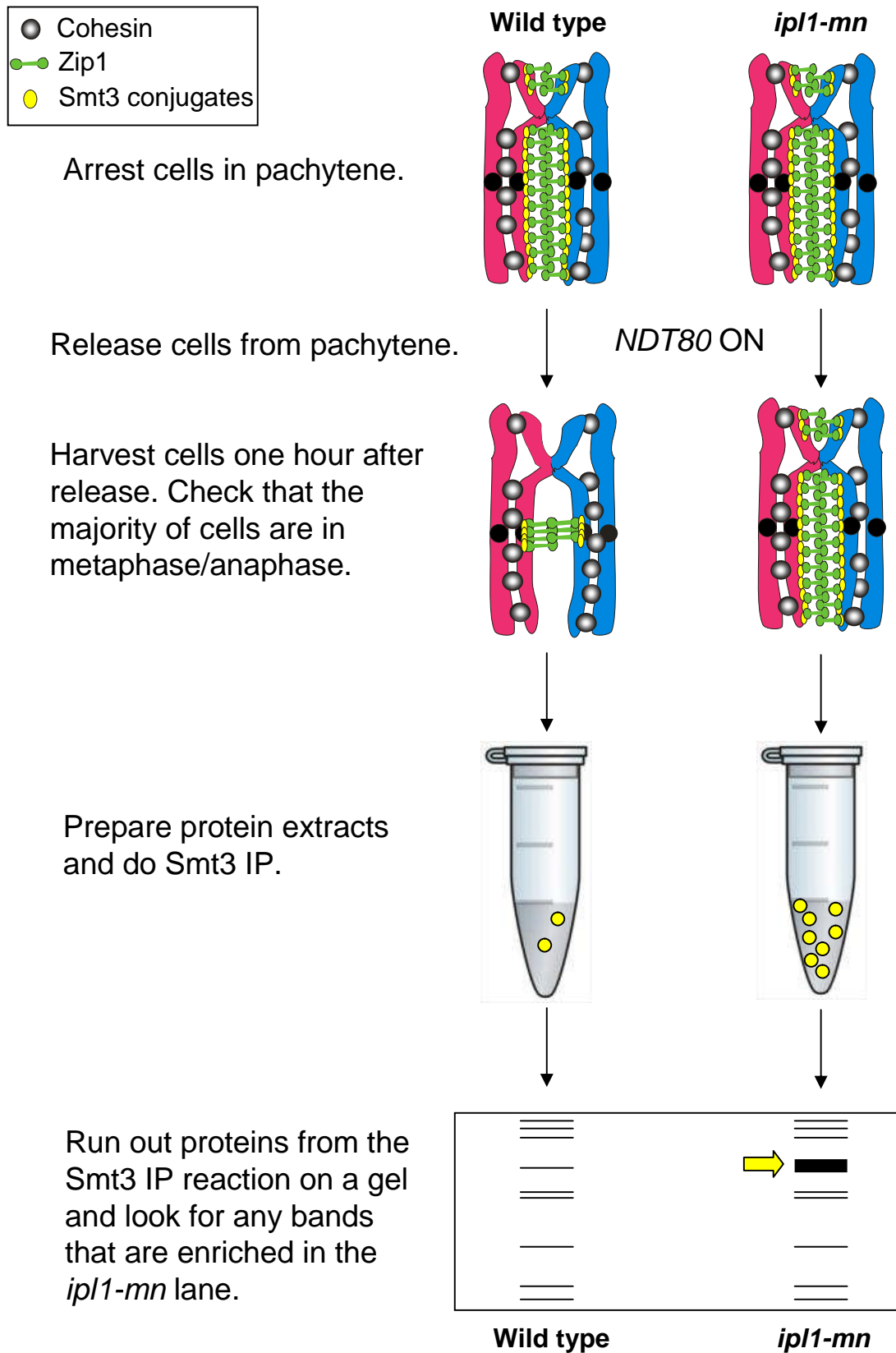
**Figure 6.4.** The synaptonemal complex fails to disassemble in *ip1-mn* cells. Representative images of spread *ip1-mn* nuclei in diplotene (A), metaphase I (B), and anaphase I (C) all with extensive stretches of Zip1 present. Bars: 2  $\mu$ m. Strains: Y991 (*ip1-mn*).

**Figure 6.5.** Smt3<sup>SUMO</sup> fails to become diffuse or dotted following exit from pachytene in *ipl1-mn* cells. (A) Representative images showing Smt3<sup>SUMO</sup> staining during pachytene, diplotene, metaphase I, and anaphase I in wild type nuclei. (B) Representative images showing Smt3<sup>SUMO</sup> staining during pachytene, diplotene, metaphase I, and anaphase I in *ipl1-mn* nuclei. Quantification of the proportions of nuclei containing linear, dot-linear, dotted or no Smt3<sup>SUMO</sup> staining during pachytene (Pa), diplotene (Dip), metaphase I (Met I) and anaphase I (Ana I) are shown for wild type (C) and *ipl1-mn* (D). Anaphase spindles often appear 'broken'. Quantification and scoring of nuclei was performed by Phil Jordan. Representative images of Smt3<sup>SUMO</sup> and Zip1 co-staining in post-pachytene nuclei for wild type (E) and *ipl1-mn* (F) cells. In the merged images, Zip1 is shown in green and Smt3<sup>SUMO</sup> in magenta. Bars: 2  $\mu$ m. Strains: Y1602 (wild type) and Y1538 (*ipl1-mn*).

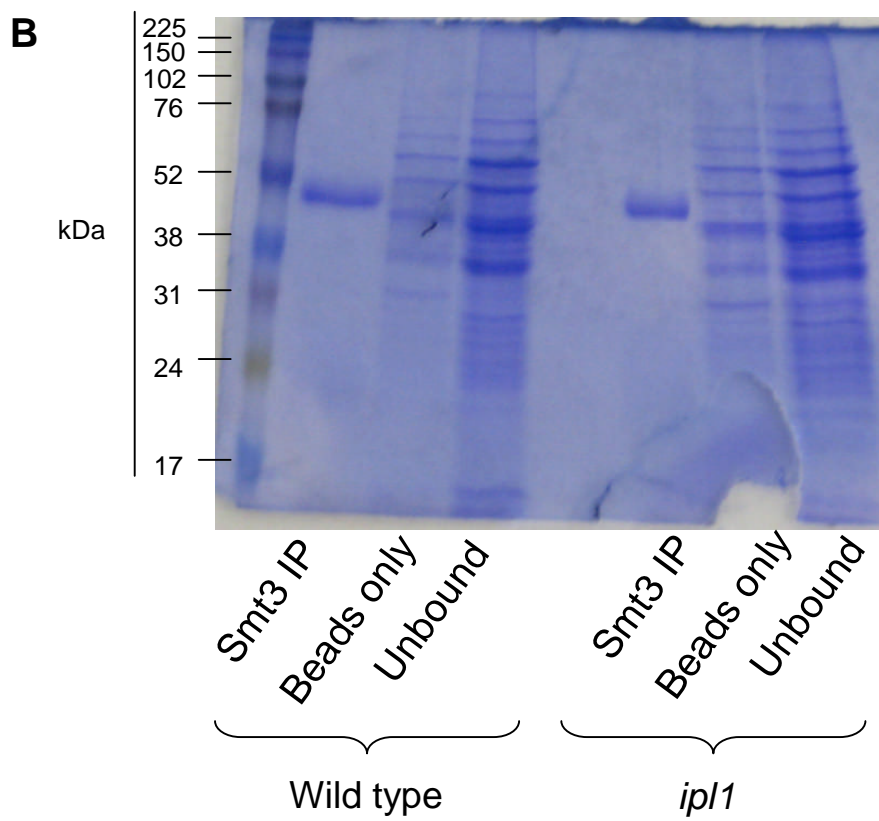
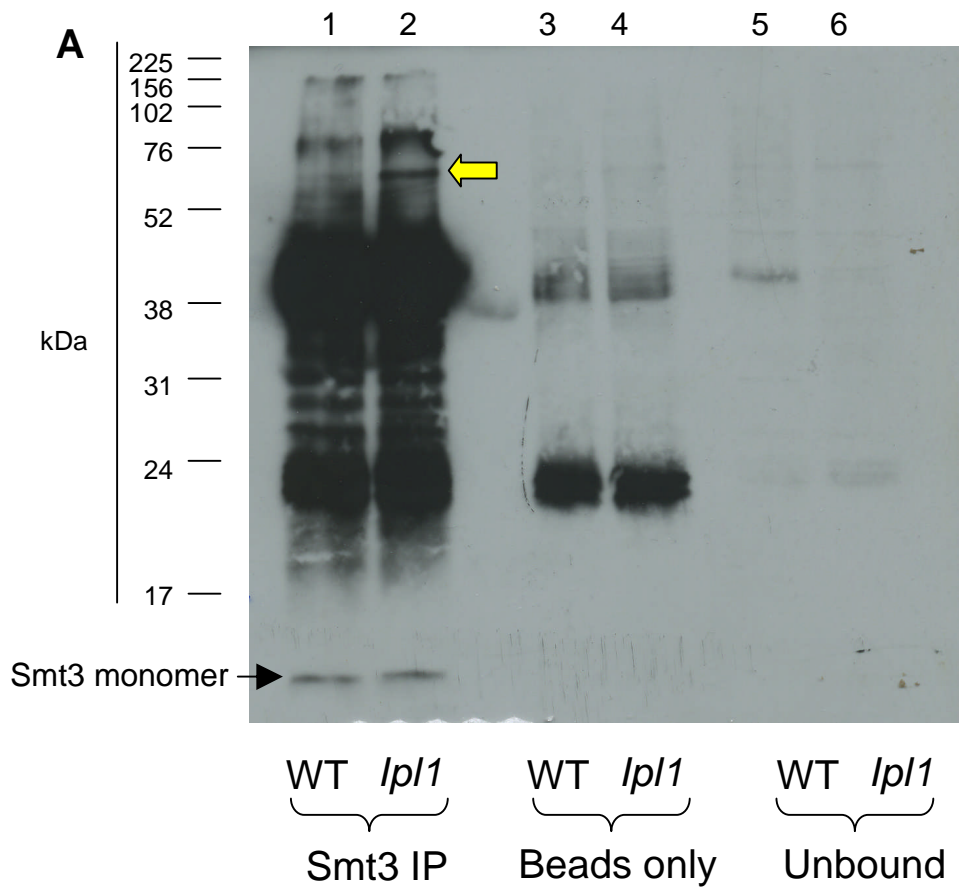


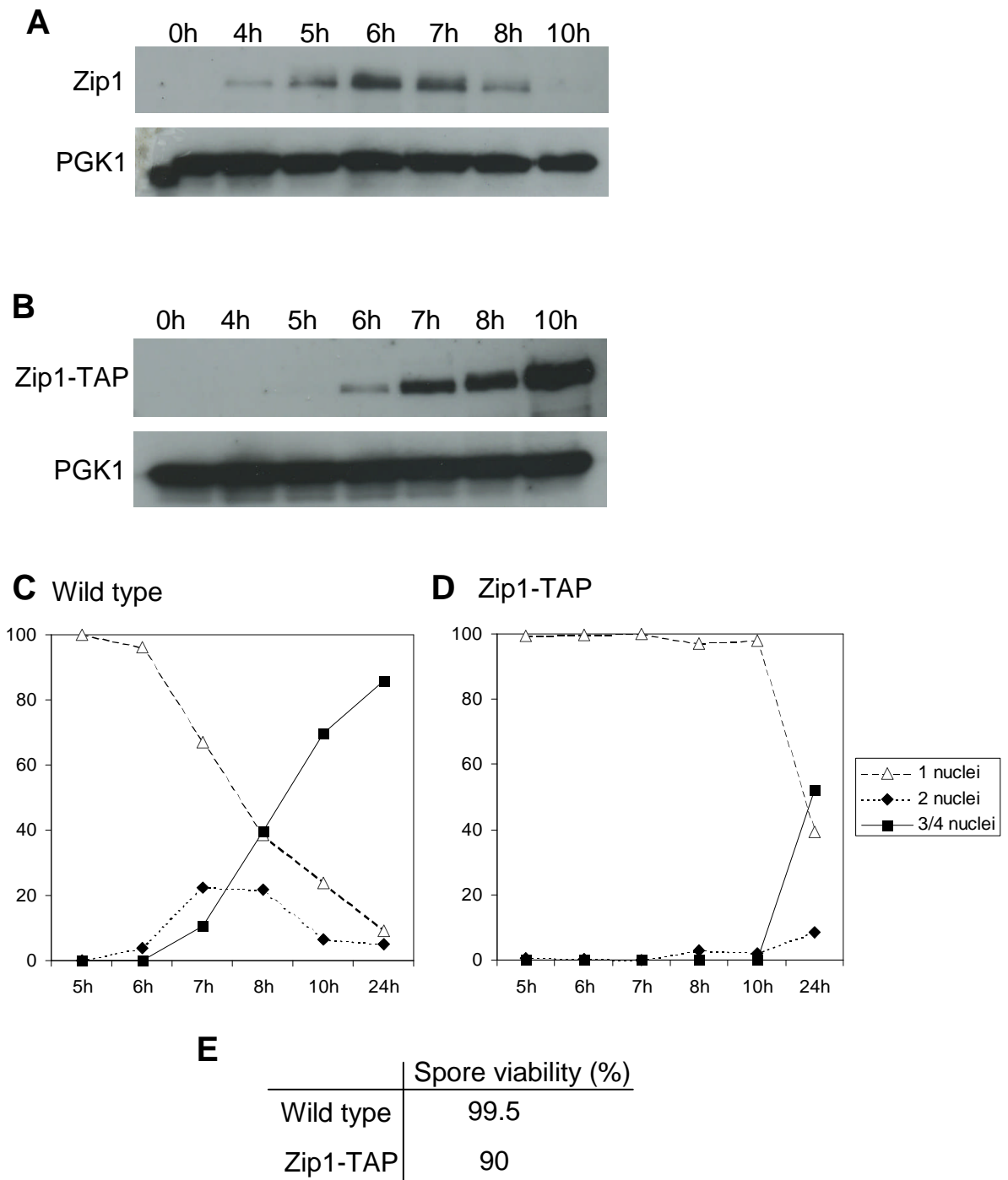
**Figure 6.6.** Experimental outline for identifying the sumoylated protein species present along the chromosomal axes. Cells were arrested in pachytene by placing the *NDT80* gene under the control of the *GAL1* promoter. Cells also expressed a Gal4-Estradiol receptor fusion protein. Upon addition of  $\beta$ -estradiol, which binds to the estradiol receptor, Gal4-ER enters the nucleus where it induces expression of *NDT80*. Ndt80 is a transcription factor inducing ~200 genes required for pachytene exit (Xu *et al.* 1995). This system allows meiotic cultures to be highly synchronised upon pachytene exit. One hour after addition of  $\beta$ -estradiol, 200 ml of wild type and *ipl1-mn* cells were harvested and stored. Additionally, 2 ml of culture was used to do meiotic spreads in order to assess the proportion of cells that had exited pachytene. Crude chromatin extracts were prepared from the stored 200 ml samples and Smt3 immunoprecipitation was performed. The immunoprecipitated proteins were then run out on large protein gels, transferred to nitrocellulose and probed for Smt3. This allows the Smt3 profiles of wild type and *ipl1-mn* cells to be compared. As there appears to be a much higher proportion of cells containing extensive linear Smt3 in the *ipl1-mn* mutant at metaphase I and anaphase I, there should be more of these protein species in the *ipl1-mn* mutant at these stages. Therefore, *ipl1-mn* samples should contain a band that appears absent or depleted in the wild type sample that correspond to the Smt3<sup>SUMO</sup> that remains with Zip1 on the chromosomes in an *ipl1-mn* mutant.

Figure 6.6.

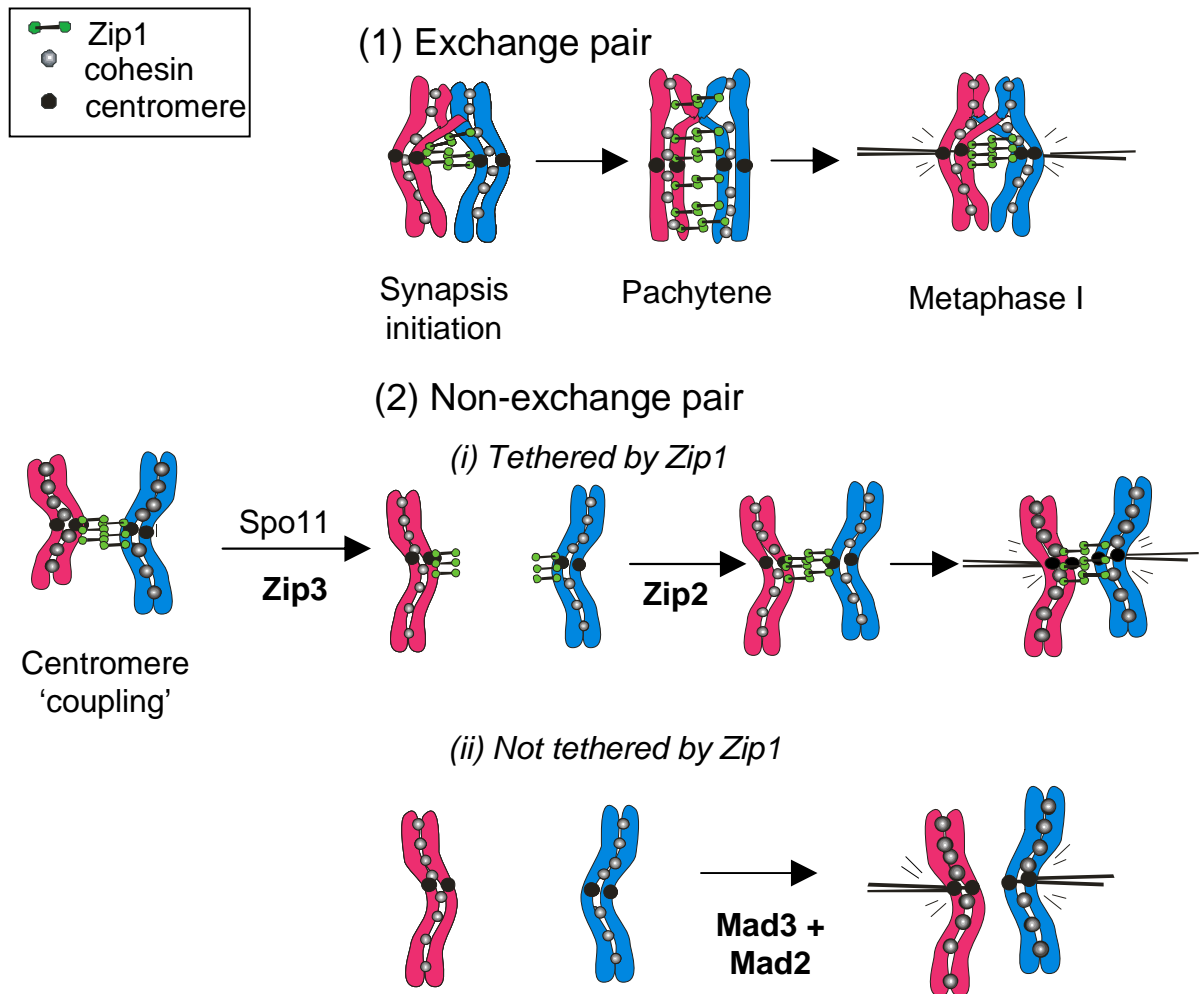


**Figure 6.7.** Smt3 immunoprecipitation on crude chromatin extracts from wild type and *ipl1-mn* cells one hour after pachytene exit. (A) Western blot showing Smt3-immunoprecipitated proteins from wild type (lane 1) and *ipl1-mn* (lane 2) cells one hour after pachytene exit. Lanes 3 and 4 contain the proteins that bound to the beads only (No Smt3 antibody) for wild type and *ipl1-mn* samples, respectively. Lanes 5 and 6 contain the proteins that did not bind to the Smt3 beads for wild type and *ipl1-mn* samples, respectively. The yellow arrow indicates a band that is enriched in *ipl1-mn* over wild type. This result was observed in two, independent experiments. Western blots were transferred from large-format 10% gels. (B) Coomassie-stained 10% gel of the same samples shown in A, with the same volumes as loaded in A. The sizes (kDa) of the protein markers are given on the left-hand side of the blot and gel.

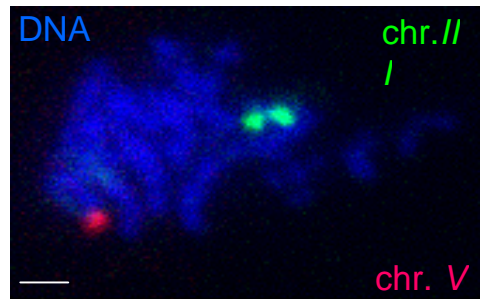
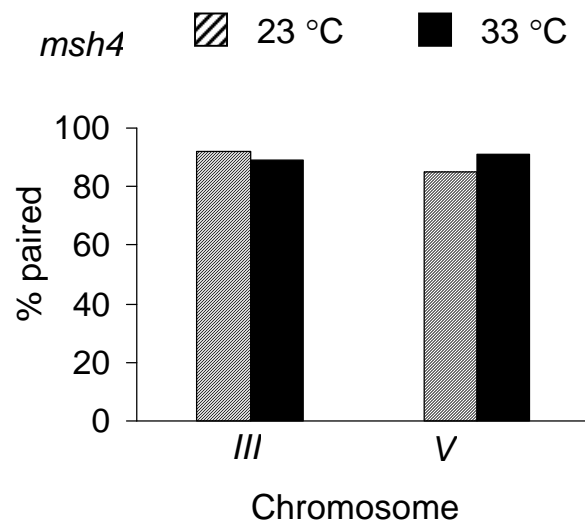




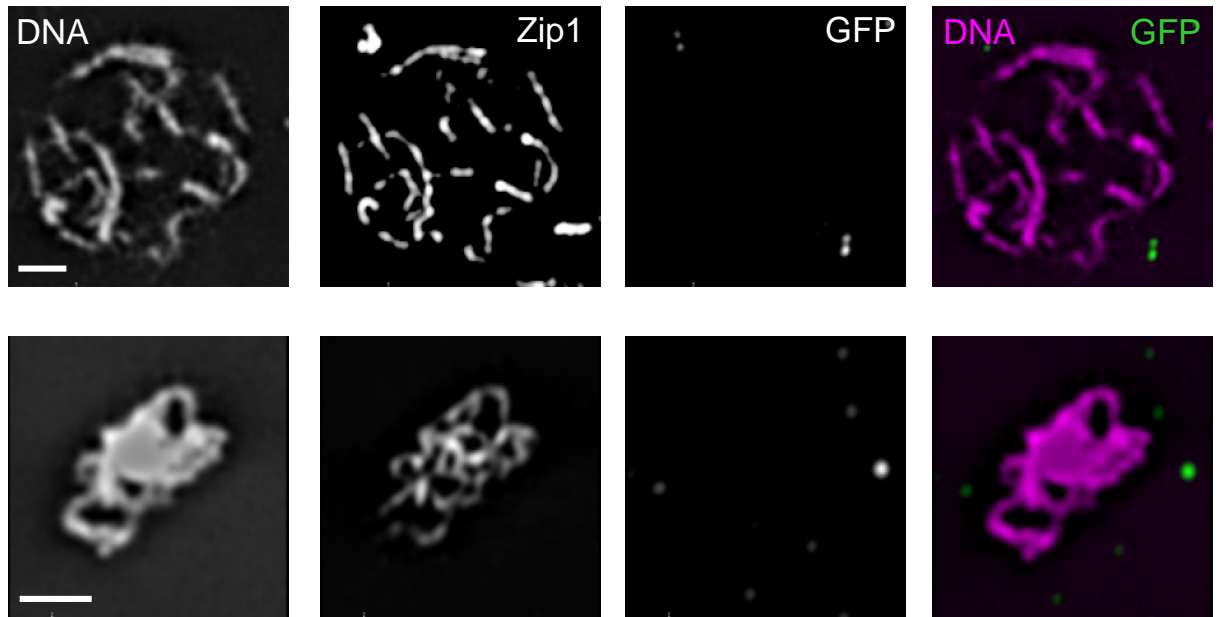
**Figure 6.8.** Preliminary work on Zip1-TAP strains. (A) Western blot showing the relative abundance of Zip1 and Pgc1 (loading control) in wild type cells throughout a meiotic time course. (B) Western blot showing the relative abundance of Zip1-TAP protein and Pgc1 (loading control) throughout a meiotic time course. The hours in sporulation media are given above the blots. (C-D) Graphs showing the completion of the first and second meiotic divisions for wild type (C) and Zip1-TAP strains (D) throughout the same meiotic time course as in A and B. (E) Shows the spore viability of wild type and Zip1-TAP strains. Strains: Y1602 (wild type) and Y2121 (Zip1-TAP).



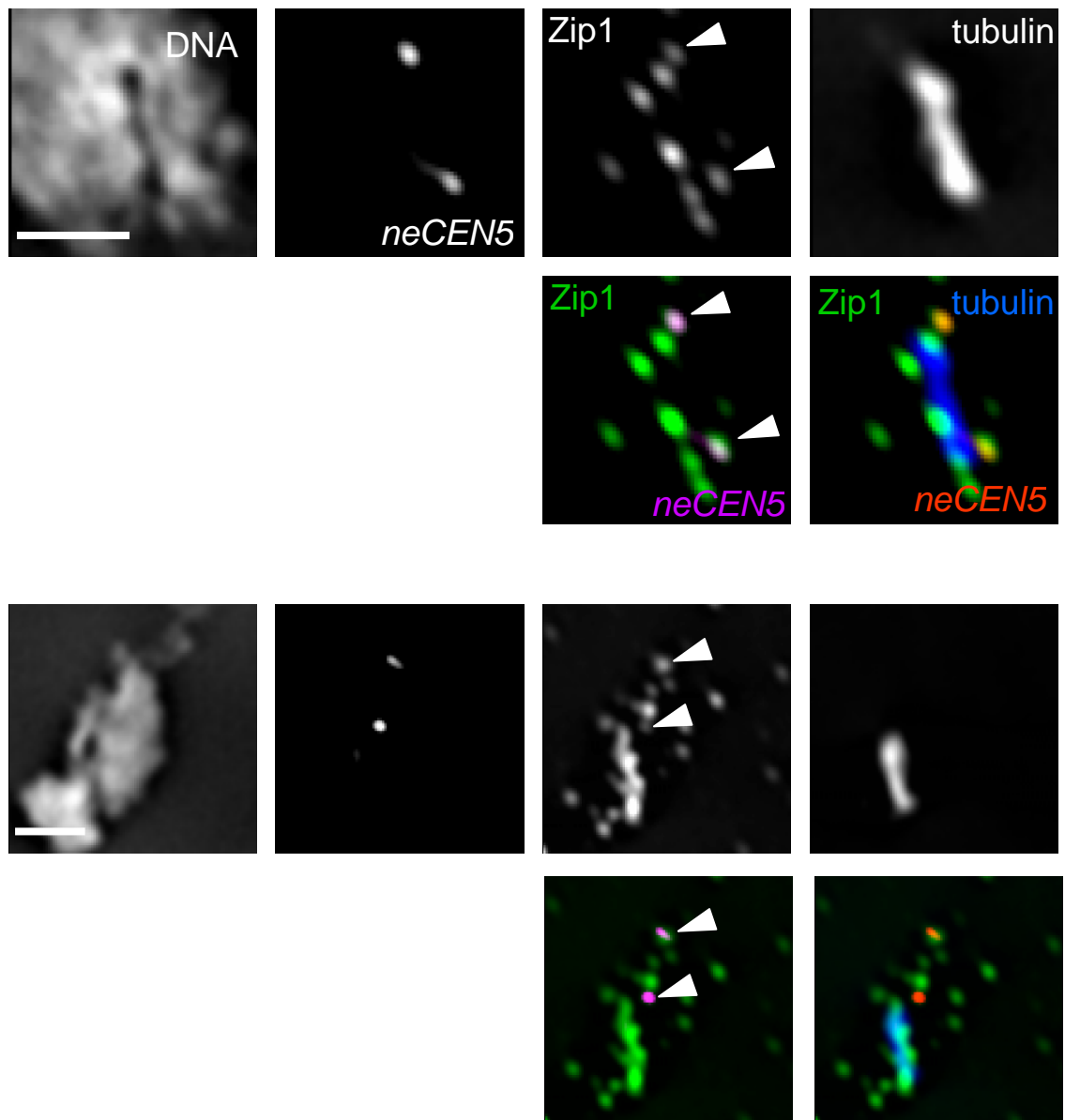
**Figure 6.9.** Model for non-exchange chromosome segregation in budding yeast. Zip1 promotes the segregation of both exchange and non-exchange chromosomes by 'tethering' centromeres throughout meiotic prophase (Chapter 4). The spindle checkpoint proteins Mad3, and possibly Mad2, aid the segregation of non-exchange chromosomes that are not 'tethered' by Zip1. In addition, they are also involved in centromere pairing of non-exchange chromosomes.

**A****B**

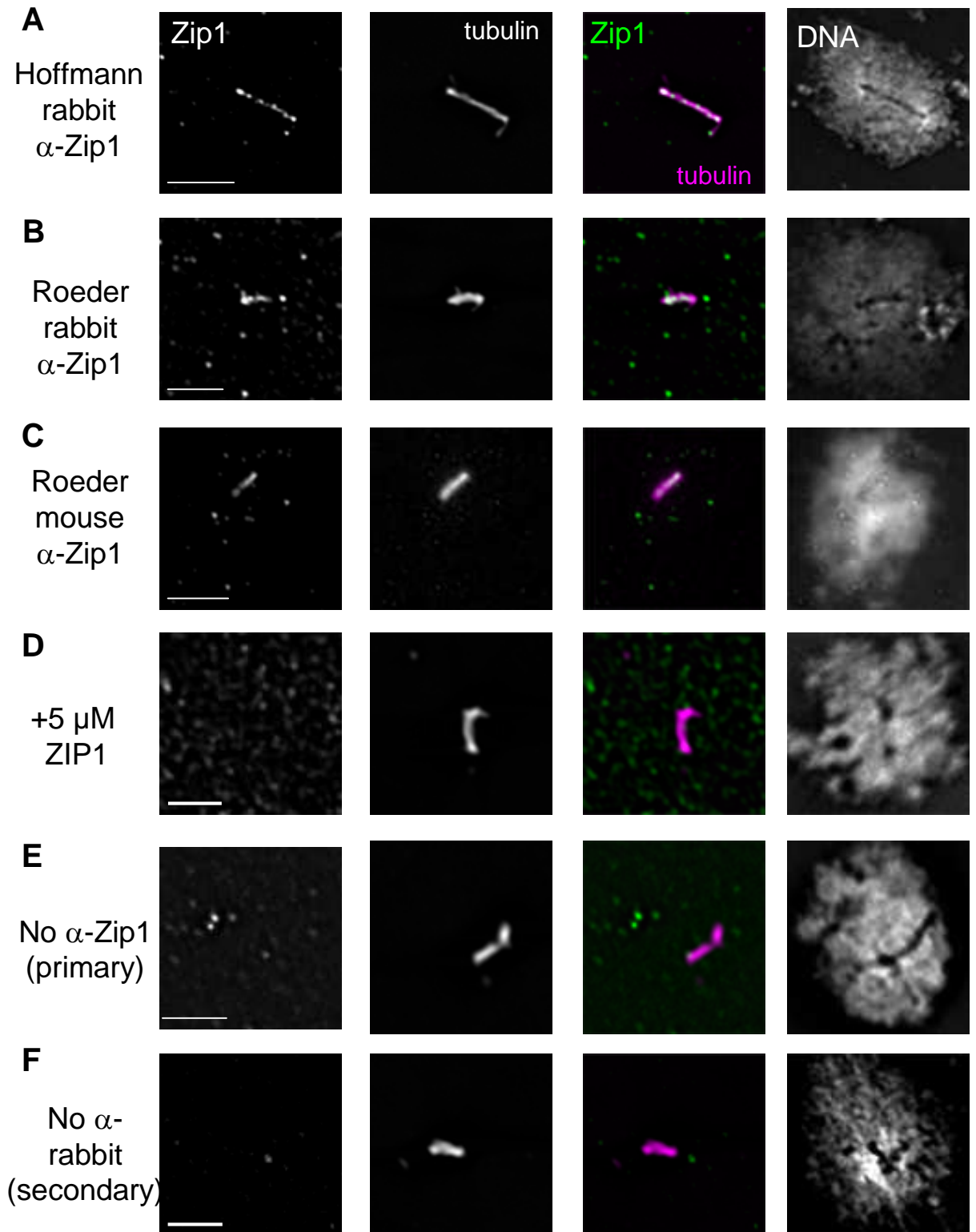
**Appendix Figure 1.** Chromosome pairing occurs normally in *msh4* strains. Fluorescent *in situ* hybridization using probes against chromosome III (green) and chromosome V (red). Meiotic nuclear spreads with highly condensed worm-like chromosomes (blue) were assessed for whether a single or two closely spaced foci ( $< 0.7 \mu\text{m}$ ) were observed. Such configurations indicate that homologous chromosomes are paired. More than 100 nuclei were assessed at each temperature. Strains (BR): Y1293 (wild type) and Y2251 (*msh4*).



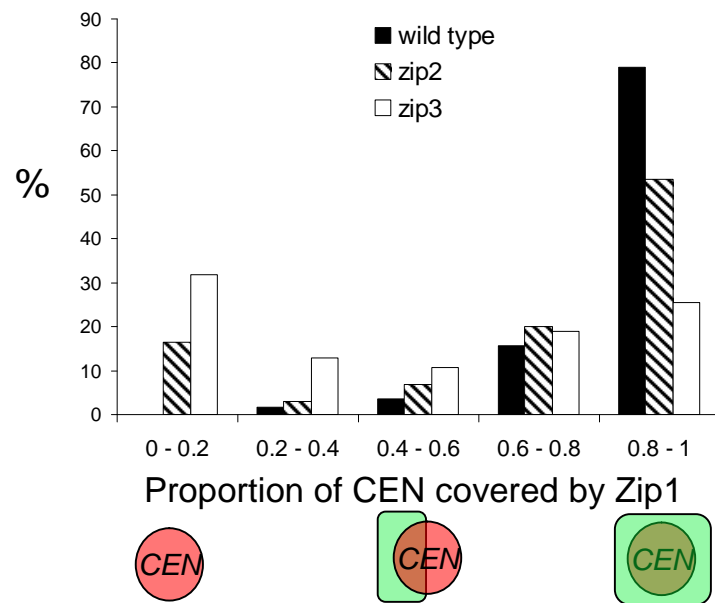
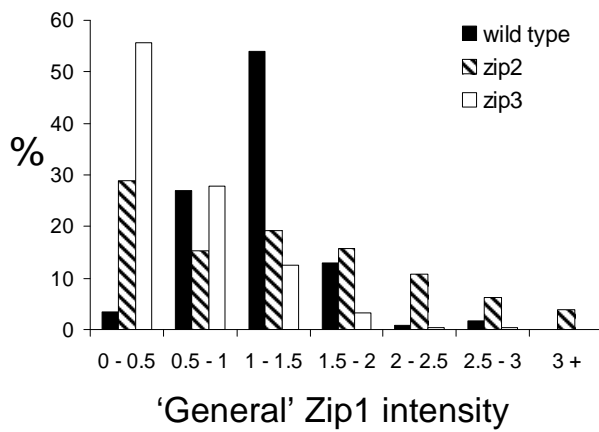
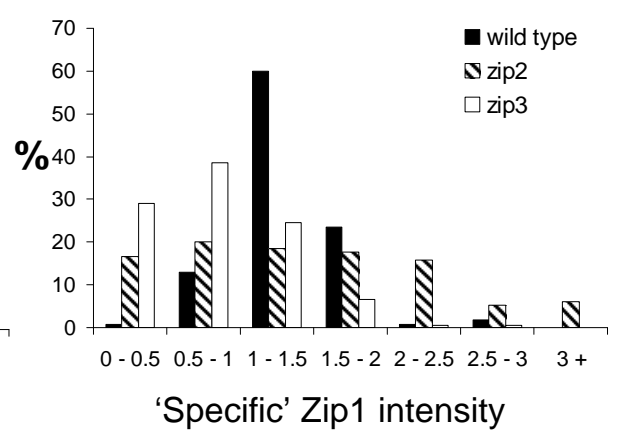
**Appendix Figure 2.** GFP signal is not detected in un-tagged Msh4 strains. Two examples of wild type (Y1293) pachytene nuclei stained with anti-GFP antibodies. The antibody only detects non-specific epitopes that are not on the DNA. In the merged images, DNA is shown in magenta and background GFP signal is shown in green. Bars: 2  $\mu$ m.



**Appendix Figure 3.** Zip1 co-localises with *neCEN5*s during metaphase I, even when they are not attached to the metaphase spindle. Bars: 2  $\mu$ m.

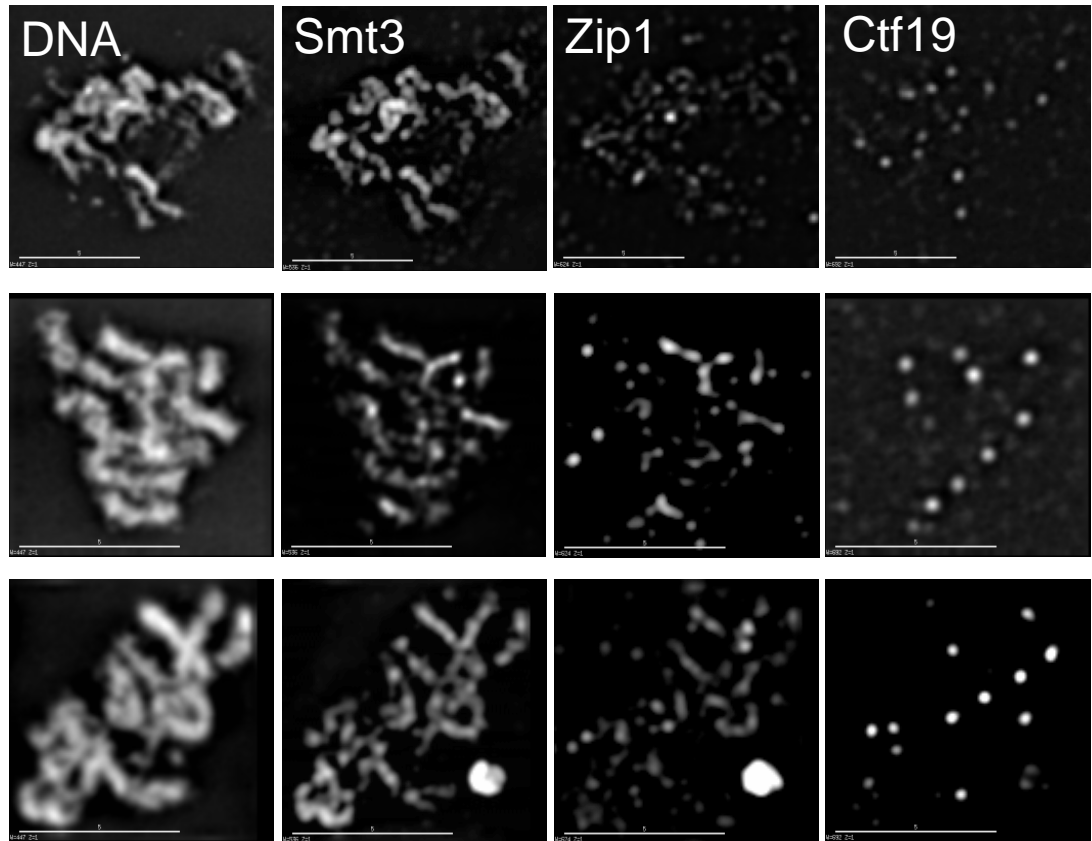


**Appendix Figure 4.** Staining controls for Zip1 localisation to metaphase I spindles. (A-C) Three different antibodies raised against Zip1 detect co-localisation of Zip1 and tubulin. This signal is not detected when the antibody was pre-incubated with 5  $\mu$ M Zip1 protein (D) or when the primary antibody against Zip1 (E) or the secondary antibody against rabbit IgG (F) is omitted. Bars: 2  $\mu$ m. Strains: Y1688 (wild type).

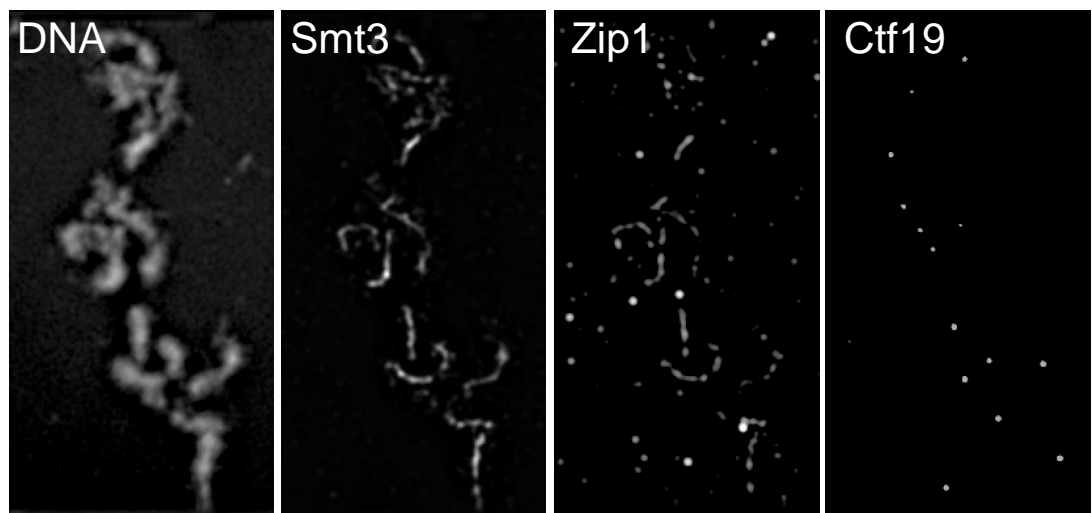
**A****B****C**

**Appendix Figure 5.** Histograms representing the same data shown in Figure 5.5.

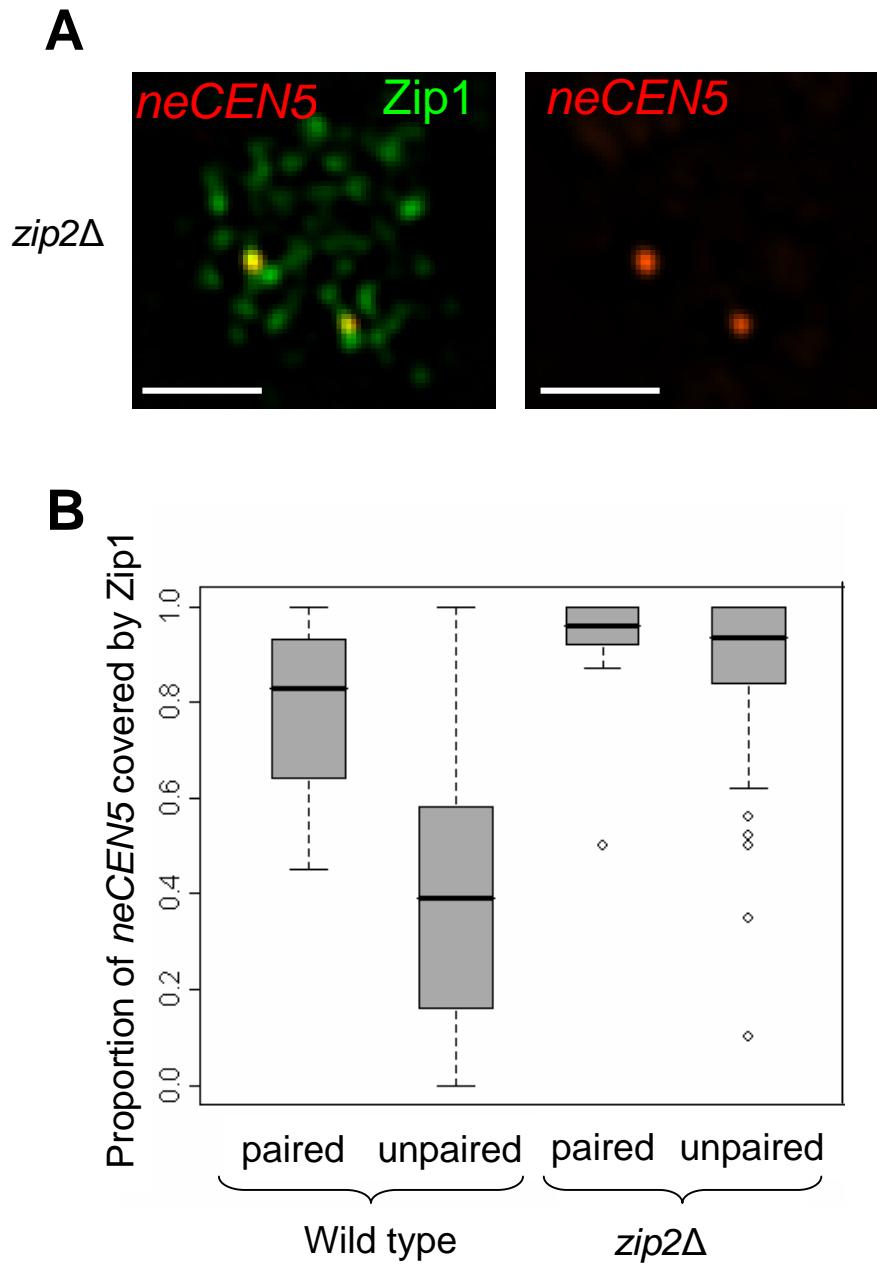
*zip2Δ*



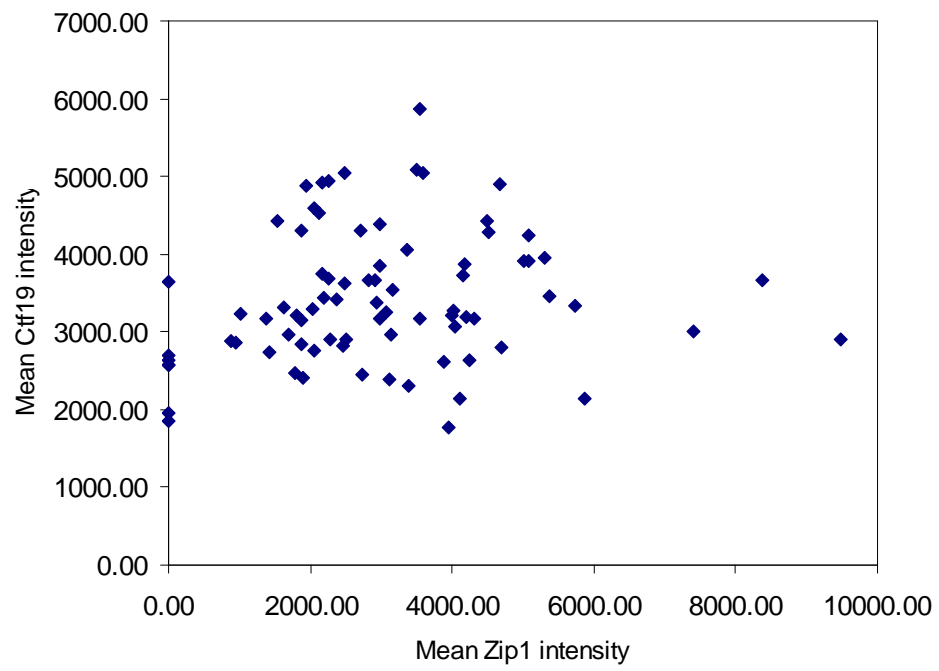
*zip3Δ*



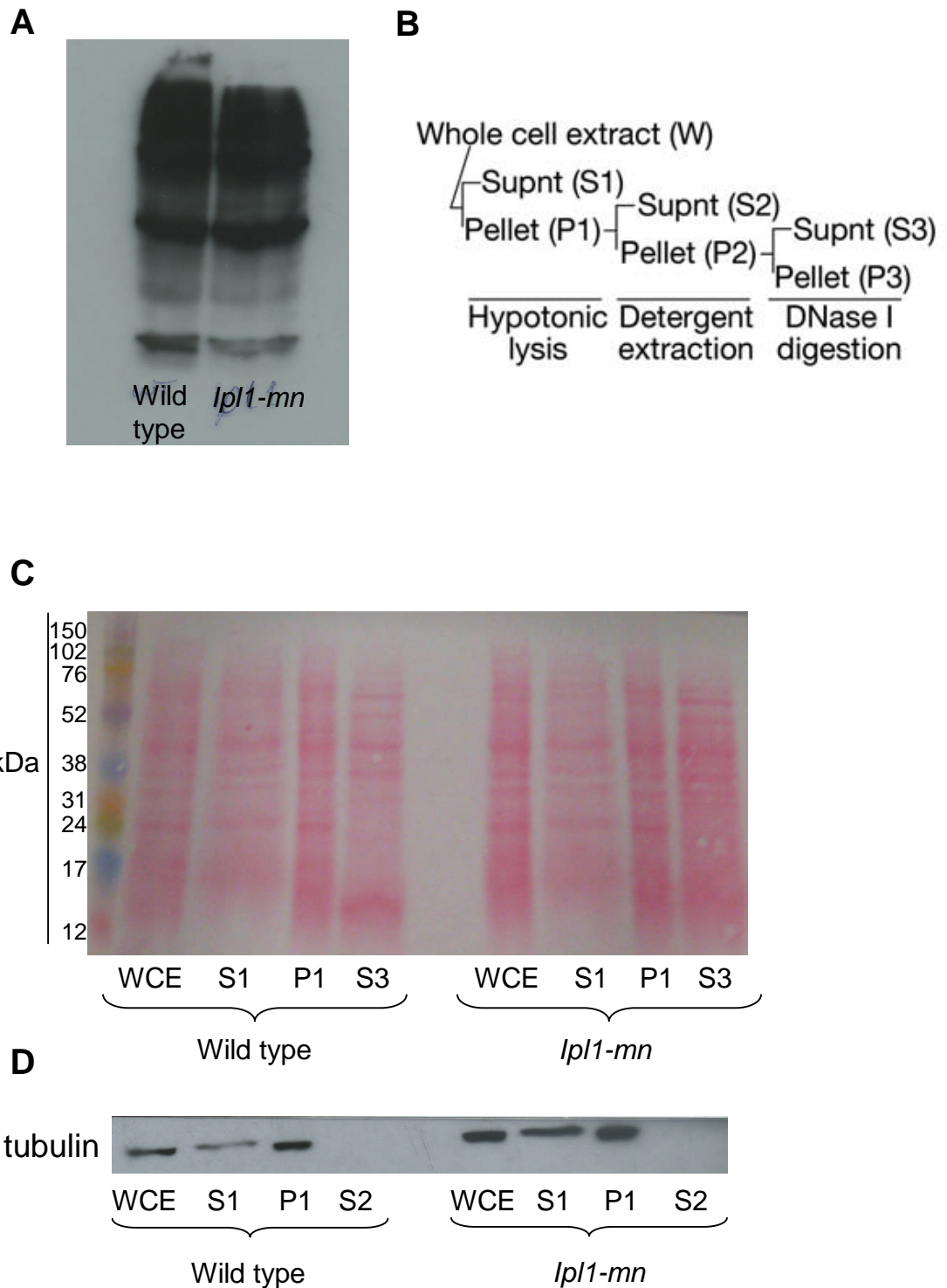
**Appendix Figure 6.** Representative images of Smt3 and Zip1 co-staining in pachytene nuclei of *zip2Δ* and *zip3Δ* mutants. The cells were defined as being in pachytene by the presence of highly condensed DNA. Bars: 5 μm.



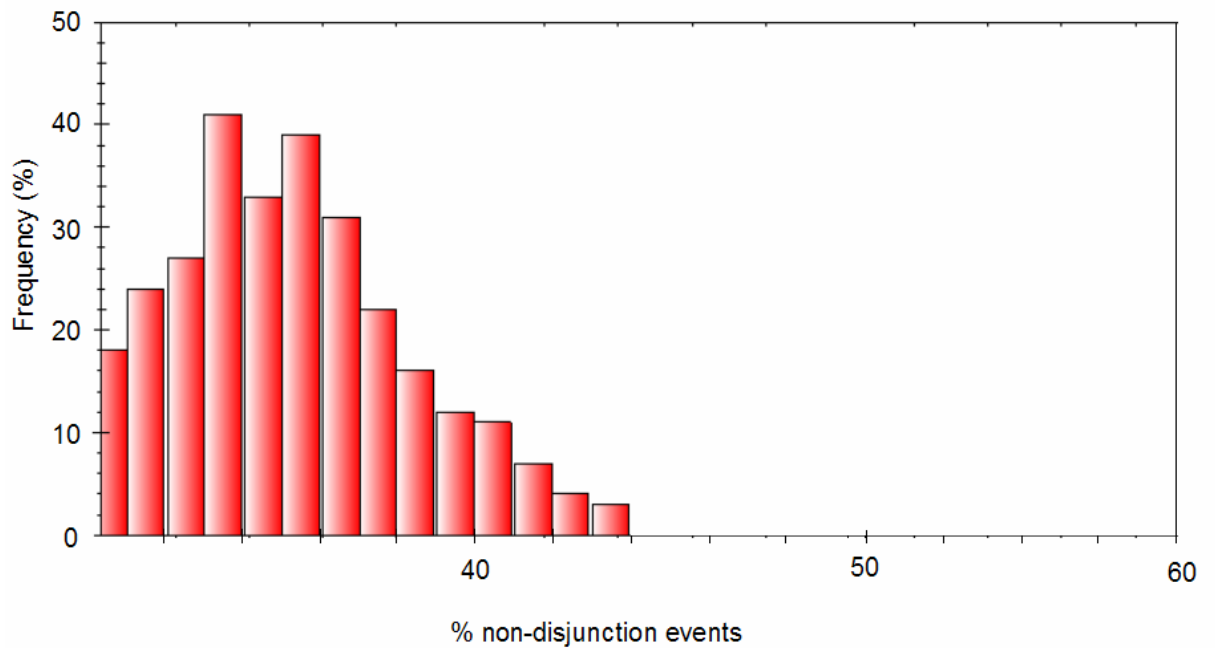
**Appendix Figure 7.** Analysis of the 'proportion' of each *neCEN5* covered by Zip1 during pachytene in *zip2Δ* mutants. 1 represents 100 % of all *neCEN5* pixels contained Zip1. See Chapter 4 for full description. 89 *neCEN5* foci were analysed from 49 nuclei.



**Appendix Figure 8.** Scatterplot of the mean Zip1 and mean Ctf19 pixel intensities for 80 randomly selected Ctf19 foci from *zip2Δ* mutants.



**Appendix Figure 9.** Protein extracts for Smt3 IP experiment. (A) Western blot for Smt3 from TCA whole-cell protein extracts from wild type and *lpl1-mn* mutant samples at 1 hour following pachytene release. Samples were run on at 10 % small-format gel. (B) Schematic outlining how the different fractions were derived. (C) Ponceau-stained western blot of the different fractions sampled during the preparation of crude chromatin extracts. WCE: whole cell extract. S1: Soluble material in supernatant following hypotonic lysis. P1: pellet containing crude nuclear fraction following hypotonic lysis and centrifugation through a 30 % sucrose cushion. S3: Soluble chromatin extract after DNase I and salt treatment of the nuclear fraction. Samples were not collected for P2 and S2. Molecular weight markers are given on the left. (D) The same western blot shown in B probed for tubulin.



**Appendix Figure 10.** A typical histogram from a single bootstrapping analysis of our dataset. In our hands, *mad3Δ* mutants experienced 34% MI non-disjunction of the non-exchange chromosome 5 pair. This percentage was obtained from examining 340 tetrads, of which 114 had experienced a MI non-disjunction event. 96 tetrads were analysed by Cheslock *et al.* (2005), who reported 50 % non-disjunction. Bootstrapping analysis was performed by sampling 96 of our 340 tetrads at random 10,000 times, each time generating a % non-disjunction. Shown here is a typical histogram of such analysis. Note that in 10,000 random samples not one returned a frequency of 50% or greater.